الجمهورية الجزائرية الديمقراطية الشعبية

République Algérienne Démocratique et populaire

وزارة التعليم العالي والبحث العلمي

Ministère de l'Enseignement Supérieur et de la Recherche Scientifique

جامعة الشهيد حمه لخضر – الوادي

Université Echahid Hamma Lakhdar – Eloued

Faculté des Sciences Exactes

Département de Chimie

Thèse

Présentée pour l'obtention du diplôme de

DOCTORAT

Domaine: Sciences de la Matière

Filière: Chimie

Spécialité: Chimie

Présentée par: **Abdellatif KEDADRA**

Thème

Etude théorique et comparative de quelques N-ferrocénylméthylamines à l'aide de la théorie de la fonctionnelle de la densité DFT et détermination de leurs activité biologique

Soutenue le: 01/12/2022

Devant le jury

LANEZ Touhami	Professeur	Univ. Eloued	Rapporteur
BENCHIKHA Naima	Professeur	Univ. Eloued	Présidente
MEDILA Ifrikia	M. C. A	Univ. Eloued	Examinatrice
BECHKI Lazhar	Professeur	Univ. Ouargla	Examinateur
SAIDI Moukhtar	Professeur	Univ. Ouargla	Examinateur
YOUCEFI Mohammed	Professeur	Univ. Laghouat	Examinateur

2022/2023

الجمهورية الجزائرية الديمقراطية الشعبية

People's Democratic Republic of Algeria

وزارة التعليم العالي والبحث العلمي

Ministry of Higher Education and Scientific Research

جامعة الشهيد حمه لخضر - الوادي

Echahid Hamma Lakhdar University - Eloued

Faculty of Sciences

Department of Chemistry

Thesis

Presented for the graduation of

DOCTORATE

Field: Material Sciences

Branch: Chemistry

Specialty: Chemistry

Presented by: **Abdellatif KEDADRA**

Theme

Theoretical and comparative study of some N-ferrocenylmethylamines using the density function theory DFT and determination of their biological activity

Graduation date: 01/12/2022

In front of the jury

Touhami LANEZ	Professor	Univ. Eloued	Raporter
Naima BENCHIKHA	Professor	Univ. Eloued	President
Medila IFRIKIA	Lecturer A	Univ. Eloued	Examiner
Bechki LAZHAR	Professor	Univ. Eloued	Examiner
Saidi MOUKHTAR	Professor	Univ. Ouargla	Examiner
Youcefi MOHAMMED	Professor	Univ. Ouargla	Examiner

2022/2023

DEDICATE

To the Piece of my heart...

To the light of my eyes...

To the love of my life...

To the soul of my mother ❤

May ALLAH have mercy on her

ACKNOWLEDGMENTS

First of all, I would like to thank God Almighty for having honored me and helped me to complete this work and present it in the way it is now.

I would also like to express my great gratitude to my supervisor in this thesis, Professor Touhami LANEZ for his guidance, sharing experience and his support in my difficult times. I really appreciate every minute you gave me and every supportive word you told me.

I cannot forget to thank the professors of the discussion committee, each in his name, Benchikha Naima, Medila Ifrikia, Bechki Lazhar, Saidi Moukhtar, Youcefi Mohammed for accepting the invitation to discuss my thesis, and I fully believe that their comments and criticism will increase the value of this thesis and improve it for the better.

All expressions of thanks and gratitude to the members of VTRS laboratory, Mr. Ali Tliba and Dr. Adika Aisha, who facilitated my work in the laboratory and did not leave me any room for complaint. To all my colleges especially Dr. Nadjiba ZEGHEB for her constant help and her priceless guidance, Dr. Hacen BEN AMARA, Dr. Hafnaoui LANEZ for their information and their valuable cooperation.

To the president of the doctoral training council Dr. Naima BEN CHIKHA, thank you so much for being there when I needed it very much. To all my Family especially my dear Father Mr. Med Tahar KEDADRA who gave me everything and all my successes are because of him being around me, my teachers my Friends and my mates Dr. Aicha KARASA, Dr. Chouaib FETHIZA, Dr. Imane CHELALBA, and Ali Khennoufa thank you so much I really appreciate your help and our experience together.

Lotfi KEDADRA

ABSTRACT

The main objective of this study is to build a QSAR model for a series of N-ferrocenylmethylaniline derivatives, the obtained model allows the prediction of their theoretical antioxidant activity and the selection of the antioxidant candidates . In order to achieve these goals, the antioxidant activity of a series of 28 N-ferrocenylmethylaniline derivatives was measured using cyclic voltammetry technique. Promising results of a half maximal inhibitory concentration of 7.719 mM have been obtained for N-(ferrocenylmethyl)-N-(acetyl)-4-(nitro)aniline (F23) which is a competitive result with that of the standard α-tocopherol (7.0581 mM). Other derivatives N-(ferrocenylmethyl)-4-(nitro)aniline (F12), N-(ferrocenylmethyl)-3-(aminobenzo)nitrile (F14), N-(ferrocenylmethyl)-N-(acetyl)-2-(nitro)aniline (F21), N-(ferrocenyl-methyl)-)-N-(acetyl)-2-(amino)benzonitrile (F24) and N-(ferrocénylmethyl)-N-(phenyl)benz-amide (F27) also gave comparable results to the standard.

Toxicity prediction studies demonstrated that among the most potent derivatives, F24 was predicted to be non-toxic. Molecular Docking study revealed that compound F24 is the most inactive compound against glutathione reductase enzyme amoung the 28 derivatives having a high inhibitory concentration of 2.61 µM and a low docking score of -7.61 kcal/mol. The compound formed only hydrophobic and π-cation interactions with amino acid residues of glutathione reductase.

The structural, electronical and spectral properties of the 28 derivatives were determined by energy optimization using Gaussian 09W with the method (DFT/B3LYP) and mixed basis sets (LANL2DZ(Fe)/6-31G(d)). Multi linear regression was used to build a quantitative relation between superoxide radical scavenging activity and structural properties. The model was validated and found to be statistically significant with a squared fitting correlation coefficient (R^2) of 0.944, adjusted squared correlation coefficient (R^2_{adj}) value of 0.842, and the cross-validation coefficient value of 0.892 with calculated F value of 17.88 showing this model with a good predictability.

Key words: ferrocene derivatives, antioxidant activity, QSAR, cyclic voltammetry, DFT.

الملخص

الهدف الرئيسي من هذه الدراسة هو بناء نموذج QSAR لسلسلة من مشتقات N-ferrocenylmethylaniline ، يسمح النموذج الذي تم الحصول عليه بالتنبؤ بنشاطها النظري المضاد للأكسدة واختيار مضادات الأكسدة المرشحة. ومن أجل تحقيق هذه الأهداف، تم قياس النشاط المضاد للأكسدة لسلسلة من 28 من مشتقات N-ferrocenylmethylaniline باستخدام تقنية قياس الفولتميتر الحلقي. تم الحصول على نتائج واعدة لتركيز مثبط نصف أقصى قدره 7.719 ميلي مولار للمشتق N- (ferrocenylmethyl) -N- (acetyl) -4- (nitro) aniline (F23) وهي نتيجة تنافسية مع تلك الخاصة بـ α-tocopherol القياسي (7.0581 ملم). مشتقات أخرى-N-(ferrocenylmethyl)-4-(nitro)aniline (F12), 5-(ferrocenylmethyl)-3-(aminobenzo)nitrile (F14), N-(ferrocenylmethyl)-N-(acetyl)-2-(nitro)aniline (F21), N-(ferrocenyl-methyl)-)-N-(acetyl)-2-(amino)benzonitrile (F24)) أيضًا أعطت نتائج جيدة ومعتبرة.

أظهرت دراسات التنبؤ بالسمية أنه من بين أكثر المشتقات فعالية ، كان من المتوقع أن يكون F24 غير سام. كشفت دراسة الإرساء الجزيئي أن المركب F24 هو المركب الأكثر فاعلية ضد إنزيم glutathione reductase بين المشتقات الـ 28 التي تحتوي على تركيز مثبط عالٍ قدره 2.61 ميكرومتر ودرجة ربط منخفضة تبلغ -7.61 كيلو كالوري / مول. شكل المركب تجاذبات كارهة للماء وبيتا مع الأحماض الأمينية من glutathione reductase.

تم تحديد الخصائص الهيكلية والإلكترونية والطيفية للمشتقات 28 عن طريق تحسين الطاقة باستخدام Gaussian 09W بالطريقة (DFT / B3LYP) ومجموعات الأساس المختلطة .((LANL2DZ (Fe) / 6-31G (d)) تم استخدام الانحدار الخطي المتعدد لبناء علاقة كمية بين نشاط الكسح الجذري للأكسيد الفائق والخصائص الهيكلية. تم التحقق من صحة النموذج ووجد أنه ذو دلالة إحصائية مع معامل الارتباط المناسب التربيعي 0.944 (R2) ، معامل الارتباط التربيعي المعدل (R2adj) بقيمة 0.842 ، وقيمة معامل التحقق المتبادل 0.892 مع قيمة F المحسوبة 17.88 كل هذه القيم تؤكد إمكانية توقع جيدة للنموذج.

الكلمات المفتاحية: مشتقات فيروسين ، نشاط مضاد للأكسدة ، QSAR، قياس الفولتميتر الحلقي، DFT.

ABBREVIATIONS

μ	Dipole moment
B3LYP	Lee-Yang-Parr nonlocal correlation function
CV	Cyclic Voltammetry
D	Diffusion coefficient
DFT	Density functional theory
DMF	Dimethylformamide
F	Fisher ratio
Fc	Ferrocene
GR	Glutathione reductase
Hf	Heat of formation
HOMO	Highest occupied molecular orbital
IC50	Half-maximal inhibitory concentration
$i_{p,a}$	Anodic peak current in $\mu A.cm^2$
$i_{p,c}$	Cathodic peak current in $\mu A.cm^2$
IR	Infra-Red
K	Binding constant
LD50	Median lethal dose
logP	Octanol/water partition coefficient
logS	water solubility
LUMO	Lowest unoccupied molecular orbital
MESP	Molecular Electro-Static Potential map
MLR	Multiple linear regression
MM^+	Molecular mechanics force field
MR	Molar refractivity

MV	Molar volume
MW	Molecular weight
$O_2^{\bullet-}$	Superoxide anion
PDB	Protein data bank
PE	Predictive error of the coefficient correlation
PM3	Semi-empirical Hamiltonian
Pol	Molar Polarizability
Q^2	Cross-validation coefficient
QSAR	Quantitative Structure-Activity relationship
R^2	Coefficient of determination
R^2_{adj}	Adjusted R squared
RMN	Resonance Magnetic Nuclear
RMSD	Root mean squared deviation
S	Standard deviation
SAG	Surface area grid
TC	Toxicity class
TPSA	Topological polar surface area
UV-Vis	Ultra Violet-Visible
ΔG	Free binding energy

CONTENTS

LIST OF FIGURES

LIST OF TABLES

GENERAL INTRODUCTION

GENERAL INTRODUCTION

Metallocenes, in particular ferrocene derivatives, are an important class of organometallic compounds [1]. Currently, ferrocene is considered as a widely applicable organometallic scaffold for the synthesis of various functional derivatives, useful in medicinal and synthetic fields [2-4].

Since its discovery in 1951, ferrocene has remained a molecule of continued interest [5], in part due to the rich chemistry of the iron(II) center and stability in aqueous and aerobic media coupled with aromaticity. Access to a wide variety of derivatives along with the ability to undergo easy iron oxidation make them fascinating targets in multiple fields such as electrochemistry, biochemistry, drug design, mediators of protein redox reactions [6, 7], internal standards in electrochemistry [8]. and organic synthesis [9], such as in the functionalization of cyclopentadienyl ligands [10, 11].

Compared to the wide use of ferrocene in new materials, ferrocene has been exceptionally applied as a structural feature in drug design, although some researchers have pointed out that ferrocene and its derivatives have potential pharmacological applications. This was due to this low polarity being limited to the bioavailability of ferrocene in vivo [12]. Since ferrocene was inert to oxidation in the atmosphere, it was inferred that synthetic derivatives of ferrocene may be a new type of antioxidant [13], in which other organic groups may enhance the bioavailability of ferrocene, or a large conjugated system formed between ferrocenyl and other organic compounds. groups can increase antioxidant efficacy [14] .

This study has two main objectives; the first is to build a quantitative structure-activity relationship (QSAR) model using multiple linear regression (MLR) method for N-ferrocenylmethylaniline derivatives, this model will be able to predict the half maximal inhibitory concentration of the antioxidant activity of these derivatives. In this regard we will perform structure optimisation of a series of 28 N-ferrocenylmethylaniline derivatives, their geometric, spectral and electronic properties will be calculated in order to use them as molecular descriptors in the QSAR study. Cyclic voltammetry assay will be applied to measure the antioxidant activity of the 28 derivatives and to obtain their IC50 which will be used as a response for the descriptors. The second objective of the study is to select the most potent derivatives as antioxidants drug candidates . Absorption, Distribution, Metabolism, and Excretion (ADME) and pharmacokinetics properties of the target derivatives will be predicted using SwissADME website tool. The toxicity of the derivatives will be also performed *in silico* using the ProTox-II web server in order to predict their toxicity properties such as hepatotoxicity, carcinogenicity, immunotoxicity, mutagenicity,

cytotoxicity, median lethal dose (LD_{50}), and toxicity class , the best candidates will be docked using AtouDockTool software to study their inhibition activity against glutathione reductase enzyme which is involved in elimination of reactive oxygen species and act as a scavenger for various oxygen radicals. The obtained *in vitro* and *in silico* results will correspond with one another and will give room for the design of novel antioxidant N-ferrocenylmethylaniline derivatives with less activity against glutathione reductase.

This thesis is structured in two main parts as follow:

- The first part contains a bibliographical and theoretical approaches and is divided into three chapters:
  - Chapter 1: Overview of ferrocene and its derivatives
  - Chaptre 2: Antioxidant activity
  - Chaptre 3: Theoretical background of the used expermintal and computetional methods
- The second part concerns the experimental part and the results of the thesis and it is also divided into three chapters:
  - Chapter 1: Structural, electronical properties and in silico toxicity of N-ferrocenylmethylaniline derivatives
  - Chapter 2: Antioxidant activity of N-ferrocenylmethylaniline derivatives by cyclic voltammetry and molecular docking studies
  - Chapter 3: QSAR modeling.

PART 1

BIBLIOGRAPHICAL AND THEORETICAL APPROACHES

CHAPTER I

OVERVIEW OF FERROCENE AND ITS DERIVATIVES

I.1. Introduction

Since Ferrocene (Figure I-1) was independently discovered in 1951 by Kealy, Pauson, and Miller [15], the impact of this revolutionary work has been enormous. It opened up new areas of chemistry, deepened our understanding of structure, binding, and reactivity, and thus paved the way for the burgeoning field of organometallic chemistry itself. Ferrocene and Ferrocene molecules are not simple trophy molecules for the plateau; rather the synthesis of this sandwich system in all its flavors, its polyvalent reactional chemistry, its structural characteristics, the mechanistic and theoretical studies which accompany it, its use in homogeneous catalysis, in particular in stereoselective and asymmetric transformations [16-18], in electrochemistry, in particularly in electron transfer processes [19], as new materials, including polymer chemistry [20-27], as fuel additives [28-30], as anticancer reagents [31], in bioorganometallic chemistry [32, 33], etc. has contributed to the rapid growth and therefore rapid shifting of the boundaries of this family of compounds over the past 60 years [34].

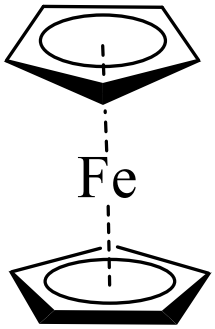

Figure I-1 Ferrocene

I.2. Discovery of ferrocene

The chemistry of transition metals was mastered by German chemists before World War II. This discipline was transferred to the English and Americans after World War II. In 1951, Kealy and Pauson [15] published for the first time in a famous article in the journal Nature, the synthesis of bis(cyclopentadienyl)iron or ferrocene. T.J. Kealy and P.L. Pauson attempted to prepare dihydrofulvalene by oxidation of a Grignard reagent of cyclopentadienyl according to Equation I-1. The compound obtained from this reaction was an orange product and thermally very stable.

$$2C_5H_5MgBr + FeCl_3 \longrightarrow (C_5H_5)_2Fe$$ *Equation I-1*

The structure proposed by Pauson for this compound has a resonance form in which iron is bonded to cyclopentadienyl through a sigma bond with a canonical ionic formula (Figure I-2).

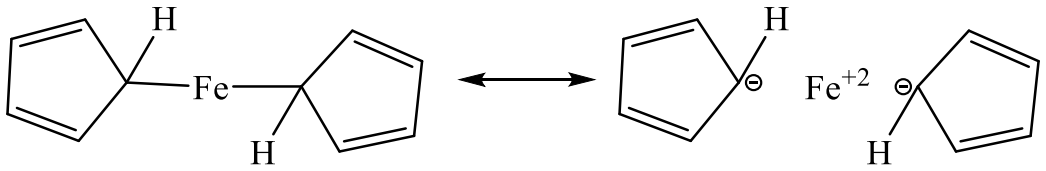

Figure I-2 The resonance structure proposed by Kealy and Pauson

English chemist Geoffrey Wilkinson and the German physicist Ernst Fischer, who were instrumental in the correction of the structure proposed by Pauson, and the discovery of the exact nature of the iron-carbon bond in bis(cyclopentadienyl)iron, called ferrocene [35, 36].

In 1952 E. O. Fischer independently began studying the structure of ferrocene in his laboratory at the Technische Hochschule in Munich. His conclusions were based on data from x-ray crystallography, from which he concluded that the molecule must consist of an iron (II) atom located between the two cyclopentadienls as ligands.

L. E. Orgel began the description of the molecular orbitals of this new structure which has already been determined by Dunitz [37]. The title of his publication contained the description sandwiched [38].

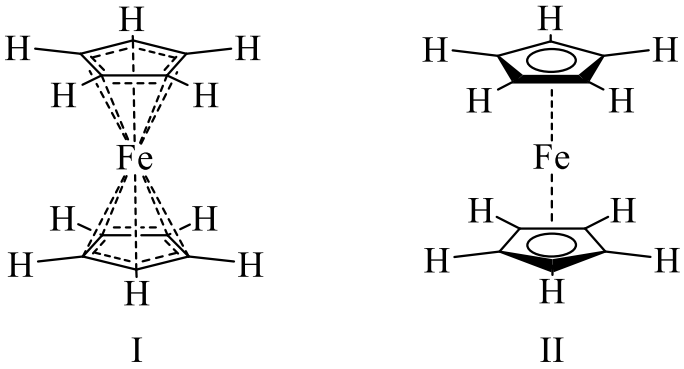

Figure I-3 The corrected structure of ferrocene

I.3. Properties of ferrocene

I.3.1. Physical properties

Ferrocene is an orange crystalline solid, with a molar mass of 186.04 g.mole^{-1} [39], stable in air, boiling point 249 °C and melting point 173-174 °C. Ferrocene is soluble in most organic solvents, its solubility in water is approximately 0.1 mg/ml at 21 °C, 100 mg/ml in DMSO at 19.5 °C. It is stable at high temperature, up to 400 °C [40].

At room temperature, Ferrocene is the most stable of the metallocenes, smelling like camphor [41]. Studies have shown that it is sensitive to prolonged exposure to air and light.

Ferrocene forms with dilute nitric acid and concentrated sulfuric acid dark red solutions with blue fluorescence [42, 43].

I.3.2. Electrochemical properties

Many studies and analyzes by electrochemical methods have been carried out on the redox properties of ferrocene. In general, the usual cathodic behavior of ferrocene in organic media such as dichloromethane, acetonitrile and DMF can be described by a one electron reversible reduction, leading to the ferrocerium ion [44, 45], Figure I-4.

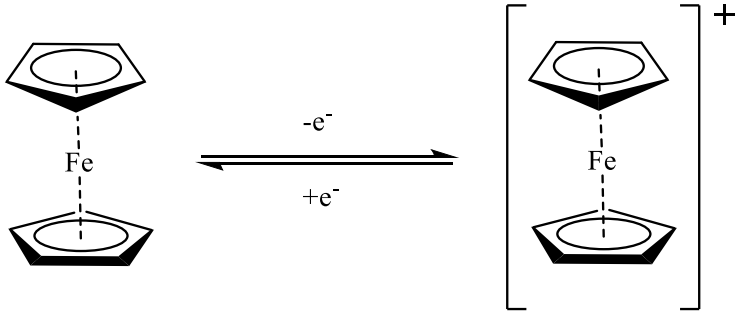

Figure I-4 Reversible monoelectronic oxidation of ferrocene

The reversibility of the redox reaction was demonstrated by cyclic voltammetry, the electrochemical parameters taken from ferrocene voltammogram show that the redox process does this in a rapid, reversible and monoelectronic way.

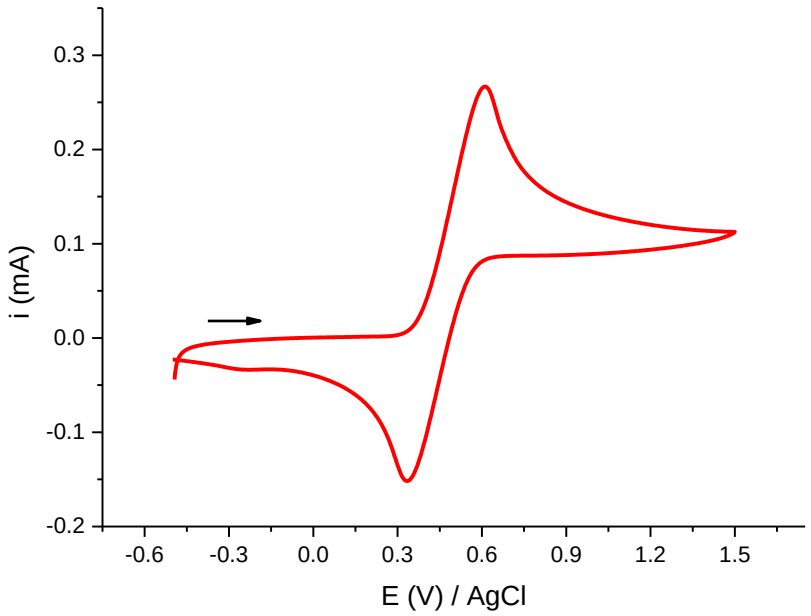

Figure I-5 Ferrocene voltammogram recorded on a platinum electrode in acetonitrile 10^{-3} M in the presence of Tetrabutylammoniumpairchlorate 10^{-1} M at υ = 100 mv/s, my own work .

The values of the electrochemical parameters taken from the voltammogram of Figure I-5 are grouped together in Table I-1. These values provide information on the speed and reversibility criteria.

Table I-1 Characteristic values of the electrochemical parameters of ferrocene

Ep_a (V)	Ep_c (V)	Ip_a (mA)	Ip_c (mA)	$E_{1/2}$ (V)	ΔEp (V)
0.609	0.339	0.267	-0.151	0.480	0.27

I.3.3. Spectral properties

I.3.3.1. InfraRed

Ferrocene infrared spectroscopy (Figure I-6) is relatively simple because of its symmetrical structure. It exhibits an absorption band at 3075 cm^{-1} equivalents to the elongation of the aromatic C-H bond. There are only four apparent bands: two at 811 and 1002 cm^{-1} are equivalent to the bending vibration of C-H, and one at 1108 cm^{-1} is equivalent to the antisymmetric vibration of the pentadienyl ring. The absorption band at 1411 cm^{-1} is equivalent to the antisymmetric C-C removal vibration of unsubstituted cyclopentadienyl.

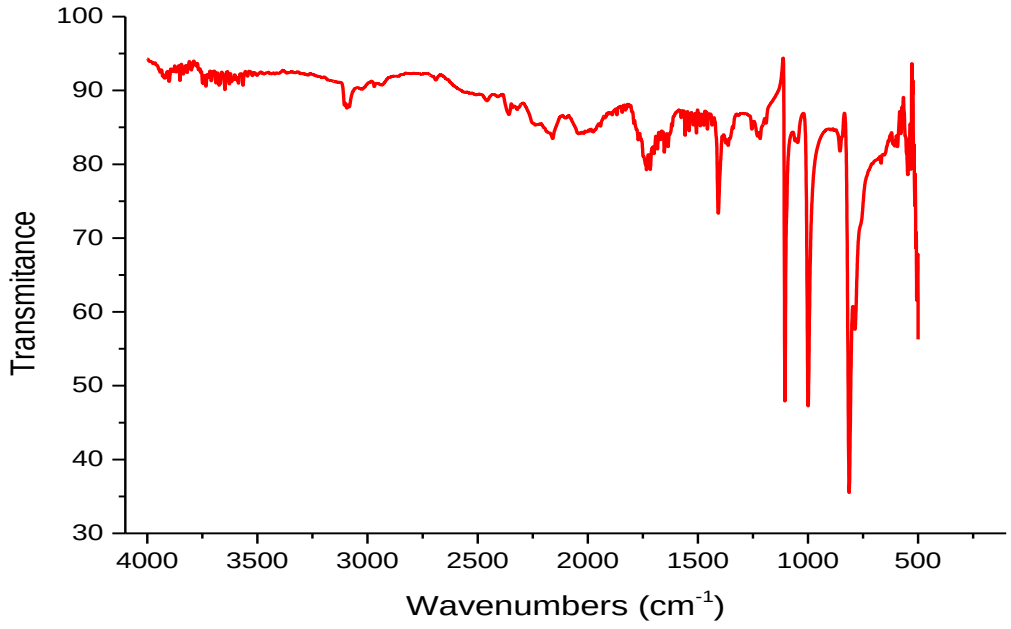

Figure I-6 IR spectrum of Ferrocene [46]

I.3.3.2. Uv-Visible

W. Albert Noyes et al. found that the ultraviolet and visible absorption spectra of ferrocene in ethanol are characterized mainly by two bands. One is at 325 nm and the other (which is somewhat broader) is centered at 440 nm [47].

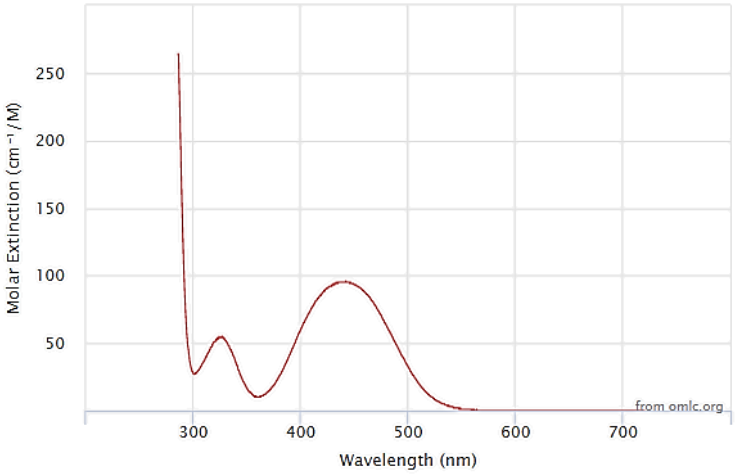

Figure I-7 UV-Vis spectrum of Ferrocene [47]

I.3.3.3. Nuclear Magnetic Resonance (NMR)

I.3.3.3.1. NMR ^{1}H

The NMR ^{1}H spectral of the Ferrocene molecule is very simple, it shows a single peak corresponds to the ten protons of two cyclopentadienyl cycles at 4.15 ppm (Figure I-8) [48].

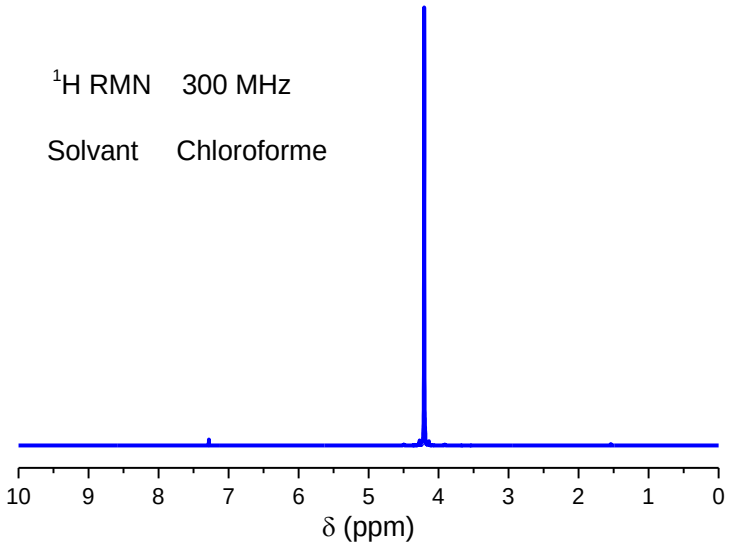

Figure I-8 NMR ^{1}H spectrum of Ferrocene [48]

I.3.3.3.2. NMR ^{13}C

Likewise, the NMR ^{13}C spectral of ferrocene shows a single peak at 68 ppm corresponds to the ten carbon atoms of two cyclopentadienyl rings (Figure I-9) [48].

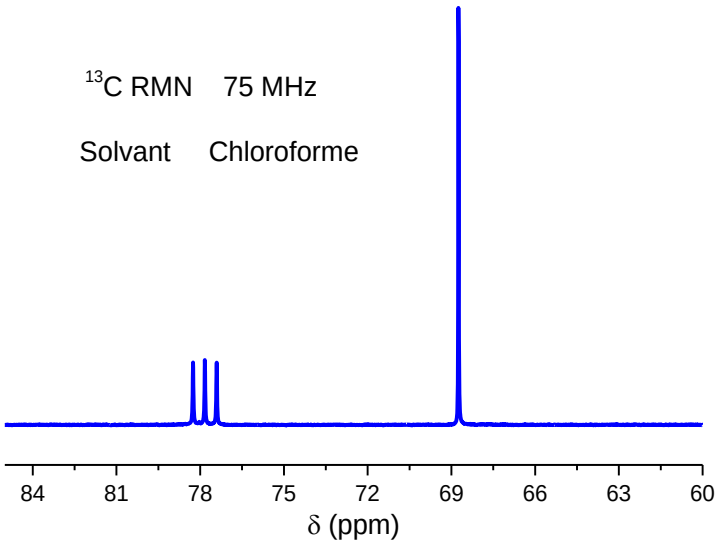

Figure I-9 NMR ^{13}C spectrum of Ferrocene [48]

I.3.3.4. Crystalline structure

The crystal structure of ferrocene (Figure I-10) has been studied by Wilkinson et al. [49] by X-ray diffraction. These analysis led to the determination of the exact lengths of the C-C, C-Fe, and C-H bonds.

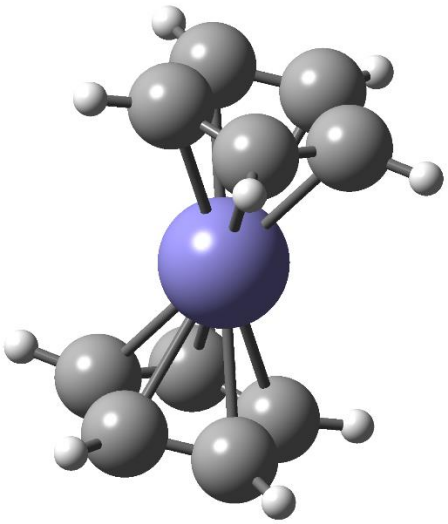

Figure I-10 Ferrocene crystal structure

The average length of the C-C bond in the two pentadienyl rings of ferrocene is 1.389Å, a value which is very close to that of benzene (1.395Å). The length Fe-C is equal to 2.03Å. C-H bonds have an average length of 1.389Å. Ferrocene is the most stable of the metallocenes series. Each ligand $C_5H_5^-$ being a donor of six electrons, with the six electrons of Fe(II) led to the stable configuration of 18 electrons [49].

I.4. Synthesis of ferrocene

I.4.1. Chemical process

The acidity of cyclopentadiene (pKa = 20) is relatively high in comparison with alkanes (the pKa of methane is of the order of 60) (Equation I-2).

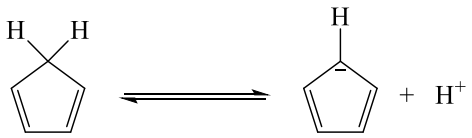

Equation I-2

This acidity is sufficient to react with the sodium hydroxide in DMSO and produce the cyclopentadienyl anion. DMSO is an aprotic dipolar solvent which enhances the basicity of the OH^- ion by very efficiently solvating the Na^+ counterion (Equation I-3).

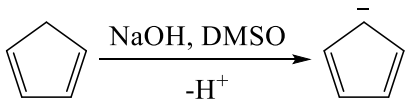

Equation I-3

A sufficiently basic amine such as diethylamine can be used to form the cyclopentadienyl ion from cyclopentadiene.

The direct reaction of cyclopentadiene with ferrous chloride in the presence of diethylamine, can be adopted to synthesize cyclopentadienyl ion from cyclopentadiene, and even a diamine can play the role of an HCl acceptor (Equation I-4) [50].

Equation I-4

Cyclopentadiennylthalliume can also be used as a starting material for the preparation of ferrocene as shown in Equation I-5 and Equation I-6 [51].

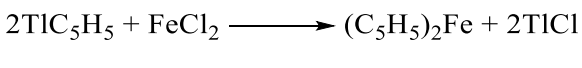

Equation I-5

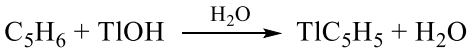

Equation I-6

Grignard's reagent of cyclopentadiene, an easily obtained intermediate, was used by Kealy and Pauson [15] for their historical preparation of ferrocene (Equation I-7). This technique was developed by Pauson in 1955 [52].

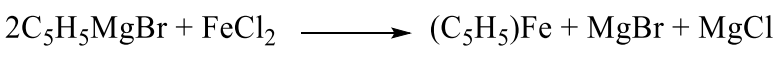

Equation I-7

The success of this method is due to the solubility of ferric chloride in organic solvents. No reaction occurs if the ferrous halide is insoluble in the solvent, but high yields of ferrocene are obtained if the ferrous ion is "solubilized" by chelation. In the Grignard reaction, an excess of the reagent is required.

Several other methods for the synthesis of ferrocene have been proposed. It can be prepared by the direct reaction of cyclopentadiene with metallic iron [53], by the reaction of ferrous chloride with sodium cyclopentadienyl in an ammonia solvent and the reaction of cyclopentadiene with the ferrous complex of acetylacetone- dipyridine [54].

A method for preparing ferrocene and analogous compounds was developed following a synthesis of the work of several research teams [55-63]. This method is essentially based on the deprotonation of cyclopentadiene by redox with sodium in xylene (Equation I-8), followed by a reaction of the cyclopentadienyl salt with ferrous chloride in THF (Equation I-9).

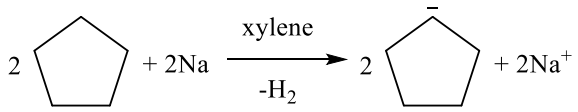

Equation I-8

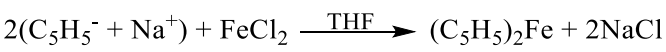

Equation I-9

I.4.2. Electrochemical process

The cation of the transition metal obtained by the loss of one or more electrons can be facilitated by the use of this metal as a cathode in an electrochemical cell. Although this process is useful for some organometallic compounds, ferrocene cannot be synthesized efficiently by this technique [64].

The anodic process is still rarely used in the synthesis of derivatives of organometallic compounds. In 1968 Valcher and Aluni [64] proposed the synthesis of ferrocene by electrolysis of

a solution of cyclopentadienylthallium using dimethylformamide and an iron anode which oxidizes to Fe^{+2}, and which then easily replaces thallium at the cathode (Equation I-10).

$$Fe + 2TlCp \longrightarrow Cp_2Fe + 2Tl^{+} + e^{-} \qquad \textit{Equation I-10}$$

I.5. Reactivity

Substituted ferrocenes can be prepared directly or indirectly. In the indirect preparation, the ferrocene molecule is used as a starting point for the synthesis of other ferrocene derivatives, while in the direct synthesis, the substituted ferrocene is prepared by the reaction of a suitably substituted cyclopentadiene derivative compound with the iron by methods similar to those used for the preparation of ferrocene itself. Only strong bases such as Grignard's reagent, organothalliums, lithium or sodium reagents can give good yields of ferrocene derivatives from substituted cyclopentadienes [65, 66].

I.5.1. Substitution reaction

The similar properties between ferrocene and benzene contributed to the development of the chemistry of this new molecule, and facilitated the performance of a wide variety of substitution reactions on ferrocene. The mechanism of substitution reactions on the pentadienyl ring is based on the direct formation of a sigma complex without the participation of the metal. Two mechanisms are proposed [67].

Mechanism (I): It has a two-step process. The first is a rapid step where the electrophile E destroys the metal-carbon bond in a reaction of SE2 with conservation of configuration, followed by limiting the rate of removal of the proton from outside the molecule, the second step is an SE2 reversal reaction (Figure I-11).

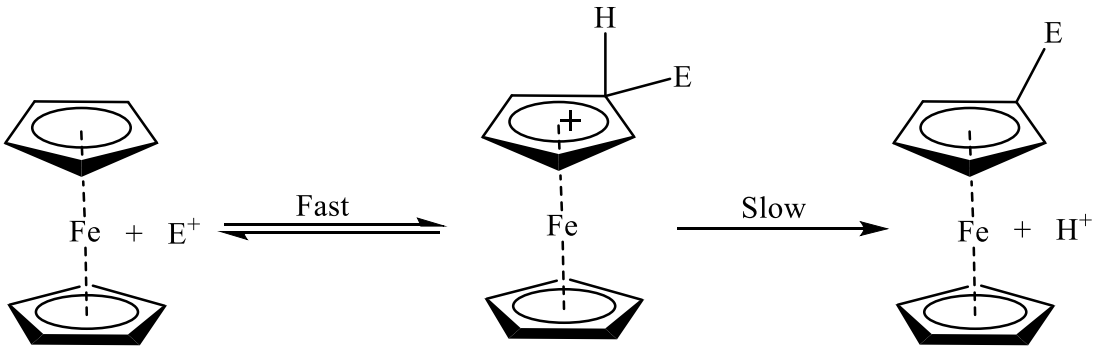

Figure I-11 Substitution mechanism (I)

Mechanism (II): this mechanism has a speed limitation of the attack by the electrophile from the outside in an SE2 displacement with a reversal of the configuration, followed by the rapid departure of a proton from the inside, with configuration conservation (Figure I-12).

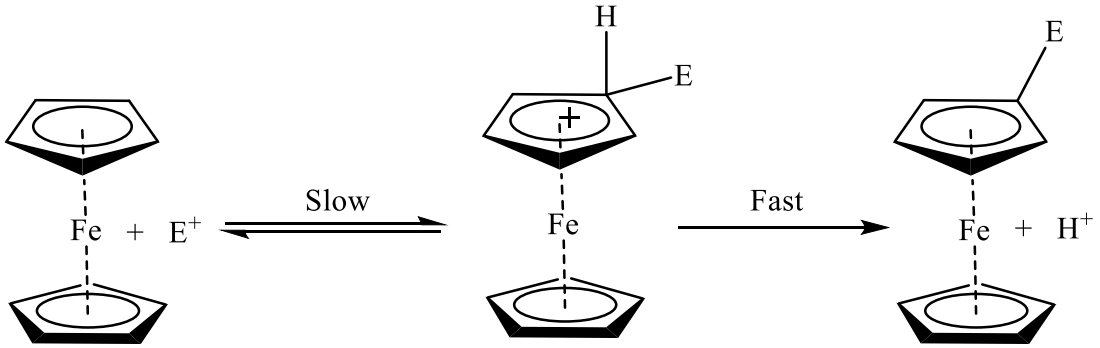

Figure I-12 Substitution mechanism (II)

I.5.2. Oxidation reaction

Ferrocene can be oxidized to the ferrocenium ion by a wide variety of oxidizing agents. During this oxidation, the iron atom, which can formally be considered as Fe (II) in ferrocene, is oxidized to the Fe (III)state . This can happen even when air is passed through a solution of ferrocene at low pH values. This oxidation occurs during attempts of nitration or halogenation of ferrocene using nitric acid or bromine respectively. Thus, the ferrocene molecule carries a positive charge and resists any electrophilic attack.

Numerous studies on the controlled oxidation of ferrocene and its derivatives have been reported [68, 69]. In order to decrease the conversion of ferrocene and its derivatives into relatively unstable and unreactive ferrocenium ion, most reactions must be carried out under an inert atmosphere.

Electrochemical reduction of ferrocene carried by the teams of Laviron in Dijon in DMF and by Bard in Austin in SO_2 was able to demonstrate the existence of extreme degrees of oxidation Fe (I) and Fe (IV). The potentials shown on Figure I-13 are given relative to the saturated calomel reference electrode (SCE) [70, 71].

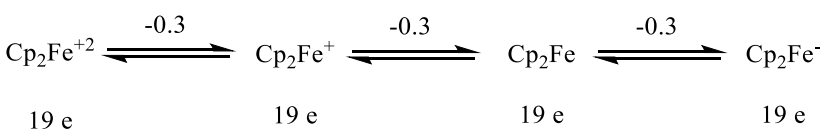

Figure I-13 The change in the oxidation state of the metal in ferrocene

Ferrocenium ion is a fairly stable, water-soluble ion with a blue-glass color; a number of its salts have been isolated and they are widely used as mild oxidants in organometallic chemistry. They are accessible by contact of ferrocene with sulfuric acid (or concentrated nitric acid). It happens that one wishes to reduce the corresponding ferrocenium salts to ferrocene derivatives, which is easily achievable using an aqueous solution of dithionite, stannous chloride and ascorbic acid or $TiCl_3$ as shown on Figure I-14.

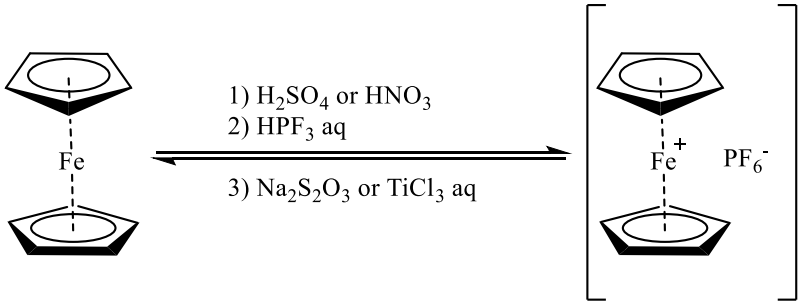

Figure I-14 Oxidation reaction of ferrocene

I.5.3. Reaction with electrophiles

Ferrocene behaves like most aromatic compounds, allowing the synthesis of substituted derivatives. A typical demonstration experiment is a Friedel Crafts reaction with acetic anhydride in the presence of phosphoric acid as a catalyst. In the presence of aluminum chloride, Me_2NPCl_2 and ferrocene react to give ferrocenyldichlorophosphine [72], while treatment with phenyldichlorophosphine under the same conditions leads to P,P-diferrocenyl-P-phenyl phosphine [73]. Figure I-15 represents some of the main reactions of ferrocene with electrophiles.

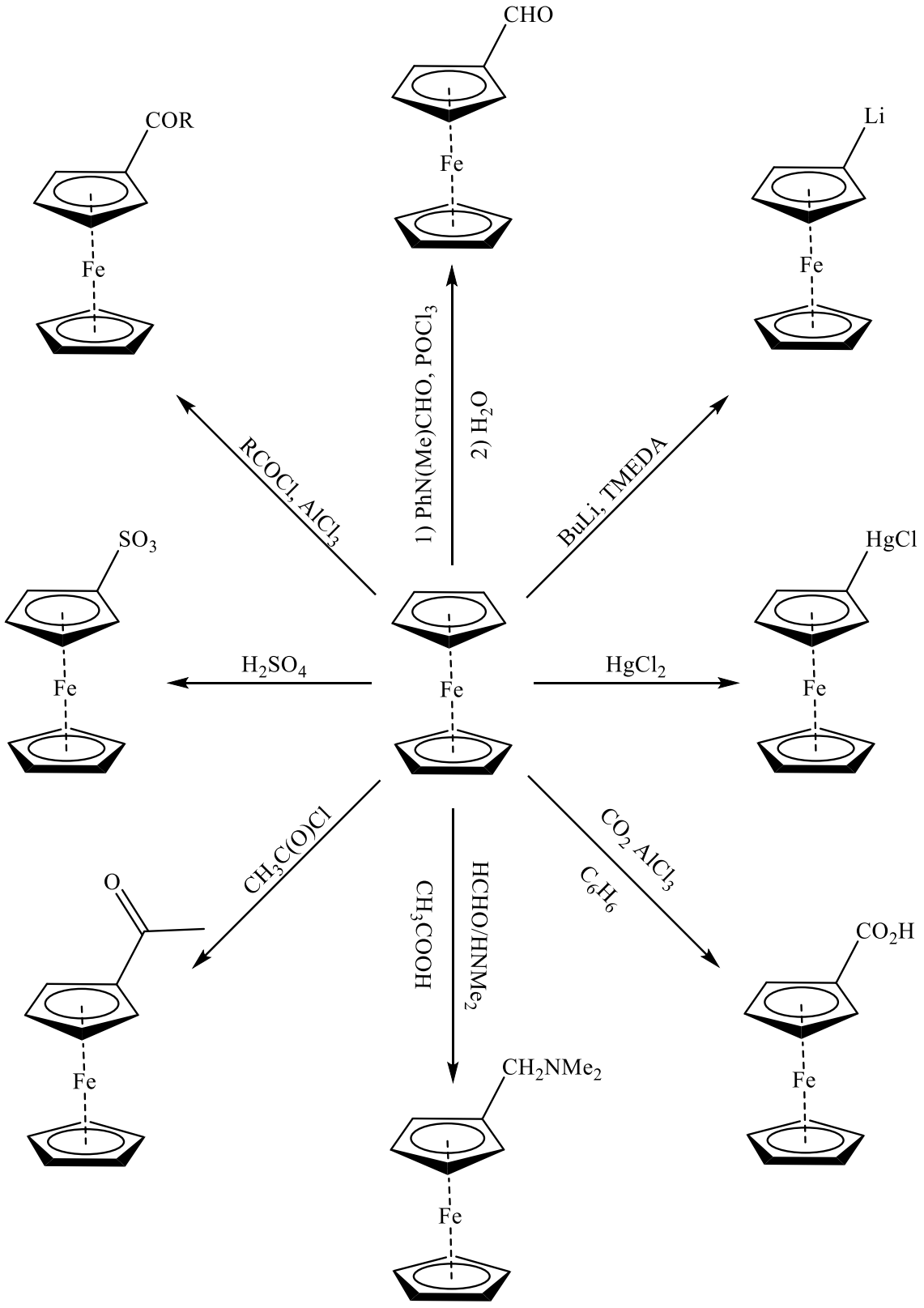

Figure I-15 The main reactions of ferrocene with electrophiles.

I.5.4. Acylation reaction

The acylation of ferrocene, according to Fridel and Crafts reaction, can be carried out under very mild conditions with, for example, acetic anhydride containing phosphoric acid as a catalyst, this acylation leads to the monoacetylferrocene as major product together with the disubstituted acetylferrocene as minor product. Using aluminum chloride as a catalyst, a good yield of both mono- and diacetylferrocene can also be obtained, their ratio depends on the proportions of the acylating reagent [74-81]. Figure I-16 illustrated the reaction scheme.

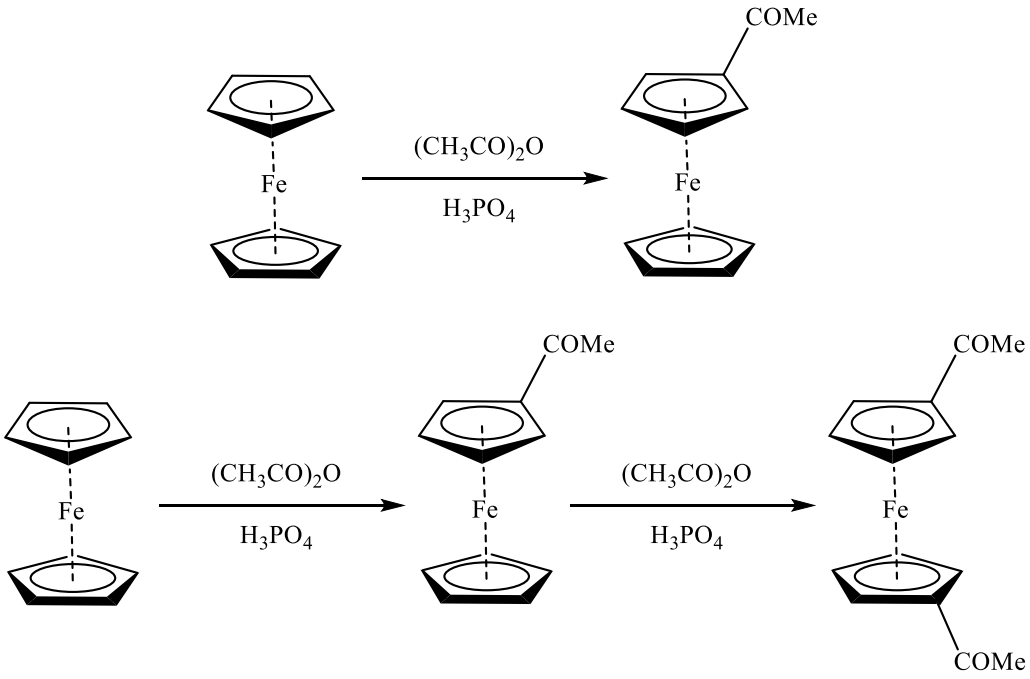

Figure I-16 Mono- and biacylation of ferrocene

I.6. Synthesis of some ferrocene derivatives

The aromatic character and the very high reactivity of ferrocene have allowed the synthesis of a very large number of its derivatives which are used as main intermediates in organic synthesis [77, 81]. These derivatives can be easily prepared and are sufficiently reactive to produce intermediates useful for the synthesis of new organic compounds difficult to synthesize by ordinary routes using organic compounds.

These intermediates are more useful for the synthesis of monosubstituted ferrocene derivatives than for disubstituted ferrocenes. Thus, although monoacetylated ferrocenes have been employed for the preparation of a large family of substituted ferrocene derivatives [82].

The N,N-dialkylaminomethylferrocene derivatives, such as N,N-dimethylaminomethyl-ferrocene [83] are among the most widely used intermediates for the synthesis of substituted

ferrocenes. Ferrocenylmethyltrimethylamonium iodide [84], Figure I-17 is used as a starting material for the preparation of a large number of monosubstituted ferrocene derivatives.

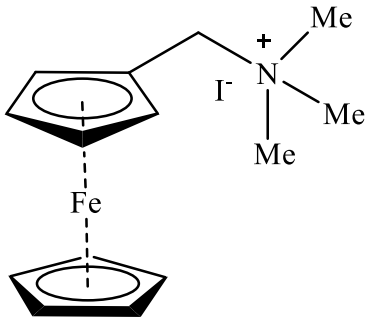

Figure I-17 Ferrocenylméthyltriméthylamonium iodide

The trimethylamine group in the ferrocenylmethyltrimethylamonium salt can be easily substituted by nucleophiles, such as alkoxide and cyanide anions, Grignard reagents, carbanionic reagents and amines.

Many methods have appeared in the literature for the preparation of ferrocenylmethyl-trimethylamonium iodide [83-85]. Thus, the modification of phosphoric acid has also been successfully employed for the aminomethylation of phenyl and methylferrocene [86], Figure I-18 illustrated the reactivity of ferrocenylmethyltrimethylamonium iodide and its use for the preparation of many other reactive ferrocene derivatives.

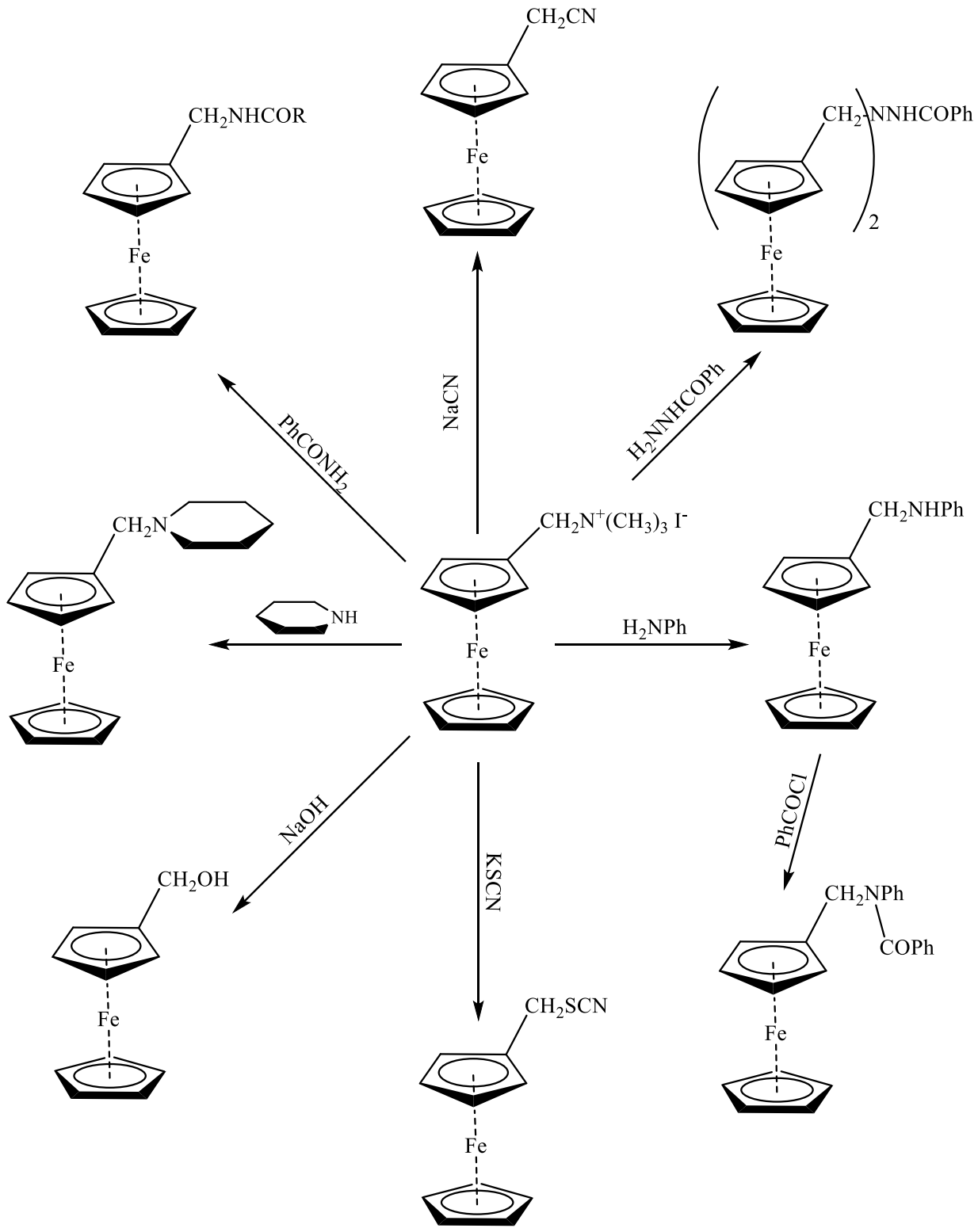

Figure I-18 Synthesis of some ferrocene derivatives from ferrocenylméthyltriméthylamonium iodide

I.6.1. N-ferrocenylmethylanilines synthesis

Using a wide range of substituted anilines as nueoclophiles, many N-ferrocenylmethylanilines can be obtained from ferrocenylmethyltrimethylamonium iodide in moderate yields. In the first step, the synthesis of N-ferrocenylmethylanilines is carried out by treating the quaternary salt ferrocenylmethyltrimethylamonium iodide with an excess of anilines in distilled water, at a temperature between 100 to 110 °C [87]. Figure I-19 shows an example of this reaction.

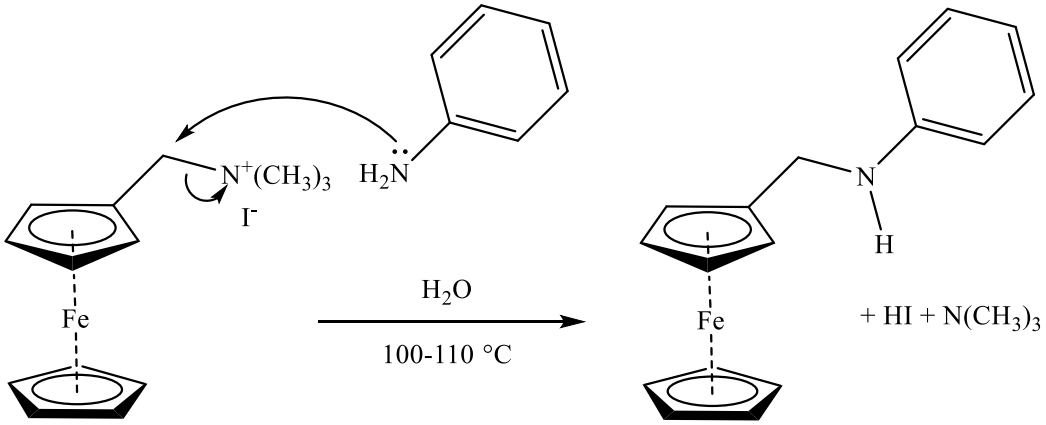

Figure I-19 N-ferrocenylmethylaniline synthesis

I.7. Ferrocene applications

The applications of ferrocene in chemistry are indeed vast. The unique structure and aromatic character of ferrocene [88] led to its ancient use in reducing carbon deposition and smoke formation upon addition to fuel oils [52]. Ferrocene and its derivatives have been used in many applications, including their use as radiation absorbers, combustion regulators, highly effective non-toxic medicinal substances, components of various redox systems, etc… [89-91] In addition, many journals have focused on the biological chemistry of ferrocene [92], its bioorganometallic chemistry [93], its applications in glucose biosensors [94] and bioelectronics [95], the synthesis and electrochemical properties of nucleic acid containing ferrocene acids [96]. Below are some of its most important applications:

I.7.1. Applications of ferrocene polymers

The introduction of metal atoms into polymers is a good method for the preparation of promising materials for use in different applications and therefore, much literature to date relates to polymers containing metals [20]. The metal atom can be arranged in a variety of different ways relative to the polymer backbone [21], as shown in Figure I-20. In type I, the metal atom can be

attached to the polymer backbone using a linker such as an alkyl group. While in type II the metal atom is electronically bonded to the backbone of the polymer. On the other hand, in type III, the metal atom is found in the backbone of the polymer itself. In addition, Fc-containing polymers are considered to be an important class of metal-containing polymers which have different applications due to the combination of polymer properties and metal properties [20].

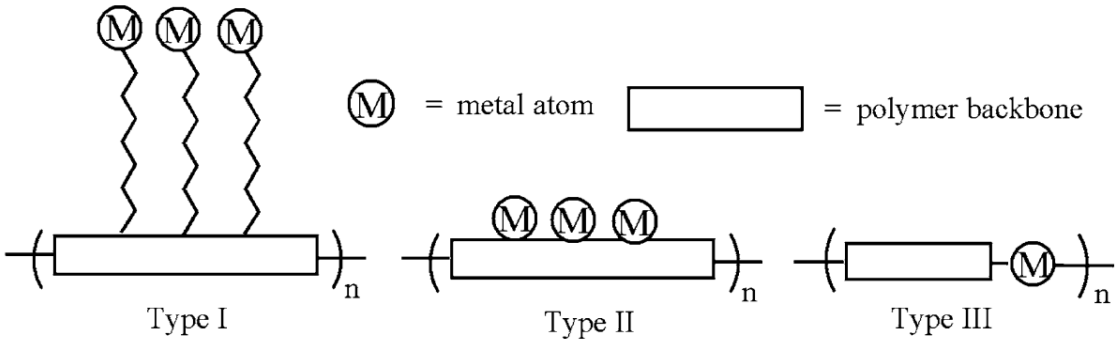

Figure I-20 Possible arrangements of the metal atoms relative to the polymer backbone [21]

Fc-based polymers have a variety of applications, including amperometric biosensors [22], protein, DNA [23, 24], and hepatitis B surface antigen (HBsAg) immunosensors [25], and monoxide sensors [26]. They can also be employed in the manufacture of optical logic devices [27].

I.7.2. Catalytic applications of unsymmetrical ferrocene ligands

Catalysis with 1,1A-asymmetric ligands is an area of research that is still in its infancy and only preliminary results have been reported to date (apart from 1,1A-ferrocenyl oxazolines which reported 1,2-homologs). This is in part due to the fact that selective monolithiation of dibromoferrocene, which represents a high yielding systemic route for the synthesis of these types of ligands, has only recently been developed [97-101].

I.7.2.1. Ferrocenylphosphate–carbene ligands

Asymmetric catalysis using transition metal complexes is a good strategy to obtain chiral compounds according to Sorádová et al. [102] Ferrocenylphosphate-carbene ligands formulated to catalyze "domino" reactions comprising the conjugated addition of Grignard reagents to an α, β-unsaturated lactone followed by entrapment of the enolate with an alkene. Promising results obtained with high enantiomeric purity.

I.7.2.2. Ferrocene-based palladium catalyst

Hanhan et al. [103] describes an efficient method for the synthesis of ortho-substituted sterically hindered biaryls by the Suzuki-Miyaura coupling reaction of aryl chlorides and heterocyclic chlorides not activated with boronic acid, using a Pd(II)-diimine containing ferrocene as a catalyst (Figure I-21). A small amount of catalyst (0.1%) has been found to be very effective. The stability of the catalyst in water, its bulk due to the presence of two ferrocene units and its electronic properties play an essential role in the success of the catalyst. Hydrolysis of ionic diimines and their complexes in water results in the deactivation of the catalyst and the reaction is completed in 15 min.

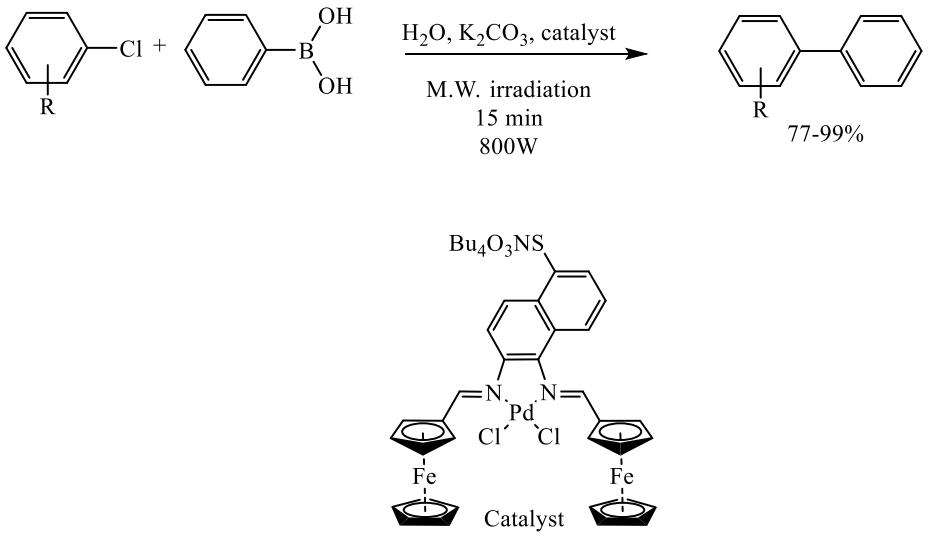

Figure I-21 Suzuki–Miyaura coupling reaction [103]

I.7.2.3. Ferrocene-based compartmental ligands

Chandrasekhar et al. [104] used the ferrocene group to prepare compartmental ligands which selectively bring together Zn(II)/4f heterobimetallic complexes (Figure I-22). Two phenolate oxygen atoms and an acetate ligand form a bridge between the metal ions Zn(II) and Dy(III). It was expected that with the use of this ligand magnetically interesting 3d/4f heterobimetallic compounds could be produced.

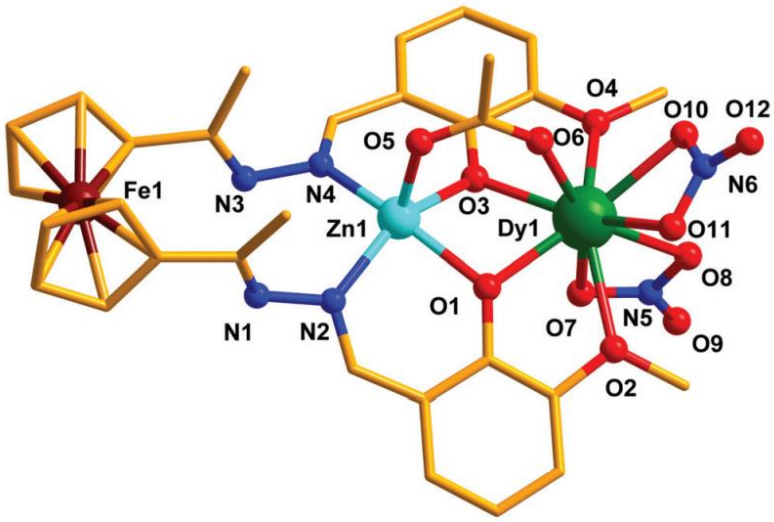

Figure I-22 Molecular structure of LZn(μ-OAc)Dy(NO3)2 complex [104]

I.7.2.4. Chiral ferrocenyldiphosphine ligands

Brunner and Janura [105] studied the phosphorus-chiral ferrocényldiphosphines, in which the chirality arises from the optically active substituents (1R,3R,4S)-menthyl, prepared by a selective lithium-halogen exchange and a P-1-ferrocenophane ring opening. Its rhodium complex has been used as an asymmetric hydrogenation catalyst giving high yields but with moderate enantiomeric excess with a variety of different substrates. The use of in the nickel catalyzed Grignard cross coupling of 1-phenylethylmagnesium chloride with vinyl bromide was also demonstrated, but the results revealed only a low enantiomeric excess.

I.7.3. Conducting applications

Several ferrocene-tetrathiafulvalenes have been synthesized as donors to drive charge transfer complexes because to the excellent structural and electrochemical features of the ferrocene-containing tetrathiafulvalene ring. The first compound in this class of donor conductive materials was discovered by Ueno et al. [106], and Bryce et al. [107] recently reported a very similar sort of donor molecule.

I.7.4. Industrial applications

The increased interest in ferrocene derivative research can be ascribed to their good water and air stability, attractive electrochemical characteristics, and non-toxic behavior [108, 109]. Fuel oil additives to reduce the creation of soot, which contains iron, are one of their industrial applications. Rocket and satellite fertilizers, UV absorbers, burn rate modifiers, and protective coatings.

I.7.5. Agricultural applications

In agriculture, crop protection is a critical concern. Ferrocene derivatives have a wide range of uses in agriculture, including as agrochemicals and catalysts for selective agrochemical production. They can also be employed as soil remediation surfactants and as selective colorimetric and electrochemical chemosensors. Triazole heterocycles are found in the majority of ferrocene agrochemicals (fungicides, herbicides) [110, 111].

I.7.6. Medical and biological applications

Beside the fact that ferrocene attracted attention in medicinal studies by being a non-toxic compound [112] ferrocene derivatives also have attracted attention as potential anticancer, antibacterial, antifungal, and antiparasitic medicines.

I.7.6.1. Antiviral and Anticancer agents

The two most prominent derivatives, ferroquine (Figure I-23) and ferrocifene (Figure I-24), were discovered in the 1990s and have since been extensively explored for the treatment of malaria and cancer, respectively [113, 114]. The ferrocenyl group of these two compounds participates in important metal-specific modes of action which contribute to the overall therapeutic efficacy of the molecules. Despite the fact that ferroquine is in Phase II clinical trials and ferrocifene is in preclinical studies, no other ferrocene derivative - indeed, no other non-radioactive organometallic compound of any kind has progressed in clinical trials [115].

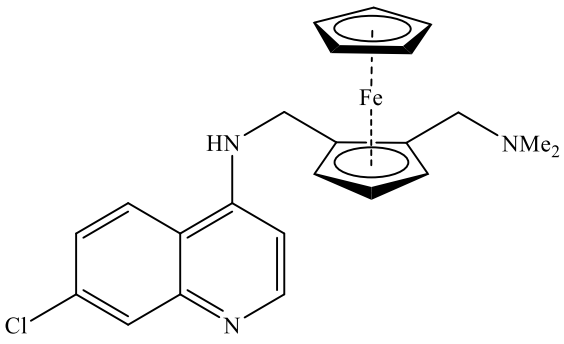

Figure I-23 Ferroquine (FQ)

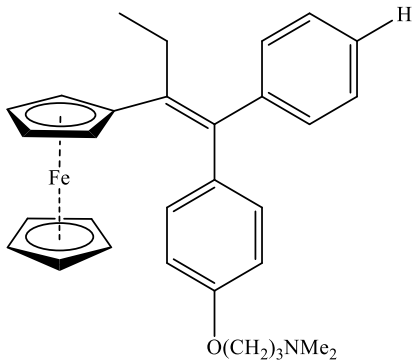

Figure I-24 Ferrocifen (Fc-TAM)

This perspective provides techniques for systematically incorporating ferrocenyl groups into established medications or drug candidates in order to discover new pharmacological avenues.

Zegheb et al. [31] studied the anti-proliferative effect of 29 N-ferrocenylmethylaniline derivatives against MCF-7 cell lines and the results indicated that among the studied derivatives,

five were very active; the binding affinity of these five active derivatives to estrogen and progesterone receptors was further investigated by molecular docking. The results of the anti-proliferative tests and the molecular docking were in good agreement. Moreover, the application of drug-likeness rules shows that most of these compounds, theoretically, can be bioavailable orally.

I.7.6.2. Antimicrobial agents

Champdore et al. [116] were inspired by the medical applications of ferrocene to create adducts by incorporating the ferrocenemethyl group in a heterocyclic base, which have been tested against HIV-1, HBV, YFV, BVDV, and a variety of bacteria. Only compounds containing thymine [117-119] were found to be cytotoxic to MT-4 cells. The only compounds that were effective against HIV-1 were the ferrocenyl derivatives of 3-deoxy-3-azidothymidine [119, 120]. However, they were found to be 10 to 300 times less potent than the reference medicine, 3-azidothymidine (AZT).

I.7.6.3. DNA/BSA binding studies

One of the recent areas of research in organometallic chemistry is the synthesis and development of detection systems for DNA detection [121, 122]. These systems (chips) allow rapid, simple, sensitive and inexpensive genetic diagnosis by the method electrochemical detection. To construct such a system, it is important to develop a reproducible method for immobilizing a capture DNA probe on the surface of gold, and many types of immobilization methods have been reported [123, 124]. Electrochemical systems for the DNA detection are potentially cheaper and more reliable than conventional systems. fluorescence spectroscopy. Ferrocene and its derivatives are often used in such devices due to their favorable electrochemical properties [125, 126]. Several reviews have recently been published on this subject [127, 128].

Khannoufa et al. [129] studied the binding interaction of 3 N-ferrocenylmethylaniline derivatives which are N-ferrocenylmethyl-2-nitroaniline (2FMNA), N-ferrocenylmethyl-3-nitroaniline (3FMNA) and N-ferrocenylmethyl-4-nitroaniline (4FMNA) with albumin bovine serum (BSA) by absorption spectroscopy, cyclic voltammetry and molecular docking techniques. The results indicated that these derivatives could bind to BSA. Molecular docking study indicated the preferred binding site, binding mode and further suggested that the binding mode of the three compounds to BSA is hydrogen bonding and hydrophobic forces.

I.7.6.4. Antioxidant agents

The antioxidant capabilities of ferrocene derivatives were studied by Khelef and Lanez [130]. They used three different ferrocene derivatives bearing amine, amide, and hydrazine groups (Figure I-25), and evaluaed their antioxidant activities using four different methods, including 2,2-Diphenyl-1-picrylhydrazyl (DPPH) free radical scavenging activity, superoxide ($O_2^{\bullet-}$) anion radical scavenging activity, phosphomolybdenum, and decrease in peak oxidation current of oxygen methods. The ferrocene derivative (B) showed the highest DPPH and ($O_2^{\bullet-}$) radical scavenging activity and was determined to be closest to that of standard antioxidant ascorbic acid.

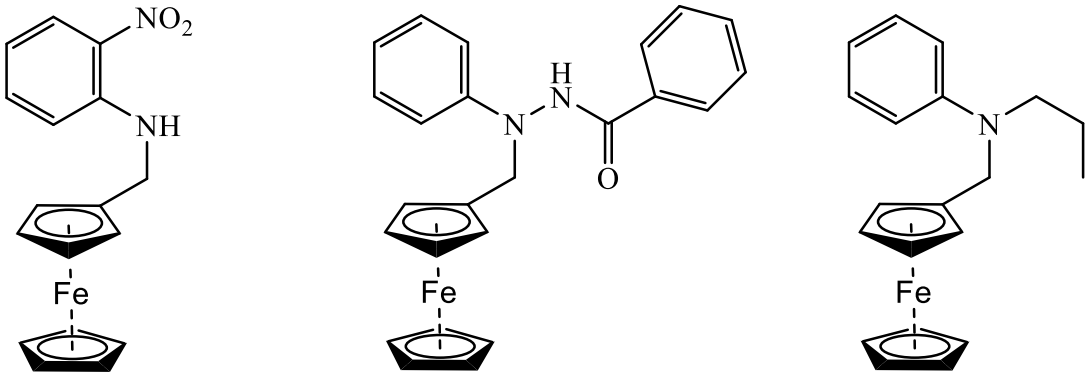

(A) (B) (C)

Figure I-25 three different derivatives of ferrocene containing amine, amide and hydrazin

Lanez et al. [131] have been also evaluated the superoxide anion radical binding parameters with 2-(ferrocenylmethylamino)benzonitrile and 3-(ferrocenylmethylamino)benzonitrile using cyclic voltammetry techniques. The antioxidant activity of the two compounds was also measured. The results indicated an electrostatic interaction of the superoxide anion radical with the two compounds as the dominant mode.

CHAPTER II

ANTIOXIDANT ACTIVITY

II.1. Introduction

The measurement of the antioxidant potential and the monitoring of the oxidation processes are approached globally by determining products resulting from the oxidation or by evaluating the ability to scavenge radicals of reaction models. The first, older mode requires prior knowledge of the compounds resulting from oxidation. Indeed, these methods look for certain functional groups (aldehydes, ketones, dicarbonyls, etc.) in the derivatives of the original constituents. The second relates the amount of radicals trapped to that of the antioxidant used [132].

Due to their high reactivity, reactive oxygen species (ROS) are responsible for a great deal of damage to cellular constituents. This production of deleterious species is generally balanced by their consumption at equal speed by the endogenous antioxidant system. The disruption of the balance between pro- and anti-oxidant species is referred to as oxidative stress. [133].

II.2. Oxidative stress

Oxidative stress is an imbalance between the generation of ROS and the body's ability to neutralize them and separate oxidative damage [134]. It corresponds to a disturbance of the intracellular oxidative status [135].

Free radicals are produced by various physiological mechanisms because they are useful for the body in reasonable doses. This physiological production is perfectly mastered by defense systems. Under normal circumstances, the antioxidant / prooxidant balance is said to be in equilibrium. If this is not the case, whether through antioxidant deficiency or as a result of overproduction of radicals, the excess of these radicals is called Oxidative Stress. It is now accepted that the phenomenon of oxidative stress is involved in the etiology of many neurodegenerative diseases (Alzheimer's, Parkinson's, Huntington's), pathological disorders (ischemia reperfusion syndrome), but also in the phenomena of aging [136].

II.3. Free radicals

A free radical is a molecule or an atom having one or more unpaired electrons, which makes it extremely reactive [137]. The collection of free radicals and their precursors is often referred to as reactive oxygen species [136]. The term "reactive oxygen derivatives" is not restrictive. It includes the free radicals of oxygen itself, but also certain non-radical reactive oxygenated derivatives of significant toxicity such as hydrogen peroxide H_2O_2.

Due to the involvement of free radicals in various pathologies, research into new molecules that can compensate for a deficit in the natural anti-free radical protection system has been greatly intensified [138].

Recently, chemists have been developing analogs of natural antioxidants by chemically modifying them to increase their free radical scavenging properties. They are interested in the development of more specific traps based on the particular reactivity of certain chemical groups towards radical species [138].

II.3.1. Free radical formation

At the cellular level, ROS and reactive nitrogen species (RNS) can be produced in response to a variety of stimuli, such as metabolic overload caused by an excess of macronutrients. The main determinants of the generation of ROS or RNS are the family of nicotinamides adenine dinucleotide phosphate oxidases (NOX), mitochondrial respiration, endoplasmic reticulum function (ER) and nitric oxide synthase (NOS) [139].

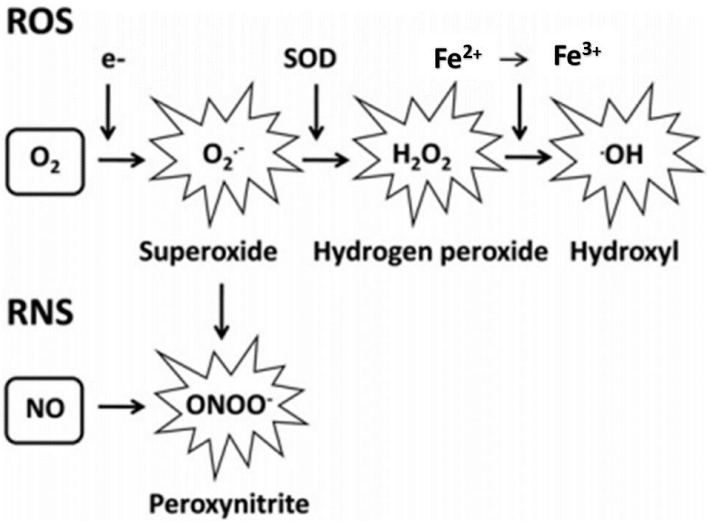

Figure II-1 Generation of the major reactive species of oxygen (ROS) and nitrogen (RNS)[140].

II.3.1.1. Redox reaction

The most common free radicals have a single celibate electron. They can be formed from a radical species which undergoes a redox reaction. There is then loss or gain of electron (Equation II-1, Equation II-2) [141].

$$\text{Oxydation:} \quad R - X \rightarrow R - X^{\bullet +} + e^{-} \rightarrow R^{\bullet} + X^{+} + e^{-} \qquad \textit{Equation II-1}$$

$$\text{Reduction:} \quad R - X + e^{-} \rightarrow R - X^{\bullet -} \rightarrow R^{\bullet} + X^{-} \qquad \textit{Equation II-2}$$

One of the best-known examples is the Fenton reaction, which reacts ferrous iron and hydrogen peroxide is presented in the following Equation II-3:

$$H_2O_2 + Fe^{2+} \rightarrow HO^{\bullet} + OH^{-} + Fe^{3+}$$ *Equation II-3*

II.3.1.2. Homolytic rupture

The production of free radicals can also be done by homolytic breaking of a covalent bond, which results in the formation of two entities each having a single electron (Equation II-4).

$$R - X \rightarrow R^{\bullet} + X^{\bullet}$$ *Equation II-4*

Homolytic rupture is the symmetrical partitioning of the common valence doublet, as opposed to heterolytic rupture which gives rise to ions of opposite charge. This most commonly occurs in the gas phase or in the liquid phase for molecules having weakly polarized bonds.

The oxygen molecule is representative of this type of rupture, the bond energy that connects the two oxygen atoms (150 $kJmol^{-1}$) is relatively low compared to the carbon-carbon bond (346 $kJmol^{-1}$) [142]. This bond being fragile, it is more apt to undergo homolytic rupture.

II.3.2. Radical reactive oxygen species

II.3.2.1. Superoxide radical ($O_2^{\bullet-}$)

In the human body, part of the molecular oxygen can univalent and sequentially capture an electron, leading to the formation of the leader of reactive oxygen species: one of these reactive species is known as superoxide anion [143], it generates as indicated in the following equation (Equation II-5).

$$O_2 + e^{-} \rightarrow O_2^{\bullet-}$$ *Equation II-5*

II.3.2.2. Hydroxyl radical

It mainly produces from superoxide anion and hydrogen peroxide in the presence of ferric ions, during the Haber-Weiss reaction (Equation II-6):

$$O_2^{\bullet-} + H_2O_2 \rightarrow {}^{\bullet}OH + OH^{-} + O_2$$ *Equation II-6*

The hydroxyl radical has a very high reactivity in biological media, being able to combine with many molecules with a rate constant of the order of 10^{10} $M^{-1}. s^{-1}$. It is able to react with almost all cellular components by electron exchange, addition on double bonds or tearing of a hydrogen

atom, it is a very powerful oxidant, certainly constituting the most toxic free radical in biology. The hydroxyl radical is therefore a very powerful oxidant and is believed to be at the origin of the production of secondaryfree radicals, following its reaction with various cellular compounds [144].

II.3.2.3. Perhydroxyl radical $HO_2^{\bullet}$

This is obtained after protonation of the superoxide radical in a pH<4.8 medium. The perhydroxyl radical is more reactive than superoxide because the standard redox potential is higher as well as its rate constants, especially with respect to polyunsaturated fatty acids (linoleic, linolenic, arachidonic acids) [145].

II.3.3. Non-Radical reactive oxygen species

II.3.3.1. Hydrogen peroxide H_2O_2

Hydrogen peroxide H_2O_2 which is not a free radical can be formed secondarily to the dismutation of ($O_2^{\bullet-}$) by superoxide dismutase or produced by bivalent reduction of oxygen thanks to a large number of dehydrogenases, in particular acyl CoA dehydrogenase, NADH dehydrogenase, xanthine oxidase, uricase, mono-amine oxidase… etc (Equation II-7, Equation II-8) [146].

$$O_2^{\bullet-} + 2H^+ \rightarrow H_2O_2 + O_2 \qquad \textit{Equation II-7}$$

$$O_2 + 2e^- + 2H^+ \rightarrow H_2O_2 \qquad \textit{Equation II-8}$$

Hydrogen peroxide is also a very reactive oxidizing agent; this is why it is often used as a disinfectant and as a bleaching agent. If not quickly destroyed, it can decompose and produce hydroxyl radicals that attack macromolecules in the cell [147].

II.4. Diseases linked to oxidative stress

By revealing abnormal biological molecules and by overexpressing certain genes, oxidative stress will be the main initial cause of several diseases: cancer, cataracts, amyotrophic lateral sclerosis, acute respiratory distress syndrome, pulmonary edema, accelerated aging, Alzheimer's, Parkinson's, intestinal infections, rheumatism, atherosclerosis, diabetes [148, 149].

II.5. Diet and oxidative stress

The production of ROS can occur at the cellular level in response to various stimuli, such as the metabolic overload itself caused by an overabundance of macronutrients. Indeed, when the calorie intake exceeds the energy expenditure, the increase induced by the excess substrate activates the Krebs cycle which causes the formation of ROS.

Thus, excessive ingestion of macronutrients induces the production of ROS [140]. In this sense, a study has shown that the ingestion of 75g of glucose induces an increase in the production of superoxide in leukocytes, which are then released into the extracellular environment. A similar response has also been observed following the ingestion of saturated fat [150]. Thus, a meal rich in fat and carbohydrates induces a more intense and prolonged oxidative and inflammatory response with increased production of ROS. in obese patients compared to normo-weighted subjects [151].

For this, it is possible to choose antioxidant and non-inflammatory foods to minimize inflammation and postprandial oxidative stress. The advent of molecular biology shows the role of certain small molecules in antioxidant defense; indeed, this defense can be reinforced by exogenous inputs.

Diagram (Figure II-2) shows that a good diet directly provides most of the elements that can ensure good antioxidant defense. This power supply guarantees:

- A supply of vitamins A and C, carotenoids and flavonoids which have the role of neutralizing radical entities by trapping them (Scavangers).
- Trace elements such as iron, Selenium, copper, zinc and manganese essential for the activity of antioxidant enzymes (Cu, Zn-SOD, Se-GPx).

Based on these data, scientists are attaching more and more importance to a diet rich in fruits and vegetables, this finding therefore leads to an important reflection on the effect of long-term antioxidant therapy in the context of prevention of pathologies where oxidative stress is involved (eg cardiovascular disease). With this in mind, the SUVIMAX study proposed to evaluate the impact of a daily intake for 8 years of a mixture of antioxidants at physiological doses (30 mg of Vit E, 120 mg of Vit C, 6 mg of b-Carotene, 100µg of selenium and 20 mg of zinc on the incidence of the onset of cardiovascular diseases [152].

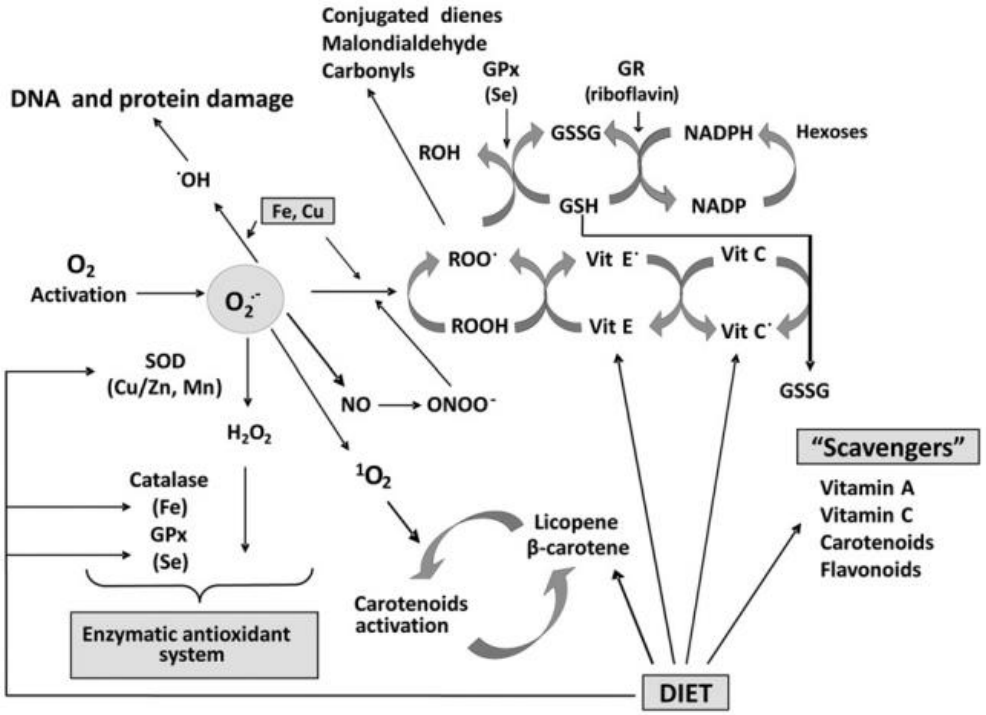

Figure II-2 Role of diet in oxidative metabolism [140].

II.6. Antioxidants

Antioxidants are molecules with the ability to neutralize free radicals which are responsible for many diseases. Antioxidants are compounds that inhibit or delay the oxidation process by blocking the initiation or propagation of chains of oxidative reactions [153].

Natural or synthetic antioxidants are used to prevent many diseases (cardiovascular and neurodegenerative, inflammation, diabetes, etc.) and aging, due to the excessive formation of free radicals. Antioxidants are also used in foods to delay spoilage, rancidity or discoloration which is often due to oxidation caused by light, heat and certain metals [154].

II.6.1. Enzymatic antioxidants

One of the enzymatic antioxidant defense systems is made up of three enzymes: superoxide dismutase SOD, glutathione peroxidase GSH-Px and catalase. These enzymes have a complementary action on the radical cascade at the level of superoxide and hydrogen peroxide, ultimately leading to the formation of water and molecular oxygen [155].

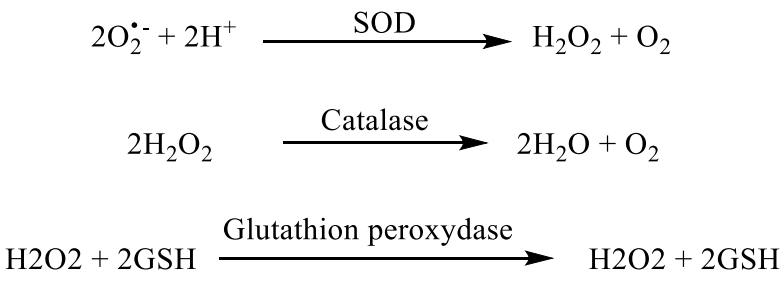

Figure II-3 Enzymatic reactions trapping reactive oxygenated species ROS

There are many other antioxidant enzymes such as peroxyredoxins, heme oxygenase, glutathione transferase, thioredoxin reductases or thioredoxin peroxidases. Most of these enzymes, as well as the oxidative damage repair enzymes, will use a reducing equivalent donor, NADPH, which, along with glutathione, forms the hubs of antioxidant defense [156].

II.6.2. Non-enzymatic antioxidants

This group of antioxidants is made up of several compounds capable of reacting directly or indirectly with ROS. The indirect mechanism involves the chelation of transition metals which prevents the production of the highly toxic hydroxyl radical [157].

Certain antioxidant compounds such as vitamins E (tocopherol), C (ascorbic acid), Q (ubiquinone), or carotenoids provided by food, act by scavenging radicals and capturing the single electron, transforming them into stable molecules or ions. The trapping vitamin will become a radical, then will either be destroyed or regenerated by another system. Thus, vitamin E is regenerated by vitamin C which is itself regenerated by enzymes, ascorbate reductases. This type of antioxidant is called a scavenger for the Anglo-Saxons. Many food compounds can also have this behavior: polyphenols, alkaloids…. There are also endogenous compounds synthesized by cells and playing the same role; the most important is reduced glutathione which protects not only against oxygen radicals, but also against peroxides or $NO^{\bullet}$ [156, 158].

II.6.3. Antioxidants of plant origin

Carotenoids and polyphenols constitute large families of compounds (several hundred) including β-carotene, caffeic acid and quercetin. Carotenoids and polyphenols are generally good scavengers of hydroxyl $HO^{\bullet}$ and peroxyl $RO_2^{\bullet}$ radicals. They are therefore capable of inhibiting the lipid peroxidation chains, but in a less efficient manner than that of α-tocopherol. In addition, carotenoids have a specific role of capturing oxygen in gulet 1O2, which allows them to exercise protection against damage induced by the ultraviolet rays of sunlight [141].

II.6.4. Synthetic antioxidants

These are butylhydroxytoluene (BHT), butylhydroxyanisole (BHA) and gallic acid esters: propyl gallate, doctyl gallate, and dodecyl. BHT is a highly effective and inexpensive chain breaking antioxidant. BHA is a mixture of two positional isomers whose efficiency is somewhat lower than that of BHT.

There are other little used synthetic antioxidants such as tertiobutylhydroquinone (TBHQ) used for the preservation of crude oils, nordihydrogualaretic acid (NDGA), the latter is used in products for topical use and 4-hydroxymethyl 2,6-ditertiobutylphenol or Ionox 100, whose antioxidant properties are similar to those of BHT (Figure II-4) [159].

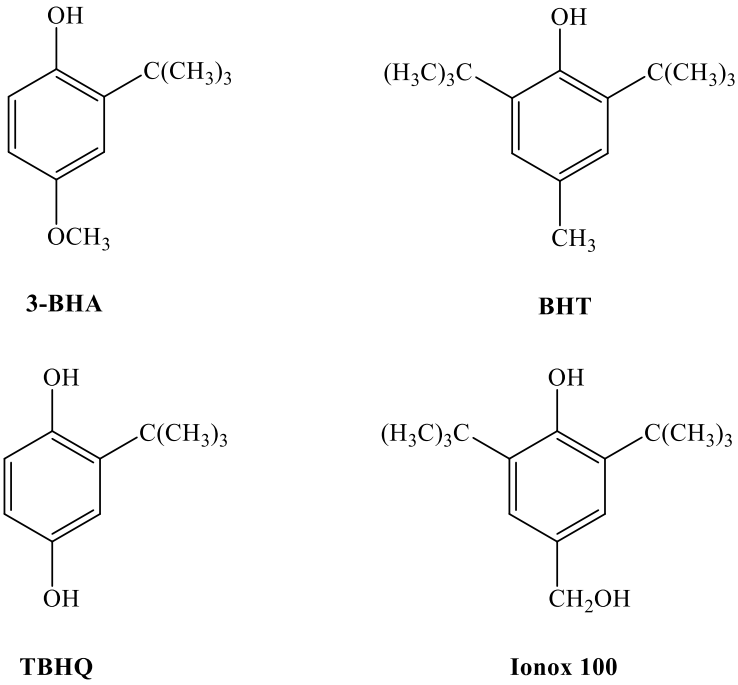

Figure II-4 Chemical structure of some synthetic antioxidants.

II.7. In vitro evaluation of antioxidant activity

Currently, a wide variety of analytical methods for determining antioxidant capacity are available. These analyzes differ from each other in terms of reaction mechanisms, oxidants and target species (probes), reaction states and the form in which the results are expressed. In addition, even when only one of these analyzes is considered, it generates other parameters to be taken into consideration such as: the solvent, the reaction time and the pH [160].

A battery of assays measuring different aspects of antioxidant behavior is recommended to produce a complete antioxidant profile. Comparing data from different studies is difficult. It is also

of great importance to choose accepted, validated and standardized methods, with data both comparable and available in the literature.

The design of such methods is based on the use of oxidizing species and probes (proteins, triacylglycerols, and cell models) with the appropriate biological significance that the reaction conditions (concentration, reaction time, pH…), closely related to which can be in vivo [160].

II.7.1. Stable radical scavenging methods and evaluation of their reduction capacity

II.7.1.1. Trapping of the 2.2-diphenyl-1-picrylhydrazyl (DPPH•) radical

In this analysis, the purple-colored DPPH• is reduced by the so-called antioxidant molecules to pale yellow hydrazine, Figure II-5. The trapping capacity is generally assessed in organic media by monitoring the decrease in absorbance at 515-528 nm until the absorbance remains constant [161].

The determination of the antioxidant capacity is based on the amperometric reduction of DPPH• to glassy carbon. The current which results from it on a glassy carbon electrode polarized at the fixed potential, is proportional to the residual concentration of DPPH• after the reaction with the antioxidants [162].

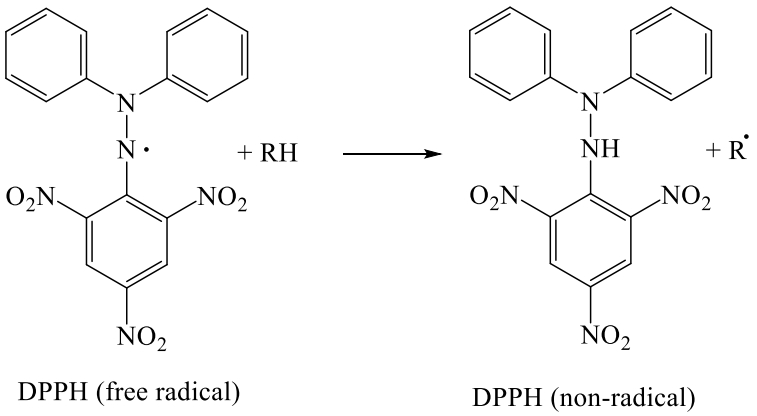

Figure II-5 Reaction of DPPH with an antioxidant

In opposition to what has always been believed, the reaction mechanism is based on an electron transfer reaction, while hydrogen atom abstraction is a marginal reaction process, because it occurs slowly in strong solvents, such as methanol and ethanol [163].

The steric accessibility of DPPH• is a determining cause of the reaction, since the small molecules which have better access to the site of the radical probably have a relatively higher antioxidant capacity [164]. Many high molecular size antioxidant compounds that react quickly

with radicals may react slowly or may even be inert in this assay. The lack of DPPH• or similar radicals in biological systems is also a weak point.

II.7.1.2. Antioxidant iron reduction power (FRAP analysis)

FRAP analysis measures the ability of antioxidants to bring back the ferric complex of tripyridyl-s-triazine 2.4.6 $[Fe(III)-(TPTZ)_2]^{3+}$ intensely to the blue-stained ferrous complex $[Fe(II)-(TPTZ)_2]^{2+}$ in an acidic medium [165]. The values are calculated by measuring the increase in absorbance at 593 nm and relating it to a standard solution of ferrous ions or a standard solution of antioxidants [166].

One point to be aware of is the concomitant production of Fe(II), which is a well-known prooxidant, and can result in the generation of additional radicals in the reaction medium. In addition, compounds which absorb at the same wavelength can mix with it, leading to overestimation of the results [167].

II.7.1.3. Analysis by the Folin-Ciocalteu (FC) reagent

The chemistry behind FC analysis is based on the transfer of electrons into an alkaline medium from phenolic compounds and all other molybdenum reducing species, forming blue complexes that can be detected spectrophotometrically at 750-765 nm [168].

Therefore, it is only recently that FC analysis has been proposed to measure the total reducing capacity of samples [164]. Excellent linear correlations between FC analysis with other analyzes (TEAC and DPPH•, for example) have been established [169].

II.7.2. Oxygen free radical scavenging methods

II.7.2.1. Peroxyl radical trapping (ROO•)

The ORAC (Oxygen-Radical Absorbance Capacity) measurement developed by Cao et al. [170] is a simple and reproducible method for assessing the antioxidant capacity of different molecules [171]. B-PE (Porphyridium cruentum β Phycoerythrin) is a fluorescent protein extremely sensitive to oxidative stress. In the presence of AAPH [(2,2'-azobis(2-amidinopropane) dichloride], a donor of the peroxyl radical, the tetrameric structure of β-PE is modified, it dimerizes. This dimerization depends on the concentration of radicals peroxyls of the reaction medium can be followed by measuring the decrease in fluorescence of β-PE as a function of time. This kinetics of decrease in fluorescence is directly related to the concentration of free radicals

present in the reaction volume under these defined conditions of time and concentrations of β-PE is from AAPH.

II.7.2.2. Superoxide radical trapping ($O_2^{\bullet -}$)

This test evaluates the ability of a product to capture a free radical, the superoxide anion $O_2^{\bullet -}$ This radical is generated in vitro by the hypoxanthine / xanthine oxidase system. In this method, the radical reduces the yellow-colored NBT2+ (Nitro-Blue Tetrazolium) to purple-colored formazan blue which absorbs at 560 nm.

Thus an antioxidant compound capable of capturing the superoxide anion will prevent the formation of formazan blue and the solution will remain yellow. The absorbances obtained make it possible to calculate a percentage inhibition of the reduction of NBT2+ compared to a control consisting of the reaction medium devoid of antioxidant compound. it can be then drawn a curve representing the logarithm of the percentage inhibition as a function of the concentration of test compound, and determine the IC50 (concentration inhibiting 50% of the activity) of the compound [172].

II.7.2.3. Trapping of hydrogen peroxide (H_2O_2 scavenging activity)

One of the most common methods to assess the scavenging capacity of hydrogen peroxide is based on the absorption of this molecule in the UV domain. As the concentration of H_2O_2 decreases by the scavenging compounds, the absorbance value of the latter at 230 nm also decreases. However, it is quite normal for samples to absorb at this wavelength as well, thus requiring a blank measurement to be performed [160].

II.7.2.4. Analysis of the scavenging capacity of the hydroxyl radical ($HO^{\bullet}$)

Due to the high reactivity of hydroxyl radicals, almost all molecules in biological systems can be considered as $HO^{\bullet}$ radical scavengers. Thus, evaluation of direct $HO^{\bullet}$ entrapment may be irrelevant for evaluating the antioxidant action of a compound, simply because very high concentrations of the scavenger are required to compete with adjacent molecules in vivo.

Several in vitro methodologies for the determination of the trapping capacity of $HO^{\bullet}$ are available in the literature, mostly based on the set Fe^{3+} + EDTA + H_2O_2 + ascorbic acid system, to produce a constant flux of $HO^{\bullet}$. These radicals attack deoxyribose at position 2 (used as a target), degrading it into a series of fragments, some react on heating with thiobarbituric acid at low pH to

give a pink chromogen [173]. If an antioxidant is added to the reaction mixture, it will compete with deoxyribose for the HO• radical, thus preventing degradation of target species [174].

CHAPTER III

THEORETICAL BACKGROUND OF EXPERMINTAL AND COMPUTETIONAL METHODS

III.1. Introduction

The electrochemistry method is one of the most popular technics for the characterization of new compounds. The basic thermodynamic quantity that is assigned to an electrode process is the standard or formal reduction potential (E_o or E_f) [175]. Electrochemistry is also an important method for demonstrating reactions involving transfers of electrons [176]. it relates electrons transfer to chemical changes. The redox potentials of an antioxidant could be determined by cyclic voltammetry which considered to be good measures of their antioxidant capacities.

The use of mathematical and theoretical methods to the solution of chemical concerns is described as computational chemistry. Molecular modeling, a subset of computational chemistry, focuses on predicting the behavior of individual molecules within a chemical system. The most precise molecular models use ab initio or “first principles” electronic structure methods, based on the principles of quantum mechanics, and are generally very computer intensive. Molecular modeling, on the other hand, has been a quickly changing and developing area due to increases in computer storage capacity and processor capability, to the point that it is now possible to solve relevant problems within a short period of time [177].

These methods are needed in this study. thus, in this chapter, some basic and important concepts will be discussed in order to make all these methods a bit familiar and clear to the reader.

III.2. Cyclic Voltammetry (CV)

Cyclic voltammetry is one of the analytical methods that make it possible to specify the conditions under which an oxidation and reduction reaction can be carried out electrochemically and possibly to establish the mechanism.

The general principle of voltammetry is therefore to obtain a response (the current) of the system under study to the excitation (the potential) responsible for the desired electrochemical reaction. This operation is carried out by carrying out an exploration by imposition and progressive variation of the electrode potential (potential sweep). Analysis of the resulting figure (response I as a function of E) provides information on the properties that determine its shape.

Knowledge of the fundamental characteristics of electrochemical reactions is obtained experimentally, by determining figures which express the relationship between current and electrode potential. These figures are called voltammograms, their determination is the object of voltammetry.

Its most frequent use consists in carrying out two linear scans, the first called “outward” and the second called “backward” in the opposite direction so as to return to the starting potential, after having therefore carried out a cycle. In this case, the method is called "cyclic voltammetry", which is its standard name. Voltammetry only reaches its true power when it is practiced back and forth. It is cyclic voltammetry, the principle of which is to perform a linear potential sweep from an initial potential E_i, given by Equation III-1:

$$E = E_i \pm \nu t \qquad \textit{Equation III-1}$$

where ν: the sweep speed, the sign + corresponds to a sweep towards positive potentials, the sign – to a sweep towards negative potentials.

The evolution of the current I(t) which crosses the electrochemical system during voltammetry, represented on a graph as a function of the value of E(t), bears the name of voltammogram or also polarization curve. In the case of cyclic voltammetry, the direction of the scan is indicated by arrows. Figure III-1 represents the general shape of a voltammogram I = f(E).

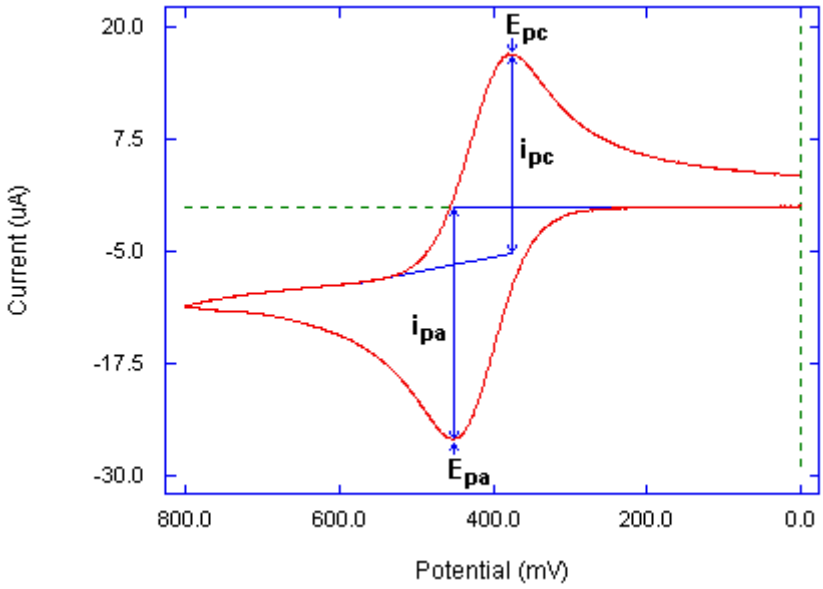

Figure III-1 General appearance of a cyclic voltammogram.

The characteristic quantities of a voltammogram are:

Ip_c, Ip_a: cathode and anode peak current, Ep_c, Epa: cathode and anode peak potential,
$Ep_{c/2}$, $Ep_{a/2}$: potential at mid-height of the cathode and anode peaks, ΔEp; potential difference between Ep_c and Ep_a.

III.2.1. Mathematical expressions of peak currents and potentials in a charge transfer

The mathematical expressions for peak current and potential were originally developed for a forward sweep (linear voltammetry) by Randals et al. [178] for fast systems, and by Delahay [179] for slow systems. This theory is extended by Matsuda et al. [180] to semi-rapid systems. The work of Nickolson et al. [181] have allowed the development of the relations describing the experimental curves of cyclic scans.

In the case of a rapid charge transfer, electrochemical parametres are linked to each other as shown in equations Equation III-2 to Equation III-6:

$$Ox + ne^- \Leftrightarrow Red \qquad \textit{Equation III-2}$$

$$I_p = 0.269An^{3/2}D_R^{1/2}C_R V^{1/2} \quad (mA) \qquad \textit{Equation III-3}$$

$$E_p = E_{p_{1/2}} + \frac{0.029}{n} \quad (mV) \qquad \textit{Equation III-4}$$

$$E_{p_a} - E_{p_c} = \frac{0.059}{n} \quad (V) \qquad \textit{Equation III-5}$$

$$\frac{I_{p_a}}{I_{p_c}} = 1 \qquad \textit{Equation III-6}$$

In the case of a semi-rapid charge transfer, the pic current denity is given by the following Equation III-7:

$$I_p = 0.269An^{3/2}D_R^{1/2}C_R K_s V^{1/2} \qquad \textit{Equation III-7}$$

In the case of a slow (irreversible) charge transfer, the current is described by Equation III-8:

$$I_p = 0.269An(\alpha n)^{1/2}D_R^{1/2}C_R V^{1/2} \qquad \textit{Equation III-8}$$

Ks: Speed constant, α: Transfer coefficient, D_R: Diffusion coefficient (cm²/s), C_R: Concentration, V: Scanning speed (V/s), A: Electrode surface (cm²), and n: Number of electrons.

III.2.2. Criteria for analysis and discrimination of the deferent systems

The study of the variations of the current and the potential according to the scanning speed ($Ip = f(v^{1/2})$ and $Ep = f(\log v)$) can inform us about the nature of the limiting stage of the current measured on the electrode mechanism.

- If $Ip = f(v^{1/2})$ is a straight line; the reaction is governed by pure diffusion.

- If Ip = f($v^{1/2}$) is a concavity curve turned towards the axis of the currents; the process at the electrode involves charge transfer accompanied by adsorption; and in the case where the concavity is turned green, the axis of the scanning speeds; the process at the electrode is associated with a chemical reaction.
- If Ep = f(logv) is a line:
    - zero slope; the reaction to the electrode is rapid.
    - with a slope other than zero and equal to -30 αn (mV); this is a slow charge transfer.
- If Ep = f(logv) is a curve and Ip = ($v^{1/2}$) is a line; we are dealing with semi - rapid processes.

In that case; note that for a process governed by diffusion; the peak current is proportional to the analytical concentration of the electroactive species.

III.3. Molecular modeling

Molecular modeling is a collection of computerized algorithms based on theoretical chemistry methodologies and experimental data that may be used to evaluate molecules and molecular systems, as well as forecast molecular, chemical, and biological properties [182, 183]. It acts as a link between theory and practice in the following ways:

- Extract results for a particular model.
- Compare experimental results of the system.
- Compare theoretical predictions for the model.
- Help understanding and interpreting experimental observations.
- Correlate between microscopic details at atomic and molecular level and macroscopic properties.
- Provide information not available from real experiments.

III.3.1. Quantum calculation methods

III.3.1.1. Schrödinger equation

The geometric structure, the modes of vibration, the enthalpies of reaction as well as other observables derive from the electronic structure of the studied system. This electronic structure is deduced from the time-independent multi-electronic Schrödinger equation, given by Equation III-9 [184]:

$$\hat{H}\Psi = E\Psi \qquad \textit{Equation III-9}$$

Where $\hat{H}$ is the Hamiltonian operator, Ψ is the wave function of the system and E is its energy. The total energy E is calculated by applying the time-independent molecular Hamiltonian to the orthogonal wave function Ψ. The Hamiltonian is written in terms of operators of kinetic and potential energies of electrons and nuclei as follows (Equation III-10):

$$\hat{H} = \hat{T}_e + \hat{T}_N + \hat{V}_{Ne} + \hat{V}_{ee} + \hat{V}_{NN} \qquad \textit{Equation III-10}$$

Where:

$\hat{T}_e$ is the operator of the kinetic energy of electrons, given by Equation III-11:

$$\hat{T}_e = -\frac{1}{2}\sum_{i=1}^{n} \nabla_i^2 \qquad \textit{Equation III-11}$$

$\hat{T}_N$ is the operator of the kinetic energy of nuclei (Equation III-12):

$$\hat{T}_N = -\frac{1}{2}\sum_{k=1}^{N} \frac{\nabla_k^2}{M_k} \qquad \textit{Equation III-12}$$

$\hat{V}_{Ne}$ is the operator of the coulombic potential energy of attraction between electrons and nuclei, given by the following Equation III-13:

$$\hat{V}_{Ne} = -\sum_{i=1}^{n}\sum_{k=1}^{N} \frac{Z_k}{d_{ik}} \qquad \textit{Equation III-13}$$

$\hat{V}_{ee}$ donate the coulomb repulsion energy between electrons (Equation III-14):

$$\hat{V}_{ee} = \sum_{i}\sum_{j>i} \frac{1}{r_{ij}} \qquad \textit{Equation III-14}$$

$\hat{V}_{NN}$ represents the Coulomb repulsion energy between nuclei (Equation III-15):

$$\hat{V}_{NN} = \sum_{k=1}^{N}\sum_{l>1}^{N} \frac{Z_k Z_l}{R_{kl}} \qquad \textit{Equation III-15}$$

Where the Hamiltonian terms are in atomic units ($m_e = 1, \hbar = 1, 4\pi\varepsilon_0 = 1$). ∇^2 is the Laplacian operator. m_e and M_k are the masses of the electron and the nucleus respectively. d_{ik} represents the distance between the electron i of coordinate r_i and the nucleus k of charge Z_k

and coordinate R_k. r_{ij} represents the distance between electrons i and j. R_{kl} is the distance between the nuclei k and l of respective charges Z_k and Z_l. Under the apparent simplicity of its formulation hides in fact several insoluble problems which have led to approximations and original resolution methods. We will detail some of them in the following paragraphs, in particular those we have used, from the density functional theory.

III.3.1.2. Born-Oppenheimer approximations

The Born-Oppenheimer approximation [185] is based on the separation of the movements of electrons and nuclei because electrons move much faster than nuclei due to the large mass difference between them ($\frac{m_e}{m_N} = \frac{1}{1836}$). We can thus imagine an image such that the electrons revolve around the fixed nuclei. This leads us to solve the problem of the movements of electrons in the field of supposedly fixed nuclei. This approximation simplifies the Schrödinger equation by decoupling the motions of nuclei from those of electrons. Here electronic and nuclear movements will be studied separately. The wave function Ψ describes the system and takes as variables the positions of electrons $\vec{r}$ and nuclei $\vec{R}$. It can be decomposed as a linear combination of products of electronic and nuclear orthonormal wave functions:

$$\Psi(r,R) = \sum_{i=1}^{N} \Psi_{ei}(r,R)\Psi_{Ni}(R) \qquad \textit{Equation III-16}$$

i being the index of the considered electron.

In the framework of the Born-Oppenheimer approximation, the Hamiltonian $\hat{H}$ will be decomposed into two terms: a purely electronic Hamiltonian $\hat{H}_e$ and a nuclear Hamiltonian $\hat{H}_N$.

The electronic Hamiltonian is written acoroding to Equation III-17:

$$\hat{H}_e = \hat{T}_e(r) + \hat{V}_{Ne}(R,r) + \hat{V}_{ee}(r) \qquad \textit{Equation III-17}$$

And the purely electronic Schrödinger equation then becomes as given by Equation III-18:

$$\hat{H}_e\Psi_e(r,R) = E_e(R)\Psi_e(r,R) \qquad \textit{Equation III-18}$$

In the electron wave function $\Psi_e(r,R)$ the nuclear coordinates R act as parameters for the electron wave function.

The nuclear Schrödinger equation is given by Equation III-19

$$\hat{H}_N \Psi_N(R) = E_N(R) \Psi_N(R) \qquad \textit{Equation III-19}$$

Where $\Psi_N(R)$ is the nuclear wave function that does not depend on the electronic coordinates r.

$\hat{H}_N$ is the nuclear Hamiltonian which is written as indicated in Equation III-20:

$$\hat{H}_N = \hat{T}_N(r) + \hat{V}_{NN}(R, r) + E_e(R) \qquad \textit{Equation III-20}$$

Nuclear energy E_N (Equation III-19), corresponds to the total energy E_T within the framework of the Born-Oppenheimer approximation and represents the electronic and nuclear energy of a given system. The Born-Oppenheimer approximation applies when electronic and nuclear Hamiltonians are separable. In other words, when nuclear motion does not cause electronic states to change.

III.3.1.3. Hartree-Fock method (HF)

One of the main electronic structure methods is the Hartree Fock (HF) method, which was developed in the 1920s after the discovery of the Schrödinger equation. The Hartree-Fock (HF) method [186, 187] is a variational method. It makes it possible to determine the orbitals and the associated energies of an atom or a molecule, taking into account in an average way the electrostatic interactions between the electrons [188, 189].

Hartree-Fock approach is based on the independent electron model approximation. We can separate the variables by assuming that each electron moves in the mean field of the other electrons. The polyelectronic wave function Ψ_e is described as a product of all the so-called spin-orbital monoelectronic functions ϕ_i. The spin-orbitals ϕ_i are written as a product of a space function φ_i relating to electron i and a spin function σ_s.

$$\phi_i = \varphi_i \sigma_s \qquad \textit{Equation III-21}$$

The function σ_s can be an α or β function depending on the nature of the electron's spin $\left(-\frac{1}{2} ou + \frac{1}{2}\right)$.

The associated electronic wave function is then written as follows:

$$\Psi_e = \phi_1(1)\phi_2(2) \dots\dots\dots \phi_n(n) \qquad \textit{Equation III-22}$$

The Pauli principle [190] is not respected by the wave function Ψ_e (Equation III-22) in this form, because it is not antisymmetric with respect to a permutation of 2 electrons. In order to satisfy the Pauli principle, the zero-order electronic wave function for an n-electron system is written as a Slater determinant defined as follows, Equation III-23:

$$\Psi_e = \frac{1}{\sqrt{n!}}\begin{bmatrix}\phi_1(1) & \cdots & \phi_n(1)\\ \vdots & \ddots & \vdots \\ \phi_1(n) & \cdots & \phi_n(n)\end{bmatrix} \qquad \textit{Equation III-23}$$

Thus, the exchange of two electrons corresponding to the permutation of two rows (or two columns) has the effect of changing the sign of the determinant on the one hand and on the other hand, the spin-orbitals must be different from each other. to have a non-zero determinant.

Electronic Hartree-Fock (HF) energy is written in the following form (Equation III-24):

$$E_e = \frac{\langle \Psi_e | H_e | \Psi_e \rangle}{\langle \Psi_e | \Psi_e \rangle} \qquad \textit{Equation III-24}$$

The operator H_e can be written as a sum of mono-electronic and bi-electronic operators:

$$H_e = \sum_{i=1}^{n} h_i + \sum_{i=1}^{n}\sum_{j>1}^{n} \frac{1}{r_{ij}} \qquad \textit{Equation III-25}$$

Where h_i is the mono-electronic operator who uses the single electron i. It is defined as follows:

$$h_i = \frac{1}{2}\nabla_i^2 - \sum_{k=1}^{N} \frac{Z_k}{d_{ik}} \qquad \textit{Equation III-26}$$

The bi-electronic term $\frac{1}{r_{ij}}$ cannot be solved exactly, because it causes the coupling of all the movements of the electrons. This term constitutes a difficulty. All methods of quantum chemistry differ in the way they take into account the term bi-electronics $\frac{1}{r_{ij}}$.

The Hartree-Fock method solves the problem of the bi-electronic term $\frac{1}{r_{ij}}$ by introducing the Fock monoelectronic operator F_i. It consists in writing the bielectronic contribution as a sum of monoelectronic operators. Each of the n monoelectronic operators represents the average influence of the electrostatic field of the n-1 electrons.

The monoelectronic operator of Fock F_i is defined according to the coulomb J_j and exchange K_j operators as follows:

$$F_i = h_i + \sum_j \left(J_j - K_j\right) \qquad \textit{Equation III-27}$$

We can express the total HF energy as a function of the mono and bi-electronic integrals:

$$E_{HF} = \sum_{i=1}^{n} \varepsilon_i + \sum_{j=1}^{n} \sum_{j>1}^{n} \left(J_{ij} - K_{ij}\right) + V_{NN} \qquad \textit{Equation III-28}$$

The term ε_i represents the energy of the spin-orbital ϕ_i.

The term J_{ij} represents the coulomb integral. It corresponds to the repulsion between the charge distributions of two electrons. It can be interpreted as a classic electrostatic repulsion. It is expressed in the following form:

$$J_{ij} = \left\langle \phi_i(i)\phi_j(j) \middle| \frac{1}{r_{12}} \middle| \phi_i(i)\phi_j(j) \right\rangle \qquad \textit{Equation III-29}$$

K_{ij} is the exchange integral. It has no physical meaning in the classical sense. It arises from the need to antisymmetrize the wave function. It is expressed in the following form:

$$K_{ij} = \left\langle \phi_i(i)\phi_j(j) \middle| \frac{1}{r_{12}} \middle| \phi_i(i)\phi_j(j) \right\rangle \qquad \textit{Equation III-30}$$

K_{ij} is the Coulomb repulsion energy of nuclei. It is introduced as a parameter.

The sign (-) comes from the antisymmetrization of the wave function Ψ_e by exchanging two electrons (to satisfy the Pauli exclusion principle). Its minimization with the constraint of orthonormalization of the set of spin-orbitals at $\langle \phi_i | \phi_j \rangle = \delta_{ij}$ leads to the so-called Hartree-Fock system of equations.

$$F_i|\phi_i\rangle = \varepsilon_i|\phi_i\rangle \qquad i = 1,2,3 \ldots \ldots n \qquad \textit{Equation III-31}$$

The Fock Operator F_i as well as the Coulomb Operator J_{ij} and the Exchange Operator K_{ij} issent operate on only one orbital. They are called monoelectronic operators. We see here that the operators J and K are expressed as a function of the solutions of Equation III-26. We are therefore in the presence of a set of n nonlinear monoelectronic equations that would have to be solved by

an iterative process. From a set of test orbitals ϕ_i, we compute the Fock operator to then deduce a new set of functions ϕ_i.

This procedure is called the "Self-Consistent Field Method" (SCF) because the iterations are continued until the electrostatic field felt by an electron (field caused by the other electrons in the other orbitals) remains. stationary. An exact solution of the HF equations, obtaining atomic orbitals, is possible for atoms comprising a nucleus and an electron. Further developments are nevertheless necessary to solve the Schrödinger equation for systems with several electrons. This requires the consideration of the LCAO [191] (Linear Combination of Atomic Orbitals) approximation which consists of developing molecular orbitals φ_i on a basis consisting of a set of atomic orbitals χ_u:

$$\varphi_i = \sum_{u=1}^{m} C_{iu}\chi_u \qquad i = 1,2,3, \dots \dots n$$

Equation III-32

With m being the number of base functions, C_{iu} designates the coefficients of the molecular orbitals assumed to be real and developed on the base functions. χ_u constitute the basic functions used in our calculations. If this base is complete, it means that the molecular orbitals φ_i are exact.

There are two types of HF methods the first one known as RHF (Restricted Hartree-Fock method) and the second is UHF (Unrestricted Hartree-Fock method).

III.3.1.4. Density Functional Theory (DFT)

Taking into account the electronic correlation requires the implementation of elaborate post-HF calculations. When the studied systems are very large, this becomes almost impossible. An alternative to all of these methods is the density functional theory. In addition, the precision of the results obtained as well as the computational performance of the DFT method currently make it an essential tool for the computation of molecular properties. It is based on two theorems established by Hohenberg and Kohn (1964) [192].

III.3.1.4.1. Hohenberg and Kohn theorems

The goal of DFT methods is to find a functional (that is to say a function dependent on a function) allowing to connect density with energy. The density functional theory is based on the postulate proposed by Thomas and Fermi [193, 194] that any electronic property of a system can be calculated from its electron density. Hohenberg and Kohn, in 1964, took up this theory and

demonstrated that there is a one-to-one correspondence between the energy of a system E and its electron density $\rho(\vec{r})$ [192]. The energy can therefore be calculated as a functional density:

$$E = F[\rho(\vec{r})] \qquad \textit{Equation III-33}$$

In a second theorem, Hohenberg and Kohn established the variational principle for energy, by showing that the electron density of the system in the ground state ρ_0 is that which minimizes the energy calculated thanks to this same functional, it is that is, $\left(\frac{\delta F}{\delta \rho}\right)_{\rho=\rho_0} = 0$. This theorem was subsequently generalized to the lowest energy state of a given symmetry, provided it was non-degenerate.

For a system made up of N nuclei and n electrons, the energy can therefore be written:

$$E = T[\rho] \int_{exp} v_{Ne}(\vec{r})\rho(\vec{r})d\vec{r} + J[\rho] + E_{XC}[\rho] \qquad \textit{Equation III-34}$$

Where:

$T[\rho]$ is the kinetic energy of the system;

$v_{Ne}(\vec{r})$ is the interaction energy of an electron with the N nuclei;

$J[\rho]$ is the bielectronic integral describing the Coulomb interaction between electrons, which is expressed simply as a function of the density $\rho(\vec{r})$;

$E_{XC}[\rho]$ is a non-classical integral, called "exchange and correlation energy", which has no known analytical expression. It ensures the exclusion of two electrons of the same spin (exchange part) and opposite spin (correlation part). The expression of this integral must therefore be approximated by physical models, which will be detailed later.

III.3.1.4.2. Theorem of Kohn and Sham

The methodology of Kohn and Sham [195] reduces to a system of monoelectronic equations, which can then be solved using the same algorithms as the Hartree-Fock method. It consists in imagining a system of electrons without interactions, which would have the same electron density $\rho(\vec{r})$ as the real system. In the case of a closed-layer system, the wave function of the system can then be constructed as the Slater determinant of n monoelectronic orbitals φ_i. The electron density of the system is then written:

$$\rho(\vec{r}) = \sum_i \varphi_i^*(\vec{r})\varphi_i(\vec{r})$$ *Equation III-35*

The kinetic energy of the fictitious system is:

$$T_s[\rho] = \sum_i \left\langle \varphi_i \left| \frac{\nabla^2}{2} \right| \varphi_i \right\rangle$$ *Equation III-36*

And the energy of the real system can be expressed as follows (Equation III-37).

$$E = T_s[\rho] = \int_{exp} v_{Ne}(\vec{r})\rho(\vec{r})d\vec{r} + J[\rho] + \tilde{E}_{XC}[\rho]$$ *Equation III-37*

where:

$$\tilde{E}_{XC}[\rho] = E_{XC}[\rho] + T_\rho[\rho] - T_S[\rho]$$ *Equation III-38*

Most often, the difference $T_\rho[\rho] - T_S[\rho]$ is negligible and $\tilde{E}_{XC}[\rho]$ can be equated with the energy of exchange and correlation $E_{XC}[\rho]$.

Using the variational principle, we then show that Equation III-37 can be transformed into a system of coupled equations whose unknowns are the monoelectronic orbitals φ_i:

$$f^{KS}[\rho]\varphi_i(\vec{r}) = \varepsilon_i\varphi_i(\vec{r})$$ *Equation III-39*

Since the Kohn-Sham operator f^{KS} is expressed as a function of the electron density ρ, which is itself calculated from the orbitals φ_i, these equations must be solved iteratively, like the Hartree equation- Fock. We therefore proceed in the same way by introducing atomic orbital bases. The resolution provides a set of monoelectronic orbitals called "Kohn Sham orbitals", from which we calculate the electron density of the system ($\vec{r}$), then the energy of the real system using Equation III-39. In the case of a system with open layers, the UDFT (unrestricted density functional theory) formalism makes it possible to apply the Kohn Sham method by defining the spin densities $\rho^\alpha(\vec{r}) = \rho^\beta(\vec{r})$. It is essential to remember that the Kohn-Sham monoelectronic orbitals are only mathematical intermediaries describing a fictitious system. However, they often have many similarities with orbitals obtained by Hartree-Fock or post-Hartree-Fock methods and as such are sometimes used for qualitative interpretations.

III.3.1.4.3. Successes and limitations of DFT

Several works have been carried out in recent years, using DFT calculations and giving good results on large chemical systems, taking into account the effects of electronic correlation. Many properties (molecular structures, vibration frequencies, ...) are well reproduced. However, the DFT method still suffers from several shortcomings, one of which is the lack of real criteria that allow functional and molecular properties to be improved [196, 197].

III.3.1.5. Time Dependent Density Functional Theory (TD-DFT)

Time Dependent Density Functional Theory (TD-DFT) is an approach that describes electronic excitations. Similar to Hohenberg and Kohn's first theorem of DFT, the Runge-Gross theorem [198] establishes a direct relationship between the time-dependent electron density and the time-dependent potential $v[\rho(r,t)]$; therefore the potential and the wave function will be density dependent. Recently van Leeuwen generalized the Runge-Gross theorem to molecular systems [199]. Likewise, the time dependent Kohn-Sham equations should be derived. Assuming that there is a time-dependent reference system without interaction with an external potential $v_s(r,t)$ whose electron density $\rho_s(r,t)$ is equal to the exact density of the real system with interaction $\rho(r,t)$.

$$\rho(r,t) = \rho_s(r,t) = \sum_i^N |\phi_i(r,t)|^2 \qquad \textit{Equation III-40}$$

If the external potential exists, we can deduce the time dependent equations of Kohn and Sham:

$$E[\rho(r),t] = T_s[\rho(r)] + \int v_{eff}[\rho(r,t)]\rho(r,t)dr \qquad \textit{Equation III-41}$$

$$v_{eff}[\rho(r,t)] = V_{ne}(r,t) + \int \frac{\rho(r',t)}{r-r'}dr' + \frac{\partial E_{XC}[\rho]}{\partial \rho(r,t)} \qquad \textit{Equation III-42}$$

Then just solve the time-dependent schrödiger equation:

$$\left[T_s + v_{eff}\right]\Psi_i(r,t) = i\frac{\partial \Psi_i(r,t)}{\partial t} \qquad \textit{Equation III-43}$$

The computation of excited states with TD-DFT is faster than ab initio methods. The theory of linear response is applied to the charge density of a molecule subjected to an electric field oscillating over time. The dynamic polarizability is obtained from the response of the dipole

moment, and the energies of excitations are then calculated as the poles and the forces of oscillators as the residues of this response, developed in the basis of the eigenstates of the operator Hamiltonian DFT. Wave functions are determined a posteriori for the excited states, in the form of linear combinations of simple excitations from the determinant Kohn Sham. This method is only true within the limit of an exact density functional. In practice, it is very sensitive to the misbehavior of the long-range exchange-correlation potential, where the density is most polarizable. As a result, the energies calculated for the excited charge transfer states can be severely affected. This method, suitable for large systems due to its low cost, is therefore not yet reliable in all cases, and should be used with caution.

III.3.1.6. Functional generations

III.3.1.6.1. Local density approximation (LDA and LSD)

In only one model case, that of the uniform gas of electrons (corresponding quite well to the electrons of the conduction band of a metal), we know the exact expressions or with an excellent approximation of the terms of exchange and correlation respectively. In this Local Density Approximation (LDA) [200], the electron density is assumed to be locally uniform and the exchange-correlation functional is of the form:

$$E_{XC}^{LDA}[\rho] = \int \rho(r)\varepsilon_{XC}\big(\rho(r)\big)dr$$ *Equation III-44*

Its extension to unrestricted systems takes the name LSD which means (Local Spin Density). the exchange-correlation functional distinguishes the density α and β in the form:

$$E_{XC}^{LSD}[\rho_\alpha, \rho_\beta] = \int \rho(r)\varepsilon_{XC}\left(\rho_\alpha(r), \rho_\beta(r)\right)dr$$ *Equation III-45*

The corresponding keywords in Gaussian are SVWN (exchange, Slater, correlation, Vosko, Wilk, Nusair) and SVWN5, these methods often provide quite good molecular properties (geometry. Frequencies) but generally lead to very bad energy data such as binding energies etc.

III.3.1.6.2. Hybrid Generalized Gradient Approximation (GGA) and Functional

To overcome the shortcomings of the LDA and LSD methods, the generalized gradient approximation considers exchange-correlation functions depending not only on the density at each point, but also on its gradient, of the general form:

$$E_{XC}^{GGA}[\rho_\alpha, \rho_\beta] = \int f(\rho_\alpha, \rho_\beta, \nabla\rho_\alpha, \nabla\rho_\beta) dv$$ *Equation III-46*

The exchange part is in general the Becke functional (B), the correlation part that of Lee, Yong and Parr (LYP) or that of Perdew-Wang (PW) with the variants 86 and 91, hence finally the keywords BLYP, BPW86 and BPW91.

Finally, it turned out that in the LDA methods, there was some good to take, that on the other hand, as we have seen, the HF method correctly handled the exchange energy.

Hence hybrid methods based on an empirical combination of these energies with energies with GGA. The most widely used is the "three-parameter Becke" method (B3); thus, the B3LYP functional [201-204] used the LYP functional for the GGA part. The parameters were adjusted to reproduce the values of the atomization energies. The GGA part can also be the functional PW91 and PW86.

III.3.1.7. Bases of atomic functions

The choice of the basis of orbitals is essential for quantum chemistry calculations. There are two basic types of functions mainly used in the calculations of electronic structures: Slater Type Orbitals (STO) and Gaussian Type Orbitals (GTO) [205].

III.3.1.7.1. Slater Type Orbitals (STO)

At the very beginning of quantum chemistry, Slater proposed the use of functions of the form:

$$X\zeta, n, l, m(r, \theta, \varphi) = NY_{l,m}(\theta, \varphi) r^{n-1} e^{\zeta, r}$$ *Equation III-47*

Where N is a normalization constant, and the functions $Y_{l,m}$ are of spherical harmonic type. The exponential dependence of the distance between the nucleus and the electrons is that of the orbitals of the hydrogen atom. Thus, a linear combination of several STOs makes it possible to correctly reproduce the true orbitals. Even if the dependence on r allows us to correctly write the behavior of orbitals when $r \to 0$, the computation of integrals with three or four centers (like bi-electronic integrals) is not analytically possible. Thus, these orbitals are generally only used for atomic and diatomic systems where high computational precision is required.

III.3.1.7.2. Gaussian Type Orbitals (GTO)

An alternative to Slater's orbitals is the use of Gaussians, which are written in the Cartesian coordinate system in the form:

$$X\zeta, l_x l_y l_z(x, y, z) = N x^{l_x} y^{l_y} z^{l_z} e^{-\alpha r^2}$$ *Equation III-48*

With $l_x l_y l_z$ determining the type of orbitals (for example, $l_x l_y l_z = 0$ represents an s-type orbital, $l_x l_y l_z = 1$ the p-type orbitals and $l_x l_y l_z = 2$ allows to obtain d and s type orbitals). The index α is called exponent. The center of the function usually coincides with the center of the nucleus.

The multiplication of two Gaussians results in a Gaussian. Thus, bi-electronic integrals are much easier to evaluate with Gaussians than with Slater functions. On the other hand, they have the drawback of not correctly describing the exact orbital in the vicinity of the nucleus ($r \to 0$), but also of decreasing too quickly as a function of r. Thus, the representation of molecular orbitals requires many more Gaussians than Slater functions (we roughly consider that three GTOs make it possible to model an STO). Despite this drawback, the ease of calculating bi-electronic integrals makes Gaussian functions the most widely used orbitals in quantum chemistry.

Gaussian bases have a fairly poor representation of atomic orbitals because they do not have the exact behavior at the origin (non-zero derivative) or at great distances (too fast decay with r) on the other hand their interest is that all the integrals involved in the calculations can be calculated explicitly without recourse to a numerical integration. To compensate for this incomplete representation of atomic orbitals by Gaussian functions, we use linear combinations of Gaussians as base functions. These functions are called contracted Gaussian functions. There are a multitude of possible Gaussian bases for performing an SCF calculation.

- The simpler base is STO-3G, also called minimal base. this means that Slater type orbitals are represented by three Gaussian functions.
- The next level includes split-valence bases such as 3-21G, 4-31G and 6-31G where the first number represents the number of Gaussians used to represent 1s orbitals. Valence orbitals are represented by two functions which are composed of the numbers of Gaussians given in the second part of the two numbers of the base denomination.

The base 6-31G will have six Gaussians for the 1s orbital. Three Gaussians for one function representing the 2s orbital and 1s Gaussian for the other function, and the 2p orbital will also have

three Gaussians for one of the functions and one Gaussian for the other. for greater flexibility, the polarization functions can be added.

III.3.1.7.3. Polarization functions

They correspond to unoccupied orbitals in the ground state atom. They will therefore be of type p, d for the hydrogen atom, and of type; d, f and g for the atoms of the second period. They must increase the flexibility of the base used and take into account the deformations of the atomic valence orbitals during the formation of the molecule. Their role in the base is decisive.

Thus, the introduction of polarization functions in the base is necessary for the determination of the geometry of particular molecules, such as for example the non-planar structure [206] of H_3O^+ or structures containing hypervalent atoms such as, for example, phosphates. Likewise, many properties could not be described correctly without the presence of polarization functions in the base: energy quantities such as inversion barriers, rotation barriers, electrical quantities, spectroscopic quantities. It exists in the literature [207, 208] many proposals for the values of the exponents of these polarization functions The presence of this type of functions in a base is generally indicated by the letter "P" except in the nomenclature of Pople where the FP are represented by an asterisk (*) if only the base of atoms other than hydrogen has FPs or two asterisks (**) if all the atoms are affected by this extension of the base. For example, using a 6-31G ** base for a molecular calculation means that the core electrons of atoms are described using a linear combination function of six Gaussians, the valence electrons by two functions, one linear combination of three Gaussians and the other consisting of a Gaussian, and that, moreover, there is a set of polarization functions on all the atoms of the molecule (p-type functions on hydrogen and functions of type d, or f or g on the other atoms depending on their nature).

III.3.1.7.4. Diffuse functions

Another type of function must necessarily expand the atomic base used whenever the physical phenomenon corresponding to the property studied requires a good description of the space located beyond the valence orbitals: these are the diffuse functions. These functions are generally uncontracted and have a low exponent which allows them to cover the diffuse space located a great distance from the nucleus. They have the same quantum number l as the valence orbitals of the atoms considered. Their role is decisive in the study of the properties of anionic species or of any phenomenon involving them, such as the determination of electron affinity, for example. They are also necessary for the treatment of molecules comprising strongly ionic bonds,

for the determination of spectroscopic quantities, for the study of excited valence states, atomic or molecular Rydberg states and also for the study of molecular interactions.

Several methods for determining the exponents of diffuse functions have been proposed, including minimizing the energy of anions, or by extrapolation using the property of exponents of functions of a given symmetry, which constitute a geometric progression [209]. It is commonly accepted that the exponent of a diffuse is generally four times smaller than the smallest exponent of a valence function.

In the nomenclature of Pople, a diffuse function is represented by the sign +. So, using a base 6-31+G** means that the core electrons are described using a linear combination of 6 Gaussians, the valence electrons using two functions, one linear combination of three Gaussians and the other made up of a single Gaussian; moreover, each atom carries a polarization function, the heavy atoms also carrying a diffuse function.

III.3.2. Molecular Mechanics (MM)

The expression "Molecular Mechanics" currently designates a method of calculation which allows, a priori, to obtain results of molecular geometries and energies based on classical mechanics. MM appeared in 1930 [210], but developed from the 1960s, when computers were more accessible and more efficient.

MM is based on the Born-Oppenheimer approximation that electrons are much faster than nuclei and nuclei are therefore implicitly processed. MM is an empirical method where atoms (nuclei) are represented by masses or spheres, and bonds by springs of different strengths. The values of these forces come from experimental data from vibrational spectroscopy, from X-ray diffraction data or from values obtained by ab-initio methods. By calculating all of these forces, according to the rules established for harmonic oscillators, we obtain molecular energy and determine the three-dimensional structure.

Today, MM is used to interpret NMR data. The main advantage of MM over other methods is the speed of calculations. This is due to a simplification of the force field equations; it is therefore possible to process very large molecular systems. On the other hand, this method does not take into account the molecular electronic structure. It is therefore impossible to study systems in which electronic effects are predominant. Thus, the validity of the results (results of the energies) depends only on the original parameterization of the constants internal to the force field.

In addition, the value of steric energy obtained in MM does not have any physical meaning in absolute terms; it is only the comparison between two values obtained for two different conformations that can be interpreted.

III.3.2.1. Interaction energy of bonded atoms

The bond stretching, bending and torsion interactions are called bonded interactions because the atoms involved must be directly bonded or bonded to a common atom. The Van der Waals and electrostatic (qq) interactions are between non-bonded atoms.

The total steric energy of a molecule can be written as a sum of the energies of the interactions:

$$E_{steric\ energy} = E_{str} + E_{bend} + E_{tor} + E_{VdW} + E_{qq} \qquad \textit{Equation III-49}$$

III.3.2.1.1. Stretching energy

Defines the energy brought into play by the variations in the length r of the links after extension and compression from their equilibrium values.

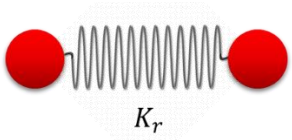

Figure III-2 Stretching between two atoms

$$E_{str} = \sum_{bonds} K_r(r - r_{eq}) \qquad \textit{Equation III-50}$$

r_{eq}: bond length at equilibrium;

k_r: force constant.

III.3.2.1.2. Bending energy

Defines the energy involved in the variations of angle θ between two contiguous bonds, around an equilibrium value θ_0.

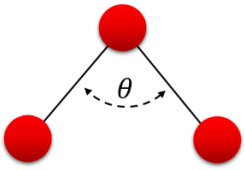

Figure III-3 Bending of valence angles

$$E_{Bend} = \sum_{bonds} K_\theta(\theta - \theta_{eq})$$ *Equation III-51*

θ_{eq}: angle at equilibrium;

k_θ: force constant.

III.3.2.1.3. Torsional energy

Defines the energy involved in rotating part of a molecule around a bond.

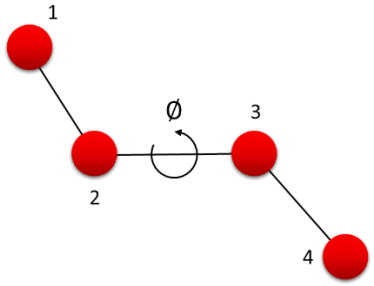

Figure III-4 dihedral angle formed by atoms 1-2-3-4

$$E_{tor} = \sum_{bonds} K_\emptyset(1 + \cos n\,\emptyset)$$ *Equation III-52*

k_φ: force constant;

n: periodicity (n = 1, 2, 3, 4, 6).

III.3.2.1.4. Van der Waals Energy

The Van der Waals energy function, reflects the attraction and repulsion between two atoms that make up a dipole.

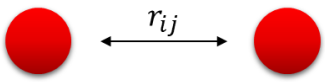

Figure III-5 Van der Waals interaction between two atoms

$$E_{VdW} = \sum_{i>j} \frac{A_{ij}}{R_{ij}^{12}} - \frac{B_{ij}}{R_{ij}^{6}}$$ *Equation III-53*

A_{ij}, B_{ij}: parameters depending on the nature of atoms i and j, distant from r_{ij}.

III.3.2.1.5. Energy of electrostatic interactions

The energy of electrostatic interactions, is written in the form of a Coulomb potential between atoms considered to carry a net charge.

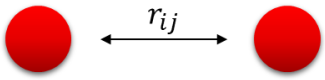

Figure III-6 electrostatic interactions

$$E_{qq} = \sum_{i>j} \frac{q_i q_j}{\varepsilon_{ij} r_{ij}}$$

Equation III-54

qi, qj: partial charges of atoms i and j, distant from r_{ij};

ε_{ij}: dielectric constant accounting for the attenuation of the electrostatic interaction by the environment (solvent or molecule itself).

III.3.2.2. Force field in molecular mechanics

A force field consists of a set of potential energy functions ("analytical energy function") associated with a series of numerical parameters, obtained experimentally (IR, microwave ...) or evaluated theoretically. It is therefore a multidimensional potential energy. that is, a sum of binding and non-binding contributions to N-bodies [211].

- For a single molecule, we can count several thousand of these individual contributions.
- The development of a new force or parameter field (parameterization), remains a major challenge for complex chemical functions, i.e., conjugated ketone, phosphonate, sulfate ...etc.
- In addition, compatibility from one force field system to another is often not possible.
- The performance of a force field can be related to certain parameters.

III.3.2.2.1. The different fields of force and their fields of application

It is difficult to define a universal force field that would be suitable for the study of small organic molecules as well as for the study of large proteins via organometallic compounds. Several force fields have therefore been developed in order to study these different classes of molecules. Here is a non-exhaustive list [212]:

- AMBER: (Assisted Model Building with Energy Refinement) Force field for proteins and nucleic acids

- CHARMM: (Chemistry at HARvard Molecular Mechanics) Force field for proteins, nucleic acids and lipids.
- MM2, MM3: Generalist force field (small molecules) by N. L. Allinger [213, 214]. This force field makes it possible to treat certain effects due to the system pi.
- MM3PRO: Version of MM3 whose parameters are suitable for the study of proteins.
- OPLS: (Optimised Potentials for Liquid Simulations) Force field for proteins as well as for certain classes of organic molecules. This force field is of the "united-atom" type. that hydrogen atoms are included in the atom that carries them, for example one type of atom would represent a $–CH_3$.

III.3.2.2.1.1. Parametrization

III.3.2.2.1.1.1. Reference parameters

The energy functions described below contain many parameters (K_φ, K_θ, dipole moments, rotational barriers, etc.) which are generally adjusted from experimental data deduced from the analysis of model compounds (spectroscopy vibrational, crystallography, thermodynamics, etc ...) or in some cases deduced from quantum mechanical calculations. These parameters are optimized so that the calculated properties (geometries, energies, heats of formation, etc.) come as close as possible to the experimental properties of the model compounds in the database.

III.3.2.2.1.1.2. Substitution parameters

The databases of the different force fields are generally very limited. The absence of reference parameters in particular for heterocyclic systems requires a choice of substitution parameters or ad hoc parameters.

III.3.3. Semi-Empirical methods

A semi-empirical method is a method in which part of the calculations necessary for Hartree-Fock calculations are replaced by parameters adjusted to experimental values (the Hamiltonian is always a parameter by comparison with reference compounds). In general, all these methods are very precise for the families of given products close to those used for parameterization (MNDO, ZDO, CNDO, NNDO…etc) [215].

- MNDO method [216] (Modified Neglect of Diatomic Overlap) which takes in account the repellencies between the electron's pairs and the electron-electron repellence directions;
- ZDO method (zero differential overlap) is based on the Huckel method for the π electrons;

- CNDO method (Complete Neglect of Differential Overlap) which takes in account only the atomic orbital of spherical symmetry and assesses the repellence integrals as the orbital would be sphere. In this case are two methods CNDO/1 and CNDO/2 which are used for the spectrum parameters;
- INDO method [217] (Intermediate Neglect of Differential Overlap) which includes the monoelectronic repellence integrals between atomic orbital of the same atom;
- NDDO method (Neglect of Differential diatomic overlap) which takes in account the orientation direction of the orbital;
- MINDO/3 [218] method is an particular case of the NNDO method which assesses the monoelectronic repellence integrals;
- SAM1 (Semi-Ab-Initio Model 1) [219] In SAM1, two-electron integrals are calculated using a standard STO-3G basis set (and hence the appearance of ab initio in the title). The resulting integrals were then scaled, and the Gaussian terms in the core–core repulsions were retained in order to fine-tune the calculations;
- AM1 (Austin Model 1) Next came Austin model 1 (AM1), due to M. J. S. Dewaret and his collaborators [220]. AM1 was designed to eliminate the problems from MNDO caused by a tendency to overestimate repulsions between atoms separated by the sum of their Van der Waals radii. The strategy adopted was to modify the core–core terms by multiplication of the Coulomb term with sums of Gaussian functions. In the original AM1 paper there are four terms in the Gaussian expansion. Each Gaussian is characterized by its position along the A–B vector and by its width. This significantly increased the number of parameters for each atom. The performances of the semiempirical method consist in the smaller cost of them and it their speed, but also in the fact they can determine some properties that cannot be established experimentally;
- PM3 (parameterized method 3) is the third parameterization of MNDO which contains essentially all the same terms as AM1. The parameters for PM3 were derived by J. J. P. Stewart [221] in a more systematic way than for AM1, many of which were derived by ‘chemical intuition’. As a consequence, some of the parameters are quite different from those of MNDO but the two models seem to predict physical properties to the same degree of accuracy.

III.3.4. Types of calculations

Computational chemistry (also called molecular modelling; the two terms are the same) is a set of techniques for investigating chemical problems on a computer. Questions commonly investigated computationally are:

III.3.4.1. Molecular geometry

The three-dimensional arrangement of the atoms that form a molecule is known as molecular geometry. It covers the molecule's overall form, as well as bond lengths, bond angles, torsional angles, and any other geometrical characteristics that govern each atom's position.

III.3.4.2. Geometry Optimization

Geometry Optimization is a standard computational chemistry calculation to find the lowest energy or most relaxed conformation for a molecule. The approach is the same for all levels of calculation, involving an iterative “jiggling” process like that described for molecular mechanics.

At each step, the molecular geometry is slightly changed and the energy of the molecule is compared to the last cycle. The computer shifts the molecule a bit, calculates the energy, shifts it a bit more, and continues until it finds the lowest energy. This is the minimum energy of the molecule and is obtained with the optimized geometry. Recall that the energies from molecular mechanics can only be used in a relative sense, while those from quantum electronic structure methods can be compared in an absolute sense, such as the heats of formation [222].

III.3.4.3. Single point calculations

Single point calculations are often used in combination with a geometry optimization to investigate steric hindrance. In this case the method only performs one computational cycle to calculate the energy of a particular fixed geometry. In a thermodynamically controlled reaction, the energetic difference between two conformations is often due to steric hindrance. If the product molecule optimizes in one conformation, you can use single point calculations to determine how much more energy is needed to form the non-preferred conformation.

The structure drawing and manipulation part of the software will allow you to move only that part of the molecule that changes in the higher energy form, leaving the rest of the molecule optimized.

The single point calculation performed on this modified molecule will give an energy that you can directly compare with the optimized energy to find the energy difference between the lower and higher energy conformers. For example, the energetic difference between having a constituent in the axial or equitorial position on a cyclohexane ring can be determined [222].

III.3.4.4. Transition state calculations

Transition state calculations can be thought of as the reverse of geometry optimizations. In this case, the method searches for a structure of maximum energy, a transient intermediate which cannot be isolated experimentally. For example, this type of calculation allows one to examine transition state energies and geometries of intermediates involved in carbocation rearrangements.

The literature contains standard models that should use as the starting point for these calculations. It takes an amount of effort and experience to properly analyze transition state structures and energies [222].

III.3.4.5. Electronic density and spin calculations

Electronic density and spin calculations allow visualization of electronic properties such as electron densities, electrostatic potentials, spin densities and the shapes and signs of molecular orbitals. The values for a particular property at each point in the 3-dimensional space around a molecule are displayed on the 2-dimensional computer screen as a surface of constant numerical value, often called an isosurface which can be rotated in any direction to study it. Alternately, numerical variations of a given property (such as electron density) at a defined distance from the molecule can be displayed as property maps using color as a key yielding what is called a property map. Carrying out surface calculations and viewing their graphical representations are major activities in computational chemistry and can provide useful insight into the mechanisms of organic reactions [222].

III.3.4.6. Chemical Reactivity

For example, knowing where the electrons are concentrated (nucleophilic sites) and where they want to go (electrophilic sites) enables us to predict where various kinds of reagents will attack a molecule [222].

III.3.4.7. IR, UV-Vis and NMR spectra:

IR, UV-Vis and NMR spectra can be calculated, and if the molecule is unknown, someone trying to make it knows what to look for. allow the calculation of infrared stretching and bending absorption frequencies and it is a lot of fun to view animations of these types of motions in molecules. The vibrational frequency of a two-atom system is proportional to the square root of the force constant (the second derivative of the energy with respect to the interatomic distance) divided by the reduced mass of the system (which depends on the masses of the two atoms) [222].

III.3.4.8. Energies of the Frontier Molecular Orbitals HOMO and LUMO

The energies of the frontier orbitals HOMO (highest occupied molecular orbital) and LUMO (lowest unoccupied molecular orbital) are descriptors commonly used in QSAR analysis. They reflect the reactivity of a molecule. Higher HOMO energy suggests a higher affinity of a molecule to react as a nucleophile, lower LUMO energy suggests a stronger electrophilic nature of a molecule.

In addition, electrophilic and nucleophilic attacks will most likely occur at atoms where the coefficients of the corresponding atomic orbitals in HOMO and LUMO, respectively, are large [223].

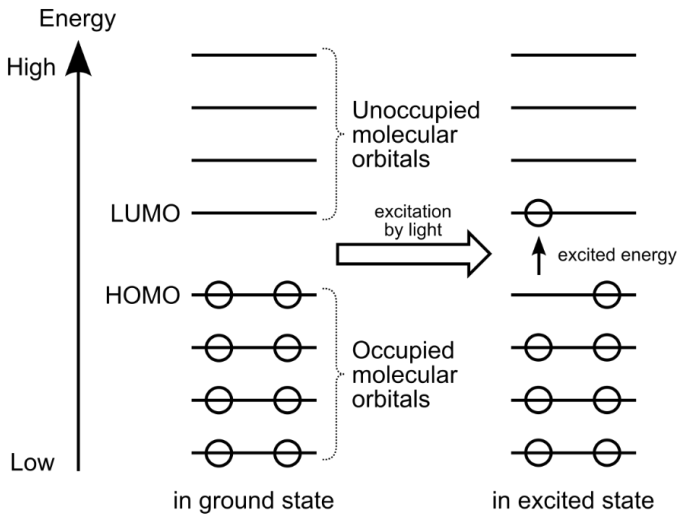

Figure III-7 Diagram of the HOMO and LUMO of a molecule (each circle represents an electron).

III.4. Quantitative Structure-Activity Relationship (QSAR) Modeling

Quantitative Structure-Activity Relationship (QSAR) analysis is based on the general principle of medicinal chemistry that the biological activity of a ligand or compound is related to its molecular structure or properties, and structurally similar molecules may have similar biological activities [224]. This molecular structural information is encoded in molecular descriptors and a QSAR model defines the mathematical relationships between the descriptors and the biological activities of known ligands to predict the activities of unknown ligands. QSAR methods have been applied in several scientific studies including chemistry, biology, toxicology and drug discovery to predict and classify the biological activities of virtual or newly synthesized compounds [225-228].

III.4.1. Main Steps in QSAR Analysis

To develop QSARs, a series of compounds, called a training set, is used. The compounds in the training set ideally, the same or similar mechanism of biological action to ensure that the same factors influence the activity of all compounds under investigation. For all compounds in the series, biological activities are evaluated and compound structural descriptors are calculated. Statistical tools are then used to derive QSARs.

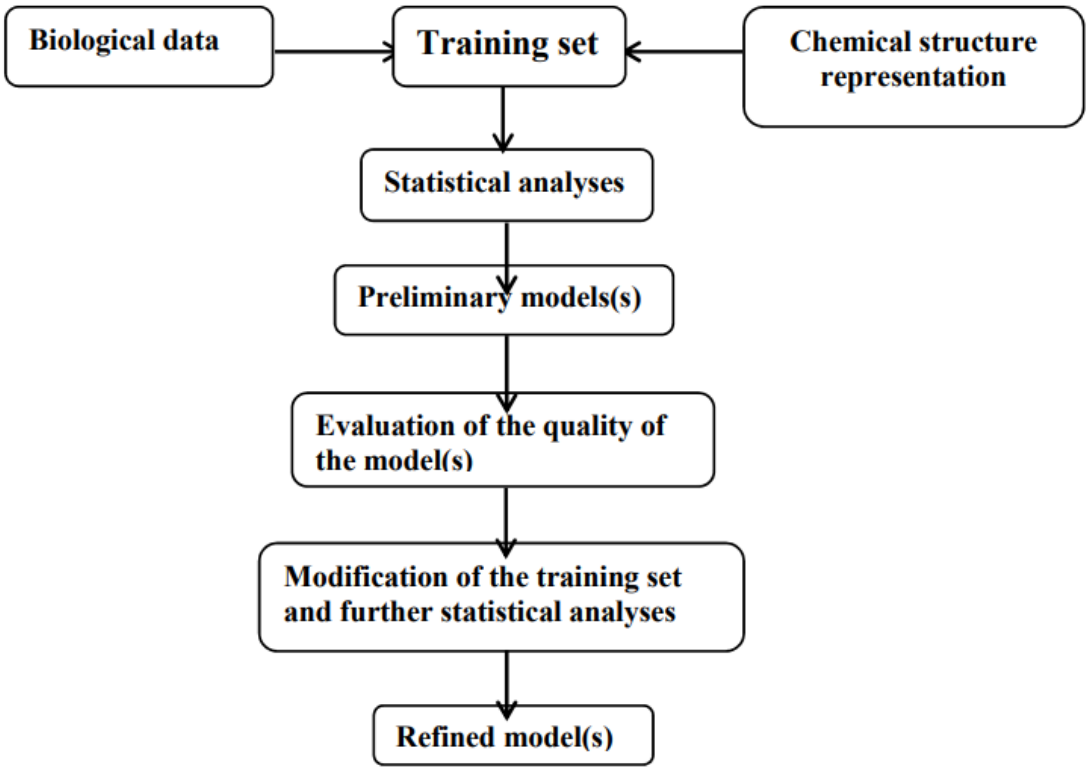

Figure III-8 The main steps in QSAR analysis

III.4.2. Tools and Techniques of QSAR

III.4.2.1. Molecular Descriptors

The crucial point in the QSPR approach is an appropriate description of the molecular structures. The chemical descriptors take account of the different aspects of the chemical information. The molecular descriptor expresses chemical information transformed and encoded from a molecule and effectively solves chemical, pharmaceutical, and toxicological problems. The advantage of theoretical molecular descriptors is in developing compounds that have never been synthesized or explored experimentally. Molecular descriptors are well known for their ability to establish linear regression relationships with physicochemical and biological properties [229].

III.4.2.1.1. Constitutional Descriptors

Constitutional descriptors can simply obtain the information from the chemical composition of the compounds. Typical constitutional descriptors include molecular weight, total numbers of atoms, bonds, and rings in the molecule. These are one-dimensional (1D) descriptors that can easily be obtained with knowledge of the molecular formula. Unfortunately, the linear relationship between constitutional descriptors and physicochemical properties cannot sufficiently prove that a physical mechanism reflects molecular interactions [229].

III.4.2.1.2. Topological Descriptors

Topological descriptors are two-dimensional (2D) descriptors obtained from information on the molecular topology; they express the atomic connectivity in the molecule and can be calculated from 2D graph representation of molecules [230].

III.4.2.1.3. Geometrical Descriptors

Geometrical descriptors are derived from three-dimensional (3D) structures of molecules defined by the coordinates of atomic nuclei and the size of the molecules represented [229]. Weighted holistic invariant molecular (WHIM) descriptors contain another prospective class of molecular geometric parameters, WHIM descriptors are obtained from the molecular (x, y, z) coordinates of the molecules with 3D structure, in which the descriptors capture detailed information on molecular size, shape, symmetry and atomic distribution. The derivation of WHIM descriptors can be obtained from centered molecular coordinates using the PCA approach from the weighted covariance matrix of atomic coordinates [231, 232].

III.4.2.1.4. Electronic Descriptors

Electronic descriptors reflect the electronic structure of the molecule, based on 3D structure and the charge distribution in the molecule. The descriptors can be obtained from the calculation with ab initio or semi-empirical approaches.

III.4.2.2. Biological Parameters

In QSAR analysis, it is imperative that the biological data be both accurate and precise to develop a meaningful model. It must be realized that any resulting QSAR model that is developed is only as valid statistically as the data that led to its development. The equilibrium constants and rate constants that are used extensively in physical organic chemistry and medicinal chemistry are

related to free energy values ΔG. Thus, for use in QSAR, standard biological equilibrium constants such as Ki or Km should be used in QSAR studies.

Likewise, only standard rate constants should be deemed appropriate for a QSAR analysis. Percentage activities (e.g., % inhibition of growth at certain concentrations) are not appropriate biological endpoints because of the nonlinear characteristic of dose-response relationships. These types of endpoints may be transformed to equi-effective molar doses.

Only equilibrium and rate constants pass muster in terms of the free-energy relationships or influence on QSAR studies. Biological data are usually expressed on a logarithmic scale because of the linear relationship between response and log dose in the mid-region of the log dose-response curve. Inverse logarithms for activity (log 1/C) are used so that higher values are obtained for more effective analogs. Various types of biological data have been used in QSAR analysis. A few common endpoints are outlined in Table III-1.

Table III-1 Types of biological data utilized in QSAR analysis

Source of Activity	Biological Parameters
Isolated receptors	
Rate constants	Log k
Michaelis-Menten Constants	Log 1/Km
Inhibition constants	Log 1/Ki
Cellular systems	
Inhibition constants	Log 1/IC50
Cross resistance	Log CR
in vitro biological data	Log 1/C
Mutagenicity states	Log TA98
In vivo systems	
Biocencentration factor	Log BCF
In vivo reaction rates	Log I (Induction)
Pharmacodynamic rates	Log T ((total clearance)

III.4.3. Statistical Methods Used in QSAR Analysis

Statistical methods are an essential component of QSAR work. They help to build models, estimate a model's predictive abilities, and find relationships and correlations among variables and activities. A suitable statistical method coupled with a variable selection method allows analysis

of this data in order to establish a QSAR model with the subset of descriptors that are most statistically significant in determining the biological activity. The statistical method can be broadly divided into two: linear and non-linear method.

In statistics a correlation is established between dependent variables (biological activity) and independent variables (physiochemical properties or molecular descriptor). The liner method fits a line between the selected descriptor and activity as compared to non-linear method which fit a curved between the selected descriptor and activity. Commonly used statistical methods are listed as follows:

1. Principal component analysis (PCA)
2. Cluster analysis
3. Simple liner regression
4. Multiple liner regression
5. Stepwise multiple liner regression
6. Principal component regression (PCR)
7. Continuum Regression
8. Partial least squares (PLS)
9. Genetic function approximation (GFA)
10. Genetic partial least squares (GPLS)
11. Logistic regression
12. K-Nearest Neighbor classification (KNN)
13. Neural Network
14. Discriminant analysis
15. Decision Trees
16. SIMCA
17. Canonical Correlation

III.4.4. Multiple Linear Regressions

The Multiple Linear Regression (MLR) [233] is an extension of the classical regression method to more than one dimension. MLR calculates QSAR equations by performing standard Multivariable regression calculations using multiple variables in a single equation. MLR expresses a single dependent variable (y) as a linear combination of multiple independent variables (x):

$$y = ax_1 + bx_2 + \cdots + k$$ *Equation III-55*

Where a, b are the coefficients of the regression, and k is a constant, the regression model can be built in a stepwise manner.

III.4.5. Statistical Parameters

III.4.5.1. Coefficient of Determination (R^2)

The coefficient of determination is found by squaring the correlation coefficient and is used as a more precise way to interpret the correlation coefficient. It is useful because it gives the proportion of the variance in one variable that is “explained” by the other variable. It represents

the percent of the data that is the closest to the line of best fit [234]. The coefficient of determination can be determined by the mathematical formula:

$$R^2 = \frac{\sum_{i=1}^{n}(y_{i,cal} - y_{i,obs})^2}{\sum_{i=1}^{n}(y_{i,cal} - \bar{y})^2} = \frac{ESS}{TSS}$$ *Equation III-56*

The coefficient of determination is such that 0 < R2 < 1, The stronger correlation R when it is closer to 1.

III.4.5.2. Correlation Coefficient (R)

Correlation coefficient is a simple statistical measure of relationship between one dependent and one or more than one independent variables and it is use as a measure of the statistical fit of a regression based model in QSAR [235].

The value of r is such that -1 < R < +1. The + and – signs are used for positive linear correlations and negative linear correlations, respectively. If the predicted and observed values have a strong linear correlation r is close to 1, however if there is no linear correlation or a weak linear correlation r is close to 0. The value of the correlation coefficient can be strongly influenced by one outlying point.

III.4.5.3. Fischer Statistic (F)

The F-statistic is used to test the statistical significance of the regression [236]. Hence, the larger the F value is above the critical value, the better the regression. As can be seen from the equation below the F-statistic increases as the number of data points increase and the coefficient of determination increases.

$$F = \frac{(n - v - 1)R^2}{(1 - R^2)v} = \frac{ESS}{P}\frac{n - p - 1}{RSS}$$ *Equation III-57*

In the above equation R^2 is the coefficient of determination, n is the number of data points, and ν represents the degrees of freedom. The degrees of freedom can be determined by subtracting one from the number of variables in the regression equation (Equation III-58) [236].

$$Y_i = f(X_i, \beta) + e_i$$ *Equation III-58*

Where, Y_i is the dependent variable, X_i is for the independent variables, β is the unknown parameters, e_i is the error terms.

III.4.5.4. Standard Deviation (S)

Standard deviation (S) is a statistical measure of the spread or uncertainty around the mean. It is defined by the equation:

$$S = \sqrt{\frac{\sum_{i=1}^{n}(y_{i,cal} - \bar{y})^2}{n-p-1}} = \sqrt{\frac{RSS}{n-p-1}}$$ *Equation III-59*

Where, $y_{i,cal}$ is each individual data point, $\bar{y}$ is the mean of the data set, *n* is the number of data points, and *p* is the number of independent variables.

If many data points are clustered tightly around the mean, then the standard deviation is small. However, if data points are scattered widely around the mean, then the standard deviation is large. A useful property of standard deviation is that, unlike variance, it is expressed in the same units as the data.

III.4.5.5. Variance (r)

The variance is the average of the squared standard deviation from the mean. Sums of squares are directly related to variances.

$$r = \sqrt{\frac{\sum_{i=1}^{n}(y_{i,obs} - \bar{y})^2}{n-1}}$$ *Equation III-60*

III.4.5.6. Quality Factor (Q)

Quality factor is calculated by equation:

$$Q = \frac{r}{s}$$ *Equation III-61*

Where r is variance and S is standard deviation. Over fitting and chance correlation, due to excess number of descriptors, can be detected by Q value. Positive value for this QSAR model suggests its high predictive power and lack of over fitting [237].

III.4.6. Validation of QSAR Model

After the model equation is obtained, moreover the stability and the goodness of fit of the model, it is also significant to estimate the power and the validity of the model before using it to predict the biological activity. Validity is to establish the reliability and significance of the method

for a particular use. Therefore, validation of a QSAR model must be done. There are two validation methods used for a QSAR model: internal and external validation techniques to establish the confidence and strength of the model. In general, QSAR modeling involves a systematic process with multiple steps. These include dataset preparation, molecular descriptors selection and generation, mathematical or statistical model's derivation, model training and validation using a training dataset and model testing on a testing dataset.

III.4.6.1. Internal Validation

III.4.6.1.1. Least Squares Fit

The most common internal method of validating the model is least squares fitting. This method of validation is similar to linear regression and is the R^2 (Equation III-56) for the comparison between the predicted and experimental activities. An improved method of determining R^2 is the robust straight-line fit, where data points are away from the central data points (essentially data points a specified standard deviation away from the model) are given less weight when calculating the R^2. An alternative to this method is the removal of outliers (compounds from the training set) from the dataset in an attempt to optimize the QSAR model and is only valid if strict statistical rules are followed. The difference between the R^2 and R^2_{adj} value is less than 0.3 indicates that the number of descriptors involved in the QSAR model is acceptable. The number of descriptors is not acceptable if the difference is more than 0.3 [238].

III.4.6.1.2. Fit of the Model

Fit of the QSAR models can be determined by the methods of chi-squared $\varkappa^2$ and root-mean squared error (RMSE). These methods are used to decide if the model possesses the predictive quality reflected in the R^2. The use of RMSE shows the error between the mean of the experimental values and predicted activities. The chi squared value exhibits the difference between the experimental and predicted bioactivities:

$$\chi^2 = \sum_{i=1}^{n} \frac{(y_i - \hat{y}_1)^2}{\hat{y}} \qquad \textit{Equation III-62}$$

$$RMSE = \sqrt{\left(\sum_{i=1}^{n} \frac{(y_i - \hat{y}_m)^2}{n-1}\right)} \qquad \textit{Equation III-63}$$

Where, y and ŷ are the experimental and predicted bioactivity for an individual compound in the training set, $\hat{y}_m$ is the mean of the experimental bioactivities, and n is the number of

molecules in the set of data being examined. Large chi-square or RMSE values reflect the model's poor ability to accurately predict the bioactivities even the model is having large R^2 value (≥0.7). For good predictive model the chi-squared and RMSE values should be low (<0.5 and <0.3, respectively). However, excellent values of R^2, $\varkappa^2$ and RMSE are not sufficient indicators of model validity. Thus, alternative parameters must be provided to indicate the predictive ability of models. In principle, two reasonable approaches of validation can be envisaged one based on prediction and the other based on the fit of the predictor variables to rearranged response variables.

III.4.6.1.3. Cross-validation

Cross-validation is one of the most extensively used methods for internal validation. It involves partitioning a sample of data into complementary subsets, performing the analysis on one subset (the training set), and validating the analysis on the other subset (the validation set or testing set) [239, 240]. Correlation coefficient of the regression between experimental and estimated data obtained by cross validation is known as cross-validated correlation coefficient or Q_{cv}^2 parameter.

The cross-validation parameter, Q_{cv}^2 is mentioned in the Equation III-64:

$$Q_{CV}^2 = \frac{(SSY - PRESS)}{SSY} \qquad \textit{Equation III-64}$$

Where the PRESS (predictive residual sum of squares) and SSY or SD (the sum of squared deviations of the dependent variable values from their mean) values are obtained as:

$$PRESS = \sum (y_i - \hat{y}_i)^2 \qquad \textit{Equation III-65}$$

$$SSY = SD = \sum (y_i - \bar{y}_i)^2 \qquad \textit{Equation III-66}$$

Where y_i is the experimental activity value, $\bar{y}_i$ is the mean of the experimental activity values, $\hat{y}_i$ is the activity value predicted by the model and n in number of samples.

A model is considered to be significant when Q_{CV}^2 > 0.3. A Q_{CV}^2= 0.5 is considered as good and a Q_{CV}^2 > 0.9 as excellent. To be a reasonable QSAR model the PRESS/SSY ratio must be smaller than 0.4. A PRESS/SSY value < 0.1 is considered to be indicative of an excellent model [241].

For calculating $R_{CV}^2(Q_{CV}^2)$, each sample in the training set needs to be eliminated once and the activity of the eliminated sample will be predicted by using the model developed by the remaining samples. $R_{CV}^2(Q_{CV}^2)$ calculated according to the below formula [242]:

$$R^2_{CV}(Q2) = 1 - \frac{\sum_{i=1}^{n}(\hat{y}_i - y_i)^2}{\sum_{i=1}^{n}(\hat{y}_i - \bar{y})^2} > 0.5$$ *Equation III-67*

A model is considered acceptable when the value of R^2_{CV}(Q2) exceeds 0.5.

III.4.6.2. External validation

According to Tropsha et al. [243], for considering the validity of the developed models, in addition to the internal validation, the models should be externally validated using the test set compounds. According to their study, the following criteria could be considered as of acceptable predictability:

$$R^2_{pred} = 1 - \frac{\sum_{i=1}^{n}(y_{i,cal} - y_{i,obs})^2}{\sum_{i=1}^{n}(y_{i,cal} - \bar{y}_{train})^2} > 0.6$$ *Equation III-68*

Where R^2_{pred} is squared correlation coefficient between the experimental and predicted biological activities of dataset compounds (training and test sets).

y_{cal} and y_{obs} indicate predicted and observed activity values for the test set and $\bar{y}_{train}$ indicates mean activity value of the training set.

$$\frac{R^2 - R_0^2}{R^2} < 0.1 \quad or \quad \frac{R^2 - R'^2_0}{R^2} < 0.1$$ *Equation III-69*

$$|R_0^2 - R'^2_0| < 0.3$$ *Equation III-70*

Where R^2 is the determination coefficient between the experimental and predicted activity values of test set compounds with intercept. R_0^2 and R'^2_0 are determination coefficients of predicted versus experimental and experimental versus predicted biological activity values in which their regression line must pass through the origin, respectively.

$$0.85 \leq K \leq 1.15 \quad or \quad 0.85 \leq K' \leq 1.15$$ *Equation III-71*

The slope of regression line through the origin which mentioned in the above was indicated by K and K' respectively.

III.5. Molecular docking

Molecular docking is a key tool in structural molecular biology and computer-assisted drug design. The goal of ligand-protein docking is to predict the predominant binding mode(s) of a ligand with a protein of known three-dimensional structure. Successful docking methods

efficiently search high-dimensional spaces and use a scoring function that correctly ranks candidate dockings. Docking can be used to perform virtual screening on large compound libraries, categorize results, and offer structural hypotheses on how ligands inhibit the target, which is invaluable in lead optimization.

Figure III-9 shows key steps common to all docking protocols. The 3D structures of the target macromolecule and the small molecule must first be chosen, and then each structure must be prepared according to the requirements of the docking method used. After docking, the results should be analyzed, selecting the binding modes with the best scores.

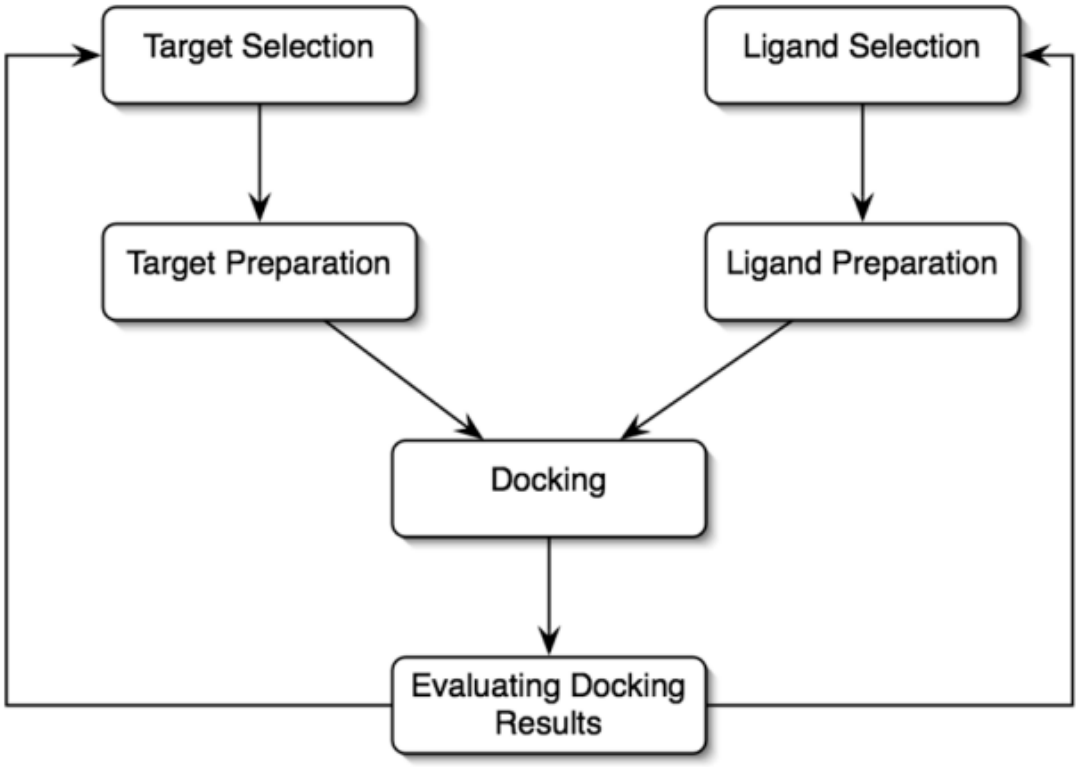

Figure III-9 A typical docking workflow.

All docking methods require a scoring function to rank the different candidate binding modes and a search method to explore state variables. Scoring functions can be empirical, force field-based, or knowledge-based, while research methods fall into two broad categories: systematic and stochastic. Systematic search methods sample the search space at predefined intervals and are deterministic. Stochastic search methods iteratively perform random changes to state variables until a user-defined termination criterion is satisfied, so that the search result varies; Sousa et al. discuss these classes of algorithms in more detail [244].

Search methods can also be classified according to their degree of exploration of the search space, such as local or global. Local search methods tend to find the nearest or local minimum

energy to the current conformation, while global methods search for the best or the global minimum energy in the defined search space. Hybrid global-local search methods have been shown to perform even better than global methods alone, being more efficient and able to find lower energies [245].

In AutoDock 4, for example, there is the choice of two local search methods (Solis and Wets [246] and Pattern Search [247]); two global search methods: Monte Carlo (MC) simulated annealing (SA) [248], and the genetic algorithm (GA) [249-251]; and one hybrid global–local search method, the Lamarckian GA (LGA) [245].

III.5.1. AutoDock

AutoDock is distributed with a GUI called AutoDockTools (ADT; see http://autodock. scripps.edu/resources/adt). ADT helps prepare ligand and receptor input files and configure AutoGrid and AutoDock calculations. BDT [252] is an alternative preparatory tool to ADT (see http://www.quimica.urv.cat/~pujadas/BDT/) which helps to set up virtual analyzes with AutoDock and set up collections of AutoGrid maps for blind docking and also by combining grid maps to incorporate structural variability in the receiver. AutoDock's AutoGrid program precalculate the necessary grid maps that describe the chemical potential at regular intervals around the target.

III.5.1.1. Target Selection and Preparation

- First of all, we need to gather structures of the target, ideally with bound ligands, from internal and external sources. Good publicly available sources include the Protein Data Bank [253], http://www.rcsb.org/pdb; ReLiBase from The Cambridge Crystallographic Data Centre (CCDC) [254], http://relibase.ccdc.cam.ac.uk; and Binding MOAD [255, 256] http://www.bindingmoad.org. (See Note 1)
- Discard any structures that lack the biologically necessary cofactors is also necessary, if any are required for biological activity. Structures that are incomplete or missing side chains should also be disregarded.
- If there is more than one target structure, we need to overlay them by superimposing the key residues in the binding site or region of interest using a least-squares superimposition method. SwissPdbViewer [257], a freely available tool from http://www.expasy.org/spdbv, offers several superimposition options under its “Fit” menu, such as “Magic Fit” and “Fit molecules (from selection)”. Note also that SwissPdbViewer can also automatically reconstruct incomplete side chains.

- Identify the extent of the structural variability and select a representative structure (see Note 2).
- Add all hydrogen atoms to the target at the desired pH; under physiological conditions at pH 7.2, the following residues have ionized side chains: arginine, lysine, aspartic acid, and glutamic acid. This defines the formal charges (see Note 3). Each histidine side chain can be either neutral or positively charged at physiological pH. If it is neutral, either the delta or the epsilon nitrogen can be protonated (see Note 4).
- The atomic assignments of imidazole rings in histidine and amido groups in asparagine and glutamine side chains can be ambiguous; tools such as REDUCE and its web interface, MOLPROBITY [258, 259] can evaluate 180◦ flips of these groups to optimize the hydrogen-bond network, and add hydrogen atoms appropriately.
- Remove all water molecules, except those that are integral to your binding hypothesis (see Note 5).
- If the representative target structure is complexed with a ligand, remove the ligand.
- Calculate the partial charges, if required by the docking tool. Some tools may use a dictionary of amino acid partial charges to simply assign the charges. If there are any cofactors in the target structure, it will be necessary to compute the appropriate partial charges if required by the docking method.
- When using AutoDock, merge nonpolar hydrogens, because it uses a unitedatom representation (see Note 6).
- AutoDock uses grid maps that must be calculated using AutoGrid. Each map describes a 3D grid of interaction energies with the target, one for each atom type in the ligand (see Note 7).

III.5.1.2. Ligand Selection and Preparation

Most docking tools require a 3D structure for each ligand, including explicit hydrogens. Depending on the source of the ligand's real molecules, molecules that have yet to be synthesized, or vendor libraries the steps required to process the molecules will vary. The following steps exemplify how to obtain these structures, and how to process them for use in AutoDock.

- ZINC is one of the largest collections of commercially available compounds; it is well curated and has 4.6 million compounds (http://blaster.docking.org/zinc) [260]. It is particularly useful for molecular docking because it provides 3D structures in SYBYL MOL2 formats, and is also free of charge. Subsets of compounds can be created by

composing a query that specifies constraints on both molecular properties and two-dimensional (2D) molecular topology.

- Ligands in the form of SMILES strings [261] can be converted into full 3D atomic coordinates, including hydrogens, using tools such as CORINA [262, 263] or ZINC [260].
- Ligands in 2D SD format [264] can be converted into full 3D atomic coordinates using CORINA [262, 263] or Chemical [265]. Chemical can be used to sketch the ligand in 3D and then perform energy minimization, molecular dynamics, or conformational search to identify low energy conformations. PRODRG [266, 267] can take PDB format, MDL MOL files, or even ASCII–text drawings of the molecule, instead of SD format. PRODRG is available as a standalone executable or as a web service, where the user can sketch the molecule in 2D and then convert the molecule into 3D; PRODRG is convenient for AutoDock 2.4 and 3, because it outputs PDBQ format.
- It is important that the protonation, tautomeric, and stereoisomeric forms of the ligand be correct, otherwise subsequent calculations will be highly suspect. The enumeration of all possible ligand tautomers can be achieved with such programs as QUACPAC (Open Eye), TAUTOMER (Molecular Networks), and LigPrep (Schrodinger).
- When preparing ligands for AutoDock, the GUI AutoDockTools (ADT) can be used to set up the necessary input files. The first step for AutoDock is to calculate Gasteiger partial charges [268] and assign AutoDock atom types to each atom in the ligand (see Notes 8–10).
- Define the “root” of the torsion tree and the rotatable bonds interactively using ADT. The “Ligand > Torsion Tree > Detect Root...” option automatically examines all the rotatable bonds in the ligand and chooses the atom that is nearest to the center of the torsion tree. The “Ligand > Torsion Tree > Choose Torsions...” option displays all rotatable bonds as green or magenta, indicating that they are active or inactive, respectively. Clicking on these bonds toggles whether they are active or not. Make sure any conjugated bonds are not rotatable.
- AutoDock 4 requires the ligand to be in PDBQT format, which is very similar to PDB format, but also includes the partial atomic charge and the AutoDock atom type for each atom. The ligand should be saved using the “Ligand > Output > Save as PDBQT...” option in ADT.

III.5.1.3. Docking

- Define the search space. There are two possibilities, depending on how much is known about the binding site:
    - If there is no previous information regarding the location of the binding site, then the translational search space should encompass the entire surface of the receptor. This is known as "blind docking," and is possible with AutoDock [269]. If the docking tool cannot encompass the whole target, then probable sites such as cavities large enough to contain the ligand(s) should be investigated separately; the third-party tool BDT [252] can be used to set up staggered grid boxes for AutoGrid.
    - If there is previous information, such as ligands with known binding modes, active site residues, or mutagenesis data, then the search space can be reduced to focus on the region of interest, thus, simplifying the search problem.
- Set the target to be docked to, using the ADT menu item "Docking > Macromolecule > Set Rigid Filename..."
- Select the search method (if there is more than one), and set the appropriate parameters. AutoDock offers MCSA, a traditional GA, and a hybrid global–local search method called LGA. The best search algorithm was shown to be LGA [245], therefore, it is recommended for most dockings (see Note 11).
- Save the input parameter file for the docking tool, if necessary. For AutoDock, use the "Docking > Output > Lamarckian GA..." option in ADT to save an AutoDock docking parameter file (DPF) set up to perform LGA dockings.

III.5.1.4. Evaluating Docking Results

When evaluating the results of dockings, there are two main criteria to consider:

1) how well did the binding mode predicted by the docking match known structural data? where available;

2) how well did the docking rank the ligands? If the method's scoring function is designed to predict binding affinities, how well did it match experimental binding data?

To answer the first criteria, a crystal structure of the complex of the ligand bound to the target must be known, and then the Root Mean Square Deviation (RMSD) between the docked and the "reference" crystallographic binding mode of the ligand can be calculated; success is usually counted as RMSD less than 2 Å. To answer the second criteria, inhibition constants, or Ki values, must be known for the ligands and the target system.

When the search method used is stochastic, it is important to consider how often a given binding mode was predicted across all the dockings that were run. This is usually achieved using conformational clustering, building families of related conformations using RMSD tolerances to decide whether two conformations belong in the same cluster.

- Read in all of the docked conformations into the docking analysis tool. For AutoDock, use ADT with the menu option “Analyze > Dockings > Open...” for one docking log (DLG) (see Note 12).
- It is useful to view the dockings in the context of the target, therefore, if necessary, load the structure of the target. In ADT, use “Analyze > Macromolecule > Open...” to read in the target PDBQT structure used to compute the AutoGrid maps.
- Perform conformational cluster analysis on the dockings to assess the level of agreement in the results. In ADT, use “Analyze > Clusterings > Recluster...”, and type in a list of RMSD tolerances in angstroms separated by spaces. This performs clustering for each RMSD tolerance value, grouping the docked conformations accordingly.
- Display the conformational clustering as a histogram, and visually inspect each cluster. In ADT, use “Analyze > Clusterings > Show...” and then choose the RMSD tolerance value. This displays a histogram of number of docked conformations in the cluster, versus the energy of the most tightly binding conformation in that cluster. The histogram is interactive, thus, clicking on a histogram bar sets up the “play” buttons in the “Conformation Player” window to play through the conformations in that cluster. This window has buttons to play forward and backward, and to step through the conformations one at a time.
- It is possible to examine AutoDock-docked conformations in more detail using the “Conformation Player” in ADT, by clicking on the “&” button. This displays a panel in which it is possible to show more information regarding the current docking, by clicking on the “Show Info” check-button. It is also possible to monitor which hydrogen bonds are formed between the ligand and the target using the “Build H-bonds” check-button. The atoms in the ligand can be colored by a color scale that goes from dark blue to green to yellow to orange to red, indicating more favorable to less favorable interaction energies, using the “Color by” option; “vdw” colors by van der Waals or H-bond plus desolvation free energy, “elec stat” colors by electrostatic interaction energy, and “total” colors by the total interaction energy; and “atom” returns to the default color-by-atom coloring.
- If the docking results do not cluster into at least one significantly populated cluster, with an RMSD tolerance of between 2 and 3 Å, this is an indication that the dockings did not

search for long enough. In AutoDock and ADT, increase the number of energy evaluations used in the LGA, and rerun the dockings. To get decent statistics, it is advisable to repeat the docking at for at least 50 runs.

- If the docked conformations are too far from the target structure, make sure that the AutoGrid grid box is centered on or near the target; the grid box can be visualized in ADT using the "Analyze > Grids > Open...", then choosing one of the grid maps files. The x-, y-, and z-axes are color-coded red, green, and blue, respectively. The energy values in the grid map can be isocontoured by dragging the blue solid triangle on the "IsoValue" slider, with lower energy values indicating pockets of tighter binding affinity, and higher-resolution isocontours can be plotted using a "Sampling" value of 1 instead of the default value, 3.

III.5.1.5. Notes

1) It is preferable to use only high-resolution structures where available, ideally better than 2.5 Å.
2) A representative structure or "leader" for a 90% homology family of structures is already precalculated and available from Binding MOAD [255] http://www.bindingmoad.org.
3) In AutoDockTools, use the "Edit > Hydrogens > Add" then choose "All Hydrogens"; all hydrogens are required for the initial Gasteiger partial charge calculation, but the nonpolar hydrogens will be merged later on.
4) AutoDockTools offers a tool to help set the desired protonation state of each its side chain, under the "Edit > Hydrogens > Edit Histidine Sidechains" menu. Which protonation state a, its adopts will depend on its environment in the target.
5) Consolv [270], freely available from http://www.bch.msu.edu/labs/kuhn/software. html, "predicts whether water molecules bound to the surface of a protein are likely to be conserved or displaced in other, independently solved crystallographic structures of the same protein."
6) AutoDockTools calculates the partial charges and merges the nonpolar hydrogens automatically when the user selects the "Grid > Macromolecule > Choose..." menu items.
7) AutoGrid requires the target to be saved in PDBQT format, and it requires a Grid Parameter File (GPF). To save the receptor, use the "File > Save > Write PDBQT..." option. Set which types of grid maps should be calculated using either "Grid > Set Map Types > Directly..." or "Grid > Set Map Types > Choose Ligand...". To set up the location and grid spacing of the grid maps, use "Grid > Grid Box...". Finally, to save the GPF, use "Grid > Output > Save GPF...".

8) Note that ADT can read in a ligand with partial charges using SYBYL mol2 format. Use “File > Read Molecule...” and change the “Files of type” button to “MOL2 files (∗.mol2)”.
9) If the ligand is missing hydrogen atoms, then they must be added before calculating the Gasteiger charges. After selecting the ligand in ADT, use the menu option “Edit > Hydrogens > Add”. It is very important to consider the tautomeric and ionization states when adding hydrogens.
10) AutoDock atom types are assigned automatically in ADT by choosing the “Ligand > Input > Choose...” option. This command will also merge the nonpolar hydrogens, making the ligand suitable for use with the united-atom force field in AutoDock.
11) It is important to make sure that the number of energy evaluations is increased from the default value of 250,000 if the ligand has any rotatable bonds. Use the ADT menu option “Docking > Search Parameters > Genetic Algorithm...” and change the “Maximum number of energy evaluations” to at least 2,500,000. It is also possible to increase the “Number of GA runs” in the panel from the default value 10. One other important parameter is the “Population Size”; the default is 150, although Hetenyi et al. showed that larger values up to 300 can improve the efficiency of the search [269]. Note also that this panel works for both the traditional and LGA search methods.
12) Alternatively, if the same ligand has been docked to the same target, but separate runs of AutoDock have produced uniquely named DLG files, as is the case when running dockings in parallel on computational clusters, use the “Analyze > Dockings > Open All...” option to read in all the dockings.

PART 2

EXPERIMENTS

CHAPTER IV

STRUCTURAL, ELECTRONICAL PROPERTIES AND IN SILICO TOXICITY OF N-FERROCENYLMETHYLANILINE DERIVATIVES

IV.1. Introduction

To achieve molecular docking, the structure of the ligand must be optimized by molecular modeling which is a set of theoretical methods consisting in modeling a three-dimensional structure of a complex, and more generally its interface, from the known structures of its constituents. The level and quality of the details obtained, depending on the type of experimental techniques, which will weigh on the capacity of the modeling methods to obtain a good resolution of the three-dimensional structures of the complex studied and which represent the molecular structure of these molecules [271, 272].

Based on the fundamental laws of quantum mechanics, the Gaussian software allows us to predict the energies, molecular structures and vibration frequencies of complex molecular systems, and to anticipate their chemical properties. Molecules and reactions can be studied under a wide range of conditions not only for stable species or complex compounds but also for compounds that cannot be observed experimentally, such as ephemeral intermediates or transition states [273].

Molecular mechanics is a calculation method used in classical mechanics to calculate the lowest energy of conformation of molecules. This makes it possible to calculate the relative energies between different configurations or between different molecules, as well as the geometries of equilibrium and the transition states, which correspond to the local surface minima of potential energy corresponding to stable conformations [273, 274].

IV.2. N-ferrocenylmethylaniline derivatives

For this study 28 derivatives were synthesized at VTRS laboratory (laboratoire de valorisation et technologie des ressources sahariennes) at El-Oued University. All the derivatives have the same basic core which can be represented with the first derivative (N-ferrocenyl-methylaniline) (Figure IV-1). All the derivatives and their commun names are tabulated in Table IV-1.

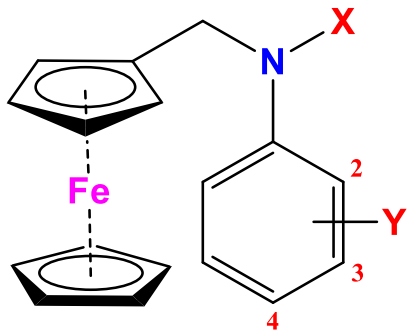

Figure IV-1 General formula of the basic core (N-ferrocenylmethylaniline) of the derivatives

Table IV-1 List of N-ferrocenylmethylaniline derivatives

Code Name	X	Y	commun Name
F1	H	H	N-ferrocenylmethylaniline
F2	H	2-Me	N-(ferrocenylmethyl)-2-(methyl)aniline
F3	H	3-Me	N-(ferrocenylmethyl)-3-(methyl)aniline
F4	H	2-Et	N-(ferrocenylmethyl)-2-(ethyl)aniline
F5	H	2-Cl	N-(ferrocenylmethyl)-2-(chloro)aniline
F6	H	3-Cl	N-(ferrocenylmethyl)-3-(chloro)aniline
F7	H	4-Cl	N-(ferrocenylmethyl)-4-(chloro)aniline
F8	H	3-Br	N-(ferrocenylmethyl)-3-(bromo)aniline
F9	H	4-Br	N-(ferrocenylmethyl)-4-(bromo)aniline
F10	H	2-NO_2	N-(ferrocenylmethyl)-2-(nitro)aniline
F11	H	3-NO_2	N-(ferrocenylmethyl)-3-(nitro)aniline
F12	H	4-NO_2	N-(ferrocenylmethyl)-4-(nitro)aniline
F13	H	2-CN	N-(ferrocenylmethyl)-2-(aminobenzo)nitrile
F14	H	3-CN	N-(ferrocenylmethyl)-3-(aminobenzo)nitrile
F15	H	4-CN	N-(ferrocenylmethyl)-4-(aminobenzo)nitrile
F16	H	3-CF_3	N-(ferrocenylmethyl)-4-(trifluoromethyl)aniline
F17	H	2-COMe	N-(ferrocenylmethyl)-2-(acetyl)aniline

Code Name	X	Y	commun Name
F18	H	4-COMe	N-(ferrocenylmethyl)-4-(acetyl)aniline
F19	H	4-SO_2-NH_2	4-((ferrocenylmethyl)amino)benzenesulfonamide
F20	COMe	H	N-(ferrocenylmethyl)-N-(phenyl)acetamide
F21	COMe	2-NO_2	N-(ferrocenylmethyl)-N-(acetyl)-2-(nitro)aniline
F22	COMe	3-NO_2	N-(ferrocenylmethyl)-N-(acetyl)-3-(nitro)aniline
F23	COMe	4-NO_2	N-(ferrocenylmethyl)-N-(acetyl)-4-(nitro)aniline
F24	COMe	2-CN	N-(ferrocenylmethyl)-)-N-(acetyl)-2-(amino)benzonitrile
F25	COMe	3-CN	N-(ferrocenylmethyl)-)-N-(acetyl)-3-(amino)benzonitrile
F26	COMe	4-CN	N-(ferrocenylmethyl)-)-N-(acetyl)-4-(amino)benzonitrile
F27	COPh	H	N-(ferrocénylmethyl)-N-(phenyl)benzamide
F28	NHCOMe	H	N'-(ferrocenylmethyl)-N'-(phenyl)acetohydrazide

IV.3. Calculation methods

All the calculation were carried out using Gaussian software (Gaussian 09W) and visualised by GaussView to show the final optimized structure of the derivatives and their properties. The optimization process was done using DFT/B3LYP method. The basis sets were chosen in order to be suitable for different atoms that compose the N-ferrocenylmethylaniline derivatives. LANL2DZ [275-279] basis set has been selected for the big atoms which are iron (Fe) in all N-ferrocenylmethylaniline derivatives and bromine which is included in the composition of the derivatives F9 and F10. Another basis set has been chosen (6-31+G(d)) [207, 208, 275-277, 280-284] for the rest of the atoms (C, H, N, O, Cl).

In order to confirm that the mixed basis set (LANL2DZ(Fe)/6-31G(d)) is suitable for the N-ferrocenylmethylaniline derivatives calculations, the derivative F1 was chosen in order to compare its calculated and experimental data [285]. F1 represents the basic core of all the derivatives. In the study case, due the absence of experimental geometric data of F1. F10 has been chosen to confirm only the ability of geometric optimization of the mentioned mixed bases sets.

Mulliken atomic charges were also calculated for F1 using Gaussian 09W with the same method (DFT/B3LYP) and the same mixed basis sets (LANL2DZ(Fe)/6-31G(d)). Moreover, the calculations of molecular electrostatic potential (MESP) map were carried out using the same computational method with the same mixed basis sets. In order to predict the reactivity of our derivatives, HOMO and LUMO energies, as well as the gap (HOMO-LUMO) were calculated using single point energy.

Furthermore, spectroscopic properties such as IR, ^{1}H NMR, and ^{13}C NMR spectrums have been predicted for F1 using the same method and mixed basis sets. in addition, the calculations of UV-Vis spectrum was carried out using TD-DFT/B3LYP method with the same mixed basis sets, the number of solved states was equal to 55 states and the used solvation model was CPCM and the solvent was ethanol.

IV.4. Geometric properties

The optimized structure of F10 is shown in Figure IV-2 with numbering of the atoms, bond lengths and bond angles of the compound calculated by DFT/B3LYP method with the mentioned mixed basis sets LANL2DZ(Fe)/6-31G(d) were compared with the experimental data. Both of the experimental and theoretical values are tabulated in Table IV-2. For the bond lengths it can be seen that there is a good agreement between the calculations and the experimental data, for example the bond Fe1-C2 is calculated at 2.084 Å where the experimental value was at 2.031 Å and the percent error of this calculation was δ=2.610 % which makes this calculation very accurate, the X-Ray value of the bond lengths of Fe1-C9, Fe1-C6 and Fe1-C10 were equal to 2.044 Å, 2.041 Å and 2.036 Å respectively, the calculated values were equal to 2.078 Å, 2.076 Å and 2.078 Å respectively with percent error equal to 1.663%, 1.715% and 2.063%, carbon-carbon bonds of the cyclopentadiene of the ferrocenyl group had a good agreement with the experimental values. For example, C10-C9 was observed by X-Ray to be equal to 1.430 Å and the calculated value was 1.433 Å with a percent error equal to 0.210 %, C4-C5 and C6-C7 were equal to 1.41 Å and 1.425 Å respectively, theoretically they were equal to 1.429 Å and 1.428 Å respectively and the percent error was 1.348% and 0.211% for each. Also, the X-Ray value of C10-C11 was equal to 1.50 Å and was calculated at 1.51 Å with percent error equal to 0.667%. For Amine group the bond C11-N1 was at 1.466 Å by X-Ray and calculated at 1.462 Å with a good percent error equal to 0.273%, in the other side C12-N1 was equal to 1.356 Å and calculated at 1.359 Å and its percent error was equal to 0.221%. As for the phenyl group the bonds C12-C17 and C15-C16 were observes to be at 1.419 Å and 1.40 Å respectively, theoretically they were calculated to be at 1.423 Å and 1.407 Å with percent error equal to 0.282% and 0.500% for each one respectively. Moreover, the bonds of Nitro group C13-N2 and N2-O2 are experimentally equal to 1.438 Å and 1.238 Å were they have been calculated at 1.446 Å and 1.252 Å respectively, and their percent error aqual to 0.556% and 1.131%. It should also be noted that the maximum percent error of bond length was equal to 2.610 % and its average was 0.716 % which makes it a pretty good calculation.

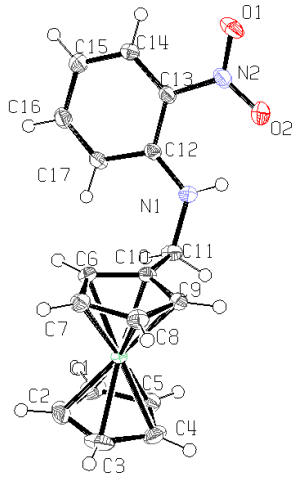

Figure IV-2 ORTEP view of F10 represents atomic labelling obtained from X-ray data [285].

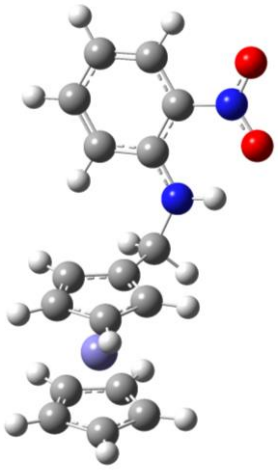

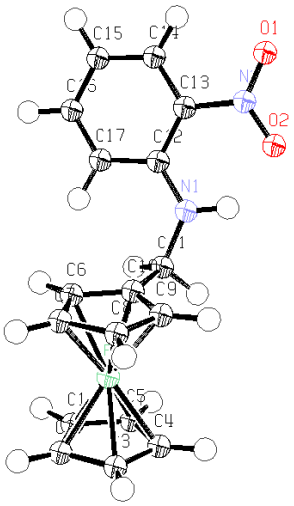

Figure IV-3 A view of F10 DFT optimized structure represented by GaussView AND ORTEP.

For the bond lengths it can be seen that there is a good agreement between the calculations and the experimental data, for example the bond Fe1-C2 is calculated at 2.084 Å where the experimental value was at 2.031 Å and the percent error of this calculation was $\delta = 2.610\,\%$ which makes this calculation very accurate, the X-Ray value of the bond lengths of Fe1-C9, Fe1-C6 and Fe1-C10 were equal to 2.044 Å, 2.041 Å and 2.036 Å respectively, the calculated values were equal to 2.078 Å, 2.076 Å and 2.078 Å respectively with percent error equal to 1.663%, 1.715% and 2.063%, carbon-carbon bonds of the cyclopentadiene of the ferrocenyl group had a good agreement with the experimental values. For example, C10-C9 was observed by X-Ray to be equal to 1.430 Å and the calculated value was 1.433 Å with a percent error equal to 0.210 %, C4-C5 and C6-C7 were equal to 1.41 Å and 1.425 Å respectively, theoretically they were equal to 1.429 Å and 1.428 Å respectively and the percent error was 1.348% and 0.211% for each. Also, the X-Ray value of C10-C11 was equal to 1.50 Å and was calculated at 1.51 Å with percent error equal to 0.667%. For Amine group the bond C11-N1 was at 1.466 Å by X-Ray and calculated at 1.462 Å with a good percent error equal to 0.273%, in the other side C12-N1 was equal to 1.356 Å and calculated at 1.359 Å and its percent error was equal to 0.221%. As for the phenyl group the bonds C12-C17 and C15-C16 were observes to be at 1.419 Å and 1.40 Å respectively, theoretically they were calculated to be at 1.423 Å and 1.407 Å with percent error equal to 0.282% and 0.500% for each one respectively. Moreover, the bonds of Nitro group C13-N2 and N2-O2 are experimentally equal to 1.438 Å and 1.238 Å were they have been calculated at 1.446 Å and 1.252 Å respectively, and their percent error aqual to 0.556% and 1.131%. It should also be noted

that the maximum percent error of bond length was equal to 2.610 % and its average was 0.716 % which makes it a pretty good calculation.

Moreover, for the bond angels of F10 it can be seen for the Ferrocenyl group in the experimental values of C-C-C angles are between 107.38° and 108.44° where the calculated values were between 107.28° and 108.38°, the angles between Iron and the carbon atoms of sandwiched cycles had a good agreement for example C10-Fe1-C6 from the X-Ray was equal to 41.14° and the calculated value was at 40.38° and its percent error was equal to 1.847% which makes the calculated value very accurate. C11-N1-C12 was also calculated to be found at 126.70° which is pretty close to the X-Ray value at 125.05° with percent error equal to 1.319%. furthermore, for the phenyl group the angles C-C-C were between 118.70° - 121.23° and their calculated values were between 118.64° - 121.20°. For the Angles the maximum percent error was 10.660% and its average was equal to 0.496% which means the calculation are super accurate.

Table IV-2 Bond lengths (Å), bond angles (°) experimental and optimized of F10 by using LANL2DZ(Fe)/6-31G(d) basis sets.

Atoms		Exp [285]	Gauss	Percent error (%)	Atoms		Exp [285]	Gauss	Percent error (%)
Bonds distances(Å)									
C10	C11	1.5	1.51	0.667	C4	C5	1.41	1.429	1.348
C10	C6	1.433	1.434	0.070	C5	C1	1.408	1.429	1.491
C10	Fe1	2.036	2.078	2.063	C5	C4	1.41	1.429	1.348
C11	C10	1.5	1.51	0.667	C5	Fe1	2.047	2.085	1.856
C11	N1	1.466	1.462	0.273	C6	C7	1.425	1.428	0.211
C12	C17	1.419	1.423	0.282	C6	Fe1	2.041	2.076	1.715
C13	N2	1.438	1.446	0.556	C7	C6	1.425	1.428	0.211
C15	C16	1.4	1.407	0.500	C7	Fe1	2.048	2.083	1.709
C16	C15	1.4	1.407	0.500	C8	C7	1.424	1.429	0.351
C16	C17	1.374	1.384	0.728	C8	C9	1.42	1.427	0.493
C1	C2	1.411	1.429	1.276	C9	C10	1.43	1.433	0.210
C1	C5	1.408	1.429	1.491	C9	C8	1.42	1.427	0.493
C1	Fe1	2.039	2.084	2.207	C9	Fe1	2.044	2.078	1.663
C2	C1	1.411	1.429	1.276	Fe1	C2	2.031	2.084	2.610
C2	C3	1.42	1.43	0.704	N1	C11	1.466	1.462	0.273
C2	Fe1	2.031	2.084	2.610	N1	C12	1.356	1.359	0.221
C3	C2	1.42	1.43	0.704	N2	C13	1.438	1.446	0.556

Atoms		Exp [285]	Gauss	Percent error (%)	Atoms		Exp [285]	Gauss	Percent error (%)
C3	C4	1.416	1.43	0.989	N2	O2	1.238	1.252	1.131
C4	C3	1.416	1.43	0.989	O2	N2	1.238	1.252	1.131
Maximum percent error of bond distance = 2.610 %									
Percent error average of bond distances = 0.716 %									
Bonds angles (°)									
C10	C6	Fe1	69.25	69.89	0.924	C4	C3	C2	107.5	108	0.465
C10	C9	Fe1	69.19	69.83	0.925	C4	C3	Fe1	70.08	70	0.114
C10	Fe1	C1	112.64	124.08	10.156	C4	C5	Fe1	70.06	69.95	0.157
C10	Fe1	C3	174.4	159.32	8.647	C5	C4	C3	108.08	107.97	0.102
C10	Fe1	C6	41.14	40.38	1.847	C5	C4	Fe1	69.71	69.97	0.373
C11	C10	Fe1	125.09	126.9	1.447	C5	Fe1	C4	40.23	40.09	0.348
C14	C15	C16	118.7	118.64	0.051	C6	C10	Fe1	69.6	69.73	0.187
C15	C14	C13	120.72	121.09	0.306	C6	C7	Fe1	69.35	69.66	0.447
C17	C16	C15	121.23	121.2	0.025	C6	Fe1	C5	133.1	124.53	6.439
C1	C5	C4	108.34	108.03	0.286	C6	Fe1	C9	68.77	67.53	1.803
C1	C5	Fe1	69.52	69.89	0.532	C7	C6	C10	108.03	108.42	0.361
C1	Fe1	C3	68.31	67.42	1.303	C7	C6	Fe1	69.85	70.18	0.472
C1	Fe1	C4	67.9	67.41	0.722	C7	C8	Fe1	69.53	69.88	0.503
C1	Fe1	C5	40.31	40.11	0.496	C7	Fe1	C8	40.66	40.09	1.402
C1	Fe1	C7	133.18	123.62	7.178	C8	C7	C6	108.14	107.87	0.250
C1	Fe1	C9	144.47	159.87	10.660	C8	C7	Fe1	69.81	70.04	0.329
C2	C3	Fe1	69.11	69.95	1.215	C8	C9	C10	108.44	108.38	0.055
C2	Fe1	C3	40.8	40.14	1.618	C8	C9	Fe1	69.99	70.21	0.314
C2	Fe1	C6	112.74	123.38	9.438	C9	C10	C6	107.38	107.28	0.093
C2	Fe1	C9	174.69	158.63	9.193	C9	C8	C7	108.01	108.05	0.037
C3	C4	Fe1	69.48	69.88	0.576	C9	C8	Fe1	69.43	69.7	0.389
C3	Fe1	C7	114.71	122.68	6.948	C11	N1	C12	125.05	126.70	1.319
Maximum percent error of bond angle = 10.660 %									
Percent error average of bond angles = 0.496 %									

Apparently the comparation between the experimental and calculated geometric parameters shows almost perfect agreement with coefficient of determination R^2 equal to 0.9992 for the bonds lengths and 0.9755 for the bonds angles both of them are represented in Figure IV-4 and Figure IV-5 respectively.

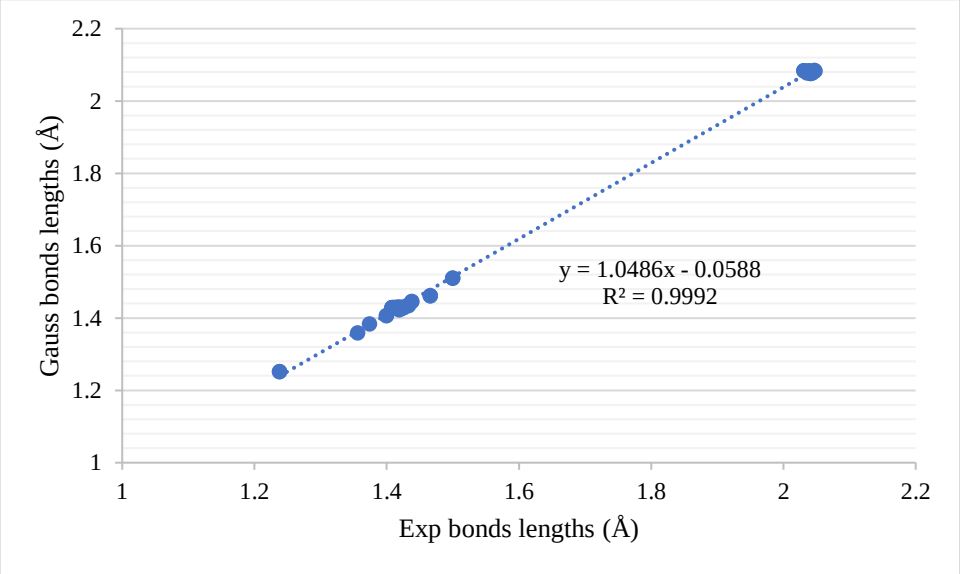

Figure IV-4 Correlation graphic between the experimental and calculated bond lenghts of F10

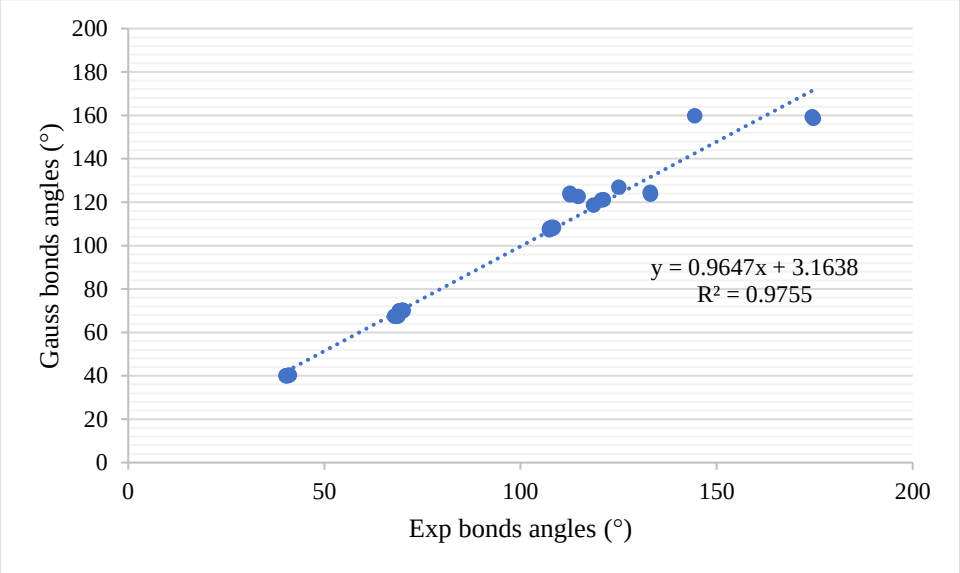

Figure IV-5 Correlation graphic between the experimental and calculated bond angles of F10.

IV.5. Spectroscopic properties

IV.5.1. IR

Vibration frequencies (Table IV-3) and IR Spectrum (Figure IV-6) of F1 were calculated using DFT/B3LYP method with the mixed basis sets LANL2DZ(Fe)/6-31G(d). The computational frequencies were compared to experimental frequencies [286].

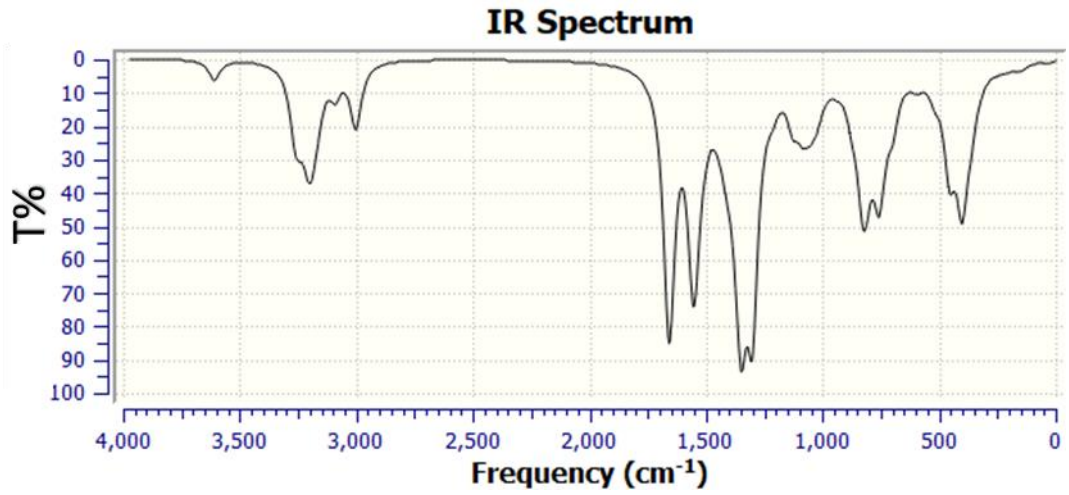

Figure IV-6 Calculated IR spectrum of F1

The comparison shows great agreement between computational and experimental frequencies. Generally, Amine group has two special bonds which are N-H bond and C-N bond the frequency of the stretching vibration of N-H bond appeared at 3405 cm^{-1} in the experimental spectrum where the computational frequency calculated at 3609.85 cm^{-1}, on the other hand the bending vibration of the same bond calculated to be at 1555.01 cm^{-1} where the stretching vibration of C-N bond appeared at 1100 cm^{-1} the calculation gave a good prediction of the frequency at 1301.02 cm^{-1}. Stretching vibration of C-H aliphatic and aromatic (phenyl) experimentally appeared at 2840 and 3090 cm^{-1} respectively where the computational values calculated at 3002.24 and 3189.32 cm^{-1}. Furthermore, the bending vibration of C-H bond from the cyclopentadiene of ferrocene part appeared at 999 cm^{-1} and its calculated value is at 812 cm^{-1}. C=C bond has the strongest peak on theoretical IR spectrum at 1658.08 cm^{-1}, this peak appeared at 1602 cm^{-1} in the experimental data. The last calculated vibration of F1 is the one of Fe-$C_{(Cp)}$ which is a stretching vibration at 451.08 cm^{-1}.

Table IV-3 Types of vibration of F1 and their frequencies

Bond	Vibration type	Experimental Frequency (cm^{-1})	Calculated Frequency (cm^{-1})	Peak strenght
N-H	Stretching	3405	3609.85	Medium
$C\text{-}H_{(Ph)}$	Stretching	3090	3189.32	Medium
$C\text{-}H_{(Aliphatic)}$	Stretching	2840	3002.24	Medium
$C{=}C_{(Ph)}$	Stretching	1602	1658.08	Strong
N-H	Bending	--	1555.01	Strong
C-N	Stretching	1100	1301.02	Strong
$C\text{-}H_{(Cp)}$	Bending	999	812	Medium
Fe-Cp	Stretching	--	451.08	Medium

It is clear that the comparison between the experimental and calculated values of vibration frequency shows great agreement with coefficient of determination R^2 equal to 0.9884. the graph is represented in Figure IV-7.

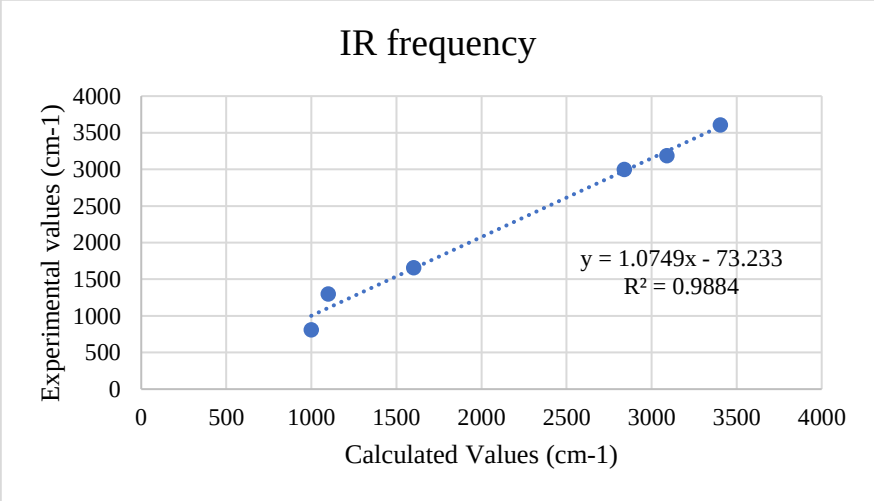

Figure IV-7 Correlation graphic between the experimental and calculated vibration frequencies

IV.5.2. NMR

NMR Spectrums of F1 were calculated using DFT/B3LYP method with the mixed basis sets LANL2DZ(Fe)/6-31G(d). The computational shifts were compared to experimental shifts. This comparison shows an agreement between the calculated values and the experimental shifts of NMR analyses.

Experimental NMR 1H analysis shows that all the hydrogen atoms of the ferrocene part resonance appeared between 4.20 and 4.24 ppm where the computational values where between

3.07 and 4.25 ppm. The computational values shows that H atoms of the ferrocene part are not in the same environment due the bounding of ferrocene with the substitution part in one side of its cyclopentadiene. The aliphatic hydrogens of C11 appeared on the experimental spectrum at 4.30 ppm where the calculated shift is equal to 3.59 ppm. the hydrogen of the amine part appeared experimentally at 4.01 ppm and theoretically at 3.52 ppm. The last type of hydrogen in F1 is the aromatic hydrogens of the phenyl part of the substitution, these hydrogens appeared between 6.71 and 6.81 ppm and the computational values are between 5.89 and 6.96 ppm.

In the case of NMR 13C the agreement between the experimental and the computational values was even much better than then the agreement in NMR 1H case. All the carbons of ferrocene part had shift values between 68.04 and 86.60 ppm where the computational values calculated to be between 57.56 and 78.75 ppm. C11 appeared at 43.52 ppm experimentally and its calculated value is 37.89 ppm which is very close to the experimental value. The last type of carbons is the type of the phenyl group which appeared in the interval of 117.68 - 129.44 ppm on the experimental spectrum. On the other hand, the theoretical spectrum shows the same type of carbons between 95.07 and 115.84 ppm. For both cases of NMR 1H and NMR 13C it can be clearly seen that there is a little shift to the right (TMS).

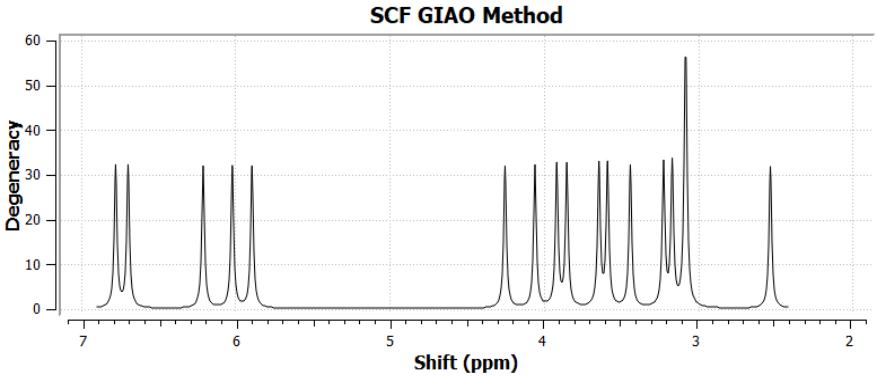

Figure IV-8 Calculated NMR ^{1}H spectrum of F1

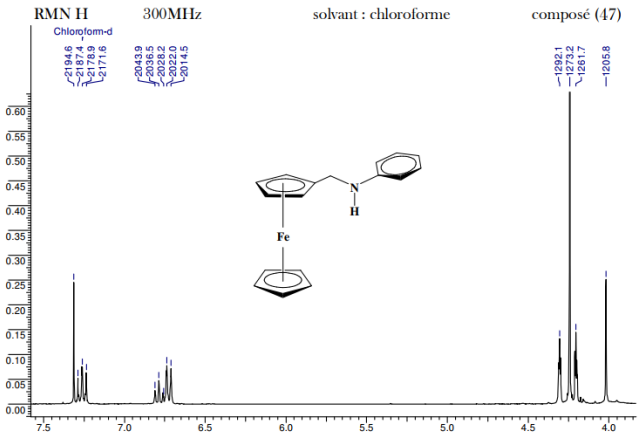

Figure IV-9 Experimental NMR ^{1}H spectrum of F1

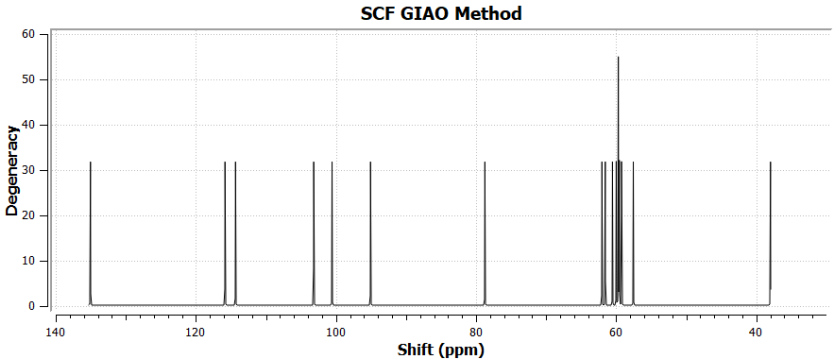

Figure IV-10 Calculated NMR ^{13}C spectrum of F1

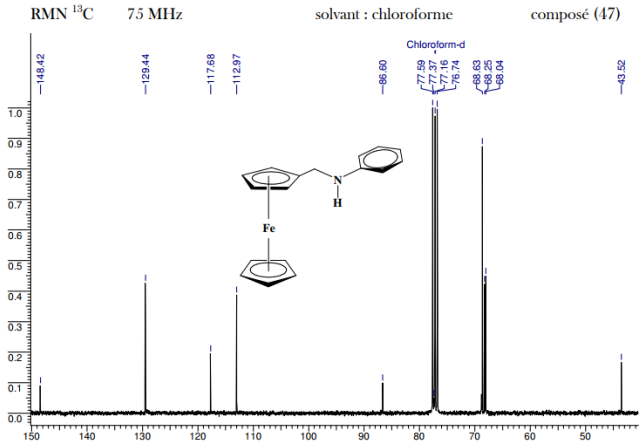

Figure IV-11 Experimental NMR ^{13}C Spectrum of F1

Table IV-4 Experimental and calculated NMR ^{1}H and NMR ^{13}C chemical shifts (ppm) of F1

NMR ^{1}H			NMR ^{13}C		
Atom	**Exp.**	**Cal.**	**Atom**	**Exp.**	**Cal.**
H6	4.20	3.22	C1	68.04	59.24
H9	4.20	3.44	C2	68.04	59.55
H7	4.24	3.85	C3	68.04	59.70
H8	4.24	4.06	C4	68.04	60.01
H5	4.24	4.25	C5	68.04	62.04
H1	4.24	3.07	C6	68.25	59.70
H2	4.24	3.92	C7	68.25	60.54
H3	4.24	3.25	C8	68.25	57.56
H4	4.24	3.64	C9	68.63	61.56
H11a	4.30	3.59	C10	86.60	78.75
H11b	4.30	3.59	C11	43.52	37.98
H-(N)	4.01	3.52	C12	148.42	135.04
H13	6.73	6.02	C13	117.68	95.07
H14	6.81	6.96	C14	129.44	115.84
H15	6.76	6.21	C15	129.44	103.18
H16	6.78	6.77	C16	129.44	114.34
H17	6.71	5.89	C17	117.68	100.56

The comparison between the experimental and calculated values of NMR shifts shows a satisfying agreement with R^2 equal to 0.9278 for NMR 1H and 0.9817 for NMR 13C both of them are represented in Figure IV-12 and Figure IV-13 respectively.

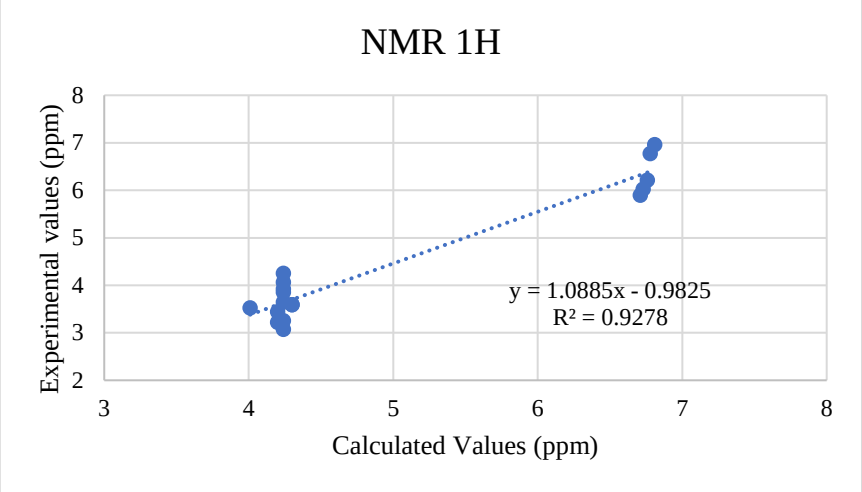

Figure IV-12 Correlation graphic between the experimental and calculated shifts of NMR 1H

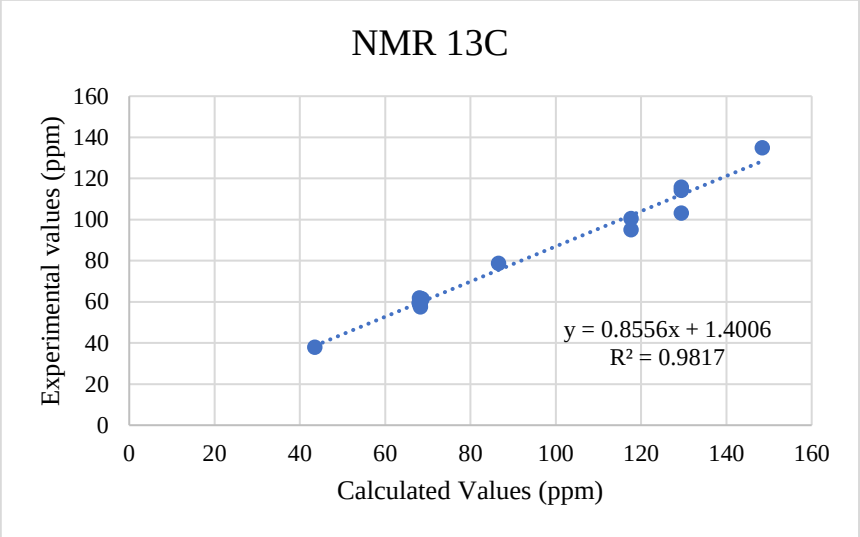

Figure IV-13 Correlation graphic between the experimental and calculated shifts of NMR 13C

IV.6. Atomic Mulliken charges

For many years, chemists have had a genuine interest in describing electron density distributions in terms of atomic charges [287]. With the increasing power of computers and the increasing use of methods that include electronic correlations we can now consistently get fairly accurate density matrices as part of geometric optimizations.

Atomic Mulliken charges of F1 have been calculated by DFT/B3LYP method with the mixed basis sets LANL2DZ(Fe)/6-31G(d). the values of atomic Mulliken charges are tabulated in Table IV-5.

The results show that all carbon atoms have negative charges except C12 and C17 of the benzene group. The iron and nitrogen also have negative charges.

Table IV-5 Atomic Mulliken charges of F1

Atom	Atomic charge	Atom	Atomic charge	Atom	Atomic charge
		Fe	-1.023		
C1	-0.060	C7	-0.369	C13	-0.819
C2	-0.065	C8	-0.026	C14	-0.293
C3	-0.132	C9	-0.178	C15	-0.196
C4	-0.045	C10	0.999	C16	-0.387
C5	-0.182	C11	-0.855	C17	0.549
C6	-0.087	C12	0.232	N1	-0.364

IV.7. Molecular electrostatic potential (MESP) map

Mapping molecular electrostatic potential (MESP) maps for chemical structure has become a major concern. Since it can explain valuable information about the interaction, active sites as well as determining the nature of the chemical addition, through which a molecule is most likely to undergo; electrophilic or nucleophilic addition. Calculations at the mentioned DFT high theoretical level and MESP maps for N-ferrocenylmethylaniline derivatives were carried out.

Generally, The MESP shows the preferred sites for nucleophilic and electrophilic attack the maximum positive region which preferred site for nucleophilic attack is colored in blue, while the maximum negative region which preferred site for electrophilic attack takes red color. The green regions signify electrically neutral regions. The order of potential decreasing is: red < orange < yellow < green < blue.

MESP Surface and contour map for F1 in Figure IV-14 shows one preferred site for the nucleophilic attack which colored in blue around the amine function (Nitrogen atom N) this makes the nitrogen atom is the most preferred site for the nucleophilic attack in any reaction or preparation of a new derivative from F1. The map also shows three red surfaces on the benzene group and on both cycles (cyclopentadiene) of ferrocene group, that makes them the best sites for the electrophilic attack especially the benzene group which involves in many reactions of synthesis new derivatives.

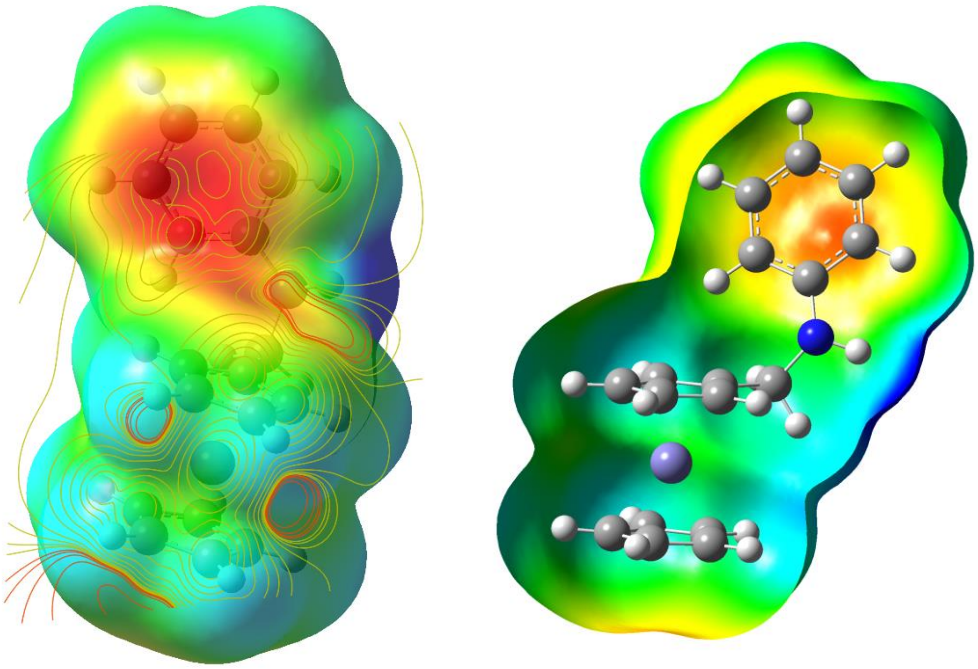

Figure IV-14 MESP Surface and contour map for F1.

MESP Surface and contour map of all the derivatives are listed below.

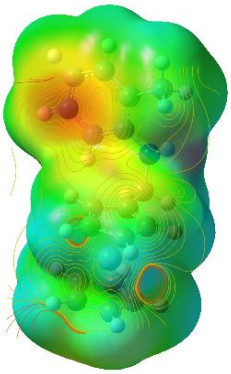	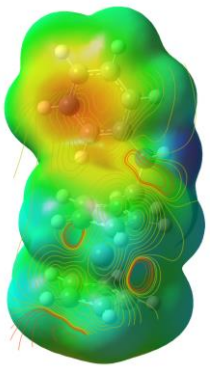	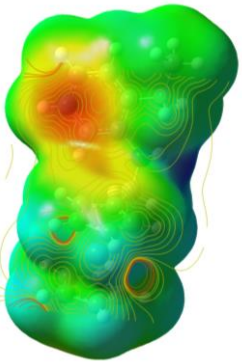
F2	F3	F4
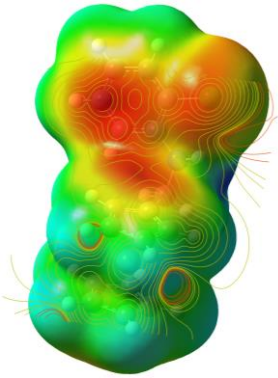	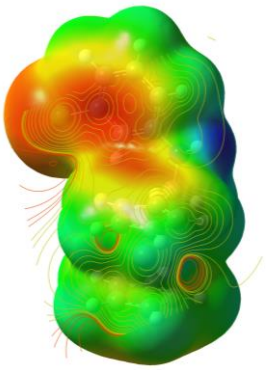	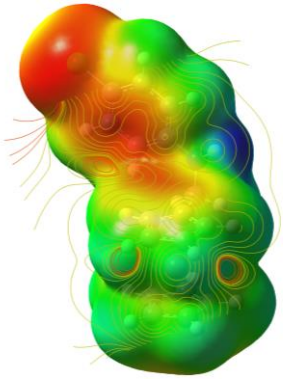
F5	F6	F7

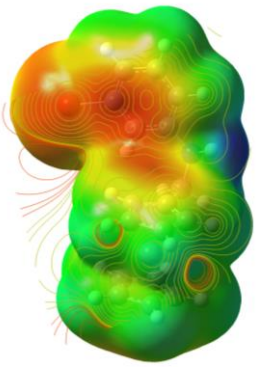		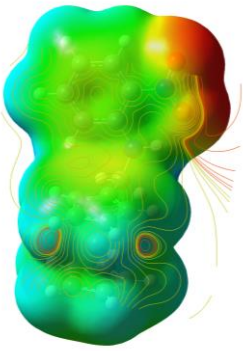
F8	F9	F10
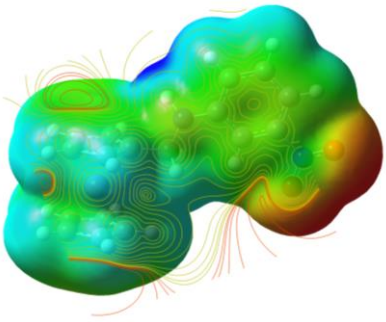	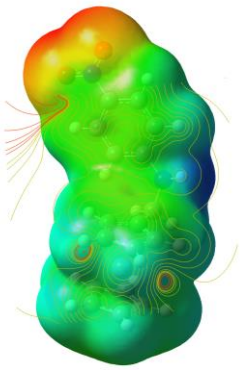	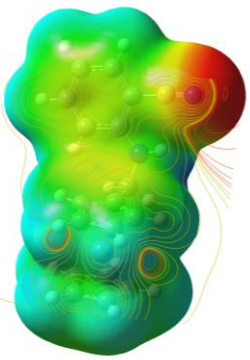
F11	F12	F13
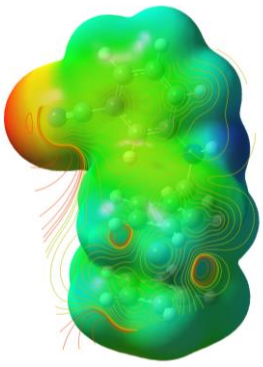	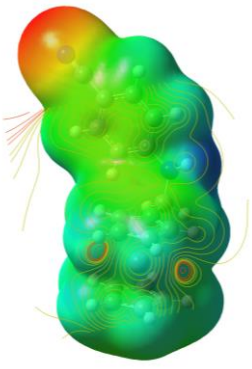	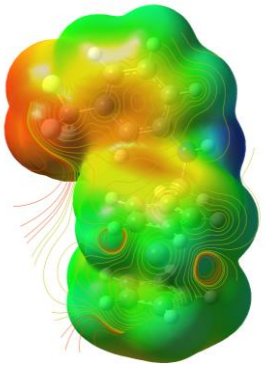
F14	F15	F16
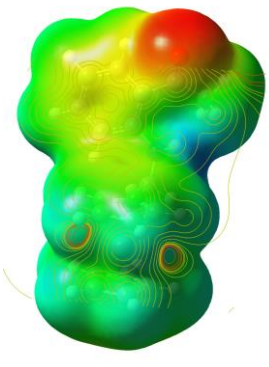	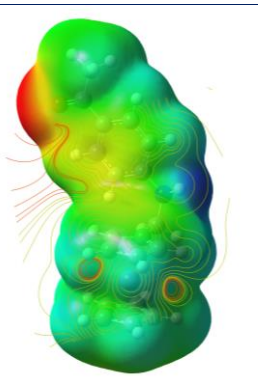	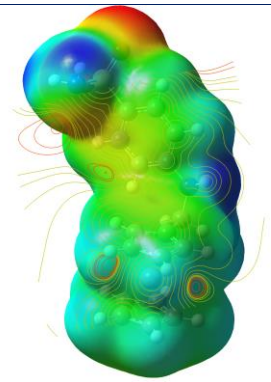
F17	F18	F19

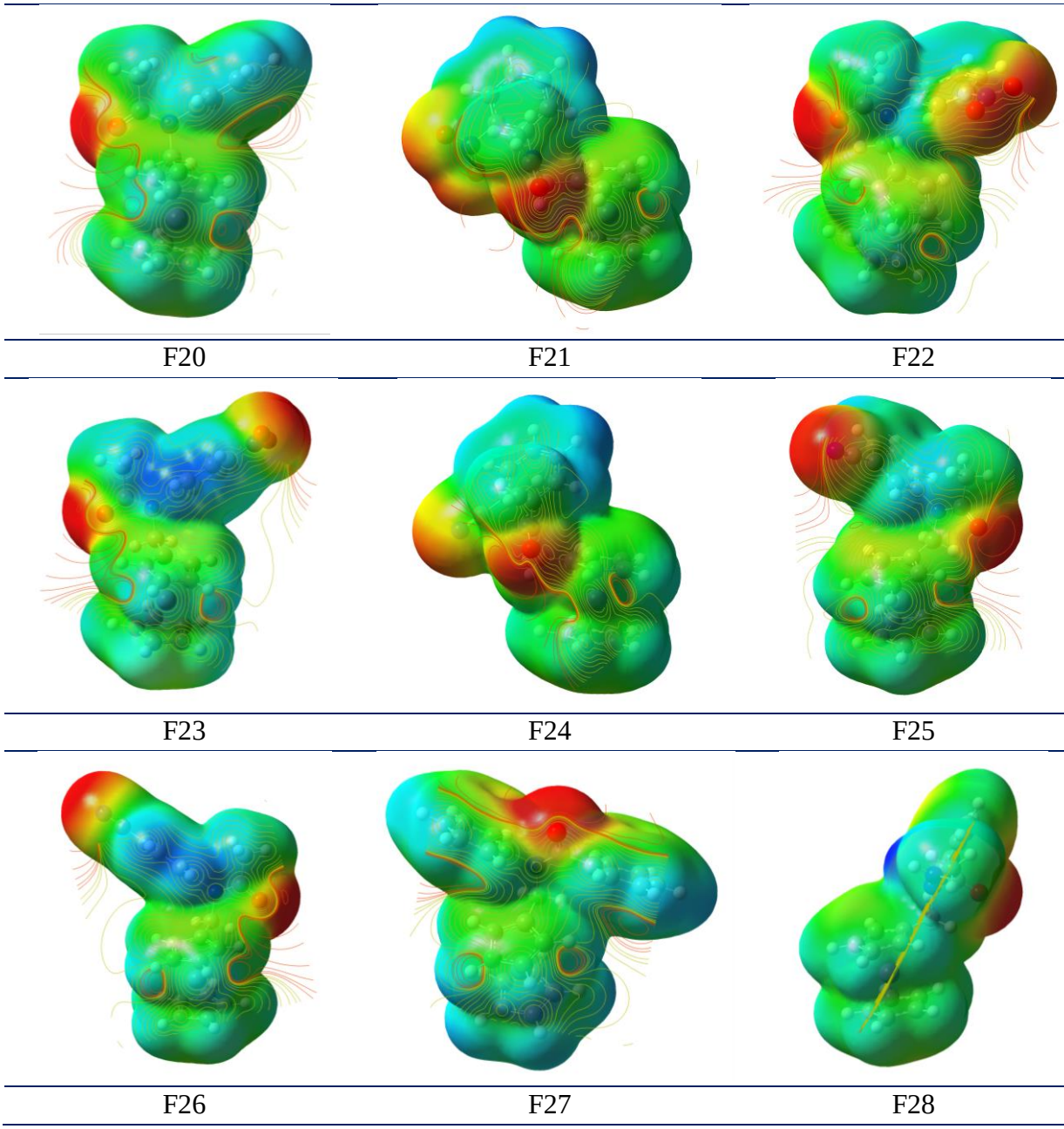

Figure IV-15 MESP Surface and contour map of N-ferrocenylmethylaniline derivatives

IV.8. Energies of the Frontier Molecular Orbitals HOMO and LUMO

Basically, all species (atoms, ions, molecules) are considered to have frontier orbitals which are simply the highest energy (HO) and lowest unoccupied energy (LU) occupied orbitals. When molecular orbits are involved, the abbreviations HOMO and LUMO are used. The kinetic characteristics of the reagents and reactions are assessed by considering only FMO interactions. The energy difference between the highest energy occupied molecular orbit (HOMO) of a molecule and its lowest unoccupied molecular orbit (LUMO) is known as HOMO-LUMO gap.

HOMO, LUMO and HOMO-LUMO gap of F1 were calculated at the mentioned DFT high theoretical level. The energies and the contour diagrams of these molecular orbitals are shown in

Figure IV-16. The diagram shows that HOMO is around the iron of ferrocene part of F1 and its energy is equal to -5.437 eV. On the other hand, the LUMO is distributed around the benzene part and its energy is -0.506 eV. HOMO-LUMO gap (ΔG) of the derivative F1 is equal to 4.931 eV. F1 derivative then is reactive and its reactivity is considerable.

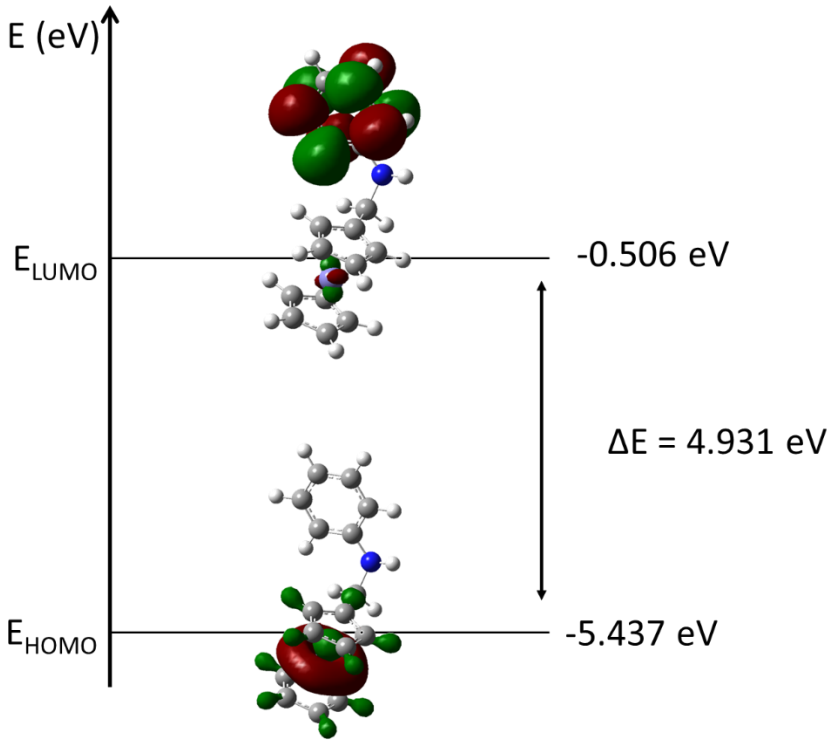

Figure IV-16 HOMO, LUMO and HOMO-LUMO gap of F1

HOMO, LUMO and HOMO-LUMO gap (ΔE) values of all the derivatives are tabulated in Table IV-6.

Table IV-6 The calculated HOMO, LUMO and HOMO-LUMO gap of N-ferrocenylmethylaniline derivatives

Code	-E_{HOMO} (eV)	-E_{LUMO} (eV)	ΔE (eV)	Code	-E_{HOMO} (eV)	-E_{LUMO} (eV)	ΔE (eV)
F1	5.437	0.506	4.931	F15	5.852	1.131	4.721
F2	5.341	0.501	4.840	F16	5.703	0.982	4.721
F3	5.412	0.502	4.910	F17	5.726	1.528	4.197
F4	5.314	0.494	4.819	F18	5.712	1.345	4.368
F5	5.584	0.553	5.031	F19	5.815	0.903	4.911
F6	5.628	0.594	5.034	F20	5.528	0.880	4.648
F7	5.548	0.619	4.929	F21	5.634	2.959	2.676
F8	5.641	0.595	5.046	F22	5.694	3.096	2.598

Code	$-E_{HOMO}$ (eV)	$-E_{LUMO}$ (eV)	ΔE (eV)	Code	$-E_{HOMO}$ (eV)	$-E_{LUMO}$ (eV)	ΔE (eV)
F9	5.574	0.633	4.941	F23	5.757	3.092	2.665
F10	5.837	2.555	3.282	F24	5.634	2.068	3.566
F11	5.889	2.632	3.257	F25	5.685	2.062	3.623
F12	5.937	2.335	3.602	F26	5.729	2.089	3.640
F13	5.777	1.397	4.380	F27	5.696	1.031	4.665
F14	5.774	1.488	4.286	F28	5.606	0.553	5.053

A molecule with a high frontier orbital gap (HOMO-LUMO energy gap) has low chemical reactivity and high kinetic stability and versa [288-290], because it is energetically unfavorable to add an electron to the high-lying LUMO in order to remove electrons from the low-lying HOMO. Among the 28 derivatives some of them are predicted to be more reactive than others as F10-F12 and F21-F26 where it is obvious that their HOMO-LUMO gaps are lower.

IV.9. ADME and Pharmacokinetics properties

In pharmacokinetics and pharmacology, ADME is an abbreviation for "absorption, distribution, metabolism, and excretion" which explains the disposition of a pharmacological substance in an organism [291]. Development of new drugs were shown to be caused by the undesirable pharmacokinetic properties of these drugs, therefore, it has been increasingly demanded to evolve new approaches that are able to predict drugs ADME properties [292].

SwissADME webserver was used to study the ADME and Pharmacokinetics properties, this webserver allows computing physicochemical descriptors and estimate ADME parameters, pharmacokinetic properties, druglike nature of N-ferrocenylmethylaniline derivatives, ensuring that they are not only promising candidates in terms of biological efficacy but also pharmacokinetics [293].

IV.9.1. Pharmacokinetic properties

Pharmacokinetics is one of the major branches of pharmacology. It refers to the way that the body reacts on and affects a pharmaceutical substance in it. When a drug enters the body, it will be soon recognaised by the body and processes it in a special way, according to its characteristics. The information that provided by a pharmacokinetics study is very necessary to improve the administration and use of medicines [294, 295].

Every drug takes the oral rout has a set of conditions that must be fulfilled to be effective, one of these conditions is the need to across the gut wall. The absorption of substance across this

wall is a complex process, that is why gastrointestinal drug absorption (GI absorption) is one of the most important conditions that the drug needs to achieve [296].

Drugs directed to the brain to treat certain neurodegenerative diseases such as Alzheimer's disease and Parkinson’s disease or to treat Inflammatory diseases (Infection, Multiple sclerosis and Brain tumors), these drugs need to be able to across the blood–brain barrier (BBB) and this condition is as much important as the first one in our candidates to treat the oxidation reactions that occur in the brain [297].

P-glycoprotein (Pgp) is an important protein of the cell membrane that pumps many foreign substances out of cells. The importance of this protein is to transport drugs across the cell membrane, its ability to transport drugs accounts for regulating the distribution and bioavailability of drugs [298].

Cytochromes P450 (CYPs) are a super family of enzymes that oxidize steroids, fatty acids, and xenobiotics [299, 300]. The importance of these enzymes in pharmacokinetics is that they are the main enzymes involved in drug metabolism, accounting for about 75% of the total metabolism. effects on CYP isozyme activity are a major source of adverse drug interaction, since changes in CYP enzymes activity may affect the metabolism of various drugs [301].

It can be seen from Table IV-7 that most of the derivatives are strongly drug candidates due to their ability to across the gut wall which allows them to take the oral route except F16. They also have the ability to pass the Blood-Brain Barrier except F16 and F19. Moreover, the results show that only F10-F12, F19, F21-F23 are not predicted to be Pgp substrate while all the rest are predicted to be Pgp substrate which can allow them across the cell membrane. Also, the ADME prediction indicated that the most derivatives are not CYP inhibitors, thus makes them good drug candidates, although some derivatives have been considered as inhibitors of CYP1A2 and CYP3A4.

Table IV-7 ADME prediction of N-ferrocenylmethylaniline derivatives.

Compound	GI absorption	BBB permeant	Pgp substrate	CYP1A2 inhibitor	CYP2C19 inhibitor	CYP2C9 inhibitor	CYP2D6 inhibitor	CYP3A4 inhibitor
F1	High	Yes	Yes	No	No	No	No	No
F2	High	Yes	Yes	No	No	No	No	No
F3	High	Yes	Yes	No	No	No	No	No
F4	High	Yes	Yes	No	No	No	No	No

Compound	GI absorption	BBB permeant	Pgp substrate	CYP1A2 inhibitor	CYP2C19 inhibitor	CYP2C9 inhibitor	CYP2D6 inhibitor	CYP3A4 inhibitor
F5	High	Yes	Yes	Yes	No	No	No	No
F6	High	Yes	Yes	Yes	No	No	No	No
F7	High	Yes	Yes	Yes	No	No	No	No
F8	High	Yes	Yes	Yes	No	No	No	No
F9	High	Yes	Yes	Yes	No	No	No	No
F10	High	Yes	No	Yes	No	No	No	Yes
F11	High	Yes	No	Yes	No	No	No	No
F12	High	Yes	No	Yes	No	No	No	No
F13	High	Yes	Yes	Yes	No	No	No	No
F14	High	Yes	Yes	Yes	No	No	No	No
F15	High	Yes	Yes	Yes	No	No	No	No
F16	Low	No	Yes	No	No	No	No	No
F17	High	Yes	Yes	No	No	No	No	No
F18	High	Yes	Yes	No	No	No	No	No
F19	High	No	No	No	No	No	No	Yes
F20	High	Yes	Yes	No	No	No	No	No
F21	High	Yes	No	Yes	No	No	No	Yes
F22	High	Yes	No	Yes	No	No	No	Yes
F23	High	Yes	No	Yes	No	No	No	Yes
F24	High	Yes	Yes	No	No	No	No	No
F25	High	Yes	Yes	No	No	No	No	No
F26	High	Yes	Yes	No	No	No	No	No
F27	High	Yes	Yes	No	No	No	No	No
F28	High	Yes	Yes	No	Yes	No	No	No

IV.9.2. Drug-likeness properties

Oral administration is the most common of the possible routes of administration for a pharmacological molecule authorized by the US Food and Drug Administration (FDA). Rather of receiving an injection intravenously, a patient prefers to open the lid of a bottle and consume the tablets/capsules. Orally administered pharmaceuticals are swallowed, then travel through the human body on a long journey before they reach the interaction site and exert their pharmacological effect [302].

Table IV-8 shows the predicted results of all N-ferrocenylmethylaniline derivatives and their violations of the roles of Lipinski's (Pfizer) [303], Ghose's (Amgen) [304], Veber's (GSK) [305], Egan's (Pharmacia) [306] and Muegge's (Bayer) [307]. The results shows that most of the derivatives have the necessary characteristics and have no violations of the roles that allow them to be drug candidates. On the other hand, some of the compounds have shown 1 violation (MLOGP>4.15) with Lipinski rule of five. Furthermore, other derivatives such as F2-F8 shows other violations in Muegge rule (XLOGP3>5, Heteroatoms<2). Bioavailability score was predicted to be 0.55 for all derivatives, which means that all the derivatives have a good oral administration [308].

Table IV-8 Drug-likeness and bioavailability of N-ferrocenylmethylaniline derivatives.

Compound	Lipinski #violations	Ghose #violations	Veber #violations	Egan #violations	Muegge #violations	Bioavailability Score
F1	0	0	0	0	1	0.55
F2	0	0	0	0	2	0.55
F3	0	0	0	0	2	0.55
F4	1	0	0	0	2	0.55
F5	1	0	0	0	2	0.55
F6	1	0	0	0	2	0.55
F7	1	0	0	0	2	0.55
F8	1	0	0	0	2	0.55
F9	1	0	0	0	2	0.55
F10	0	0	0	0	1	0.55
F11	0	0	0	0	0	0.55
F12	0	0	0	0	0	0.55
F13	0	0	0	0	1	0.55
F14	0	0	0	0	0	0.55
F15	0	0	0	0	0	0.55
F16	1	1	0	1	2	0.55
F17	0	0	0	0	0	0.55
F18	0	0	0	0	0	0.55
F19	0	0	0	0	0	0.55
F20	0	0	0	0	0	0.55
F21	0	0	0	0	0	0.55
F22	0	0	0	0	0	0.55

Compound	Lipinski #violations	Ghose #violations	Veber #violations	Egan #violations	Muegge #violations	Bioavailability Score
F23	0	0	0	0	0	0.55
F24	0	0	0	0	0	0.55
F25	0	0	0	0	0	0.55
F26	0	0	0	0	0	0.55
F27	1	0	0	0	1	0.55
F28	0	0	0	0	0	0.55

IV.10. *In* silico toxicity studies

The *in silico* toxicity study aims to help in optimizing the compounds regarding its toxicity proprieties, the study could offer an important improvement to the awareness of full perspective of virtual screening for the identification of target compounds with negligible or no toxicity which may open a path for the selection of novel nontoxic N-ferrocenylmethylaniline derivatives with high antioxidant activity.

The *in silico* toxicity study of the derivatives was performed using ProTox-II webserver [309]. It aims to predict the hepatotoxicity (dili), carcinogenicity (carcino), immunotoxicity (immuno), mutagenicity (mutagen), and cytotoxicity (cyto), also it predicts the median lethal dose (LD50) and the toxicity class (TC). Paracetamol also have been studied as a standard (Table IV-9).

Table IV-9 In silico toxicity profiles of the most five potent compounds

Molecule	Dili	carcino	immuno	mutagen	cyto	LD50 (mg/Kg)	TC
Paracetamol	Active	Inactive	Inactive	Inactive	Inactive	338	4
F1	Inactive	Inactive	Inactive	Inactive	Inactive	300	3
F2	Inactive	Inactive	Active	Inactive	Inactive	400	4
F3	Inactive	Inactive	Active	Inactive	Inactive	400	4
F4	Inactive	Inactive	Inactive	Inactive	Inactive	920	4
F5	Inactive	Inactive	Active	Inactive	Inactive	500	4
F6	Inactive	Inactive	Active	Inactive	Inactive	700	4
F7	Inactive	Inactive	Active	Inactive	Inactive	700	4
F8	Inactive	Inactive	Active	Inactive	Inactive	300	3
F9	Inactive	Inactive	Active	Inactive	Inactive	300	3
F10	Inactive	Active	Active	Active	Inactive	300	3

Molecule	Dili	carcino	immuno	mutagen	cyto	LD50 (mg/Kg)	TC
F11	Inactive	Active	Active	Active	Inactive	300	3
F12	Inactive	Active	Active	Active	Inactive	400	4
F13	Inactive	Inactive	Inactive	Active	Inactive	400	4
F14	Inactive	Inactive	Inactive	Active	Inactive	400	4
F15	Inactive	Inactive	Inactive	Active	Inactive	400	4
F16	Inactive	Inactive	Active	Inactive	Inactive	500	4
F17	Inactive	Inactive	Active	Inactive	Inactive	1296	4
F18	Inactive	Inactive	Active	Inactive	Inactive	2400	5
F19	Inactive	Active	Inactive	Inactive	Inactive	3000	5
F20	Inactive	Inactive	Inactive	Inactive	Inactive	237	3
F21	Inactive	Active	Inactive	Active	Inactive	210	3
F22	Inactive	Active	Inactive	Active	Inactive	237	3
F23	Inactive	Active	Inactive	Active	Inactive	237	3
F24	Inactive	Inactive	Inactive	Inactive	Inactive	256	3
F25	Inactive	Inactive	Inactive	Inactive	Inactive	237	3
F26	Inactive	Inactive	Inactive	Inactive	Inactive	256	3
F27	Inactive	Active	Inactive	Inactive	Inactive	1500	4
F28	Inactive	Active	Inactive	Active	Inactive	1000	4

ProTox-II webserver successfully predicted the hepatoxicity of Paracetamol which is known [310]. F1, F4, F20, F24, F25 and F26 were predected non toxic derivatives with LD50 equal to 300, 920, 237, 256, 237 and 256 respectevly and their TC were 3, 4, 3, 3, 3 and 3 respectivly. The toxicity class of F14 and F27 was detected to be equal to 4 and were predicted as non-toxic in hepatotoxicity, immunotoxicity, mutagenicity, and cytotoxicity, F27 possess the highest LD50, compounds F21 and F23 were predicted as toxic in mutagenicity, finally compound F12 was predicted to be immunetoxic. All derivatives did not show any hepatotoxicity or cytotoxicity.

IV.11. Conclusion

The mixed basis sets of LanL2DZ(Fe)/6-31G(d) gave accurate results. That can be observed from values of R^2 of the comparison between the bond lengths and angles where R^2 was equal to 0.9992 and 0.9755 respectively. Also, the mixed basis sets show a high ability to predict the spectral properties. Moreover, the energetic properties such as HOMO, LUMO, and HOMO-LUMO gap have been calculated to predict the reactivity of the derivatives. Using Gaussian 09, the MESP maps have been also calculated to predict the reactive sites of the derivatives. basically,

the electrophilic sites concentrated on the nitrogen of the amine group of all derivatives where the nucleophilic sites predicted to be concentrated on the phenyl group.

ADME and Pharmacokinetics properties of N-ferrocenylmethylaniline derivatives have been predicted using SwissADME webserver tool, the predicted results show that most derivatives have the needed properties of bioavailability which nominates them to be strong drug candidates.

The *in-silico* toxicity study predicted the toxicity of the derivatives to put in mind their toxicity in order to select the best condidates as antioxidants.

CHAPTER V

ANTIOXIDANT ACTIVITY OF N-FERROCENYLMETHYLANILINE DERIVATIVES BY CYCLIC VOLTAMMETRY AND MOLECULAR DOCKING STUDIES

V.1. Introduction

Antioxidants appear today as the keys to longevity and our allies in the fight against modern diseases. These are protective elements that act as free radical scavengers [311]. These are produced daily by the body; they are very reactive compounds comprising a single electron, they are necessary for vital mechanisms but, they become harmful when they are in excess and induce certain damage at the level of the structure of the organs by causing an oxidative stress which contributes to the creation of different diseases such as cardiovascular disease, cancer, etc.

Defense systems make it possible to prevent free radical formation or to limit the resulting oxidation lesions. These systems can be endogenous or exogenous, of nutritional origin [312]. These systems depend on several molecules which called antioxidants. That makes the investigation of new antioxidants such an interesting research field.

Glutathione plays an essential antioxidant intracellular role [313] and is involved in elimination of reactive oxygen species and act as a scavenger for various oxygen radicals. The enzyme glutathione reductase (GR), also called glutathione-disulfide reductase, reduces the oxidized form of glutathione disulfide (GSSG) to the reduced glutathione form (GSH). Elevated levels of the ratio GSH / GSSG, intracellular signal transduction, elimination of free radicals and reactive oxygen species, and the preservation of intracellular redox status [314]. Thus, inhibition of glutathione reductase results to a decrease in GSH and an increase in GSSG and consequently high rate of GSH / GSSG, So, studding the glutathione reductase inhibition by potentially antioxidant compounds could serve as a good means for choosing antioxidants candidates. A good antioxidant candidate should inhibit glutathione reductase enzyme less. Therefor, molecular docking study will be performed to afford an insight about the inhibition and binding partialities of the most potent compounds with glutathione reductase.

V.2. Materials and Methods

The derivatives were dissolved in dimethylformamide (DMF), the concentrations of the derivatives are tabulated in Table V-1

Table V-1 the concentration of the derivatives in DMF

Code	C [mM]	Code	C [mM]	Code	C [mM]
F1	30.242	F11	60.981	F21	52.881
F2	9.2	F12	61.278	F22	79.321
F3	65.531	F13	48.072	F23	52.881
F4	73.928	F14	43.012	F24	55.832
F5	92.132	F15	117.018	F25	47.457
F6	107.487	F16	83.526	F26	60.019
F7	92.132	F17	108.04	F27	53.127
F8	232.388	F18	90.033	F28	117.738
F9	54.044	F19	86.428		
F10	63.956	F20	16.506		

V.2.1. Experimental devices

The electrochemical study was carried out at VTRS laboratory using a Voltalab 40 (PGZ 301) with the three-electrode assembly controlled by a microcomputer (Voltamaster 04 Software).

V.2.1.1. Classic three-electrode assembly

In all the experiments, the assembly with three electrodes was used: a reference electrode, an auxiliary electrode and a working electrode (the substrate).

V.2.1.1.1. Electrochemical cell

The cell used is in PYREX glass, with a capacity of 15 ml, a volume sufficient for the concentration of electroactive species to remain constant during handling. The latter has a double wall and a cover with 5 holes to pass the three electrodes, the gas tube and the last hole to inject the derivatives into the solution.

V.2.1.1.2. Electrodes

- The working electrode: a glassy carbon electrode of an area equal to 0.013 cm^2
- The auxiliary electrode (counter electrode): a platinum wire was used as a counter electrode.
- The reference electrode: all the potential measurements are taken in relation to the saturated calomel electrode (SCE) with potassium chloride KCl, constituted by the calomel system (mercurous chloride / mercury + potassium chloride) represented by:

$$Hg_2Cl_2 \downarrow +2e^- \Leftrightarrow 2Hg \downarrow +2Cl^- \qquad \textit{Equation V-1}$$

Its potential in relation to the normal hydrogen electrode is equal to +0.2444 V at 25 °C.

V.2.1.1.3. Electrolyte

In general, solutions are used which contain electroactive species, a completely dissociated support electrolyte salt allowing the solution to be saturated. Under these conditions the trace of a voltammogram is from a few milliseconds to a few minutes. In order to remove dissolved oxygen when needed, the generally used procedure is to bubble an inert gas for a few minutes [315].

In all electrochemical processes, there are several types of phenomena associated with a transfer of electric charge at the interfaces formed by the contacting of electrodes (electronic conduction) and an electrolyte (ionic conduction). During this charge transfer, chemical transformation (redox) is occurring (Figure V-1).

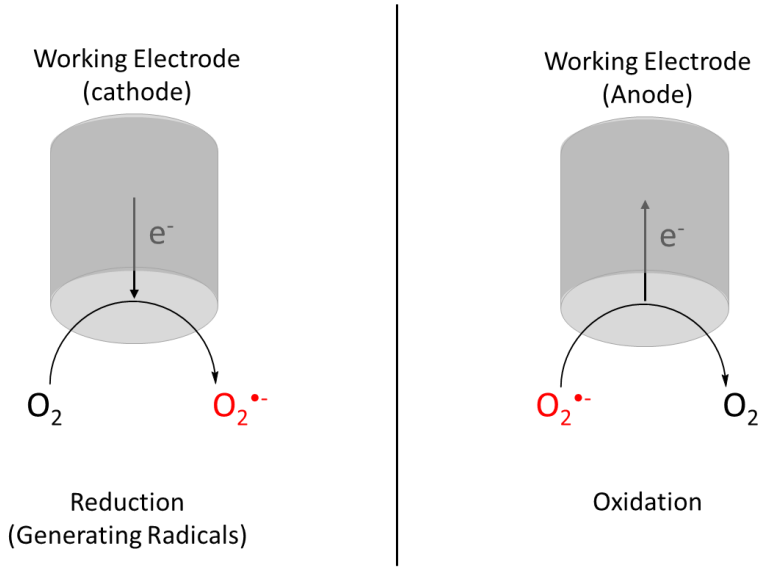

Figure V-1 charge transferring process between the electrode and the electrolyte

V.2.1.2. Experimental conditions

- The potential E: -1600 up to 0 mV.
- Scanning speed is constant: 100 mV/s.
- The solvent: Dimethylformamide (DMF).
- Supporting electrolyte: Tetrabutylammonium tetrafluoroborate ($C_{16}H_{36}BF_4N$).

V.3. Results and discussion

V.3.1. Electrochemical study of the behavior of the electrolyte

Before starting the electrochemical study of our system, the solution has been examined in the absence of O_2 in order to determine its electroactivity domain. For the plotting of the cyclic voltammetry curves, a potential sweep has been performed between 0 and -1600 mV, to analyze the electrochemical behavior of our electrolyte. The shape of the cyclic voltammogram is given in Figure V-2.

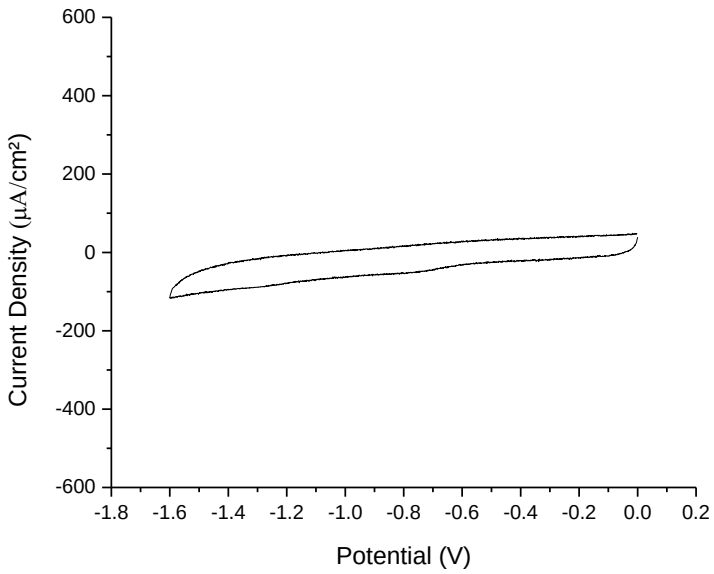

Figure V-2 cyclic voltammogram of the electrolyte

This voltammogram prove that there are no other reactions that can occur during the experiment in the electrolyte which could mislead the results. Therefore, the only reactions that can occur in the electrolyte are the redox reactions of the superoxide anion.

V.3.2. Electrochemical study of the behavior of the complex (F-$O_2^{\bullet-}$)

After getting a voltamogramm of the solution in the presence of only the support electrolyte, O_2 was then bubbled into the solution and a second voltammogram of O_2 was obtained under the same conditions. Then, this experiment was reapeted after successive addition of a solution of each ferrocene derivative, the volume of each addition is equal to 1ml.

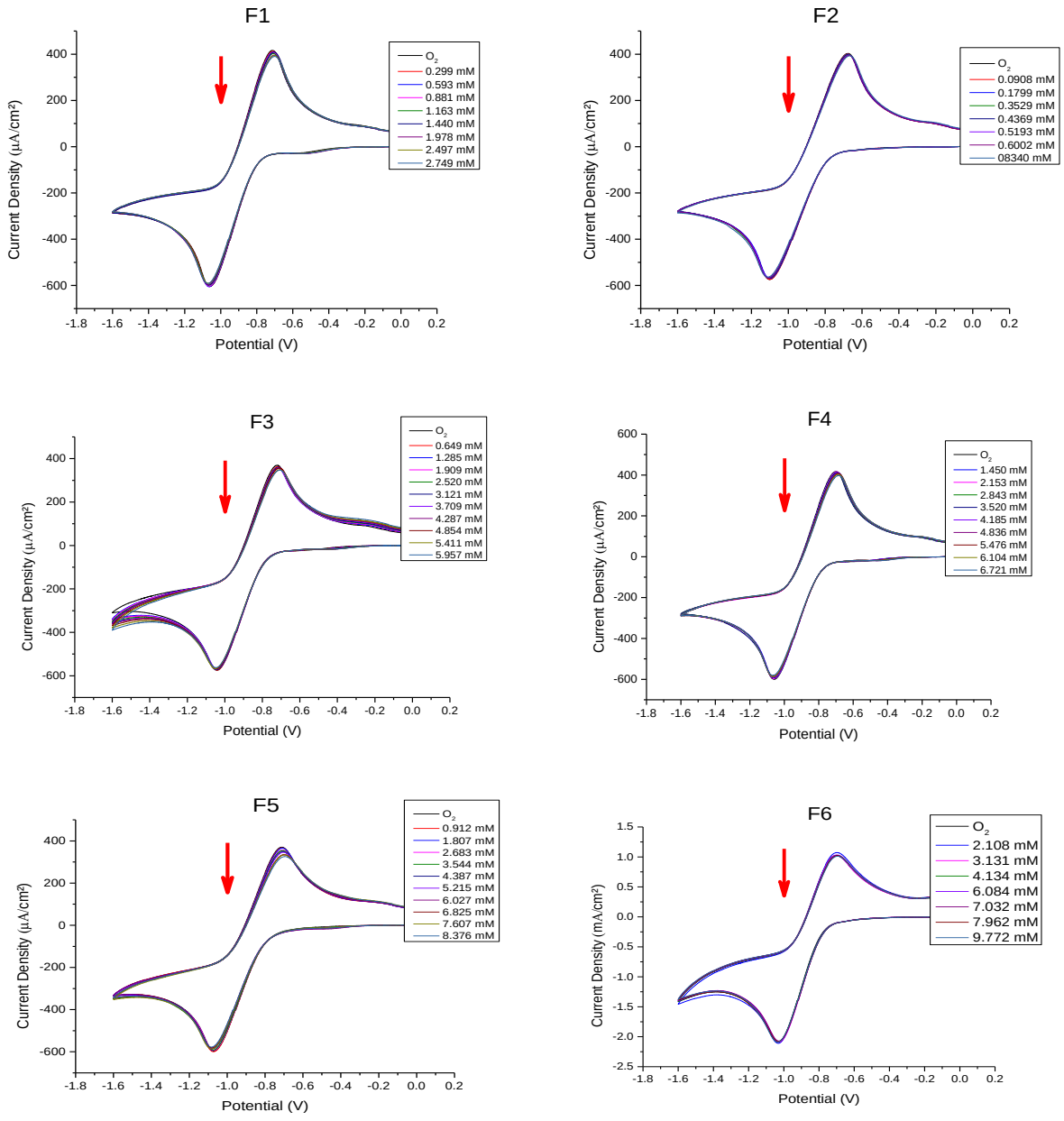

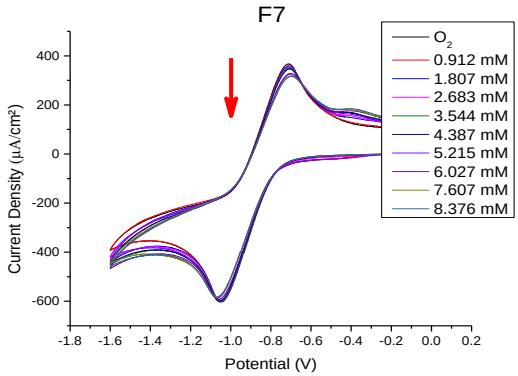
F7
O2
0.912 mM
1.807 mM
2.683 mM
3.544 mM
4.387 mM
5.215 mM
6.027 mM
7.607 mM
8.376 mM
Current Density (μA/cm²)
Potential (V)

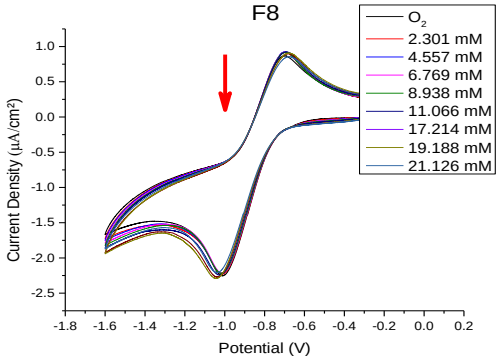
F8
O2
2.301 mM
4.557 mM
6.769 mM
8.938 mM
11.066 mM
17.214 mM
19.188 mM
21.126 mM
Current Density (μA/cm²)
Potential (V)

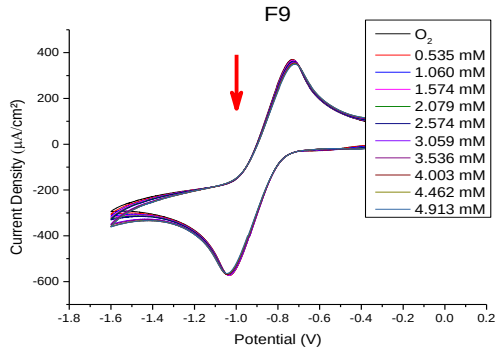
F9
O2
0.535 mM
1.060 mM
1.574 mM
2.079 mM
2.574 mM
3.059 mM
3.536 mM
4.003 mM
4.462 mM
4.913 mM
Current Density (μA/cm²)
Potential (V)

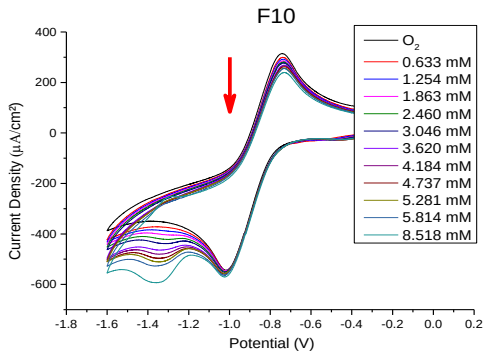
F10
O2
0.633 mM
1.254 mM
1.863 mM
2.460 mM
3.046 mM
3.620 mM
4.184 mM
4.737 mM
5.281 mM
5.814 mM
8.518 mM
Current Density (μA/cm²)
Potential (V)

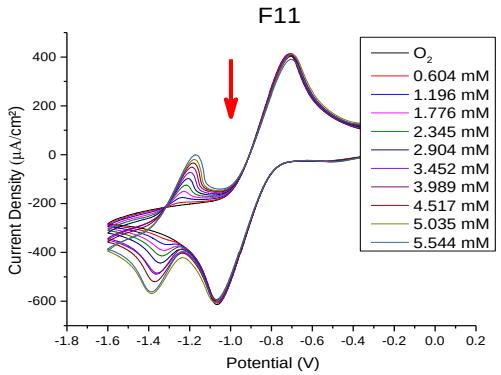
F11
O2
0.604 mM
1.196 mM
1.776 mM
2.345 mM
2.904 mM
3.452 mM
3.989 mM
4.517 mM
5.035 mM
5.544 mM
Current Density (μA/cm²)
Potential (V)

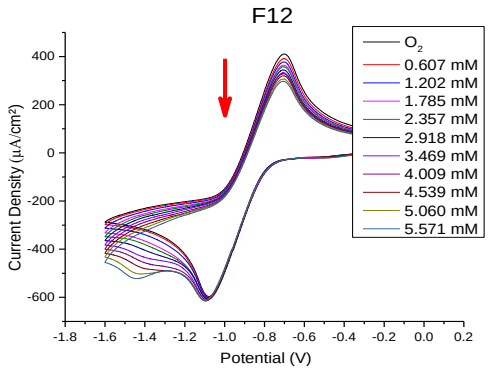
F12
O2
0.607 mM
1.202 mM
1.785 mM
2.357 mM
2.918 mM
3.469 mM
4.009 mM
4.539 mM
5.060 mM
5.571 mM
Current Density (μA/cm²)
Potential (V)

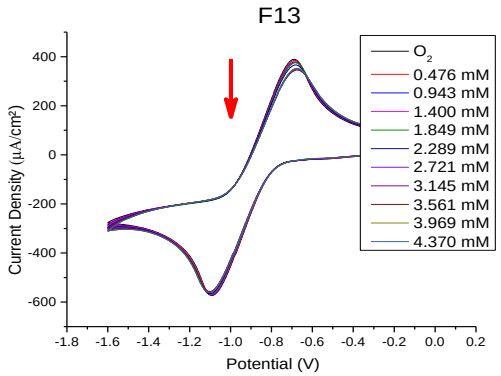
F13
O2
0.476 mM
0.943 mM
1.400 mM
1.849 mM
2.289 mM
2.721 mM
3.145 mM
3.561 mM
3.969 mM
4.370 mM
Current Density (μA/cm²)
Potential (V)

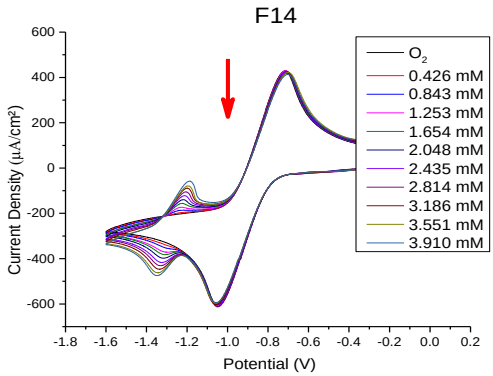
F14
O2
0.426 mM
0.843 mM
1.253 mM
1.654 mM
2.048 mM
2.435 mM
2.814 mM
3.186 mM
3.551 mM
3.910 mM
Current Density (μA/cm²)
Potential (V)

F15

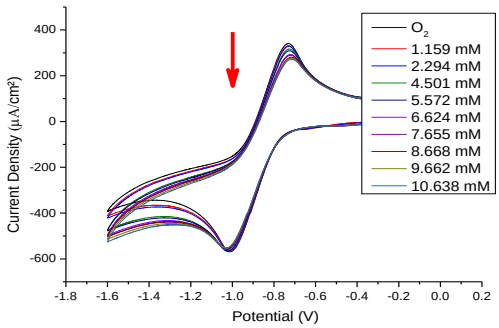

F16

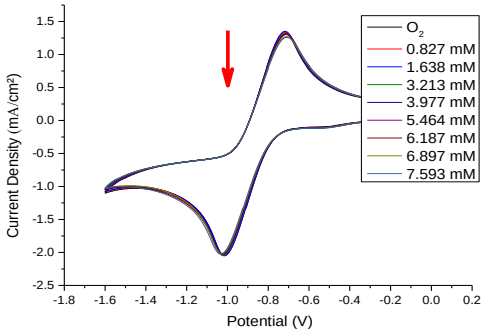

F17

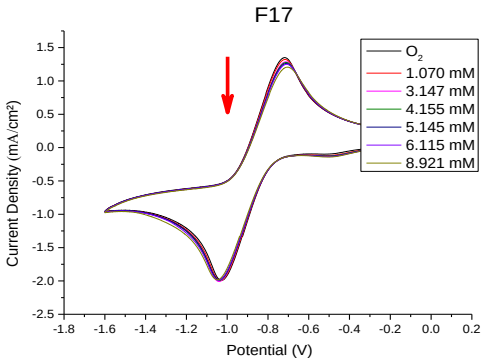

F18

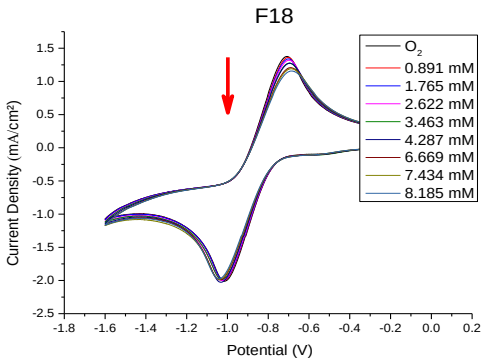

F19

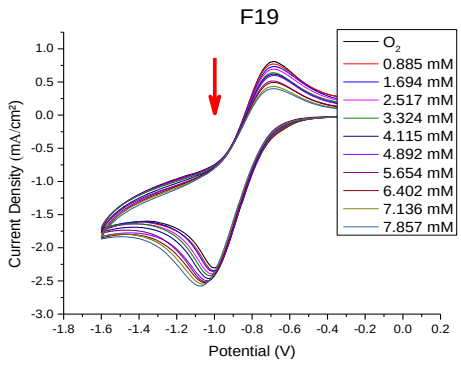

F20

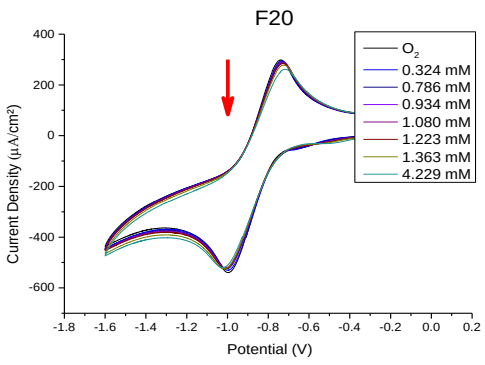

F21

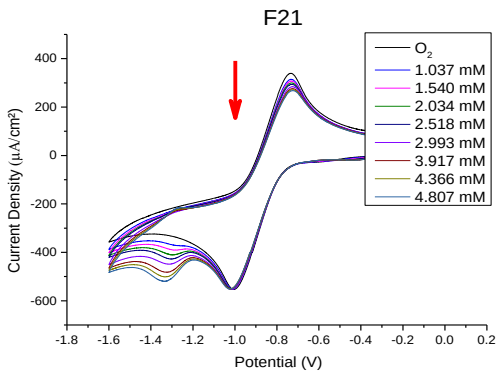

F22

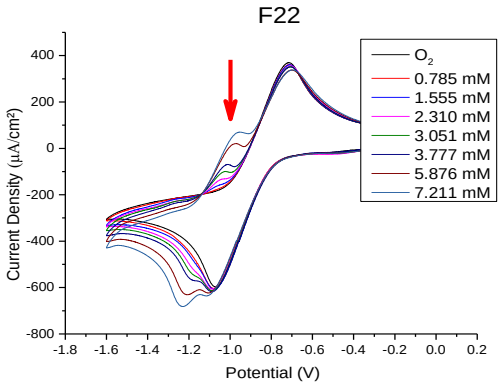

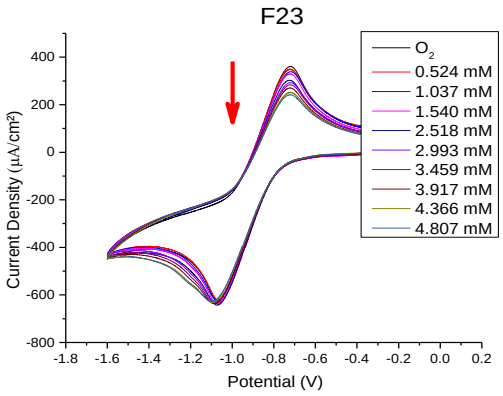

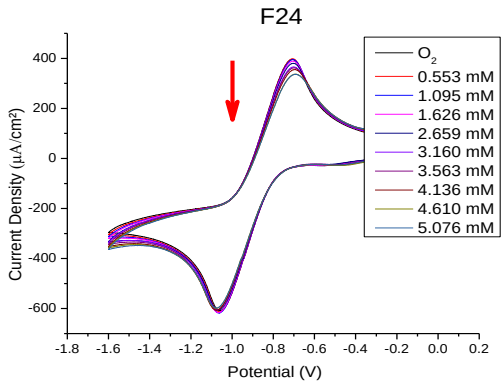

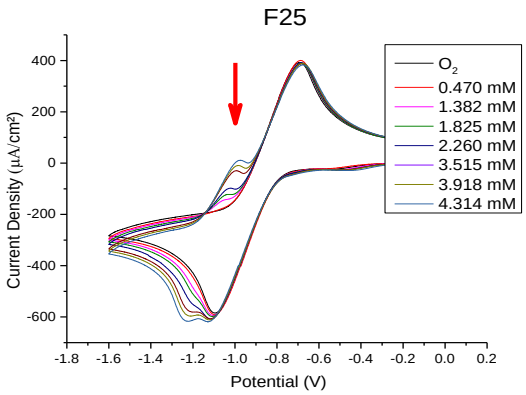

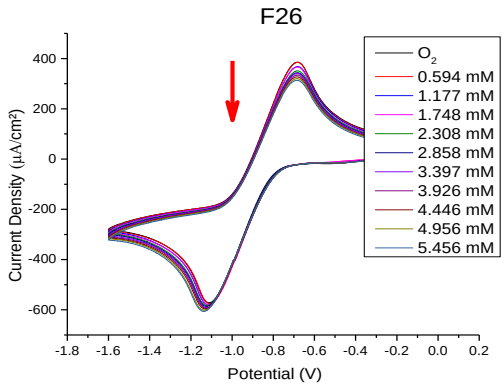

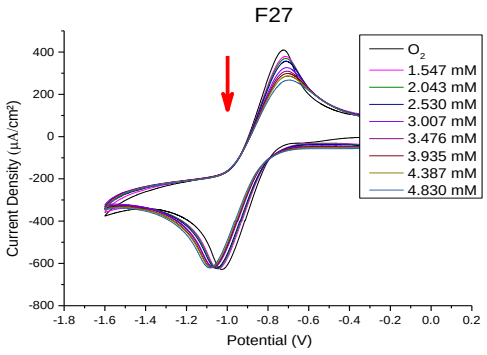

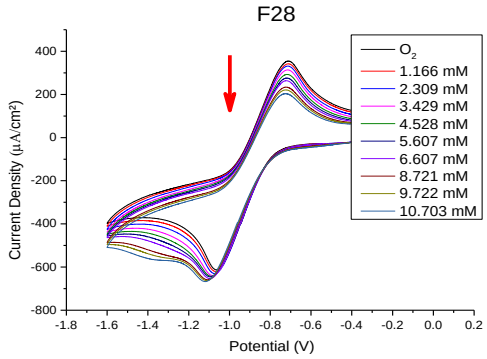

The reduction peak is obviously stable in every addition of the derivatives which means that initial amount of O_2 is the same in every cycle, the fixed amount of O_2 in the solution gives us the same concentration of the superoxide radical in the reduction process of O_2. Therefore, it is possible to compare the oxidation peak of each addition to each other. Most of the voltammograms shows a good response upon addition of ferrocene derivatives, the decreasing of the oxidation peak is clearly observed for compounds F12, F15, F19, F21, F23, F27 and F28.

From these voltammograms the binding constant (K), the free binding energy (ΔG), the diffusion coefficient (D) and the half-maximal inhibitory concentration (IC50) were calculated.

V.3.3. Binding constant (K)

The bonding affinity between two or more molecules at equilibrium is measured by a binding constant, which is a special case of general equilibrium constants. According to authors of references [5, 316, 317] K is calculated using the following equation:

$$\log\left(\frac{1}{[F]}\right) = \log\left(\frac{i}{i_0 - i}\right) + \log(K) \qquad \textit{Equation V-2}$$

where K is the apparent binding constant, i_0 and i are the peak current of the free radical ($O_2^{\bullet-}$) and the complex (F-$O_2^{\bullet-}$), respectively. Under the assumption of reversible, diffusion-controlled electron transfer and the complex F-$O_2^{\bullet-}$ is a 1:1 association complex, then the plot of log(1/[F]) versus log(i/(i$_0$-i)) becomes linear with the intercept of log(K) (Equation V-2).

The plots of log(1/[F]) versus log(i/(i$_0$-i)) used to calculate the binding constants of each derivative with $O_2^{\bullet-}$ are represented in Figure V-3, and the values of K are tabulated in Table V-2.

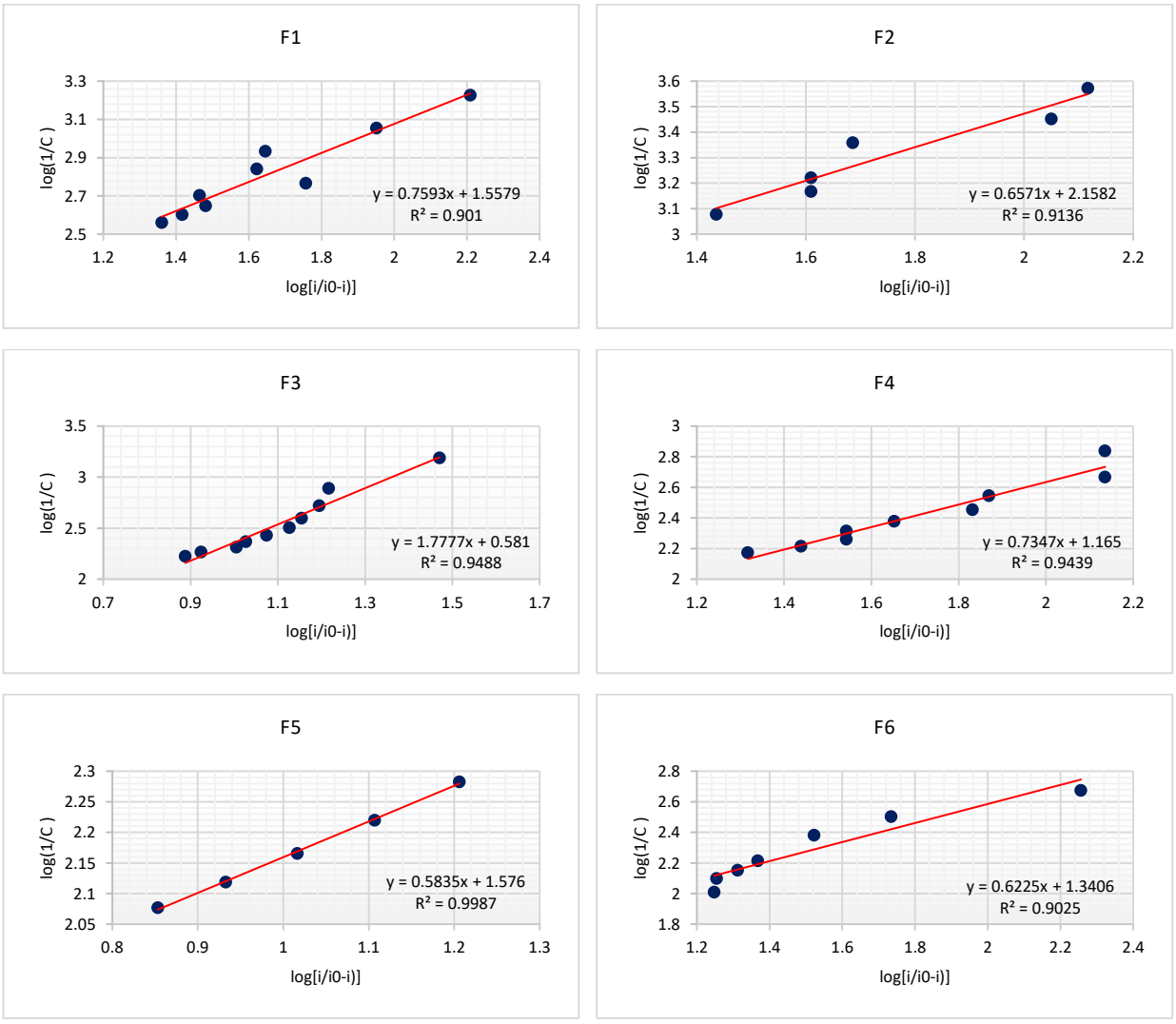

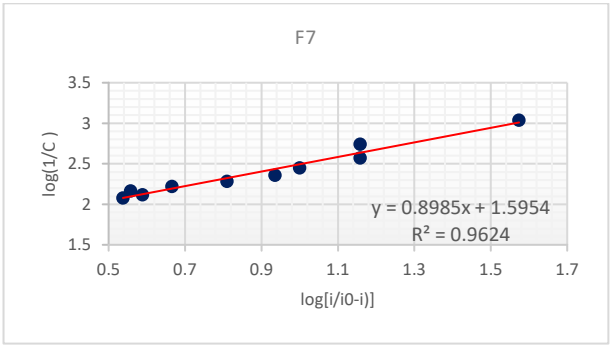
F7
log(1/C)
log[i/i0-i)]
y = 0.8985x + 1.5954
R² = 0.9624

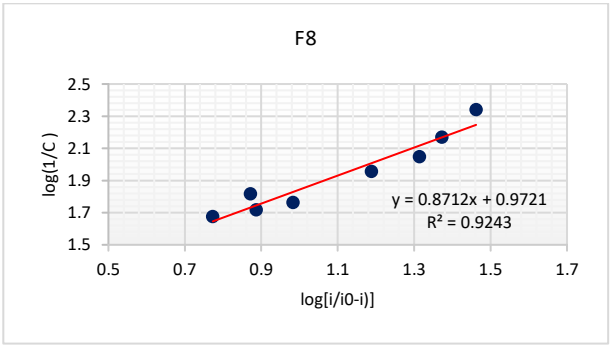
F8
log(1/C)
log[i/i0-i)]
y = 0.8712x + 0.9721
R² = 0.9243

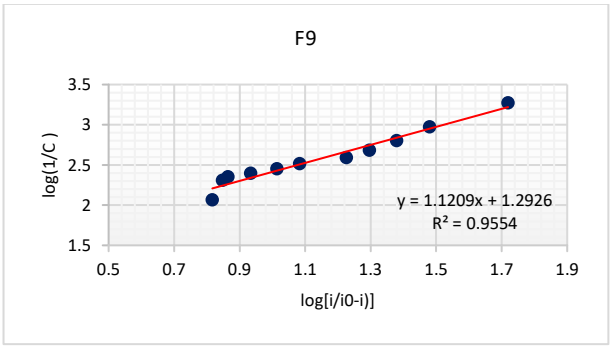
F9
log(1/C)
log[i/i0-i)]
y = 1.1209x + 1.2926
R² = 0.9554

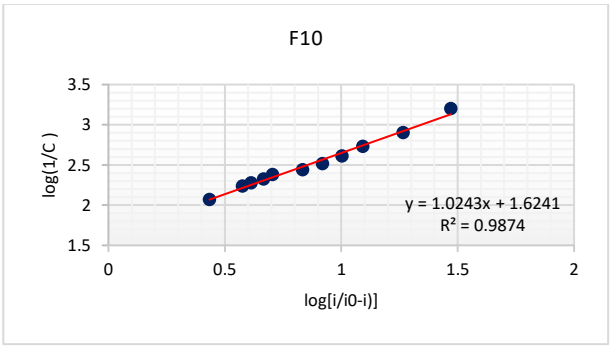
F10
log(1/C)
log[i/i0-i)]
y = 1.0243x + 1.6241
R² = 0.9874

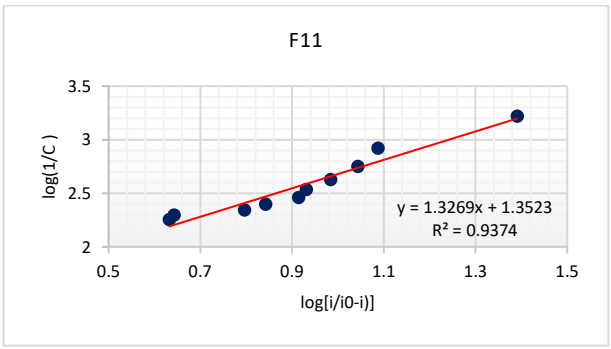
F11
log(1/C)
log[i/i0-i)]
y = 1.3269x + 1.3523
R² = 0.9374

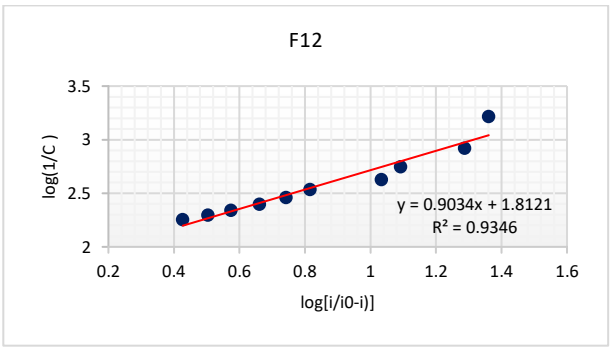
F12
log(1/C)
log[i/i0-i)]
y = 0.9034x + 1.8121
R² = 0.9346

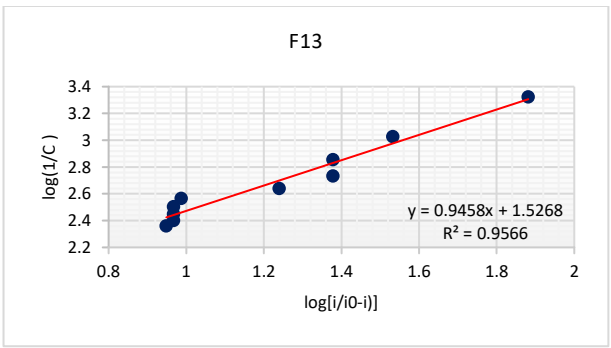
F13
log(1/C)
log[i/i0-i)]
y = 0.9458x + 1.5268
R² = 0.9566

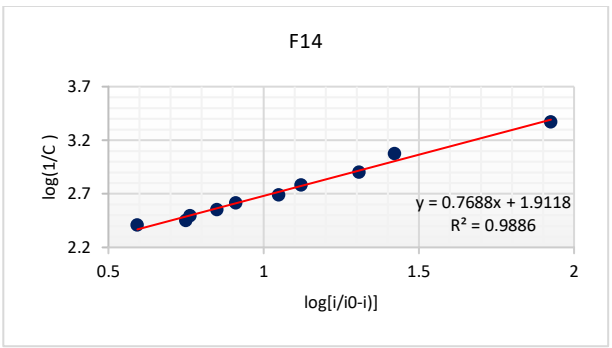
F14
log(1/C)
log[i/i0-i)]
y = 0.7688x + 1.9118
R² = 0.9886

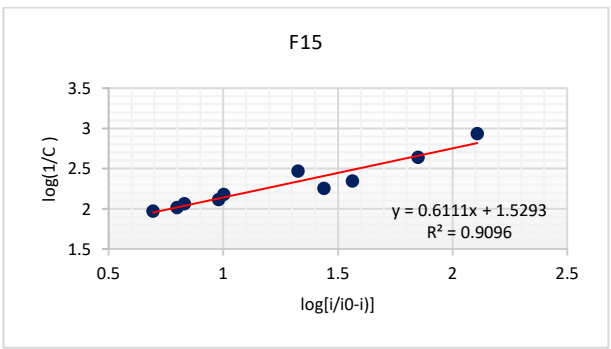
F15
log(1/C)
log[i/i0-i)]
y = 0.6111x + 1.5293
R² = 0.9096

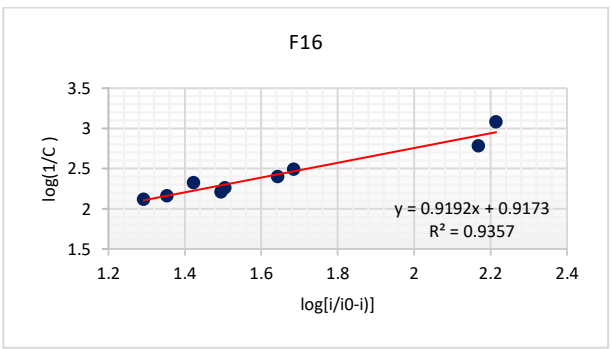
F16
log(1/C)
log[i/i0-i)]
y = 0.9192x + 0.9173
R² = 0.9357

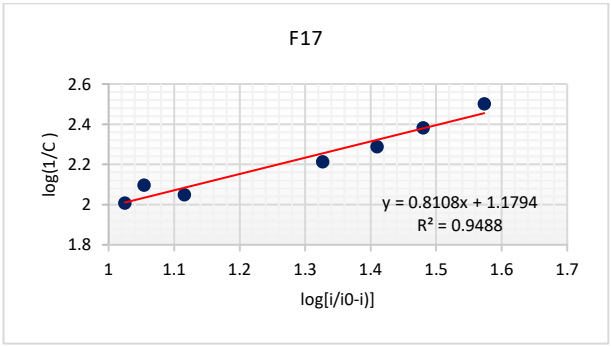
F17
log(1/C)
log[i/i0-i)]
y = 0.8108x + 1.1794
R² = 0.9488

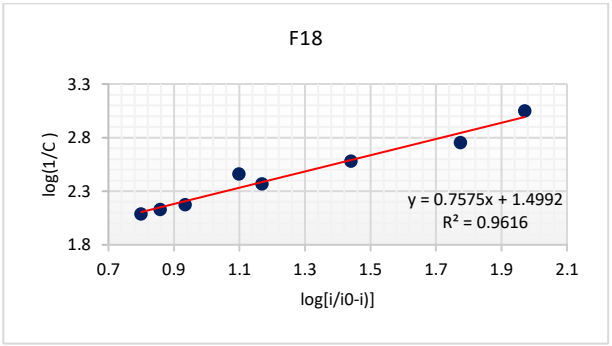
F18
log(1/C)
log[i/i0-i)]
y = 0.7575x + 1.4992
R² = 0.9616

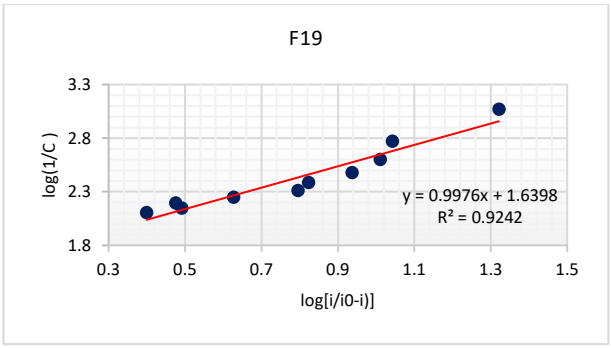
F19
log(1/C)
log[i/i0-i)]
y = 0.9976x + 1.6398
R² = 0.9242

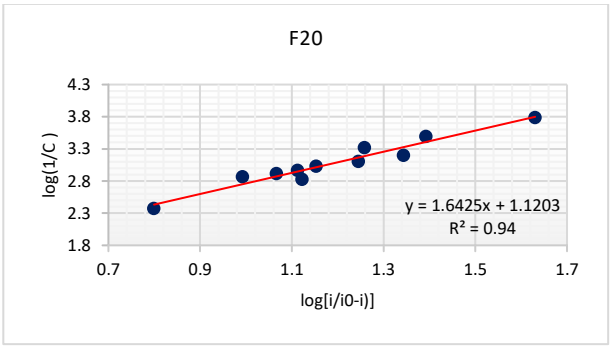
F20
log(1/C)
log[i/i0-i)]
y = 1.6425x + 1.1203
R² = 0.94

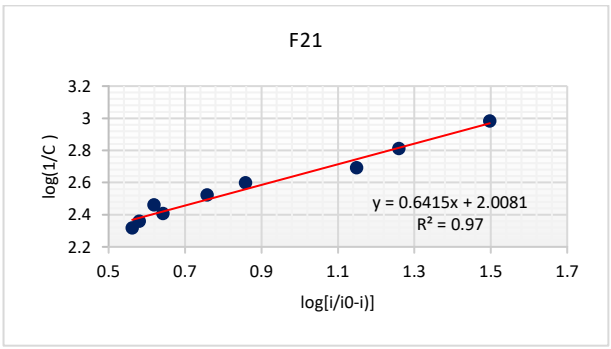
F21
log(1/C)
log[i/i0-i)]
y = 0.6415x + 2.0081
R² = 0.97

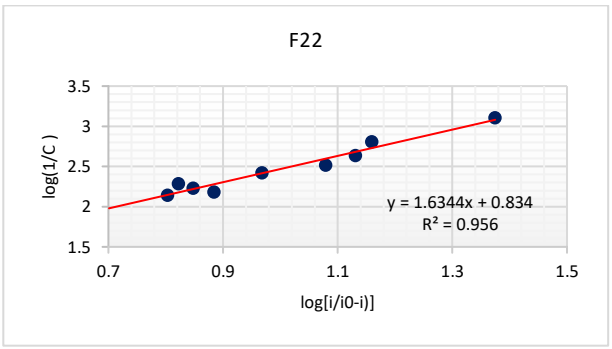
F22
log(1/C)
log[i/i0-i)]
y = 1.6344x + 0.834
R² = 0.956

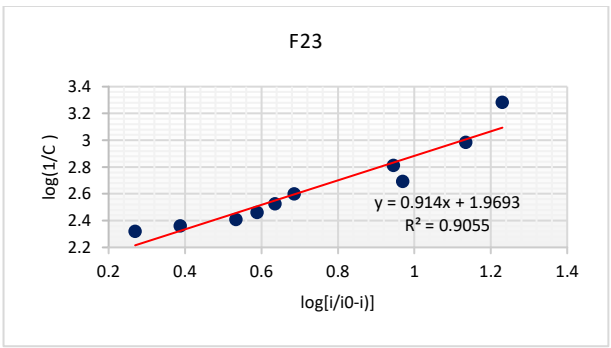
F23
log(1/C)
log[i/i0-i)]
y = 0.914x + 1.9693
R² = 0.9055

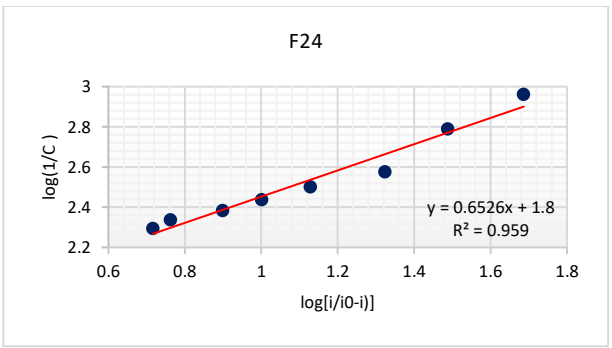
F24
log(1/C)
log[i/i0-i)]
y = 0.6526x + 1.8
R² = 0.959

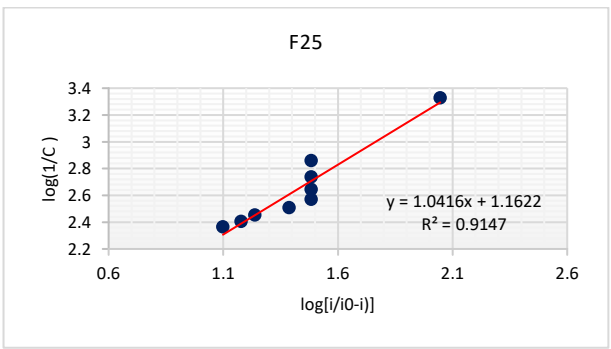
F25
log(1/C)
log[i/i0-i)]
y = 1.0416x + 1.1622
R² = 0.9147

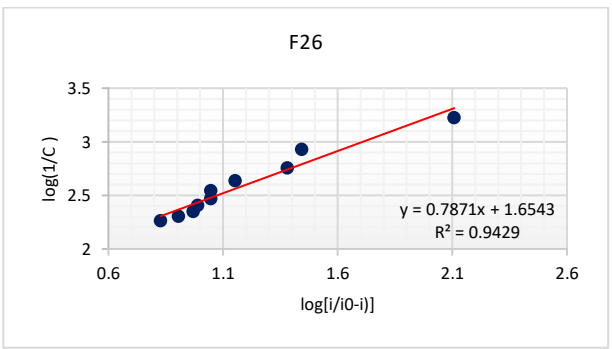
F26
log(1/C)
log[i/i0-i)]
y = 0.7871x + 1.6543
R² = 0.9429

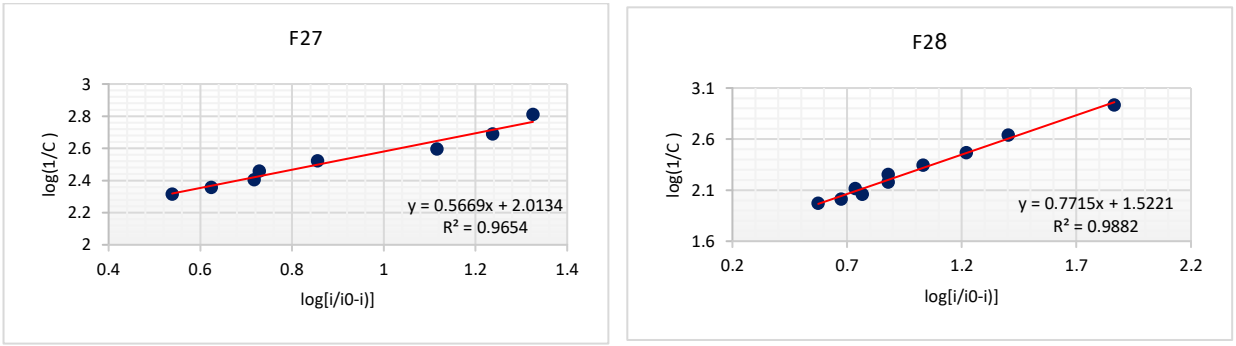

Figure V-3 plots of log(1/[N-ferrocenylmethylaniline Derivative]) versus log(i/(i$_0$-i)) of each derivative

All the results have good R^2 values between 0.9010 and 0.9987. It can be seen from Table V-2 that F2, F21and F27 had the highest values of K which equal to 143.95 M^{-1}, 101.89 M^{-1} and 103.14 M^{-1} respectively, where the smallest values belong to the binding of F3, F8, F16 and F22 which were between 3 and 9 M^{-1}.

Table V-2 binding constant of N-ferrocenylmethylaniline derivatives with the superoxide radical.

Code	K [M^{-1}]	R^2	Code	K [M^{-1}]	R^2	Code	K [M^{-1}]	R^2
F1	36.1364	0.9010	F11	22.5071	0.9374	F21	101.8880	0.9700
F2	143.9536	0.9136	F12	64.8739	0.9346	F22	6.8228	0.9560
F3	3.8108	0.9488	F13	33.6393	0.9566	F23	93.1798	0.9055
F4	14.6208	0.9439	F14	81.6259	0.9886	F24	63.0959	0.9590
F5	37.669	0.9987	F15	33.8337	0.9096	F25	14.5291	0.9147
F6	21.9091	0.9025	F16	8.2663	0.9357	F26	45.1163	0.9429
F7	39.3898	0.9624	F17	15.1131	0.9488	F27	103.1360	0.9654
F8	9.3785	0.9243	F18	31.5633	0.9616	F28	33.2720	0.9882
F9	24.5592	0.9705	F19	43.6316	0.9242			
F10	42.0157	0.9841	F20	16.8658	0.9083			

V.3.4. Free binding energy (ΔG)

The values of free binding energy ΔG were calculated from binding constant K, using the following Equation V-3:

$$\Delta G = -RT\ln(K) \qquad \textit{Equation V-3}$$

Where ΔG represents the binding free energy in KJ.mol^{-1}, R is the gas constant 8.31 J.$mol^{-1}K^{-1}$ and T is the absolute temperature 298 K.

The calculated values of ΔG are summerised in Table V-3. It can be seen from the obtained results that the interactions between the radical and ferrocene derivatives are physical interaction. The F-$O_2^{\bullet-}$ bond occurs through multiple noncovalent bonds: electrostatic, hydrogen, hydrophobic, and Van der Waals. Long-range forces such as electrostatic and hydrogen bonds are important in the rate of formation of F-$O_2^{\bullet-}$ complexes at the points of contact. The strongest interactions between the radical and the derivatives that observed are those with F2 (12.306 KJ/mol), F21 (11.450 KJ/mol), F23 (11.229 KJ/mol) and F26 (9.433 KJ/mol). On the other hand F3, F16 and F22 had the weakest interactions with the superoxide radical and their energy equal to 3.313, 5.231 and 4.755 respectively, these interactions are most likely to be Van der Waals interactions type.

Table V-3 Free binding energy of N-ferrocenylmethylaniline derivatives with the superoxide radical.

Code	-ΔG (KJ/mol)	Code	-ΔG (KJ/mol)	Code	-ΔG (KJ/mol)
F1	8.884	F11	7.711	F21	11.450
F2	12.306	F12	10.333	F22	4.755
F3	3.313	F13	8.706	F23	11.229
F4	6.643	F14	10.901	F24	10.264
F5	8.986	F15	8.720	F25	6.627
F6	7.644	F16	5.231	F26	9.433
F7	9.097	F17	6.725	F27	11.481
F8	5.543	F18	8.548	F28	8.679
F9	7.927	F19	9.350		
F10	9.257	F20	6.996		

V.3.5. Diffusion coefficient (D)

The scanning speed was varied between 5 values (100, 200, 300, 400 and 500 mV/s) for the blank solution ($O2^{\bullet-}$) and the F-$O_2^{\bullet-}$ complex in order to measure the current density of the oxidation using Randles-Sevcik equation [318] (Equation V-4)

$$i_{p,a} = 2.69.10^5.n^{\frac{3}{2}}.A.C.D^{\frac{1}{2}}.v^{\frac{1}{2}} \qquad \textit{Equation V-4}$$

Where $i_{p,a}$ is the anodic peak current in µA.cm^{-2}, n is the number of electrons transferred through the oxidation reaction, A is the surface area of the electrode in cm^2, C is the bulk concentration of the electroactive species within the electrolyte solution in mol.cm^{-3}, D is the diffusion coefficient in cm^2.s^{-1} and *v* is the scan rate in Vs^{-1}.

The values of anodic currents increase upon increasing the scan rate used to monitor the diffusion phenomena.. The diffusion coefficient D is obtained from the slop of the linear plot of the anodic current density versus thesequare root of the scan rate using Equation V-4

The measurement allows to know the diffusion coefficient D of the free radical and the F bounded radical. Thus, it becomes possible to determine the deference between the diffusion speed of the free and the F bonded radical which further confirm the interaction between the radical and the derivative.

All the obtained results of diffusion coefficient are tabulated in Table V-4, from this table it is obvious that the diffusion speeds of the complexes are slower than diffusion of the free radical $O2^{\bullet-}$. The percent decrease of the diffusion has been also calculated. F12, F19 and F28 gave the highest values of percent decrease 66.50 %, 95.19 % and 74.21 % respectively. It can be noted that the decrease in diffusion coefficient values of the complexe $F\text{-}O_2^{\bullet-}$ does not depend only on the molecular weight of the derivative attached to it, however the strength of the interactions between the radical and the derivative can be also considered.

Table V-4 Diffusion coefficient of the free and bonded radical

Code	D $\times 10^5$ O_2 [cm²/s]	D $\times 10^5$ O_2-D [cm²/s]	Decrease of D [%]	Code	D $\times 10^5$ O_2 [cm²/s]	D $\times 10^5$ O_2-D [cm²/s]	Decrease of D [%]
F1	10.30	8.23	20.09	F15	6.89	2.85	58.60
F2	5.32	5.21	1.99	F16	98.94	90.11	8.93
F3	9.11	8.30	8.83	F17	106.68	90.08	15.56
F4	9.55	7.68	19.60	F18	112.29	84.54	24.71
F5	6.83	5.55	18.70	F19	18.23	0.88	95.19
F6	69.99	61.97	11.47	F20	5.46	2.62	52.03
F7	9.28	4.78	48.47	F21	7.17	4.87	32.07
F8	55.32	31.63	42.82	F22	7.86	4.74	39.71
F9	8.78	7.94	9.61	F23	7.78	4.24	45.44
F10	5.95	3.82	35.74	F24	8.45	4.79	43.25
F11	10.05	8.32	17.20	F25	8.19	5.50	32.79
F12	8.47	2.84	66.50	F26	6.22	5.06	18.55
F13	7.48	6.06	19.00	F27	10.93	4.42	59.57
F14	11.44	10.64	6.97	F28	8.30	2.14	74.21

V.3.6. Half-maximal inhibitory concentration (IC50)

The half-maximal inhibitory concentration IC50 is a measure of the effectiveness of a given compound to inhibit a specific biological or biochemical function. Often the compound in question is a possible drug. This quantitative measure indicates how much of a drug or other substance (inhibitor) is needed to half-inhibit a given biological process. in the study case IC50 refers to the needed concentration to half-scavenge the superoxide anion. IC50 can be calculated according to the following equation:

$$\%\, O_2^{\cdot -}{}_{radicalscavengingactivity} = \frac{i_{pa_0} - i_{pa}}{i_{pa_0}} x100 \qquad \textit{Equation V-5}$$

Where i_{pa_0} is the anodic current density of the blank with the derivative and i_{pa} is the anodic current density of the radical in each addition.

The plot of the $\%\, O_2^{\cdot -}{}_{radicalscavengingactivity}$ values versus the concentration gives a linear equation $y = ax + b$, where x is concentration of the derivative and y is the radical scavenging activity. Thus, IC50 can be calculated as follow:

$$IC50 = \frac{50 - b}{a} \qquad \textit{Equation V-6}$$

The plots of the $\%\, O_2^{\cdot -}{}_{radicalscavengingactivity}$ versus the concentration for all the derivatives are represented in the following Figure V-4.

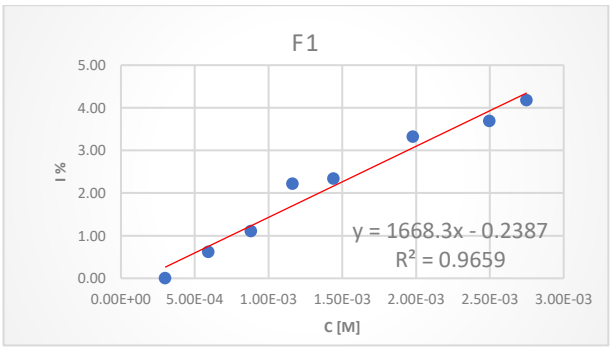

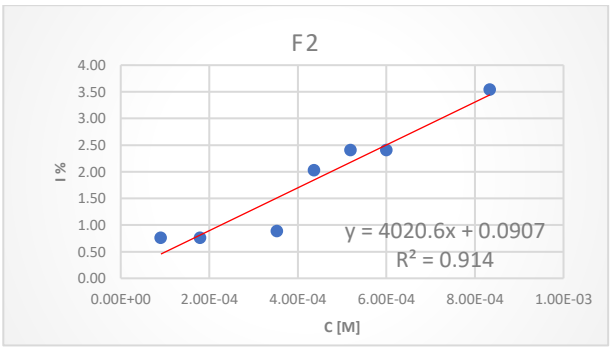

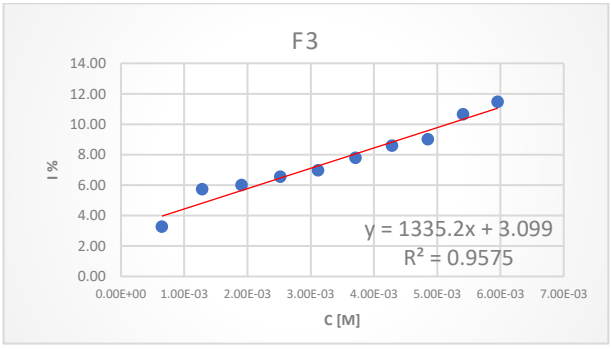
F3
I %
C [M]
y = 1335.2x + 3.099
R² = 0.9575

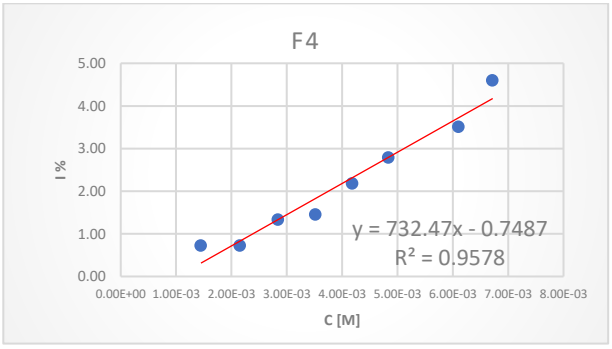
F4
I %
C [M]
y = 732.47x - 0.7487
R² = 0.9578

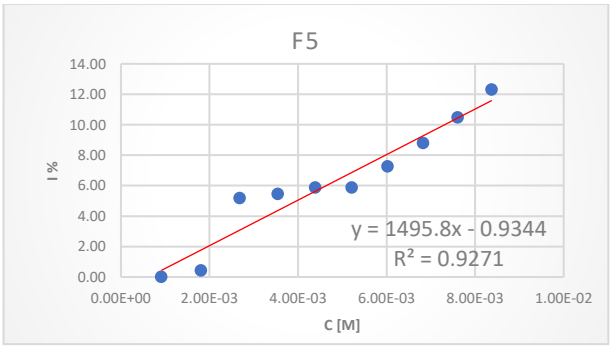
F5
I %
C [M]
y = 1495.8x - 0.9344
R² = 0.9271

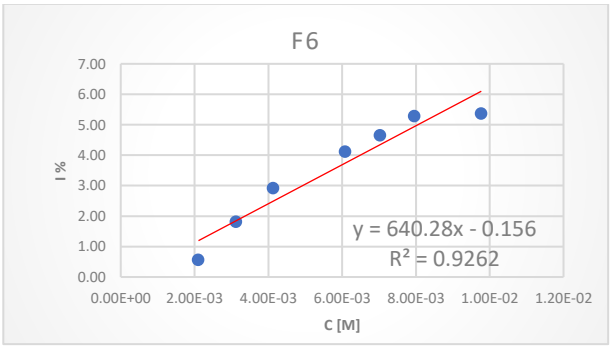
F6
I %
C [M]
y = 640.28x - 0.156
R² = 0.9262

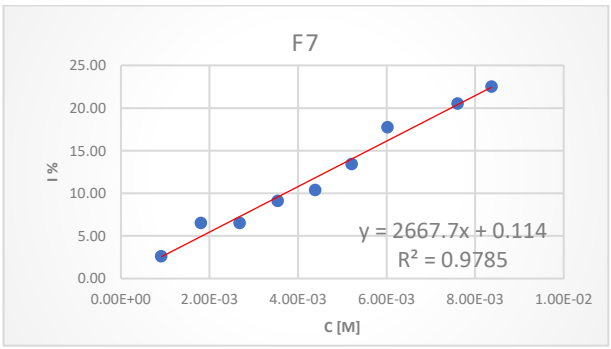
F7
I %
C [M]
y = 2667.7x + 0.114
R² = 0.9785

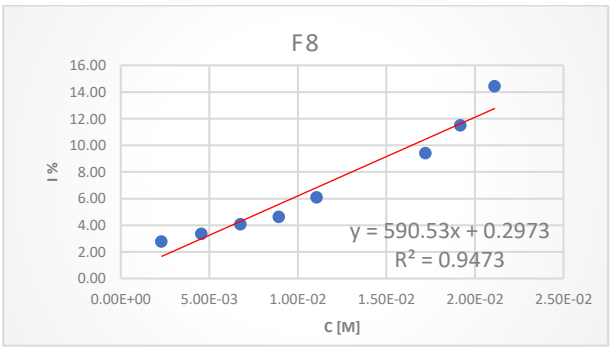
F8
I %
C [M]
y = 590.53x + 0.2973
R² = 0.9473

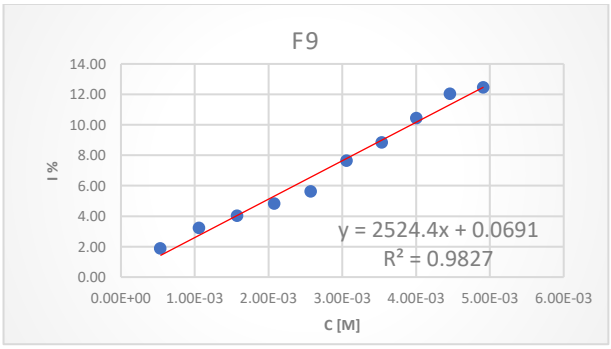
F9
I %
C [M]
y = 2524.4x + 0.0691
R² = 0.9827

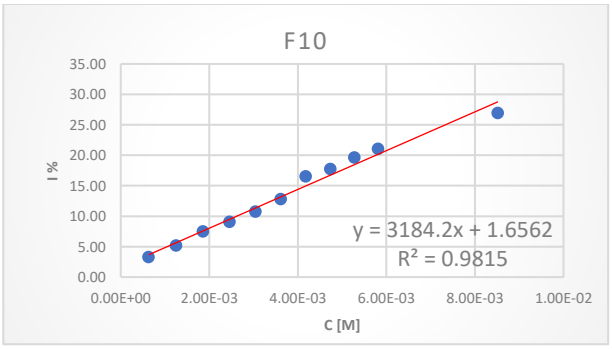
F10
I %
C [M]
y = 3184.2x + 1.6562
R² = 0.9815

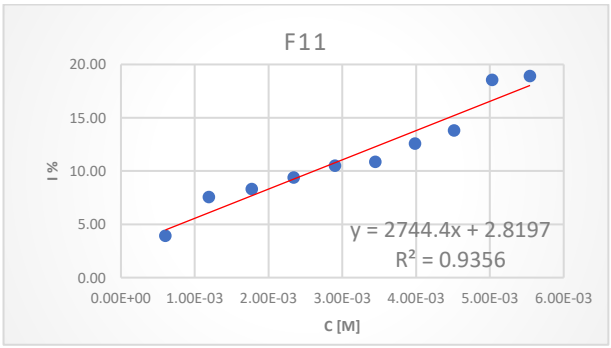
F11
I %
C [M]
y = 2744.4x + 2.8197
R² = 0.9356

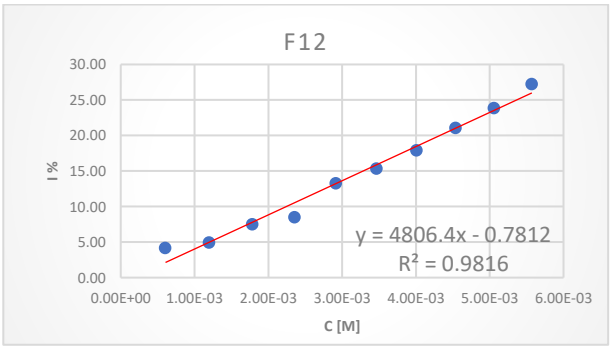
F12
I %
C [M]
y = 4806.4x - 0.7812
R² = 0.9816

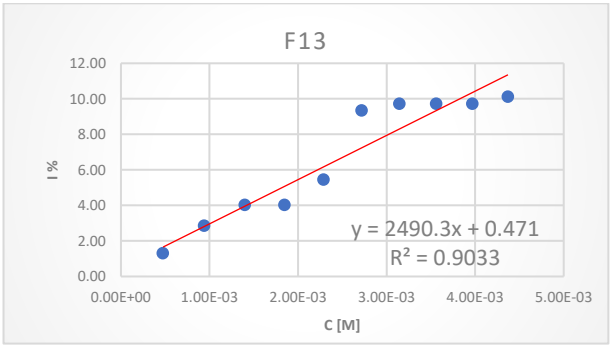
F13
I %
C [M]
y = 2490.3x + 0.471
R² = 0.9033

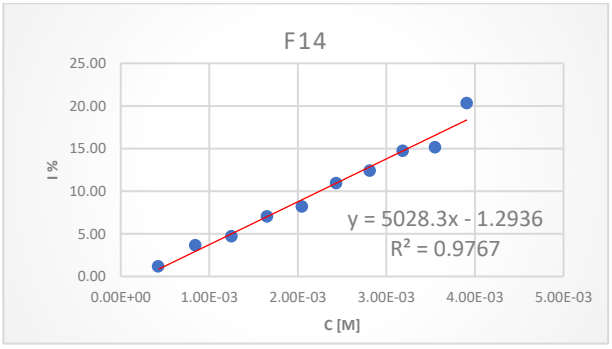
F14
I %
C [M]
y = 5028.3x - 1.2936
R² = 0.9767

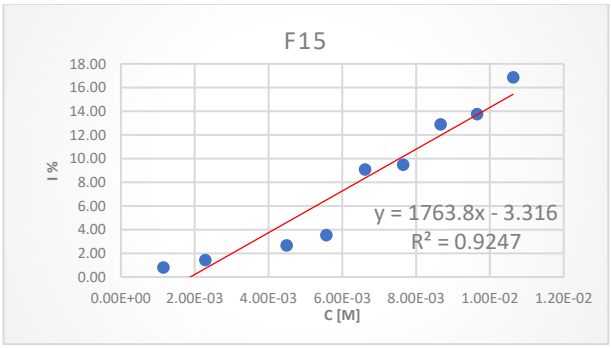
F15
I %
C [M]
y = 1763.8x - 3.316
R² = 0.9247

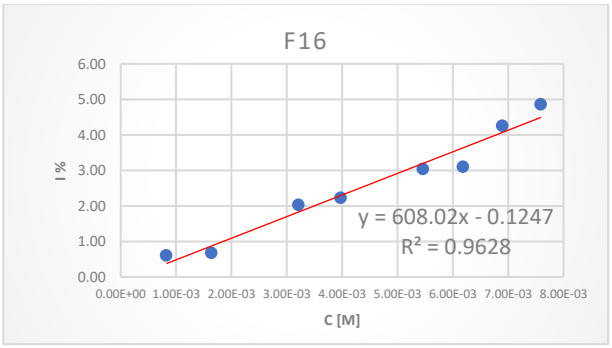
F16
I %
C [M]
y = 608.02x - 0.1247
R² = 0.9628

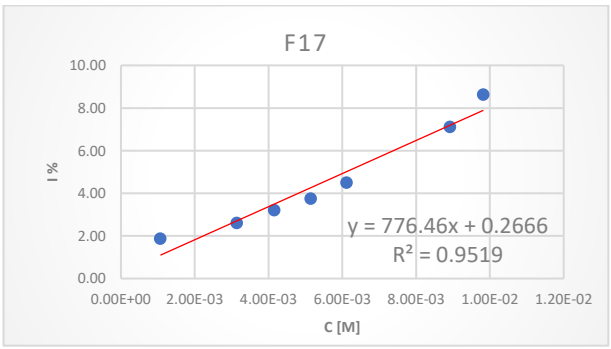
F17
I %
C [M]
y = 776.46x + 0.2666
R² = 0.9519

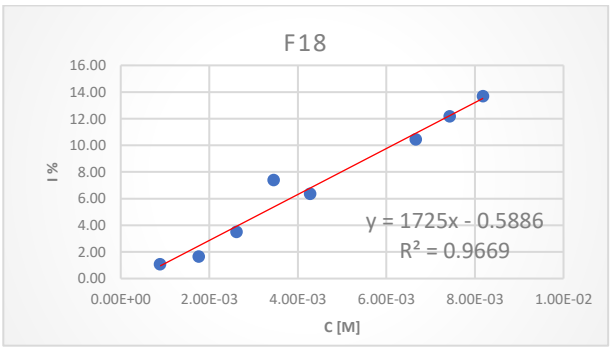
F18
I %
C [M]
y = 1725x - 0.5886
R² = 0.9669

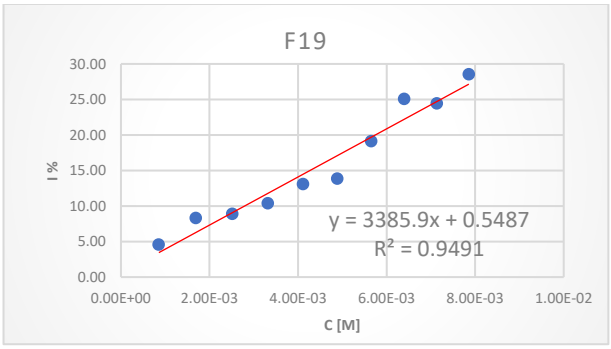
F19
I %
C [M]
y = 3385.9x + 0.5487
R² = 0.9491

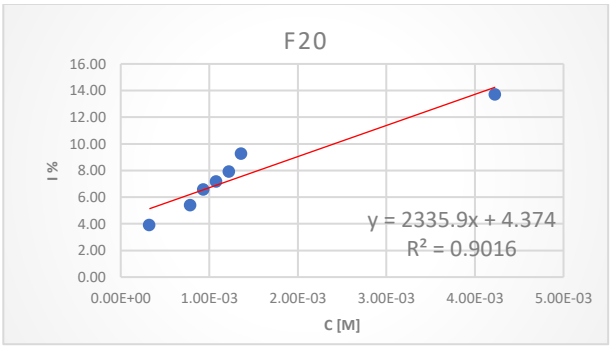
F20
I %
C [M]
y = 2335.9x + 4.374
R² = 0.9016

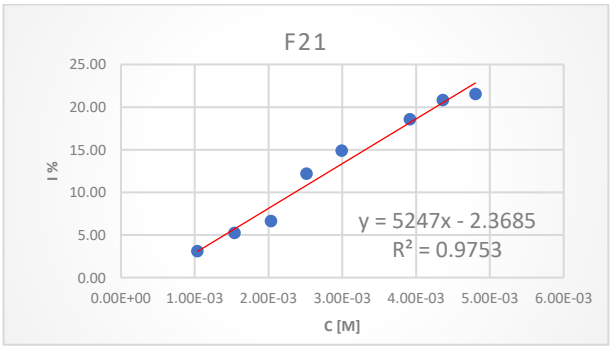
F21
I %
C [M]
y = 5247x - 2.3685
R² = 0.9753

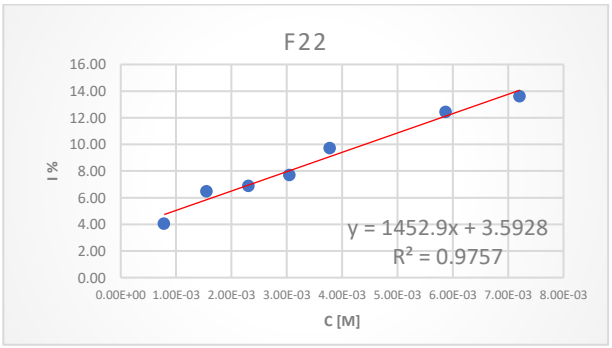
F22
I %
C [M]
y = 1452.9x + 3.5928
R² = 0.9757

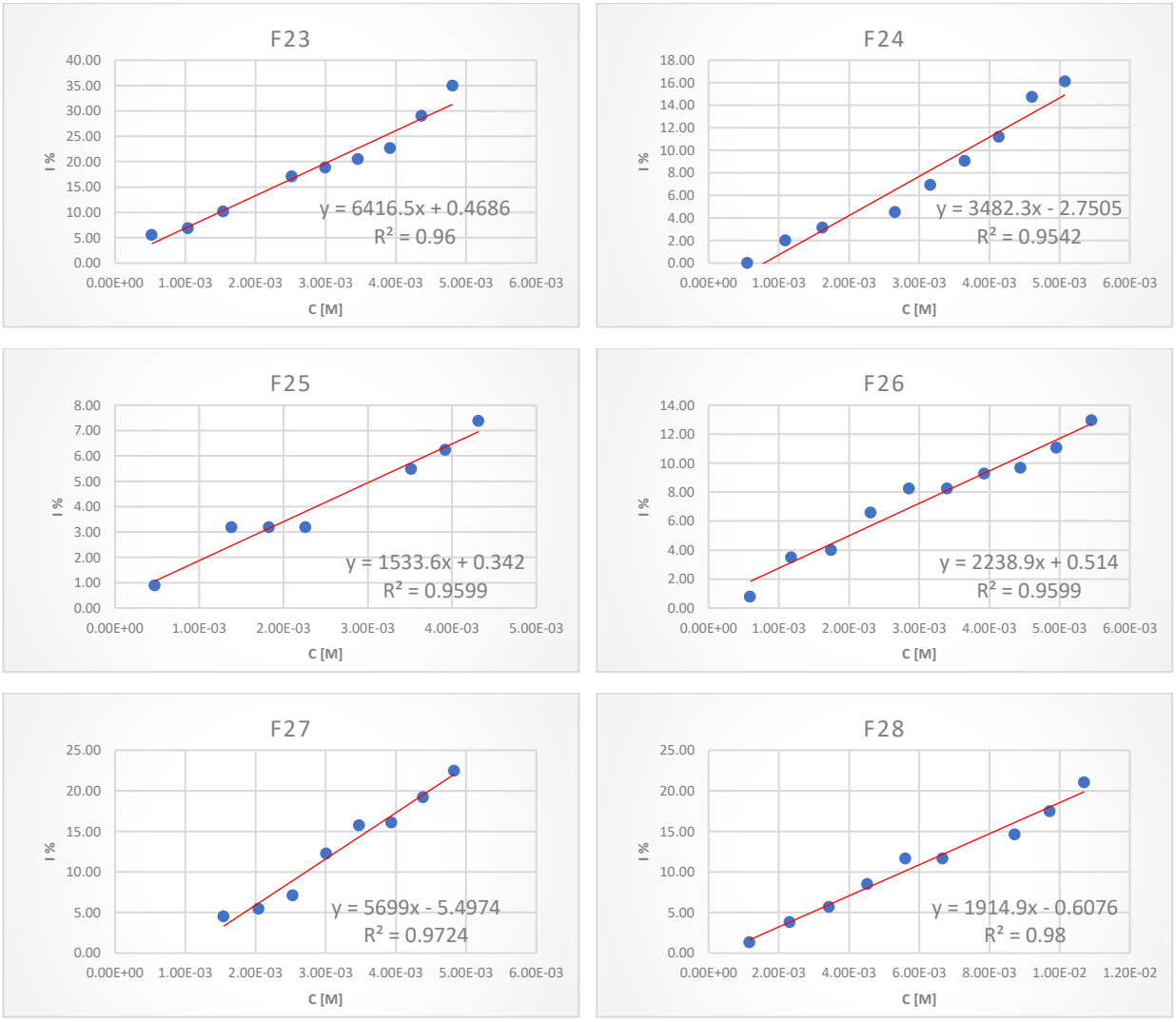

Figure V-4 plots of % $O_2^{\cdot-}$ $_{radicalscavengingactivity}$ versus the concentration of ferrocene derivative included their equation and linear regression.

All IC50 values are summarized in Table V-5 side by side with the linear regression of each derivative. It can be seen from the Table V-5 that all the derivatives have considerable values of IC50. However, F2, F12, F14, F21 and F27 show the best values of 9.981, 12.414, 10.565, 10.201 and 9.738 mM for IC50 respectively, the highest value is attributed to F23 (7.719 mM, $R^2 = 0.96$). R^2 confirms the accuracy of the results where it can be clearly seen that all the results are with a high values of R^2 (>0.9).

Table V-5 Half-maximal inhibitory concentration of N-ferrocenylmethylaniline derivatives.

Code	IC50 mM	R^2	Code	IC50 mM	R^2	Code	IC50 mM	R^2
F1	30.114	0.9659	F11	17.191	0.9356	F21	9.981	0.9753
F2	12.414	0.914	F12	10.565	0.9816	F22	31.941	0.9757
F3	35.126	0.9575	F13	19.889	0.9033	F23	7.719	0.96

Code	IC50 mM	R^2	Code	IC50 mM	R^2	Code	IC50 mM	R^2
F4	69.284	0.9578	F14	10.201	0.9767	F24	15.148	0.9542
F5	34.052	0.9271	F15	30.228	0.9247	F25	32.379	0.9599
F6	78.334	0.9262	F16	82.439	0.9627	F26	22.103	0.9599
F7	18.700	0.9785	F17	64.051	0.9558	F27	9.738	0.9724
F8	84.166	0.9473	F18	29.327	0.9669	F28	26.428	0.98
F9	19.779	0.9827	F19	14.605	0.9491			
F10	15.182	0.9815	F20	19.533	0.9016			

Obtained values of IC50 indicated that most N-ferrocenylmethylaniline derivatives showed promising scavenging activity against $O_2^{\cdot-}$ radicals, the compounds F2, F10, F12, F14, F19, F21, F23, F24 and F27 emerged to display the most significant potency, with the activity of compounds F23 is almost comparable to that of the standard α-tocopherol (7.0581 mM) [319] used as positive control because it is the most potent biological [320-322] and antioxidant form of the vitamin [323-326] values were summarized in Figure V-5. Although it didn't give the best IC50 value, F24 is obviously the safer choice between the derivatives considering the toxicity risks of F23 and the other derivtives while F24 is non toxic.

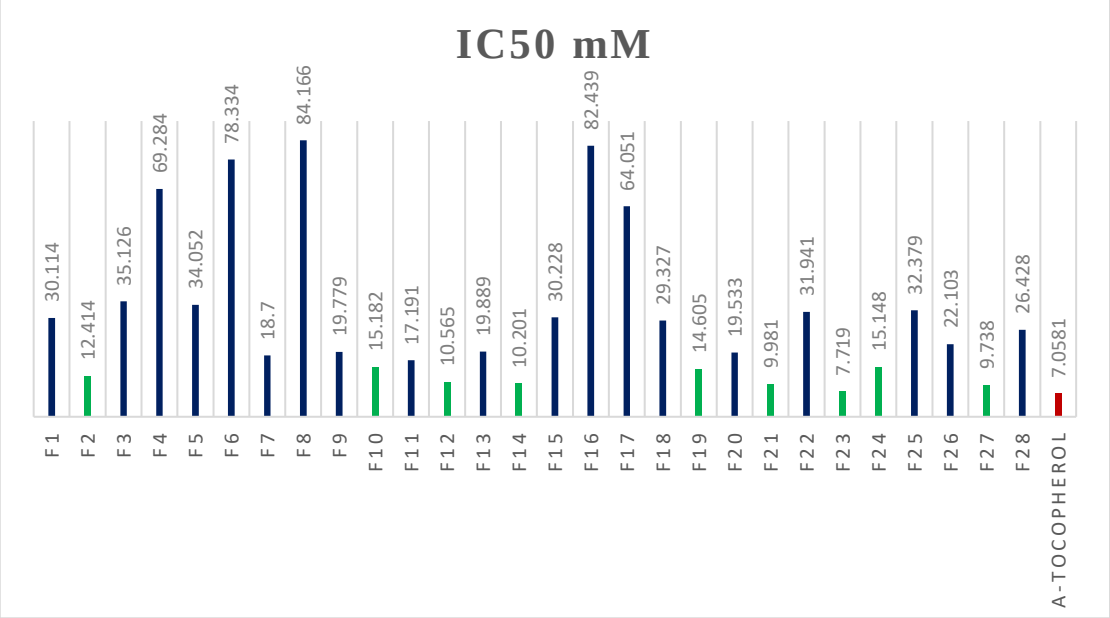

Figure V-5 IC50 values of N-ferrocenylmethylaniline derivatives and α-tocopherol as positive control.

V.4. Molecular docking Studies

Molecular docking study was carried out to afford an insight about the inhibition and binding parameters of the most five potent compounds with the enzyme glutathione reductase. The enzyme glutathione reductase (GR), also called glutathione-disulfide reductase, reduces glutathione disulfide (GSSG) to glutathione (GSH) which is involved in elimination of reactive oxygen species and act as a scavenger for various oxygen radicals, glutathione exists in reduced (GSH) and oxidized (GSSG) forms, the reaction symbolized by the following equilibrium.

$$2GSH + NADP^{+} \rightarrow GSSG + NADPH + H^{+}$$

Inhibition of glutathione reductase results in a decrease in reduced glutathione (GSH) and an increase in glutathione disulfide (GSSG) using NADPH, particularly from the pentose phosphate pathway in bacteria, plants and animals in order to regenerate glutathione, a molecule essential for resistance against oxidative stress and for the preservation of intracellular pH. So, studying glutathione reductase inhibition could serve as a good means for the selection antioxidants candidates. A good antioxidant candidate should inhibit glutathione reductase enzyme less.

Rigid receptor and flexible ligand molecular docking model were carried out to study the inhibition of glutathione reductase by the most five potent compounds against superoxide anion radical, and to understand, how strong the interactions between them. The crystal 3D-structure of glutathione reductase target involved in this study was retrieved from online data bank, RCSB PDB (https://www.rcsb.org/pdb, ID: 1XAN) as shown in Figure V-6 [327].

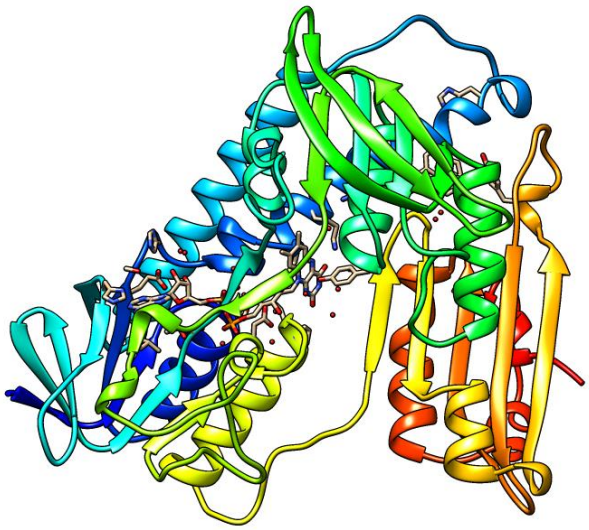

Figure V-6 UCSF chimera ribbons chemical structure view of human glutathione reductase in complex with a xanthene inhibitor (ID: 1xan).

V.4.1. Receptor preparation

The receptor was first imported into the AutoDockTools interface, missing atoms were inserted in incomplete residues, alternate conformations were deleted, all water molecules and ligands were removed, and polar hydrogen atoms and charges were added to the receptor structure.

V.4.2. Receptor-Ligand Docking

In silico molecular docking simulations studies were executed by using the software AutoDock 4.2 software [328, 329]. Lamarckian genetic algorithms were utilized, the grid box size was set at 60×60×60 (Å) in the x, y and z directions and the coordinates was fixed at x = 69.46, y = -17.32 and z = 55.62. All docking experiments consisted of 50 docking runs; the other parameters were left to their default values. The best conformation was selected with the lower docking energy for further docking analysis. The visualization of the interaction was generated with PLIP webserver (protein Ligand Interaction Profiler) [330, 331].

Results from molecular docking suggest that hydrogen bonding, hydrophobic forces and π-cation interactions are involved in the binding process. Figure V-7 illustrates the interactions of compounds F12, F14, F21, F23, F24 and F27 with the nearby residues in the active site of glutathione reductase.

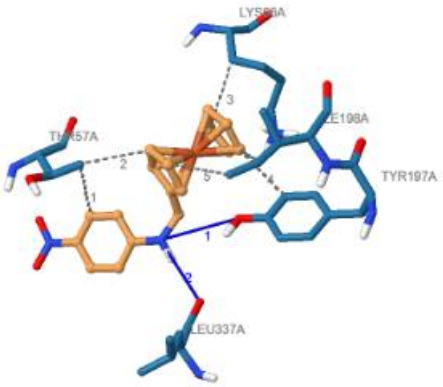

F12-GR

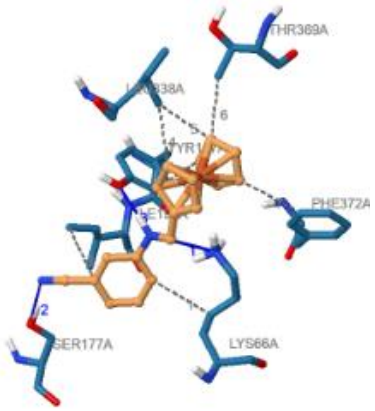

F14-GR

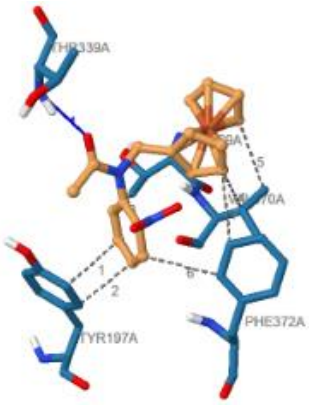

F21-GR

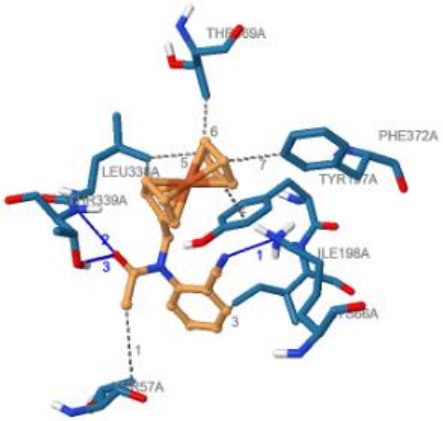

F23-GR

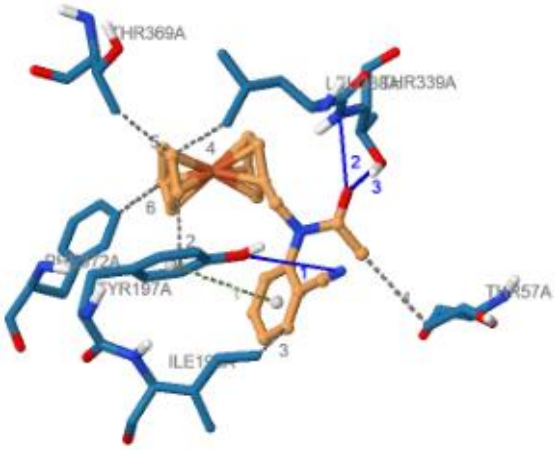

F24-GR

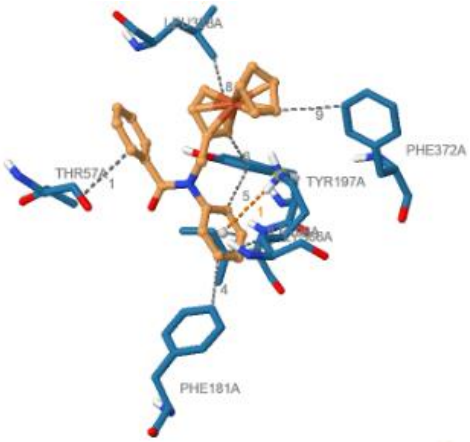

FAM27-GR

Figure V-7 Best docking poses for glutathione reductase interacting with F12, F14, F21, F23, F24 and F27 generated with PLIP web server illustrating the H-bonds, hydrophobic and π-cation interactions.

Interacting residues and their corresponding bond types and length are summarised in Table V-6, it can be seen from this table that beside hydrophobic interactions, compounds F14, F23 and F24 formed with the GR three hydrogen bonds, however, compounds F12 and F21 reacted respectively via two and one hydrogen bonds, in contrast, compounds F27 did not form any hydrogen bonding.

Table V-6 Interactions type between the ligands F12, F14, F21, F23, F24 and F27 and glutathione reductase

Molecule	Bond type	Amino acid	Distance (Å)
F12	H-bonds	TYR197, LEU327	3.54; 2.50
	Hydrophobic interactions	THR 57(2), ILE 198(2), TYR197, LYS66	3.72; 3.31; 3.52; 3.25; 3.04; 3.83
F14	H-bonds	LYS66, SER177, TYR197	2.75; 2.06; 1.99

Molecule	Bond type	Amino acid	Distance (Å)
	Hydrophobic interactions	LYS66, TYR197, ILE198, LEU338(2), THR369, PHE372	3.41; 3.33; 3.59; 2.21; 3.22; 3.46; 3.37
F21	H-bonds	THR339	1.89
	Hydrophobic interactions	TYR197(2), THR369, VAL370(2), PHE372	3.35; 3.04; 3.40 3.41; 3.50; 3.63; 3.50
F23	H-bonds	LYS66, THR339(2)	2.05; 2.32; 1.93
	Hydrophobic interactions	THR57, TYR197, ILE198, LEU338, THR369, PHE372	3.91; 3.50; 3.71; 2.99; 3.18; 3.50; 3.45
F24	H-bonds	TYR197, THR339 (2)	3.10, 2.65, 2.01
	Hydrophobic interactions	THR57, TYR197, ILE198, LEU338, THR369, PHE372	3.82, 3.71, 3.85, 3.25, 3.47, 3.30
	π-stacking interactions	TYR197	5.25
F27	π-cation interactions	LYS66	4.06
	Hydrophobic interactions	TRR57, LYS66(2), PHE181, TYR197(2), ILE198, LEU338, PHE372	3.74; 3.52; 3.49; 3.83; 3.27; 3.12; 3.41; 3.20; 3.34

Obtained binding free energy and the calculated inhibitory concentration (Equation V-7) from molecular docking study for the most five potent compounds are summarised in Table V-7.

$$\Delta G = RTln(IC50) \qquad \textit{Equation V-7}$$

Table V-7 Binding free energies and inhibitory concentration obtained from molecular docking study

Adduct	F12-GR	F14-GR	F21-GR	F23-GR	F24-GR	F27-GR
ΔG (Kcal/mol)	-8.09	-7.70	-7.52	-7.34	-7.61	-8.26
IC50 (µM)	1.18	2.28	3.07	4.16	2.61	0.88

The lowest binding free energy was found to be equal to -7.34 kcal/mol for compound F23, this value indicates weak binding affinity towards the enzyme glutathione reductase compared to other compounds. Compound F23 also possess the highest inhibitory concentration that is necessary to reduce the rate of glutathione reductase enzyme reaction by 50%. Thus, the compound F23 is a weaker inhibitor of glutathione reductase. Frthermore, F21 and F24 posses high IC50 value and low ΔG (-7.52 and -7.61 Kcal/mol) respectively

V.5. Conclusion

The results of studying the antioxidant activity for 28 N-ferrocenylmethylaniline derivatives show that all the derivatives have a considerable radical scavenging activity. The confirmation of the interactions between the derivatives and the radical was carried out by calculating free binding energy to determine the strength of these interaction and their type. The result goes to confirm that all the interactions between the derivatives and the radical were physical interaction. Free binding energy of all the derivatives varied from 3.313 to 12.306 KJ/mol. To further confirm the interaction between the radical and ferrocene derivative the diffusion coefficients were calculated, the results showed that the diffusion coefficient of the free radical is always higher than the bonded one, this finding further confirmed the interaction between theradical and the studied ferrocene derivatives. Half-maximal inhibitory concentration IC50 of every derivative has been also calculated

Molecular docking study revealed that compound F23 is the most inactive compounds against glutathione reductase enzyme having the highest inhibitory concentration of 4.16 µM and the lowest docking scores of 7.34 kcal/mol. F21 and F24 also predicted to be inactive compounds against glutathione reductase enzyme.

The obtained *in silico* and *in vitro* results correspond with one another and give room for the design of novel antioxidant N-ferrocenylmethylaniline derivatives with less activity against glutathione reductase and inactive toxicity or at least bearly active considering its dose.

CHAPTER VI

QSAR MODELING

VI.1. Introduction

Toward the discovery of novel biologically potent ferrocene derivatives, we herein present a series of new antioxidant compounds of N-ferrocenylmethylanilines bearing various substituted functions. Also, we build a QSAR model for description and prediction of radical scavenging activity of N-ferrocenylmethylanilines, using the multiple linear regression (MLR) method. The predicted QSAR model will guide the synthesis of potential new N-ferrocenylmethylaniline derivatives as radical scavengers.

VI.2. Training set and biological data

Data set for the QSAR study is composed of 28 sets of N-ferrocenylmethylaniline compounds for which their *in vitro* antioxidant activities against superoxide anion radical were measured using cyclic voltammetry assays. All IC50 (mM) values have been converted into positive logarithmic scale pIC50 by taking negative logarithm (-logIC50) and subsequently used as the dependent variable for the QSAR model development.

The synthesis of a series of 28 N-ferrocenylmethylaniline derivatives and their in vitro antioxidant activities (pIC50 values) used for the QSAR analysis were carried out in our laboratory and listed in Figure VI-1.

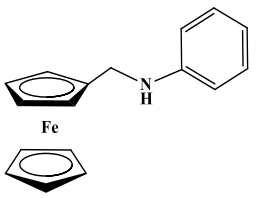

F1, pIC_{50} = 1.5212

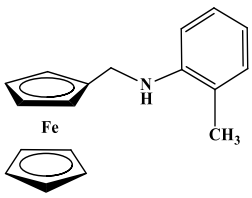

F2, pIC_{50} = 1.9061

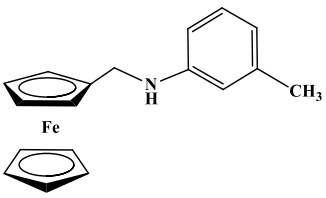

F3, pIC_{50} = 1.4544

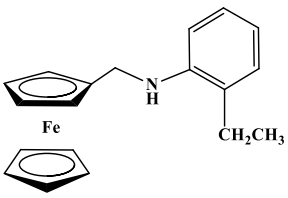

F4, pIC_{50} = 1.1594

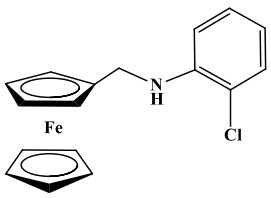

F5, pIC_{50} = 1.4679

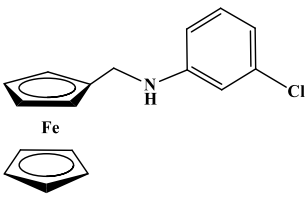

F6, pIC_{50} = 1.1060

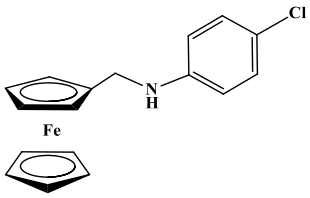

F7, pIC_{50} = 1.7282

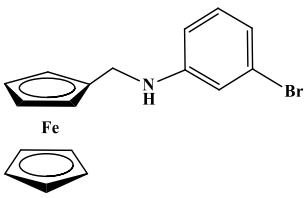

F8, pIC_{50} = 1.0749

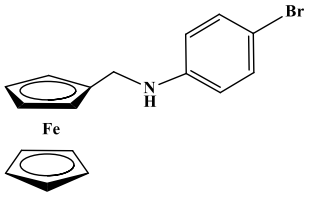

F9, pIC_{50} = 1.7038

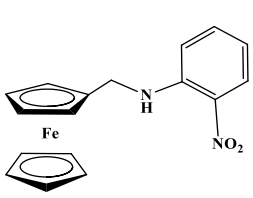

F10, pIC_{50} = 1.8187

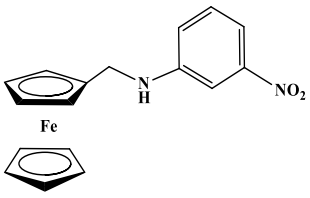

F11, pIC_{50} = 1.7647

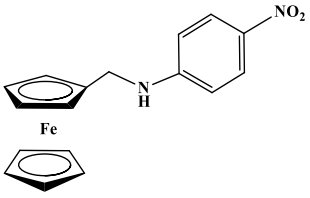

F12, pIC_{50} = 1.9761

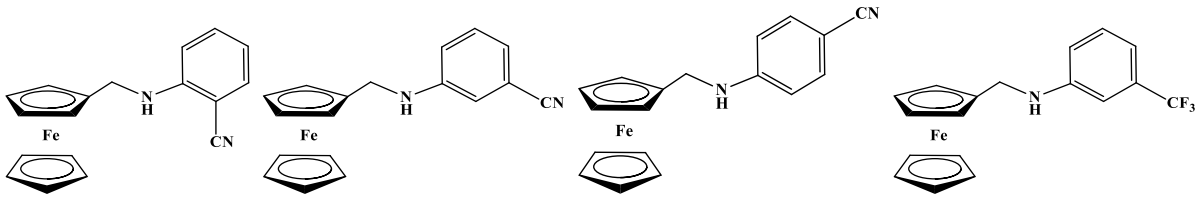

F13, pIC_{50} = 1.7014 F14, pIC_{50} = 1.9914 F15, pIC_{50} = 1.5196 F16, pIC_{50} = 1.0839

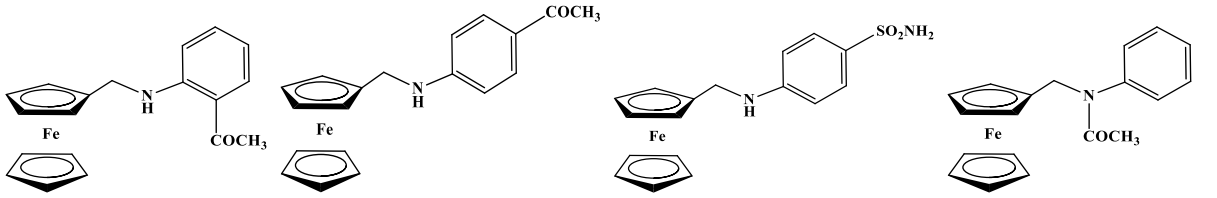

F17, pIC_{50} = 1.1935 F18, pIC_{50} = 1.5327 F19, pIC_{50} = 1.8355 F20, pIC_{50} = 1.7092

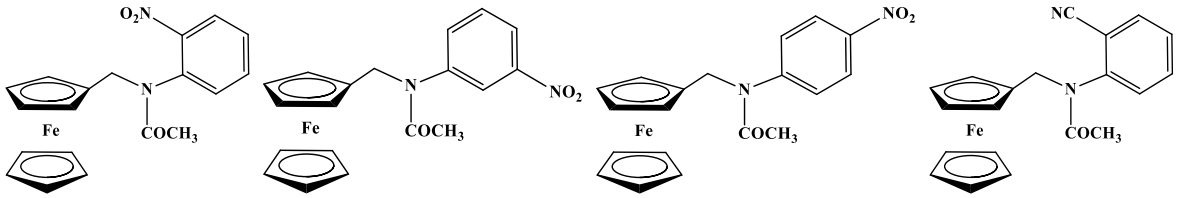

F21, pIC_{50} = 2.0008 F22, pIC_{50} = 1.4957 F23, pIC_{50} = 2.1124 F24, pIC_{50} = 1.8196

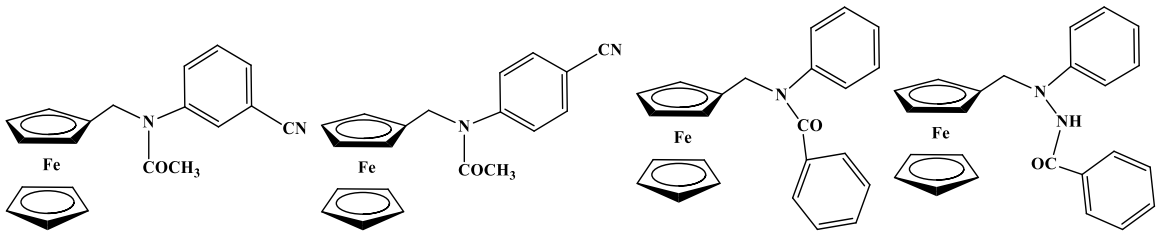

F25, pIC_{50} = 1.4897 F26, pIC_{50} = 1.6555 F27, pIC_{50} = 2.0115 F28, pIC_{50} = 1.5779

Figure VI-1 Chemical structures and observed pIC50 of N-ferrocenylmethylaniline derivatives against $O_2^{\bullet-}$ used as data set

VI.3. Molecular descriptors

Physico-chemical descriptors: such as surface area grid (SAG), molar volume (MV), heat of formation (Hf), molar polarizability (Pol) and molecular weight (MW) were identified by pre-optimizing the 28 N-ferrocenylmethylanilines by means of the Molecular Mechanics Force Field (MM+) included in HyperChem version 8.0.8 package followed by refining the resulting minimized structures using the PM3 semi-empirical Hamiltonian.

Quantum chemical descriptors: such as dipole moment (μ), energy of frontier orbital's (HOMO and LUMO), atomic net charges and total energy were obtained using Gaussian 09 program package [332] at the density functional theory level with the unrestricted Becker's three parameter hybrid exchange functional [201] combined with Lee-Yang-Parr nonlocal correlation function [333-335], a combination of basis set LanL2DZ (for iron) and 6-311G+(d) (for the rest of atoms) was used for all structure optimisation process of N-ferrocenylmethylaniline derivatives.

The rest of descriptors such as octanol/water partition coefficient (logP), topological polar surface area (TPSA) and water solubility (logS) were calculated using the free web server SwissADME [336].

VI.4. Molecular descriptors selection

In order to select the suitable predominant descriptors for establishing the QASR equation, all generated descriptors obtained using Gaussian 09W, HyperChem and SwissADME were subjected to correlation analysis with the experimentally determined radical scavenging activities, taking every one of the descriptors as an independent variable, and pIC50 as a dependent variable using multiple linear regression (MLR) method implanted in Molegro Data Modeler software version 3.0, at the end of regression analysis only 6 descriptors were selected. The molecular descriptors finally maintained are presented in Table VI-1. Moreover, the leave-one-out method was used to validate the QSAR equation, and the obtained square of the cross-validation coefficient Q^2 was used as a criterion of both robust stability and predictive ability of the model.

Table VI-1 Values of molecular descriptors

Molecule	pIC50	HOMO	LUMO	Total E	μ	MW	logP	logS	SAG	MV	pol	Hf
F1	1.5212	-0.01859	-0.19979	-836.24	1.648	291.17	3.03	-4.76	482.29	-145.48	30.25	-145.48
F2	1.9061	-0.01841	-0.19626	-875.56	1.884	305.20	3.30	-5.14	500.34	846.05	32.09	-156.57
F3	1.4544	-0.01845	-0.1989	-836.24	1.786	305.20	3.30	-5.14	480.8	798.42	30.25	-148.46
F4	1.1594	-0.01816	-0.19527	-914.87	1.944	319.22	3.56	-5.58	527.39	893.38	33.92	-160.90
F5	1.4679	-0.02032	-0.20519	-1295.83	2.137	325.61	3.50	-5.41	499.65	839.81	32.18	-155.00
F6	1.1060	-0.02182	-0.20683	-1295.83	3.393	325.61	3.50	-5.41	501.56	845.95	32.18	-155.53
F7	1.7282	-0.02276	-0.20388	-1295.83	3.865	325.61	3.50	-5.41	503.92	845.57	32.18	-155.44
F8	1.0749	-0.02186	-0.20731	-848.80	3.472	370.06	3.57	-5.48	517.84	863.4	32.88	-141.23
F9	1.7038	-0.02326	-0.20483	-848.80	3.948	370.06	3.57	-5.48	512.23	865.8	32.88	-141.23
F10	1.8187	-0.09388	-0.2145	-1040.75	5.603	336.17	2.56	-6.12	502.84	850.77	31.97	-156.89
F11	1.7647	-0.09672	-0.21641	-1040.75	6.814	336.17	2.45	-5.55	519.01	867.55	31.97	-156.40
F12	1.9761	-0.08582	-0.21818	-1040.76	8.625	336.17	2.45	-5.55	513.52	861.78	31.97	-159.57
F13	1.7014	-0.05134	-0.21231	-928.49	4.577	316.18	2.89	-5.54	506.53	853.19	32.1	-113.28
F14	1.9914	-0.05469	-0.21218	-928.49	6.113	316.18	2.78	-4.97	510.13	857.95	32.1	-113.78
F15	1.5196	-0.04156	-0.21505	-928.49	7.726	316.18	2.78	-4.97	511.1	858.74	32.1	-114.19

F16	1.0839	-0.03607	-0.20957	-1173.30	4.433	359.17	4.00	-5.68	520.15	873.88	31.81	-307.32
F17	1.1935	-0.05617	-0.21042	-988.88	4.589	333.21	3.00	-5.00	526.73	896.71	34.01	-189.36
F18	1.5327	-0.04942	-0.20993	-988.90	5.653	333.21	2.96	-4.79	533.01	905.96	34.01	-190.59
F19	1.8355	-0.03319	-0.21368	-1440.17	6.785	370.25	1.94	-4.71	553.39	930.31	32.74	-216.89
F20	1.7092	-0.03233	-0.20314	-988.90	3.954	333.21	2.85	-4.28	521.94	896.46	34.01	-188.37
F21	2.0008	-0.10873	-0.20706	-1193.40	6.488	378.20	2.15	-5.07	544.38	943.67	35.72	-194.74
F22	1.4957	-0.11378	-0.20925	-1193.41	4.192	378.20	2.15	-5.07	554.09	954.57	35.72	-196.15
F23	2.1124	-0.11364	-0.21158	-1193.41	2.183	378.20	2.15	-5.07	553.54	954.67	35.72	-196.50
F24	1.8196	-0.07599	-0.20705	-1081.15	6.500	358.21	2.63	-4.49	544.5	945.62	35.86	-151.46
F25	1.4897	-0.07578	-0.20891	-1081.15	4.082	358.21	2.63	-4.49	555.09	953.27	35.86	-152.70
F26	1.6555	-0.07678	-0.21054	-1081.15	1.716	358.21	2.63	-4.49	556.92	952.87	35.86	-152.85
F27	2.0115	-0.0379	-0.20934	-1180.63	3.660	395.27	3.90	-6.01	600.02	1051.65	41.83	-151.93
F28	1.5779	-0.02033	-0.20602	-1044.22	3.638	348.22	2.64	-4.82	546.97	938.9	35.36	-163.74
Molecule	TPSA	qFe1	qN1	qC9	qC10	qC11	qC12	qC13	qC14	qC15	qC16	qC17
F1	12.03	-1.019	-0.396	-0.086	0.0644	-0.531	-0.109	-0.837	-0.343	0.005	-0.843	1.208
F2	12.03	-1.045	-0.369	-0.236	1.039	-0.911	0.158	0.084	-1.292	0.006	-0.438	0.914
F3	12.03	-1.023	-0.364	-0.178	0.999	-0.855	0.232	-0.819	-0.293	-0.196	-0.387	0.549
F4	12.03	-1.03	-0.378	-0.16	0.957	-0.805	1.303	-0.827	-0.78	-0.531	-0.385	0.858
F5	12.03	-1.035	-0.295	-0.17	1.072	-0.893	-0.905	0.445	-0.523	-0.008	-0.416	0.457
F6	12.03	-1.022	-0.366	-0.185	0.982	-0.903	0.087	-0.777	-0.227	-0.363	0.091	0.264
F7	12.03	-1.031	-0.362	-0.19	1.031	0.9	0.067	-0.831	-0.614	0.186	-0.514	0.746
F8	12.03	-1.022	-0.375	-0.19	0.959	-0.848	0.183	-0.962	-0.165	-0.602	1.227	-0.602
F9	12.03	-1.027	-0.365	-0.187	1.009	-0.897	0.038	-0.784	-0.771	0.79	-0.799	0.593
F10	57.85	-1.005	-0.39	-0.122	0.96	-0.674	-0.198	-0.312	0.44	-0.182	-0.502	0.151
F11	57.85	-0.998	-0.417	-0.177	-0.229	-0.058	0.788	0.123	-0.403	-0.004	-0.289	-0.525
F12	57.85	-1.009	-0.372	-0.156	1.002	-0.86	0.677	-1.395	0.024	-0.166	-0.396	0.682
F13	35.82	-1.019	-0.311	-0.123	1.066	-0.843	-0.358	0.42	-0.629	0.077	-0.478	0.476
F14	35.82	-1.025	-0.362	-0.182	0.967	-0.922	0.166	-0.897	-0.182	-0.306	0.238	0.769
F15	35.82	-1.017	-0.359	-0.177	1.031	-0.899	0.245	-0.874	-0.34	0.361	-0.547	0.928
F16	12.03	-1.033	-0.395	-0.144	0.925	-0.867	0.446	-0.704	-0.285	-0.221	-1.225	0.846
F17	29.1	-1.003	-0.338	-0.14	1.022	-0.873	-0.447	0.392	-0.526	-0.013	-0.479	0.337

F18	29.1	-1.018	-0.368	-169	1.034	-0.882	0.279	-1.306	-0.858	0.527	-0.438	0.942
F19	80.57	-1.017	-0.363	-0.185	1.054	-0.898	0.349	-1.087	-0.255	-0.5	-0.663	1.053
F20	20.31	-1.16	0.183	-0.141	1.252	-1.054	-1.372	0.082	-0.365	0.002	-0.506	0.734
F21	66.13	-1.193	0.296	-0.204	1.215	-0.96	-1.068	0.082	-0.319	-0.164	-0.166	0.255
F22	66.13	-1.178	0.157	-0.143	1.271	-1.137	-0.503	-0.068	-0.555	-0.031	-0.3	0.421
F23	66.13	-1.189	0.19	-0.104	1.342	-1.245	-0.442	-0.135	-0.046	-0.154	0.076	-0.31
F24	44.1	-1.19	0.263	-0.174	1.454	-1.247	-0.814	0.264	-0.36	-0.304	0.093	0.322
F25	44.1	-1.152	0.175	-0.249	1.216	-1.01	-0.823	0.359	-0.073	-0.188	0.063	-0.184
F26	44.1	-1.169	0.24	-0.242	1.311	-1.076	-1.134	0.39	-0.318	0.502	-0.558	0.213
F27	20.31	-1.279	0.199	-0.214	1.879	-1.966	-0.611	-0.08	-0.498	-0.052	-0.429	0.635
F28	32.34	-1.139	0.278	0.175	0.937	-1.393	-0.303	0.102	-0.355	-0.117	-0.77	0.646

VI.5. Model building

To build the QSAR model and to predict pIC50 for radical scavenging activity of N-ferrocenylmethylaniline derivatives, we used a total of 20 compounds, belonging to the same class, they only differ in terms of the position of the functionalization in the aniline ring (Figure 1). All the compounds were synthesized coupling the quaternary salt (ferrocenylmethy) trimethyl-ammonium iodide with various substituted anilines [337-340].

While constructing the model, great care was taken into consideration to avoid the inclusion of highly collinear molecules using MLR regression. After a statistical analysis using MLR regression method implanted in Molegro Data Modeler software with the antioxidant activities (pIC50) as the dependent variable and the descriptors as independent variables, the best statistically QSAR model equation was obtained and the statistical parameters were given in the following model, Equation V-6:

$$pIC50 = -0.535097 \times logP - 7.16821 \times qFe1 - 1.67059 \times qN1 - 4.83885 \quad | \quad \textit{Equation VI-1}$$

N = 20; R^2 = 0.934; S = 0.333; F = 36.525; ρ < 0.005; Q = 7.202; RMSD = 0.1160

In this QSAR equation, N is the number of compounds used to build the QASR model, R^2 is the squared correlation coefficient, ρ is the significance of the model, F is the Fisher ratio, Q is the factor of quality for which Q = R/ESS (where R is the correlation coefficient and ESS is the standard error of the estimation), and RMSD is the root mean squared deviation. The positive value

of Q for QSAR's model suggests its high predictive power. The accuracy in the analysis is indicated by the low standard error of estimate value of 0.12968.

This QSAR equation suggests that the octanol/water partition coefficient (logP) and the net charges (qFe1 and qN1) are the main independent parameters contributing to the antioxidant activities of the N-ferrocenylmethylaniline derivatives.

As it can be seen from Equation VI-1, the obtained QSAR equation reach the optimal ratio of compounds to descriptors which should be according to the Topliss and Costello rule equal to at least 5:1 and thus the equation should be credible [341]. The equation also shows that all parameters have negative coefficients which means that any increase in these values result in a decrease in the antioxidant activity.

VI.6. Validation of the model

The leave-one-out cross-validation method was used to determine the predictive power of the model. Results summarized in Table 3 for the obtained QSAR model indicate that it is statistically significant. The high values of $Q^2 = 0.873$ ($Q^2 \geq 0.5$), $R^2 = 0.934$ ($R^2 > 0.6$), $R^2_{adj} = 0.849$ ($R^2_{adj} > 0.5$), and the low value of $R^2 - Q^2 = 0.061$ ($R^2 - Q^2 < 0.3$), are considered ultimate proof that the QSAR model has a high predictive power [342, 343]. The obtained predicted residual sum squares (PRESS) value of 0.269 is smaller than the sum of the squares of response (SSY) value of 2.112 which further points out that the model predicts better than chance and can be considered statically significant. Furthermore, the PRESS/SSY ratio is equal to 0.127 which is smaller than 0.4 is also proof of the predictive ability [344]. The low S_{PRESS} value of 0.130 additionally reflects the good predictive potential of the QSAR model.

The predictive error of the coefficient correlation PE is another parameter used to evaluate the predictive power of the obtained model. For the developed model, the condition $R > 6PE$ is satisfied and hence has good predictive power.

Table VI-2 Cross-validation parameters

R^2_{adj}	R^2_{cv}	Q^2	PE	6PE	SSY	PRESS	S_{PRESS}	PRESS/SSY
0.849	0.873	0.873	0.017	0.102	2.112	0.269	0.130	0.127

The comparison of the observed pIC50obs values with the predicted values pIC50pred is presented in Table VI-3. The residual values by the QASR model are also presented in this table. The calculated low residual values confirmed the high predictive power of the model.

Table VI-3 Comparison of observed (pIC50), predicted (pIC50) and residuals of the QASR model

Molecule	pIC50obs	pIC50pred	Residuals
F1	1.5212	1.5058	0.01543
F2	1.4544	1.3365	0.11789
F4	1.1594	1.2710	-0.11155
F5	1.4679	1.2257	-0.11966
F6	1.106	1.2032	-0.12834
F7	1.7282	1.6469	0.17181
F8	1.0749	1.7007	0.06402
F9	1.7038	1.7044	0.27175
F11	1.7647	1.5634	-0.0438
F12	1.9761	1.0854	-0.00151
F13	1.7014	1.3102	-0.11674
F15	1.5196	1.4893	0.04342
F18	1.5327	2.0196	-0.18406
F19	1.8355	1.6455	0.06366
F20	1.7092	2.0679	-0.06708
F23	2.1124	2.2163	-0.10389
F25	1.4897	1.8447	-0.02506
F26	1.6555	1.7326	-0.07705
F27	2.0115	1.9100	0.10153
F28	1.5779	1.4487	0.12923

A plot of predicted pIC50 versus observed pIC50 values are shown in Figure 4A. The obtained squared fitting correlation coefficient of 0.934 between the predicted and observed values confirmed the efficiency of the obtained QSAR model and further confirms that the QASR equation has satisfactory predictability for new samples and could be used to guide the design of new antioxidant N-ferrocenylmethylanilines.

A plot of the residuals (observed pIC50 - predicted pIC50) versus observed pIC50, is also presented in Figure 4B. A random distribution of the residuals on both sides of zero was observed indicating a good fit for a linear model and that no systematic error exists [345]. The applicability domain is set up inside a defined domain where all the data points were within the boundary -0.20, +0.30.

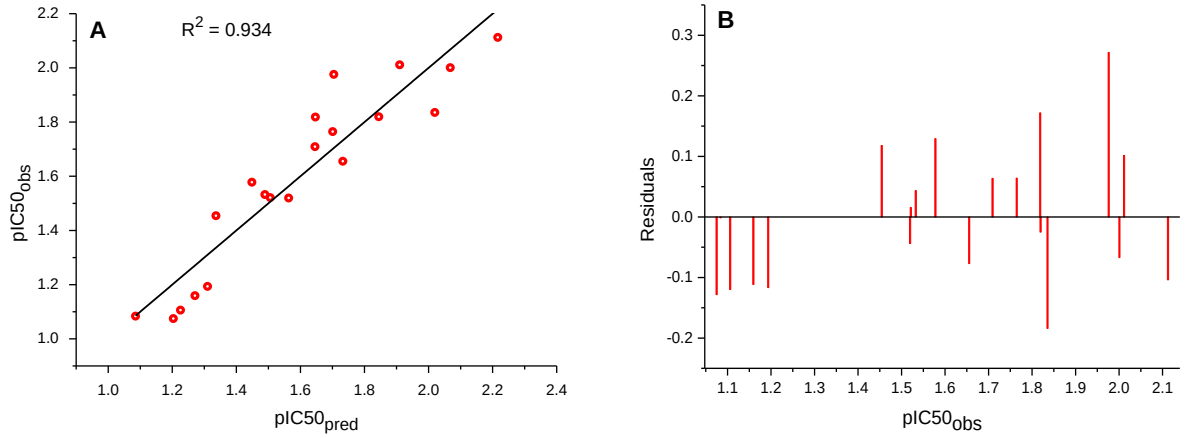

Figure VI-2 (A) Correlation plot of predicted pIC50 versus observed pIC50 value, (B) a distribution plot of the residuals versus observed pIC50

VI.9. Conclusion

The high predictive ability of the QASR model was established. The model involved logP, qFe and qN1 to predict the antioxidant activity. With the high values of Q^2 = 0.892, R^2 = 0.934 and R^2_{adj} = 0.842 cross-validation approved that the model has a high ability to predect the IC50 of new N-ferrocenylmethylaniline derivatives.

GENERAL CONCLUSION

GENERAL CONCLUSION

Optimization procedures using Gaussian 09W software have been done to optimize the 28 derivatives in order to determine their properties. The optimization method was DFT/B3LYP and the basis set wasn't the same for all atoms. In this study the mixed basis sets of LanL2DZ(Fe)/6-31G(d) was used. The accurancy of the method is confirmed by values of R^2 obtained from the linear correlation between the calculated and the experimental values of the bond lengths and angles which were equal to 0.9992 and 0.9755 respectively. Moreover, the mixed basis sets showed a high ability to predict the spectral and energetic properties. HOMO-LUMO gap values which have been calculated to predict the reactivity of the derivatives The MESP maps have also been used to predict the derivatives' reactive locations. The electrophilic sites of all derivatives were centered on the amine group, while the nucleophilic sites were projected to be concentrated on the phenyl group.

The ADME and pharmacokinetics properties of N-ferrocenylmethylaniline derivatives were predicted using the SwissADME webserver tool. The predicted results revealed that the majority of the derivatives have the required bioavailability properties. Furthermore, the in silico toxicity analysis performed, median lethal dose (LD50) and toxicity class (TC) have been predicted and they gave some promising candidates such as F24.

All compounds of the studied series of 28 N-ferrocenylmethylanilines showed remarkable *in vitro* radical scavenging activity. The obtained values of the free binding energy (-3.313 and -12.306 KJ/mol) confirmed physical interactions between the derivatives and the free radical ($O_2^{\bullet-}$). The half-maximal inhibitory concentration (IC50) of all the 28 derivatives was measured using cyclic voltametry thecnics. The compounds F2, F10, F12, F14, F19, F21, F23, F24, and F27 showed the best results, these results were compared with that of the standard vitamin E (7.0581 mM), the IC50 value of F23 (7.719 mM) is competitive to that of the standard while the others idicating that they are strong drug candidates.

We could conclude from the docking study that although the molecule F23 is the most inactive compound against glutathione reductase enzyme, with the greatest inhibitory concentration of 4.16 µM and the lowest docking scores of 7.34 kcal/mol, but it cannot be a good antioxidant candidate because it is predicted as carcinogenic and mutagenic. On the other hand, based on what it is cited above, the compound F24 can be chosen as the best and safer antioxidant candidate because it is inactive against glutathione reductase enzyme, its remarkable scavenging

activity against superoxide inion, its promising ADME and drug-likness properties and because it is predicted to be a non-toxic derivative.

Finally, the QASR model was built with high values of $Q^2 = 0.892$, $R^2_{adj} = 0.842$, and $R^2 = 0.934$ which allows it to predict IC50 Of new N-ferrocenylmethylaniline derivatves and save time and efforts for researchers.

REFERENCES

REFERENCES

1. Togni, A., *Planar-chiral ferrocenes: synthetic methods and applications.* Angewandte Chemie International Edition in English, 1996. **35**(13-14): p. 1475-1477.
2. Stepnicka, P., *Ferrocenes: ligands, materials and biomolecules*. 2008: John Wiley & Sons.
3. Tsukazaki, M., et al., *Direct and highly enantioselective synthesis of ferrocenes with planar chirality by (−)-sparteine-mediated lithiation.* Journal of the American Chemical Society, 1996. **118**(3): p. 685-686.
4. Nishibayashi, Y., et al., *Enantioselective ortho-lithiation of substituted ferrocenes.* The Journal of Organic Chemistry, 1996. **61**(3): p. 1172-1174.
5. Ibrahim, M., *Voltammetric studies of the interaction of nogalamycin antitumor drug with DNA.* Analytica Chimica Acta, 2001. **443**(1): p. 63-72.
6. Jaouen, G., *Bioorganometallics: biomolecules, labeling, medicine*. 2006: John Wiley & Sons.
7. Dai, Z., et al., *Direct electrochemistry of glucose oxidase immobilized on a hexagonal mesoporous silica-MCM-41 matrix.* Bioelectrochemistry, 2007. **70**(2): p. 250-256.
8. Carney, M., et al., *Ferrocene derivatives as metalloprotein redox probes: electron-transfer reactions of ferrocene and ferricenium ion derivatives with cytochrome c.* Journal of the American Chemical Society, 1984. **106**(9): p. 2565-2569.
9. Goel, A., et al., *The synthesis and structural characterization of novel N-meta-ferrocenyl benzoyl dipeptide esters: The X-ray crystal structure and in vitro anti-cancer activity of N-{meta-ferrocenyl) benzoyl}-l-alanine-glycine ethyl ester.* Journal of organometallic chemistry, 2007. **692**(6): p. 1292-1299.
10. Neuse, E.W., et al., *An iron–organic polymeric smoke suppressant for poly (vinyl chloride).* Applied organometallic chemistry, 1988. **2**(1): p. 53-57.
11. Ye, B.X., et al., *Electrochemical and spectroscopic study of the interaction of indirubin with DNA.* Electroanalysis: An International Journal Devoted to Fundamental Practical Aspects of Electroanalysis, 2005. **17**(17): p. 1523-1528.
12. Köpf-Maier, P., H. Köpf, and E.W. Neuse, *Ferrocenium salts—the first antineoplastic iron compounds.* Angewandte Chemie International Edition in English, 1984. **23**(6): p. 456-457.
13. Hurvois, J. and C. Moinet, *Reactivity of ferrocenium cations with molecular oxygen in polar organic solvents: decomposition, redox reactions and stabilization.* Journal of Organometallic Chemistry, 2005. **690**(7): p. 1829-1839.
14. Liu, Z.-Q., *Potential applications of ferrocene as a structural feature in antioxidants.* Mini reviews in medicinal chemistry, 2011. **11**(4): p. 345-358.
15. Kealy, T. and P. Pauson, *A new type of organo-iron compound.* Nature, 1951. **168**(4285): p. 1039-1040.
16. Gomez Arrayas, R., J. Adrio, and J.C. Carretero, *Recent applications of chiral ferrocene ligands in asymmetric catalysis.* Angewandte Chemie International Edition, 2006. **45**(46): p. 7674-7715.

17. Togni, A. and T. Hayashi, *Ferrocenes: Homogeneous Catalysis.* Organic Synthesis, Materials Science, 1995. **1**.
18. Sutcliffe, O.B. and M.R. Bryce, *Planar chiral 2-ferrocenyloxazolines and 1, 1'-bis (oxazolinyl) ferrocenes—syntheses and applications in asymmetric catalysis.* Tetrahedron: Asymmetry, 2003. **14**(16): p. 2297-2325.
19. Sato, S., M. Tsueda, and S. Takenaka, *Electrochemical detection of aberrant methylated gene using naphthalene diimide derivative carrying four ferrocene moieties.* Journal of Organometallic Chemistry, 2010. **695**(15-16): p. 1858-1862.
20. Masson, G., A.J. Lough, and I. Manners, *Soluble poly (ferrocenylenevinylene) with t-butyl substituents on the cyclopentadienyl ligands via ring-opening metathesis polymerization.* Macromolecules, 2008. **41**(3): p. 539-547.
21. Wolf, M.O., *Transition-Metal–Polythiophene Hybrid Materials.* Advanced Materials, 2001. **13**(8): p. 545-553.
22. Wu, S., et al., *Electron transfer in ferrocene-containing functionalized chitosan and its electrocatalytic decomposition of peroxide.* Macromolecules, 2006. **39**(20): p. 6796-6799.
23. Zhang, L., et al., *A Conjugated Polymer-Based Electrochemical DNA Sensor: Design and Application of a Multi-Functional and Water-Soluble Conjugated Polymer.* Macromolecular rapid communications, 2008. **29**(17): p. 1489-1494.
24. Wu, Y., S. Liu, and L. He, *Electrochemical biosensing using amplification-by-polymerization.* Analytical chemistry, 2009. **81**(16): p. 7015-7021.
25. Qiu, J.-D., et al., *A label-free amperometric immunosensor based on biocompatible conductive redox chitosan-ferrocene/gold nanoparticles matrix.* Biosensors, 2009. **25**(4): p. 852-857.
26. Paul, S., N. Chavan, and S. Radhakrishnan, *Polypyrrole functionalized with ferrocenyl derivative as a rapid carbon monoxide sensor.* Synthetic metals, 2009. **159**(5-6): p. 415-418.
27. Matsui, J., et al., *Quasi-solid-state optical logic devices based on redox polymer nanosheet assembly.* Langmuir, 2009. **25**(18): p. 11061-11066.
28. Zhou, X., et al., *Development of N-ferrocenyl (benzoyl) amino-acid esters stationary phase for high performance liquid chromatography.* Talanta, 2015. **144**: p. 1044-1051.
29. Corley, R.C. and F.M. Dewey, *Use of 1, 1'-bis-(1-glycidoxylalkyl) ferrocenes in rocket propellants*. 1975, Google Patents.
30. Gore, G., et al., *Evaluation of ferrocene derivatives as burn rate modifiers in AP/HTPB-based composite propellants.* Defence Science Journal, 1999. **49**(2): p. 151.
31. Zegheb, N., et al., *In Vitro and In Silico Determination of some N-ferrocenylmethylaniline Derivatives as Anti-Proliferative Agents against MCF-7 Human Breast Cancer Cell Lines.* Anti-cancer Agents in Medicinal Chemistry, 2021.
32. Kesik, M., et al., *Synthesis and characterization of conducting polymers containing polypeptide and ferrocene side chains as ethanol biosensors.* Polymer Chemistry, 2014. **5**(21): p. 6295-6306.

33. Kedadra, A., et al., *Synthesis and antioxidant activity of six novel N-ferrocenylmethyl-N-(nitrophenyl)-and-N-(cyanophenyl)-acetamides: Cyclic voltammetry and molecular docking studies*. Journal of Electrochemical Science Engineering, 2021.
34. Heinze, K. and H. Lang, *Ferrocene Beauty and Function*. 2013, ACS Publications.
35. Wilkinson, G., et al., *The structure of iron bis-cyclopentadienyl.* Journal of the American Chemical Society, 1952. **74**(8): p. 2125-2126.
36. Dunitz, J., L. Orgel, and A. Rich, *The crystal structure of ferrocene.* Acta Crystallographica, 1956. **9**(4): p. 373-375.
37. Dunitz, J. and L. Orgel, *Bis-cyclo pentadienyl Iron: a Molecular Sandwich.* Nature, 1953. **171**(4342): p. 121-122.
38. Wilkinson, G. and M. Rosenblum, J Am Chem Soc, 1952. **74**: p. 2125.
39. Werner, H., *At least 60 years of ferrocene: the discovery and rediscovery of the sandwich complexes.* Angewandte Chemie International Edition, 2012. **51**(25): p. 6052-6058.
40. RAUSCH, M., M. VOGEL, and H. ROSENBERG, *Derivatives of Ferrocene. II. Some Reduction Products of Benzoylferrocene and 1, 1'-Dibenzoylferrocene1*. The Journal of Organic Chemistry, 1957. **22**(8): p. 903-906.
41. Dyagileva, L., et al., *Reactivity of the first transition row metallocenes in thermal decomposition reaction.* Journal of Organometallic Chemistry, 1979. **175**(1): p. 63-72.
42. Chen, Y., et al., *Ultrasensitive ratiometric electrochemical immunoassay of N-terminal pro-B-type natriuretic peptide based on three-dimensional PtCoNi hollow multi-branches/ferrocene-grafted-ionic liquid and CoNC nanosheets.* Sensors 2021. **326**: p. 128794.
43. Williams, M., *The Merck Index: An Encyclopedia of Chemicals, Drugs, and Biologicals, Edited by MJO'Neil, Royal Society of Chemistry, Cambridge, UK ISBN 9781849736701; 2708 pages. April 2013.* 2013.
44. Molina, P., et al., *Characterization and electrochemical study of bis (ferrocenes) with a furan spacer and ferrocenophanes prepared from α-bromoacetyl substituted ferrocenes.* Journal of Organometallic Chemistry, 2001. **637**: p. 258-265.
45. Simenel, A.A., et al., *Synthesis and enantiomeric resolution of ferrocenyl (alkyl) azoles.* Journal of organometallic chemistry, 2003. **688**(1-2): p. 138-143.
46. *Ferrocene*. 2018 [cited 2021; Available from: https://webbook.nist.gov/cgi/cbook.cgi?ID=B6000428&Mask=80.
47. Bozak, R., *Photochemistry in the metallocenes.* Advances in photochemistry, 1971. **8**: p. 227-244.
48. KHELEF, A., *Synthèse et étude du comportement anodique de quelques N-ferrocenyl-N-phenylalkanamides et N'-ferrocenyl-N'-phenylalkanehydrazides et étude structurale de leurs phases cristallines*, in *Industrial chemistry*. 2014, Mohamed Khider University - Biskra: Biskra. p. 163.
49. North, A., D.t. Phillips, and F.S. Mathews, *A semi-empirical method of absorption correction.* Acta Crystallographica Section A: Crystal Physics, Diffraction, Theoretical, 1968. **24**(3): p. 351-359.

50. Wilkinson, G., Org Syn 1956. **36**: p. 31-34.
51. Leigh, T., *624. Ferrocene derivatives containing tertiary alkyl groups. Synthesis by the Friedel–Crafts and other methods.* Journal of the Chemical Society, 1964: p. 3294-3302.
52. Pauson, P., *Ferrocene and related compounds.* Quarterly Reviews, Chemical Society, 1955. **9**(4): p. 391-414.
53. Miller, S., *J. A. Tebboth, and JF Tremaine.* J Chem Soc, 1952. **632**: p. 127-128.
54. Wilkinson, G., P. Pauson, and F. Cotton, *Bis-cyclopentadienyl compounds of nickel and cobalt.* Journal of the American chemical society, 1954. **76**(7): p. 1970-1974.
55. Wilkinson, G. and J. Birmingham, *Bis-cyclopentadienyl compounds of Ti, Zr, V, Nb and Ta.* Journal of the American Chemical Society, 1954. **76**(17): p. 4281-4284.
56. Wilkinson, G., F. Cotton, and J. Birmingham, *On manganese cyclopentadienide and some chemical reactions of neutral bis-cyclopentadienyl metal compounds.* Journal of Inorganic, 1956. **2**(2): p. 95-113.
57. Cotton, F. and G. Wilkinson, *Bis-cyclopentadienyl1-Verbindungen von Chrom, Molybdän und Wolfram.* Zeitschrift für Naturforschung B, 1954. **9**(6): p. 417-418.
58. Wilkinson, G., *The preparation and some properties of ruthenocene and ruthenicinium salts.* Journal of the American Chemical Society, 1952. **74**(23): p. 6146-6147.
59. Wilkinson, G., *The preparation and some properties of the cobalticinium salts.* Journal of the American Chemical Society, 1952. **74**(23): p. 6148-6149.
60. Cotton, F., R. Whipple, and G. Wilkinson, *Bis-cyclopentadienyl compounds of rhodium (III) and iridium (III).* Journal of the American Chemical Society, 1953. **75**(14): p. 3586-3587.
61. Wilkinson, G. and J. Birmingham, *Cyclopentadienyl compounds of Sc, Y, La, Ce and some lanthanide elements.* Journal of the American Chemical Society, 1954. **76**(23): p. 6210-6210.
62. Birmingham, J., D. Seyferth, and G. Wilkinson, *A new preparation of bis-cyclopentadienyl-metal compounds.* Journal of the American Chemical Society, 1954. **76**(16): p. 4179-4179.
63. Pauson, P. and G. Wilkinson, *Bis-indenyl Derivatives of Iron and Cobalt.* Journal of the American Chemical Society, 1954. **76**(7): p. 2024-2026.
64. Parkins, A.W. and R.C. Poller, *An Introduction to Organometallic Chemistry*. Vol. 1. 1986, London: Macmillan Publishers Ltd. 252
65. Nesmeyanov, A.N., et al., Dokl Akad Nauk SSSR, 1958. **120**.
66. M. A. Lynch, J. and J.C. Brantly, Brit Part, 1958. **52**.
67. Arimoto, F.S., U S Pat, 1958. **52**.
68. Hoh, G.L., W.E. McEwen, and J. Kleinberg, *Substituent effects in the chronopotentiometric oxidation of ferrocenes.* Journal of the American Chemical Society, 1961. **83**(19): p. 3949-3953.
69. Knight, D. and R. Schlitt, *Assay of Alkyl and Hydroxyalkyl Ferrocenes by Potentiometric Titration.* Analytical Chemistry, 1965. **37**(4): p. 470-471.
70. Mugnier, Y., et al., *Réduction électrochimique du ferrocène.* Journal of Organometallic Chemistry, 1980. **186**(2): p. C49-C52.

71. Bard, A.J., et al., *Electrochemistry of metallocenes at very negative and very positive potentials. Electrogeneration of 17-electron Cp2Co2+, 21-electron Cp2Co2-, and 22-electron Cp2Ni2- species.* Inorganic Chemistry, 1993. **32**(16): p. 3528-3531.
72. de Meulenaer, J.t. and H. Tompa, *The absorption correction in crystal structure analysis.* Acta Crystallographica, 1965. **19**(6): p. 1014-1018.
73. Coppens, P., *Crystallographic Computing, edited by FR Ahmed, SR Hall & CP Huber.* Copenhagen: Munksgaard, 1970: p. 255-270.
74. Lubov'V, S., et al., *Synthesis, structure and redox potentials of biologically active ferrocenylalkyl azoles.* Journal of organometallic chemistry, 2004. **689**(15): p. 2473-2479.
75. Snegur, L.V., et al., *Ferrocenylalkyl azoles: bioactivity, synthesis, structure.* Applied Organometallic Chemistry, 2008. **22**(2): p. 139-147.
76. Xie, Y.-S., et al., *Synthesis, structure characterization and preliminary biological evaluation of novel 5-alkyl-2-ferrocenyl-6, 7-dihydropyrazolo [1, 5-a] pyrazin-4 (5H)-one derivatives.* Journal of Organometallic Chemistry, 2008. **693**(7): p. 1367-1374.
77. Broadhead, G., J. Osgerby, and P. Pauson, *127. Ferrocene derivatives. Part V. Ferrocenealdehyde.* Journal of the Chemical Society, 1958: p. 650-656.
78. Weinmayr, V., *Hydrogen Fluoride as a Condensing Agent. V. Reactions of Dicyclopentadienyliron in Anhydrous Hydrogen Fluoride1.* Journal of the American Chemical Society, 1955. **77**(11): p. 3009-3011.
79. Weinmayr, V., *Hydrogen Fluoride as a Condensing Agent. V. Reactions of Dicyclopentadienyliron in Anhydrous Hydrogen Fluoride1.* Journal of the American Chemical Society, 1955. **77**(11): p. 3009-3011.
80. Graham, P., et al., *Some acyl ferrocenes and their reactions.* Journal of the American Chemical Society, 1957. **79**(13): p. 3416-3420.
81. Nesmeyanov, A.N., V.A. Sazonova, and V.N. Drozd, Dokl Akad Nauk SSSR, 1959. **126**.
82. Richards, J.H. and T.J. Curphey, Chem Ind 1956.
83. LINDSAY, J.K. and C.R. HAUSER, *Aminomethylation of Ferrocene to Form N, N-Dimethylaminomethylferrocene and Its Conversion to the Corresponding Alcohol and Aldehyde1.* The Journal of Organic Chemistry, 1957. **22**(4): p. 355-358.
84. Lednicer, D. and C.R. Hauser, Org Syn, 1960. **40**.
85. Osgerby, J.M. and P.L. Pauson, J Chem Soc, 1958.
86. Nesmeyanov, A.N., et al., Dokl Akad Nauk SSSR, 1961. **131**.
87. Argyropoulos, N. and E. Coutouli-Argyropoulou, *Synthesis of unsymmetrical 1, 1'-disubstituted ferrocenes. Formation of ferrocenophanes via intramolecular cycloaddition.* Journal of organometallic chemistry, 2002. **654**(1-2): p. 117-122.
88. Woodward, R., M. Rosenblum, and M. Whiting, *A new aromatic system.* Journal of the American Chemical Society, 1952. **74**(13): p. 3458-3459.

89. Nesmeyanov, A.N. and N.S. Kochetkova, *Principal Practical Applications of Ferrocene and Its Derivatives.* Russian Chemical Reviews, 1974. **43**(9): p. 710.

90. Kochetkova, N.S. and Y.K. Krynkina, *Practical Applications of Cyclopentadienyl Complexes of Transition Metals.* Russian Chemical Reviews, 1978. **47**(5): p. 486.

91. Fouda, M.F., et al., *On the medicinal chemistry of ferrocene.* Applied Organometallic Chemistry, 2007. **21**(8): p. 613-625.

92. Dombrowski, K.E., W. Baldwin, and J.E. Sheats, *Metallocenes in biochemistry, microbiology & medicine.* Journal of organometallic chemistry, 1986. **302**(3): p. 281-306.

93. Van Staveren, D.R. and N. Metzler-Nolte, *Bioorganometallic chemistry of ferrocene.* Chemical reviews, 2004. **104**(12): p. 5931-5986.

94. Wang, J., *Glucose biosensors: 40 years of advances and challenges.* Electroanalysis: An International Journal Devoted to Fundamental, 2001. **13**(12): p. 983-988.

95. Willner, I. and E. Katz, *Integration of layered redox proteins and conductive supports for bioelectronic applications.* Angewandte Chemie International Edition, 2000. **39**(7): p. 1180-1218.

96. Zatsepin, T.S., et al., *Ferrocene-containing nucleic acids. Synthesis and electrochemical properties.* Russian chemical reviews, 2003. **72**(6): p. 537-554.

97. Atkinson, R.C., et al., *Synthesis, coordination chemistry, and catalytic application of a novel unsymmetrical P/O ferrocenediyl ligand.* Organometallics, 2004. **23**(11): p. 2744-2751.

98. Kang, J., J.H. Lee, and K.S. Im, *Preparation of pseudo-C2-symmetric P, S-hybrid ferrocenyl ligand and its application to some asymmetric reactions.* Journal of Molecular Catalysis A: Chemical, 2003. **196**(1-2): p. 55-63.

99. Gibson, V.C., et al., *Synthesis, characterisation and catalytic activity of metal complexes of neutral, unsymmetrical P/S ferrocenediyl ligands.* Journal of the Chemical Society, Dalton Transactions 2002(17): p. 3280-3289.

100. Alexakis, A. and C. Benhaim, *Asymmetric conjugate addition to alkylidene malonates.* Tetrahedron: Asymmetry, 2001. **12**(8): p. 1151-1157.

101. Chesney, A., et al., *Synthesis of ferrocenyloxazolines incorporating secondary functionalities.* Synthesis, 1998. **1998**(04): p. 413-416.

102. Soradova, Z., et al., *Stereoselective domino conjugate addition of Grignard reagents to lactones followed by reaction with activated alkenes catalyzed by ferrocenyl carbene ligands.* Tetrahedron: Asymmetry, 2015. **26**(5-6): p. 271-275.

103. Hanhan, M.E., R. Martínez-Máñez, and J.V. Ros-Lis, *Highly effective activation of aryl chlorides for Suzuki coupling in aqueous media using a ferrocene-based Pd (II)–diimine catalyst.* Tetrahedron Letters, 2012. **53**(19): p. 2388-2391.

104. Chandrasekhar, V., A. Chakraborty, and E.C. Sañudo, *Ferrocene-based compartmental ligand for the assembly of neutral Zn II/Ln III heterometallic complexes.* Dalton Transactions, 2013. **42**(37): p. 13436-13443.

105. Brunner, H. and M. Janura, *Enantioselective Catalysis 113: New Menthylphosphane Ligands Differing in Steric and Electronic Properties.* Synthesis, 1998. **1998**(01): p. 45-55.
106. Ueno, Y., H. Sano, and M. Okawara, *Synthesis and complex formation of diferrocenyltetrathiafulvalene.* Journal of the Chemical Society, Chemical Communications, 1980(1): p. 28-30.
107. Bryce, M.R., et al., J Chem Soc, Chem Commun, 1993.
108. Wang, J.-Y., L.-C. Chen, and K.-C. Ho, *Synthesis of redox polymer nanobeads and nanocomposites for glucose biosensors.* ACS applied materials, 2013. **5**(16): p. 7852-7861.
109. Chinapang, P., et al., *Ferrocenyl derivative of 1, 8-naphthalimide as a new turn-on fluorescent sensor for Au (III) ion.* Dyes, 2015. **112**: p. 236-238.
110. Fang, J.X., et al., *Preparation, characterization and biological activities of novel ferrocenyl-substituted azaheterocycle compounds.* Applied organometallic chemistry, 2003. **17**(3): p. 145-153.
111. Jin, Z., et al., *Synthesis and Biological Evaluation of Novel Ferrocene-Substituted Triadimefon-and Triadimenol-Analogues.* Synthesis, 2007. **37**(8): p. 601-604.
112. Yeary, R.A., *Chronic toxicity of dicyclopentadienyliron (ferrocene) in dogs.* Toxicology, 1969. **15**(3): p. 666-676.
113. Neuse, E.W. and F. Kanzawa, *Evaluation of the activity of some water-soluble ferrocene and ferricenium compounds against carcinoma of the lung by the human tumor clonogenic assay.* Applied organometallic chemistry, 1990. **4**(1): p. 19-26.
114. Nourbakhsh, M., et al., *The effect of a newly synthesized ferrocene derivative against MCF-7 breast cancer cells and spheroid stem cells through ROS production and inhibition of JAK2/STAT3 signaling pathway.* Anti-Cancer Agents in Medicinal Chemistry, 2020. **20**(7): p. 875-886.
115. Patra, M. and G. Gasser, *The medicinal chemistry of ferrocene and its derivatives.* Nature Reviews Chemistry, 2017. **1**(9): p. 1-12.
116. de Champdoré, M., et al., *In-water reactivity of nucleosides and nucleotides: one-step preparation and biological evaluation of novel ferrocenyl-derivatives.* Tetrahedron, 2004. **60**(31): p. 6555-6563.
117. Köpf-Maier, P., H. Köpf, and E. Neuse, *Ferricenium complexes: a new type of water-soluble antitumor agent.* Journal of cancer research 1984. **108**(3): p. 336-340.
118. Köpf-Maier, P., *Complexes of metals other than platinum as antitumour agents.* European journal of clinical pharmacology, 1994. **47**(1): p. 1-16.
119. Köpf-Maier, P., *Tumor inhibition by ferricenium complexes: systemic effect in vivo and cell growth inhibition in vitro.* Zeitschrift für Naturforschung C, 1985. **40**(11-12): p. 843-846.
120. Köpf-Maier, P., *Complexes of metals other than platinum as antitumour agents.* European journal of clinical pharmacology, 1994. **47**(1): p. 1-16.

121. Sato, S., T. Nojima, and S. Takenaka, *Electrochemical gene detection based on supramolecular complex formation by ferrocenyl-β-cyclodextrin and adamantylnaphthalene diimide bound to double stranded DNA.* Journal of organometallic chemistry, 2004. **689**(25): p. 4722-4728.
122. Mukumoto, K., et al., *Preparation of carbodiimide-terminated dithiolane self-assembly monolayers as a new DNA-immobilization method.* Analytical sciences, 2006. **22**(3): p. 349-355.
123. Wang, Y., et al., *Voltammetric Determination of Surface-Confined Biomolecules with N-(2-Ethyl-ferrocene) maleimide.* Electroanalysis: An International Journal Devoted to Fundamental, 2005. **17**(23): p. 2163-2169.
124. JC, L., et al., J Clin Microb, 2006. **44**.
125. Baldoli, C., et al., *Electrochemical activity of new ferrocene-labelled PNA monomers to be applied for DNA detection: Effects of the molecular structure and of the solvent.* Journal of Electroanalytical Chemistry, 2005. **585**(2): p. 197-205.
126. Zocchi, G., *Analytical assays based on detecting conformational changes of single molecules.* ChemPhysChem, 2006. **7**(3): p. 555-560.
127. Szunerits, S., et al., *Comparison of different strategies on DNA chip fabrication and DNA-sensing: Optical and electrochemical approaches.* Electroanalysis: An International Journal Devoted to Fundamental, 2005. **17**(22): p. 2001-2017.
128. Lee, M.-R., et al., *Determining morphine in biologic fluids of rats by gas chromatography–mass spectrometry.* Analytica chimica acta, 2006. **559**(1): p. 25-29.
129. Khennoufa, A., et al., *Spectrophotometric, voltammetric and molecular docking studies of binding interaction of N-ferrocenylmethylnitroanilines with bovine serum albumin.* Journal of Molecular Structure, 2021. **1224**: p. 129052.
130. Khelef, A. and T. Lanez, *In vitro assays of the antioxidant activities of ferrocene derivatives bearing amine, amide or hydrazine groups.* Der Pharma Chemica, 2015. **7**(6): p. 318-323.
131. Lanez, T. and M. Henni, *Antioxidant activity and superoxide anion radical interaction with 2-(ferrocenylmethylamino) benzonitrile and 3-(ferrocenylmethylamino) benzonitrile.* Journal of the Iranian Chemical Society, 2016. **13**(9): p. 1741-1748.
132. Marc, F., et al., *Studies of several analytical methods for antioxidant potential evaluation in food.* Medecine Sciences: M/S, 2004. **20**(4): p. 458-463.
133. Bandyopadhyay, U., D. Das, and R.K. Banerjee, *Reactive oxygen species: oxidative damage and pathogenesis.* Current science, 1999: p. 658-666.
134. Boyd, B., et al., *Etude pilote ouverte de l'effet antioxydant d'Ambrotose AOTM sur des personnes en bonne santé.* GlycoScience et Nutrition, 2003. **4**(6): p. 7.
135. Morel, Y. and R. Barouki, *Repression of gene expression by oxidative stress.* Biochemical Journal, 1999. **342**(3): p. 481-496.
136. Favier, A., *Le stress oxydant: Intérêt conceptuel et expérimental dans la compréhension des mécanismes des maladies et potentiel thérapeutique.* L'actualité chimique, 2003: p. 108-115.

137. Vansant, G. *Radicaux libres et antioxydants: principes de base*. in *Symposium «Antioxydants et alimentation». Institut Danone*. 2004.
138. Novelli, G., *Role of free radicals in septic shock.* Journal of physiology, 1997. **48**(4): p. 517-527.
139. de Ferranti, S. and D. Mozaffarian, *The perfect storm: obesity, adipocyte dysfunction, and metabolic consequences.* Clinical chemistry, 2008. **54**(6): p. 945-955.
140. Codoñer-Franch, P., et al., *Oxidant mechanisms in childhood obesity: the link between inflammation and oxidative stress.* Translational Research, 2011. **158**(6): p. 369-384.
141. Gardès-Albert, M., et al., *Espèces réactives de l'oxygène.* L'actualité chimique, 2003: p. 91.
142. Mercier, J.-P. and P. Godard, *Chimie organique: une initiation*. 2001: PPUR presses polytechniques.
143. Koechlin-Ramonatxo, C., *Oxygène, stress oxydant et supplémentations antioxydantes ou un aspect différent de la nutrition dans les maladies respiratoires.* Nutrition clinique et métabolisme, 2006. **20**(4): p. 165-177.
144. Lacolley, P., et al., *Biologie et pathologie du coeur et des vaisseaux.* 2008.
145. Brahim Abba Ahmedou, G.K., *l'effet de deux plantes médicinales sur le statut antioxydant et la peroxydase lipidique induite au cours du diabète.* 2015.
146. Jadot, G., *Antioxydants et vieillissement*. 1994: John Libbey Eurotext.
147. Karp, G., *Biologie cellulaire et moléculaire: Concepts and experiments*. 2010: De Boeck Supérieur.
148. Atawodi, S., *Antioxidant potential of African medicinal plants.* African Journal of Biotechnology, 2005. **4**(2): p. 128-133.
149. Georgetti, S.R., et al., *Evaluation of the antioxidant activity of different flavonoids by the chemiluminescence method.* Aaps Pharmsci, 2003. **5**(2): p. 111-115.
150. Mohanty, P., et al., *Glucose challenge stimulates reactive oxygen species (ROS) generation by leucocytes.* The journal of clinical endocrinology metabolism, 2000. **85**(8): p. 2970-2973.
151. Patel, C., et al., *Prolonged reactive oxygen species generation and nuclear factor-κB activation after a high-fat, high-carbohydrate meal in the obese.* The Journal of Clinical Endocrinology Metabolism, 2007. **92**(11): p. 4476-4479.
152. Pincemail, J., et al., *Mécanismes physiologiques de la défense antioxydante.* Nutrition clinique et métabolisme, 2002. **16**(4): p. 233-239.
153. Behera, J. and C. Rao, *A Ni2+ (S= 1) Kagome compound templated by 1, 8-diazacubane.* Journal of the American Chemical Society, 2006. **128**(29): p. 9334-9335.
154. Meda, *Tropical Medicine & International Health.* Blackwell Synergy, 2005. **11**(2): p. 136-143.
155. Lehucher-Michel, M., et al., *Oxidative stress and human disease. Current knowledge and perspectives for prevention.* Presse medicale, 2001. **30**(21): p. 1076-1081.
156. Favier, A., *Le stress oxydant.* L'actualité chimique, 2003. **108**(10): p. 863-832.
157. Kohen, R. and A. Nyska, *Invited review: Oxidation of biological systems: oxidative stress phenomena, antioxidants, redox reactions, and methods for their quantification.* Toxicologic pathology, 2002. **30**(6): p. 620-650.

158. Flora, S.J., *Structural, chemical and biological aspects of antioxidants for strategies against metal and metalloid exposure.* Oxidative medicine cellular longevity, 2009. **2**(4): p. 191-206.

159. Johnson, D.R. and L.C. Gu, *In Autoxidation and Antioxidants*. 1988, New York: John Wiley.

160. Magalhães, L.M., et al., *Methodological aspects about in vitro evaluation of antioxidant properties.* Analytica chimica acta, 2008. **613**(1): p. 1-19.

161. Brand-Williams, W., M.-E. Cuvelier, and C. Berset, *Use of a free radical method to evaluate antioxidant activity*. LWT-Food science, Technology, 1995. **28**(1): p. 25-30.

162. Milardović, S., D. Iveković, and B.S. Grabarić, *A novel amperometric method for antioxidant activity determination using DPPH free radical.* Bioelectrochemistry, 2006. **68**(2): p. 175-180.

163. Foti, M.C., C. Daquino, and C. Geraci, *Electron-transfer reaction of cinnamic acids and their methyl esters with the DPPH• radical in alcoholic solutions.* The Journal of organic chemistry, 2004. **69**(7): p. 2309-2314.

164. Huang, D., B. Ou, and R.L. Prior, *The chemistry behind antioxidant capacity assays.* Journal of agricultural, food chemistry, 2005. **53**(6): p. 1841-1856.

165. Benzie, I.F. and J. Strain, *[2] Ferric reducing/antioxidant power assay: direct measure of total antioxidant activity of biological fluids and modified version for simultaneous measurement of total antioxidant power and ascorbic acid concentration.* Methods in enzymology, 1999. **299**: p. 15-27.

166. Tsao, R., R. Yang, and J.C. Young, *Antioxidant isoflavones in osage orange, Maclura pomifera (Raf.) Schneid.* Journal of agricultural, food chemistry, 2003. **51**(22): p. 6445-6451.

167. Ou, B., et al., *Novel fluorometric assay for hydroxyl radical prevention capacity using fluorescein as the probe.* Journal of agricultural, food chemistry, 2002. **50**(10): p. 2772-2777.

168. Singleton, V.L., R. Orthofer, and R.M. Lamuela-Raventós, *Analysis of total phenols and other oxidation substrates and antioxidants by means of folin-ciocalteu reagent.* Methods in enzymology, 1999. **299**: p. 152-178.

169. Roginsky, V. and E.A. Lissi, *Review of methods to determine chain-breaking antioxidant activity in food.* Food chemistry, 2005. **92**(2): p. 235-254.

170. Cao, G., H.M. Alessio, and R.G. Cutler, *Oxygen-radical absorbance capacity assay for antioxidants.* Free radical biology, medicine, 1993. **14**(3): p. 303-311.

171. Benderitter, M., et al., *The cell membrane as a biosensor of oxidative stress induced by radiation exposure: a multiparameter investigation.* Radiation research, 2003. **159**(4): p. 471-483.

172. Parejo, I., et al., *Comparison between the radical scavenging activity and antioxidant activity of six distilled and nondistilled Mediterranean herbs and aromatic plants.* Journal of Agricultural, Food Chemistry, 2002. **50**(23): p. 6882-6890.

173. Halliwell, B., J.M. Gutteridge, and O.I. Aruoma, *The deoxyribose method: a simple "test-tube" assay for determination of rate constants for reactions of hydroxyl radicals.* Analytical biochemistry, 1987. **165**(1): p. 215-219.

174. Hagerman, A.E., et al., *High molecular weight plant polyphenolics (tannins) as biological antioxidants.* Journal of agricultural, food chemistry, 1998. **46**(5): p. 1887-1892.

175. Gagne, R. and C. XA, *CA Koval and GC Lisensky.* Inorg Chem, 1980. **19**: p. 2854.
176. Elgrishi, N., et al., *A practical beginner's guide to cyclic voltammetry.* Journal of Chemical Education, 2018. **95**(2): p. 197-206.
177. Dorsett, H. and A. White, *Overview of molecular modelling and ab initio molecular orbital methods suitable for use with energetic materials*. 2000, DEFENCE SCIENCE AND TECHNOLOGY ORGANIZATION SALISBURY (AUSTRALIA).
178. Randles, J.E., *A cathode ray polarograph. Part II.—The current-voltage curves.* Transactions of the Faraday Society, 1948. **44**: p. 327-338.
179. Delahay, P., *New instrumental methods in electrochemistry.* 1954.
180. Matsuda, H. and Y. Ayabe, *The theory of the cathode-ray polarography of Randles-Sevcik.* Zeitschrift fuer Elektrochmie, Angewandte Physikalische Chemie, 1955. **59**: p. 494-503.
181. Shain, I. and R.S. Nicholson, *The theory of cyclic voltammetry is presented for chemical reactions presented for chemical reactions presented for chemical reactions presented for chemical reactions presented for chemical reactions coupled with electron transfer coupled with electron transfer coupled with electron transfer coupled with electron transfer coupled with electron transfer reactions. A numerical method is described for solving integral described for solving integral described for solving integral described for solving integral described for solving integral.* Anal Chem, 1964. **36**: p. 706-23.
182. Murcko, M.A., *Molecular Modeling: Basic Principles and Applications.* Drug Discovery Today, 1997. **9**(2): p. 364.
183. Schlecht, M.F., *Molecular Modeling on the PC*. 1998: Wiley-VCH.
184. Schrödinger, E., *Quantisierung als eigenwertproblem.* Annalen der physik, 1926. **385**(13): p. 437-490.
185. Born, M. and R. Oppenheimer, *Zur quantentheorie der molekeln.* Annalen der physik, 1927. **389**(20): p. 457-484.
186. Hartree, D.R., *The wave mechanics of an atom with a non-Coulomb central field. Part I. Theory and methods.* Camb Phil Soc, 1928. **24**: p. 89-110
187. Fock, V., *Näherungsmethode zur Lösung des quantenmechanischen Mehrkörperproblems.* Zeitschrift für Physik, 1930. **61**(1-2): p. 126-148.
188. Young, D.C., *A practical guide for applying techniques to real-world problems.* Computational Chemistry, New York, 2001. **9**: p. 390.
189. Jensen, F., *Introduction to computational chemistry*. 2017: John wiley & sons.
190. Pauli, W., *Relativistic field theories of elementary particles.* Reviews of Modern Physics, 1941. **13**(3): p. 203.
191. Roothaan, C.C.J., *New developments in molecular orbital theory.* Reviews of modern physics, 1951. **23**(2): p. 69.
192. Hohenberg, P. and W. Kohn, *Inhomogeneous electron gas.* Physical review, 1964. **136**(3B): p. B864.

193. Thomas, L.H. *The calculation of atomic fields*. in *Mathematical proceedings of the Cambridge philosophical society*. 1927. Cambridge University Press.

194. Fermi, E., *Eine statistische Methode zur Bestimmung einiger Eigenschaften des Atoms und ihre Anwendung auf die Theorie des periodischen Systems der Elemente.* Zeitschrift für Physik, 1928. **48**(1-2): p. 73-79.

195. Kohn, W. and L.J. Sham, *Self-consistent equations including exchange and correlation effects.* Physical review, 1965. **140**(4A): p. A1133.

196. Rabiolle, F. 2000, Toulouse university.

197. Vito, D.A. 2003, Geneve university.

198. Runge, E. and E.K. Gross, *Density-functional theory for time-dependent systems.* Physical Review Letters, 1984. **52**(12): p. 997.

199. Marques, M.A. and E.K. Gross, *Time-dependent density functional theory.* Annu Rev Phys Chem, 2004. **55**: p. 427-455.

200. Bachrach, S.M., *Population analysis and electron densities from quantum mechanics.* Reviews in computational chemistry, 1994: p. 171-228.

201. Becke, A.D., *Density-functional exchange-energy approximation with correct asymptotic behavior.* Physical review A, 1988. **38**(6): p. 3098.

202. Becke, A.D., *Density-functional thermochemistry. V. Systematic optimization of exchange-correlation functionals.* The Journal of chemical physics, 1997. **107**(20): p. 8554-8560.

203. Schmider, H.L. and A.D. Becke, *Optimized density functionals from the extended G2 test set.* The Journal of chemical physics, 1998. **108**(23): p. 9624-9631.

204. Lee, C., W. Yang, and R.G. Parr, *Development of the Colle-Salvetti correlation-energy formula into a functional of the electron density.* Physical review B, 1988. **37**(2): p. 785.

205. Slater, J.C., *Atomic shielding constants.* Physical Review, 1930. **36**(1): p. 57.

206. Lischka, H. and V. Dyczmons, *The molecular structure of H3O+ by the ab initio SCF method and with inclusion of correlation energy.* Chemical Physics Letters, 1973. **23**(2): p. 167-172.

207. Hariharan, P.C. and J.A. Pople, *The influence of polarization functions on molecular orbital hydrogenation energies.* Theoretica chimica acta, 1973. **28**(3): p. 213-222.

208. Francl, M.M., et al., *Self-consistent molecular orbital methods. XXIII. A polarization-type basis set for second-row elements.* The Journal of Chemical Physics, 1982. **77**(7): p. 3654-3665.

209. Bartlett, R.J. and J.F. Stanton, *Applications of Post-Hartree—Fock Methods: A Tutorial.* Reviews in computational chemistry, 1994: p. 65-169.

210. Dirac, P., *Lectures on Quantum Mechanics (New York: Belfer Graduate School of Science, Yeshiva University).* Lectures on Quantum Field Theory, 1964.

211. Heisenberg, W., *The physical principles of the quantum theory*. 1949: Courier Corporation.

212. Landau, L. and E.J.T.I.M.q.T.n.r. Lifschitz, Éditions Mir, Moscow, *Physique théorique ("Landau-Lifchitz").* Tome III: Mécanique quantique Théorie non relativiste, Éditions Mir, Moscow, 1967.

213. Allinger, N.L., *Conformational analysis. 130. MM2. A hydrocarbon force field utilizing V1 and V2 torsional terms.* Journal of the American Chemical Society, 1977. **99**(25): p. 8127-8134.

214. Allinger, N.L., Y.H. Yuh, and J.H. Lii, *Molecular mechanics. The MM3 force field for hydrocarbons. 1.* Journal of the American Chemical Society, 1989. **111**(23): p. 8551-8566.

215. Kohn, W., A.D. Becke, and R.G. Parr, *Density functional theory of electronic structure.* The Journal of Physical Chemistry, 1996. **100**(31): p. 12974-12980.

216. Dewar, M.J.S., G.L. Glady, and J.J.P. Stewart, J Am Chem Soc, 1978. **106**.

217. Anderson, W.P., et al., *Utility of the semiempirical INDO/1 method for the calculation of the geometries of second-row transition-metal species.* Inorganic Chemistry, 1990. **29**(1): p. 1-3.

218. Lewis, D.F., *MINDO/3: a review of the literature.* Chemical Reviews, 1986. **86**(6): p. 1111-1123.

219. Dewar, M.J., C. Jie, and J. Yu, *SAM1; the first of a new series of general purpose quantum mechanical molecular models.* Tetrahedron, 1993. **49**(23): p. 5003-5038.

220. Dewar, M.J.S., et al., J Am Chem Soc, 1985. **107**: p. 3902.

221. Stewart, J.J., *Optimization of parameters for semiempirical methods II. Applications.* Journal of computational chemistry, 1989. **10**(2): p. 221-264.

222. Williamson, K. and K. Masters, *Techniques Labs for Macroscale and Microscale Organic Experiments*. 2012: Nelson Education.

223. Lessigiarska, I., *Development of structure-activity relationships for pharmacotoxicological endpoints relevant to European Union legislation*. 2006, Liverpool John Moores University.

224. Esposito, E.X., A.J. Hopfinger, and J.D. Madura, *Methods for applying the quantitative structure-activity relationship paradigm*, in *Chemoinformatics*. 2004, Springer. p. 131-213.

225. Bradbury, S.P., *Quantitative structure-activity relationships and ecological risk assessment: an overview of predictive aquatic toxicology research.* Toxicology letters, 1995. **79**(1-3): p. 229-237.

226. Hansen, C., B.R. Telzer, and L. Zhang, *Comparative QSAR in toxicology: examples from teratology and cancer chemotherapy of aniline mustards.* Critical reviews in toxicology, 1995. **25**(1): p. 67-89.

227. Perkins, R., et al., *Quantitative structure-activity relationship methods: Perspectives on drug discovery and toxicology.* Environmental Toxicology, Chemistry: An International Journal, 2003. **22**(8): p. 1666-1679.

228. Chen, J.-Z., et al., *3D-QSAR studies of arylpyrazole antagonists of cannabinoid receptor subtypes CB1 and CB2. A combined NMR and CoMFA approach.* Journal of medicinal chemistry, 2006. **49**(2): p. 625-636.

229. Karelson, M., *Molecular descriptors in QSAR/QSPR*. 2000: Wiley-Interscience.

230. Randić, M., *The connectivity index 25 years after.* Journal of Molecular Graphics, Modelling, 2001. **20**(1): p. 19-35.

231. Todeschini, R., et al., *Modeling and prediction by using WHIM descriptors in QSAR studies: submitochondrial particles (SMP) as toxicity blosensors of chlorophenols.* Chemosphere, 1996. **33**(1): p. 71-79.

232. Todeschini, R. and P. Gramatica, *SD-modelling and prediction by WHIM descriptors. Part 5. Theory development and chemical meaning of WHIM descriptors.* Quantitative Structure-Activity Relationships, 1997. **16**(2): p. 113-119.
233. Myers, R.H., *Classical and modern regression with applications*. Vol. 2. 1990: Duxbury press Belmont, CA.
234. Solomonov, B.N., et al., journal of general chemistry, 1985. **55**(1681).
235. Rosner, B., *Fundamentals of biostatistics*. 2015: Cengage learning.
236. Plyasunov, A.V. and E.L. Shock, *Group contribution values of the infinite dilution thermodynamic functions of hydration for aliphatic noncyclic hydrocarbons, alcohols, and ketones at 298.15 K and 0.1 MPa.* Journal of Chemical, Engineering Data, 2001. **46**(5): p. 1016-1019.
237. Verma, R.P. and C. Hansch, *QSAR modeling of taxane analogues against colon cancer.* European journal of medicinal chemistry, 2010. **45**(4): p. 1470-1477.
238. Golbraikh, A. and A. Tropsha, *Beware of q2!* %J Journal of molecular graphics, modelling, 2002. **20**(4): p. 269-276.
239. Kahn, I., et al., *QSPR treatment of the soil sorption coefficients of organic pollutants.* Journal of chemical information modeling, 2005. **45**(1): p. 94-105.
240. Gramatica, P., E. Giani, and E. Papa, *Statistical external validation and consensus modeling: a QSPR case study for Koc prediction.* Journal of Molecular Graphics Modelling, 2007. **25**(6): p. 755-766.
241. Wold, S., *Validation of QSAR's.* Quantitative Structure-Activity Relationships, 1991. **10**(3): p. 191-193.
242. Tropsha, A., P. Gramatica, and V.K. Gombar, *The importance of being earnest: validation is the absolute essential for successful application and interpretation of QSPR models.* QSAR, Combinatorial Science, 2003. **22**(1): p. 69-77.
243. Gilson, M.K. and H.-X. Zhou, *Calculation of protein-ligand binding affinities.* Annu Rev Biophys Biomol Struct, 2007. **36**: p. 21-42.
244. Sousa, S.F., P.A. Fernandes, and M.J. Ramos, *Protein–ligand docking: current status and future challenges.* Proteins: Structure, Function, Bioinformatics, 2006. **65**(1): p. 15-26.
245. Morris, G.M., et al., *Automated docking using a Lamarckian genetic algorithm and an empirical binding free energy function.* Journal of computational chemistry, 1998. **19**(14): p. 1639-1662.
246. Solis, F.J. and R.J.-B. Wets, *Minimization by random search techniques.* Mathematics of operations research, 1981. **6**(1): p. 19-30.
247. Conn, A.R., N.I. Gould, and P. Toint, *A globally convergent augmented Lagrangian algorithm for optimization with general constraints and simple bounds.* SIAM Journal on Numerical Analysis, 1991. **28**(2): p. 545-572.
248. Kirkpatrick, S., C.D. Gelatt, and M.P. Vecchi, *Optimization by simulated annealing.* science, 1983. **220**(4598): p. 671-680.

249. Holland, J., *Adaptation in natural and artificial systems. Cambridge, MA: Massachusetts Institute of Technology Press*. 1992, MIT Press.
250. Goldberg, D.E. and J.H. Holland, *Genetic algorithms and machine learning.* 1988.
251. Michalewicz, Z., *Genetic algorithms+ data structures= evolution programs*. 1996: Springer Science & Business Media.
252. Vaqué, M., et al., *BDT: an easy-to-use front-end application for automation of massive docking tasks and complex docking strategies with AutoDock.* Bioinformatics, 2006. **22**(14): p. 1803-1804.
253. Berman, H.M., et al., *The protein data bank.* Nucleic acids research, 2000. **28**(1): p. 235-242.
254. Hendlich, M., *Databases for protein–ligand complexes.* Acta Crystallographica Section D: Biological Crystallography, 1998. **54**(6): p. 1178-1182.
255. Hu, L., et al., *Binding MOAD (mother of all databases).* Proteins: Structure, Function, Bioinformatics, 2005. **60**(3): p. 333-340.
256. Smith, R.D., et al., *Exploring protein–ligand recognition with Binding MOAD.* Journal of Molecular Graphics Modelling, 2006. **24**(6): p. 414-425.
257. Guex, N. and M.C. Peitsch, *SWISS-MODEL and the Swiss-Pdb Viewer: an environment for comparative protein modeling.* electrophoresis, 1997. **18**(15): p. 2714-2723.
258. Davis, I.W., et al., *MOLPROBITY: structure validation and all-atom contact analysis for nucleic acids and their complexes.* Nucleic acids research, 2004. **32**(suppl_2): p. W615-W619.
259. Lovell, S.C., et al., *Structure validation by Cα geometry: ϕ, ψ and Cβ deviation.* Proteins: Structure, Function, Bioinformatics, 2003. **50**(3): p. 437-450.
260. Irwin, J.J. and B.K. Shoichet, *ZINC− a free database of commercially available compounds for virtual screening.* Journal of chemical information modeling, 2005. **45**(1): p. 177-182.
261. James, C., D. Weininger, and J. Delany, *Daylight theory manual. 2004.* URL http://wwwdaylightcom/dayhtml/doc/theory/theorytochtml, 2007.
262. Sadowski, J., C. Rudolph, and J. Gasteiger, *The generation of 3D models of host-guest complexes.* Analytica chimica acta, 1992. **265**(2): p. 233-241.
263. Gasteiger, J., C. Rudolph, and J. Sadowski, *Automatic generation of 3D-atomic coordinates for organic molecules.* Tetrahedron Computer Methodology, 1990. **3**(6): p. 537-547.
264. Dalby, A., et al., *Description of several chemical structure file formats used by computer programs developed at Molecular Design Limited.* Journal of chemical information computer sciences, 1992. **32**(3): p. 244-255.
265. Hassinen, T. and M. Peräkylä, *New energy terms for reduced protein models implemented in an off-lattice force field.* Journal of Computational Chemistry, 2001. **22**(12): p. 1229-1242.
266. Van Aalten, D.M., et al., *PRODRG, a program for generating molecular topologies and unique molecular descriptors from coordinates of small molecules.* Journal of computer-aided molecular design, 1996. **10**(3): p. 255-262.

267. Schüttelkopf, A.W. and D.M. Van Aalten, *PRODRG: a tool for high-throughput crystallography of protein–ligand complexes.* Acta Crystallographica Section D: Biological Crystallography, 2004. **60**(8): p. 1355-1363.

268. Gasteiger, J. and M. Marsili, *A new model for calculating atomic charges in molecules.* Tetrahedron Letters, 1978. **19**(34): p. 3181-3184.

269. Hetényi, C. and D. van der Spoel, *Efficient docking of peptides to proteins without prior knowledge of the binding site.* Protein science, 2002. **11**(7): p. 1729-1737.

270. Raymer, M.L., et al., *Predicting conserved water-mediated and polar ligand interactions in proteins using a K-nearest-neighbors genetic algorithm.* Journal of molecular biology, 1997. **265**(4): p. 445-464.

271. STAMBOULI, B., *Study of Protein-Protein Interaction by Molecular Modeling. Application to Biological Processes*. 2013, Tlemcen University.

272. ABDELOUAHAB, C., *Calculations and modeling of peptide deformylase interactions - antibacterial substances using "MOLECULAR DOCKING" techniques*. 2007, CONSTANTINE MENTOURI UNIVERSITY.

273. Frisch, M., et al., *gaussian 09, Revision d. 01, Gaussian.* Inc, Wallingford CT, 2009. **201**.

274. BENAOUDA, M.N., *Theoretical study of organometallic complexes based on ruthenium by quantum chemistry calculations*. 2012, University of Oran.

275. Pritchard, B.P., et al., *New basis set exchange: An open, up-to-date resource for the molecular sciences community.* Journal of chemical information, 2019. **59**(11): p. 4814-4820.

276. Feller, D., *The role of databases in support of computational chemistry calculations.* Journal of computational chemistry, 1996. **17**(13): p. 1571-1586.

277. Schuchardt, K.L., et al., *Basis set exchange: a community database for computational sciences.* Journal of chemical information, 2007. **47**(3): p. 1045-1052.

278. Hay, P.J. and W.R. Wadt, *Ab initio effective core potentials for molecular calculations. Potentials for the transition metal atoms Sc to Hg.* The Journal of chemical physics, 1985. **82**(1): p. 270-283.

279. Wadt, W.R. and P.J. Hay, *Ab initio effective core potentials for molecular calculations. Potentials for main group elements Na to Bi.* The Journal of Chemical Physics, 1985. **82**(1): p. 284-298.

280. Clark, T., et al., *Efficient diffuse function-augmented basis sets for anion calculations. III. The 3-21+ G basis set for first-row elements, Li–F.* Journal of Computational Chemistry, 1983. **4**(3): p. 294-301.

281. Ditchfield, R., W.J. Hehre, and J.A. Pople, *Self-consistent molecular-orbital methods. IX. An extended Gaussian-type basis for molecular-orbital studies of organic molecules.* The Journal of Chemical Physics, 1971. **54**(2): p. 724-728.

282. Gordon, M.S., et al., *Self-consistent molecular-orbital methods. 22. Small split-valence basis sets for second-row elements.* Journal of the American Chemical Society, 1982. **104**(10): p. 2797-2803.

283. Hehre, W.J., R. Ditchfield, and J.A. Pople, *Self—consistent molecular orbital methods. XII. Further extensions of Gaussian—type basis sets for use in molecular orbital studies of organic molecules.* The Journal of Chemical Physics, 1972. **56**(5): p. 2257-2261.

284. Spitznagel, G.W., et al., *An evaluation of the performance of diffuse function-augmented basis sets for second row elements, Na-Cl.* Journal of computational chemistry, 1987. **8**(8): p. 1109-1116.

285. Rahim, O., et al., *N-Ferrocenylmethyl-2-nitroaniline.* Acta Crystallographica Section E: Structure Reports Online, 2012. **68**(10): p. m1318-m1318.

286. Oumelkhair, R., *Synthèse et étude électrochimique et structurale de quelques N-ferrocényl méthyle anilines substitués Applications à l'inhibition de la corrosion aqueuse*. 2014, University Kasdi Merbah of Ouergla.

287. Wiberg, K.B. and P.R. Rablen, *Comparison of atomic charges derived via different procedures.* Journal of Computational Chemistry, 1993. **14**(12): p. 1504-1518.

288. Aihara, J.-i., *Reduced HOMO− LUMO gap as an index of kinetic stability for polycyclic aromatic hydrocarbons.* The Journal of Physical Chemistry A, 1999. **103**(37): p. 7487-7495.

289. Manolopoulos, D.E., J.C. May, and S.E. Down, *Theoretical studies of the fullerenes: C34 to C70.* Chemical Physics Letters, 1991. **181**(2-3): p. 105-111.

290. Ruiz-Morales, Y., *HOMO− LUMO gap as an index of molecular size and structure for polycyclic aromatic hydrocarbons (PAHs) and asphaltenes: A theoretical study. I.* The Journal of Physical Chemistry A, 2002. **106**(46): p. 11283-11308.

291. Caldwell, J., I. Gardner, and N. Swales, *An introduction to drug disposition: the basic principles of absorption, distribution, metabolism, and excretion.* Toxicologic pathology, 1995. **23**(2): p. 102-114.

292. Balakumar, C., et al., *Ligand-and structure-based in silico studies to identify kinesin spindle protein (KSP) inhibitors as potential anticancer agents.* Journal of Biomolecular Structure, 2018. **36**(14): p. 3687-3704.

293. Daina, A., O. Michielin, and V. Zoete, *SwissADME: a free web tool to evaluate pharmacokinetics, drug-likeness and medicinal chemistry friendliness of small molecules.* Scientific reports, 2017. **7**(1): p. 1-13.

294. Mosby, A., *Mosby's dictionary of medicine, nursing & health professions*. 2006: Mosby.

295. Wolff, K., et al., *Basic pharmacokinetics of substance misuse*, in *The SAGE Handbook of Drug and Alcohol Studies: Biological Approaches*. 2016, Sage Publications. p. 37-56.

296. Löbenberg, R., et al., *Mechanism of gastrointestinal drug absorption and application in therapeutic drug delivery*. 2013, Future Medicine.

297. Garcia-Garcia, E., et al., *Colloidal carriers and blood–brain barrier (BBB) translocation: a way to deliver drugs to the brain?* International journal of pharmaceutics, 2005. **298**(2): p. 274-292.

298. Dean, M., Y. Hamon, and G. Chimini, *The human ATP-binding cassette (ABC) transporter superfamily*. Journal of lipid research, 2001. **42**(7): p. 1007-1017.

299. Rettie, A.E., et al., *Hydroxylation of warfarin by human cDNA-expressed cytochrome P-450: a role for P-4502C9 in the etiology of (S)-warfarin-drug interactions.* Chemical research in toxicology, 1992. **5**(1): p. 54-59.

300. Danielson, P.á., *The cytochrome P450 superfamily: biochemistry, evolution and drug metabolism in humans.* Current drug metabolism, 2002. **3**(6): p. 561-597.

301. Guengerich, F.P., *Cytochrome p450 and chemical toxicology.* Chemical research in toxicology, 2008. **21**(1): p. 70-83.

302. Zhong, H.A., *ADMET properties: Overview and current topics.* Drug design: Principles and applications, 2017: p. 113-133.

303. Lipinski, C.A., *Lead-and drug-like compounds: the rule-of-five revolution.* Drug Discovery Today: Technologies, 2004. **1**(4): p. 337-341.

304. Ghose, A.K., V.N. Viswanadhan, and J.J. Wendoloski, *A knowledge-based approach in designing combinatorial or medicinal chemistry libraries for drug discovery. 1. A qualitative and quantitative characterization of known drug databases.* Journal of combinatorial chemistry, 1999. **1**(1): p. 55-68.

305. Veber, D.F., et al., *Molecular properties that influence the oral bioavailability of drug candidates.* Journal of medicinal chemistry, 2002. **45**(12): p. 2615-2623.

306. Egan, W.J., K.M. Merz, and J.J. Baldwin, *Prediction of drug absorption using multivariate statistics.* Journal of medicinal chemistry, 2000. **43**(21): p. 3867-3877.

307. Muegge, I., S.L. Heald, and D. Brittelli, *Simple selection criteria for drug-like chemical matter.* Journal of medicinal chemistry, 2001. **44**(12): p. 1841-1846.

308. Martin, Y.C., *A bioavailability score.* Journal of medicinal chemistry, 2005. **48**(9): p. 3164-3170.

309. Drwal, M.N., et al., *ProTox: a web server for the in silico prediction of rodent oral toxicity.* Nucleic acids research, 2014. **42**(W1): p. W53-W58.

310. Tittarelli, R., et al., *Hepatotoxicity of paracetamol and related fatalities.* Eur Rev Med Pharmacol Sci, 2017. **21**(1 Suppl): p. 95-101.

311. Bothorel, P., *Implication du stress oxydant dans la biologie tumorale et intérêt d'une supplémentation en antioxydants au cours d'une chimiothérapie*. 2011.

312. Sahnoun, Z., K. Jamoussi, and K. Zeghal, *Free radicals and antioxidants: human physiology, pathology and therapeutic aspects.* Therapie, 1997. **52**(4): p. 251-270.

313. Corso, C.R. and A. Acco, *Glutathione system in animal model of solid tumors: From regulation to therapeutic target.* Critical reviews in oncology/hematology, 2018. **128**: p. 43-57.

314. Couto, N., J. Wood, and J. Barber, *The role of glutathione reductase and related enzymes on cellular redox homoeostasis network.* Free radical biology medicine, 2016. **95**: p. 27-42.

315. Torbiero, B., *Développement de microcapteurs électrochimiques pour l'analyse en phase liquide*. 2006, INSA de Toulouse.

316. Carter, M.T., M. Rodriguez, and A.J. Bard, *Voltammetric studies of the interaction of metal chelates with DNA. 2. Tris-chelated complexes of cobalt (III) and iron (II) with 1, 10-*

phenanthroline and 2, 2'-bipyridine. Journal of the American Chemical Society, 1989. **111**(24): p. 8901-8911.

317. Feng, Q., N.-Q. Li, and Y.-Y. Jiang, *Electrochemical studies of porphyrin interacting with DNA and determination of DNA.* Analytica Chimica Acta, 1997. **344**(1-2): p. 97-104.
318. Leftheriotis, G., S. Papaefthimiou, and P. Yianoulis, *Dependence of the estimated diffusion coefficient of LixWO3 films on the scan rate of cyclic voltammetry experiments.* Solid State Ionics, 2007. **178**(3-4): p. 259-263.
319. Lanez, E., L. Bechki, and T. Lanez, *Antioxidant Activities, Binding Parameters, and Electrochemical Behavior of Superoxide Anion Radicals Twords 1-Ferrocenylmethylthymine and 1-Ferrocenylmethylcytosine.* Current Physical Chemistry, 2020. **10**(1): p. 10-22.
320. Burton, G.W. and M.G. Traber, *Vitamin E: antioxidant activity, biokinetics, and bioavailability.* Annual review of nutrition, 1990. **10**(1): p. 357-382.
321. Landvik, S.V., A.T. Diplock, and L. Packer, *Efficacy of vitamin E in human health and disease.* Handbook of antioxidants, 2002: p. 75-97.
322. Farrell, P., *Deficiency states, pharmacological effects, and nutrient requirements.* Vitamin E: a comprehensive treatise, 1980. **1**: p. 520-620.
323. Burton, G.W., et al., *Autoxidation of biological molecules. 4. Maximizing the antioxidant activity of phenols.* Journal of the American Chemical Society, 1985. **107**(24): p. 7053-7065.
324. McCay, P.B., *Vitamin E: interactions with free radicals and ascorbate.* Annual review of nutrition, 1985. **5**(1): p. 323-340.
325. Burton, G.W. and K.U. Ingold, *Vitamin E: application of the principles of physical organic chemistry to the exploration of its structure and function.* Accounts of chemical research, 1986. **19**(7): p. 194-201.
326. Burton, G.W. and K.U. Ingold, *Vitamin E as an in Vitro and in Vivo Antioxidant a.* Annals of the New York Academy of Sciences, 1989. **570**(1): p. 7-22.
327. Savvides, S.N. and P.A. Karplus, *Kinetics and crystallographic analysis of human glutathione reductase in complex with a xanthene inhibitor.* Journal of Biological Chemistry, 1996. **271**(14): p. 8101-8107.
328. Morris, G.M., et al., *AutoDock4 and AutoDockTools4: Automated docking with selective receptor flexibility.* Journal of computational chemistry, 2009. **30**(16): p. 2785-2791.
329. Trott, O. and A.J. Olson, *AutoDock Vina: improving the speed and accuracy of docking with a new scoring function, efficient optimization, and multithreading.* Journal of computational chemistry, 2010. **31**(2): p. 455-461.
330. Adasme, M.F., et al., *PLIP 2021: Expanding the scope of the protein-ligand interaction profiler to DNA and RNA.* Nucleic Acids Res, 2021.
331. Salentin, S., et al., *PLIP: fully automated protein–ligand interaction profiler.* Nucleic acids research, 2015. **43**(W1): p. W443-W447.

332. Caricato, M., et al., *Link atom bond length effect in ONIOM excited state calculations.* The Journal of chemical physics, 2010. **133**(5): p. 054104.

333. Beck, A.D., *Density-functional thermochemistry. III. The role of exact exchange.* J Chem Phys, 1993. **98**(7): p. 5648-6.

334. Miehlich, B., et al., *Results obtained with the correlation energy density functionals of Becke and Lee, Yang and Parr.* Chemical Physics Letters, 1989. **157**(3): p. 200-206.

335. Gill, P.M., et al., *The performance of the Becke—Lee—Yang—Parr (B—LYP) density functional theory with various basis sets.* Chemical Physics Letters, 1992. **197**(4-5): p. 499-505.

336. Daina, A., O. Michielin, and V. Zoete, *SwissADME: a free web tool to evaluate pharmacokinetics, drug-likeness and medicinal chemistry friendliness of small molecules.* J Scientific reports, 2017. **7**(1): p. 1-13.

337. Khand, I.U., T. Lanez, and P.L. Pauson, *Ferrocene derivatives. Part 24. Synthesis of dihydro-2-pyrindines and dihydro-3 H-2-cyclopent [c] azepines by photolysis of their cyclopentadienyliron derivatives.* Journal of the Chemical Society, Perkin Transactions 1, 1989(11): p. 2075-2078.

338. Chérifa, B., et al., *Synthesis and electrochemical properties of N-(ferrocenylmethyl) aminobenzonitrile and N-(ferrocenylmethyl) nitroaniline derivatives.* International Letters of Chemistry, Physics Astronomy, 2015. **49**: p. 27-34.

339. Lanez, E., L. Bechki, and T. Lanez, *N 6, 9-BIS (FERROCENYLMETHYL) ADENINE: SYNTHESIS, CYCLIC VOLTAMMETRIC, SPECTROSCOPIC CHARACTERIZATION, AND DFT CALCULATIONS.* Scientific Study Research Chemistry Chemical Engineering, Biotechnology, Food Industry, 2019. **20**(4): p. 509-519.

340. Khelef, A., et al., *N-Ferrocenymethyl-N-phenylpropionamide.* Acta Crystallographica Section E: Structure Reports Online, 2012. **68**(5): p. m647-m647.

341. Topliss, J.G. and R.J. Costello, *Chance correlations in structure-activity studies using multiple regression analysis.* Journal of Medicinal Chemistry, 1972. **15**(10): p. 1066-1068.

342. Walker, J.D., et al., *Guidelines for developing and using quantitative structure-activity relationships.* Environmental Toxicology Chemistry: An International Journal, 2003. **22**(8): p. 1653-1665.

343. Clark, M. and R.D. Cramer III, *The probability of chance correlation using partial least squares (PLS).* Quantitative Structure-Activity Relationships, 1993. **12**(2): p. 137-145.

344. Alam, S. and F. Khan, *3D-QSAR, Docking, ADME/Tox studies on Flavone analogs reveal anticancer activity through Tankyrase inhibition.* Scientific reports, 2019. **9**(1): p. 1-15.

345. Srivastava, A. and N. Shukla, *Quantitative structure activity relationship (QSAR) studies on a series of imidazole derivatives as novel ORL1 receptor antagonists.* Journal of Saudi Chemical Society, 2013. **3**(17): p. 321-328.